

Modification of bioactive hyaluronic acid for stereolithography 3D printing of hydrogel conduits for peripheral nerve regeneration

Ciara Buckley



This thesis is submitted in fulfilment of the requirements for the degree of Doctor of Philosophy to the Technological University of the Shannon: Midlands Midwest.

Department of Mechanical, Polymer & Design

Engineering and Informatics

Technological University of the Shannon

Midlands

2023

CANDIDATE'S DECLARATION

I hereby declare that this thesis consists of my own work, unless otherwise stated, and has not previously been submitted to the Technological University of the Shannon, Midlands or any other university.

I agree that the library may lend or copy this thesis upon request.

Ciara Buckley

DEDICATION

**Dedicated to my Son, Joshua.
You have always been my inspiration.**

ACKNOWLEDGEMENTS

There are so many people to whom the accomplishment of this thesis belongs to. At the top of that list to thank is my wonderful PhD supervisors, Dr. Ian Major and Dr. Therese Montgomery. Your patience, knowledge and guidance over the past number of years has allowed me to grow not only as an engineer, but also as a person. I will be eternally grateful for your mentorship and friendship.

It has been an absolute honour to watch the college which has always been so welcoming and supportive of me develop into a technological university. I am so incredibly proud to have begun my journey in Athlone Institute of Technology as an undergraduate, and to close this chapter after 8 years in the Technological University of the Shannon.

A special thanks to all of the lecturers, technicians, administration staff and research staff who have helped support me in my journey right from the very beginning. A big thank you also to Dr. Mark Lynch and Dr. Crevan O' Donnell who work tirelessly keeping the research hub a safe and productive space for all.

Thank you to all of my fellow postgraduate students, it was an incredibly tough 4 years which saw us face a global pandemic together, but those zoom and teams sessions got me through some very tough times. I will always carry those memories with me.

In particular, I would like to take the opportunity to thank my dear friend, Tomasz Szank, who has been by my side since the beginning and without whom, I would not have made it this far. I can't wait to see what your next adventure holds. Tomasz Szank also conducted the HPLC testing through a biological research institute (BRI) collaboration in this project and aided in the analysis and interpretation of results.

To Declan Colbert, thank you for saving me from the madness of thesis formatting. You underestimate how much you have helped me in the writing of this thesis. I am so grateful for your friendship.

A special mention to Dr. Brian Murray of TU Dublin who collaborated in this research and provided all of the NMR testing and assisted with data analysis. Brian not only conducted the tests, but also spent a lot of time teaching me about the basics and principles of the various types of NMR, and how to read and analyse the results obtained. I am incredibly grateful for the time you took to provide me with this knowledge.

I must also take this opportunity to thank Dr. Cormac Quigley of ATU, Galway. Throughout this project, he has always been on hand to advise and instruct in all chemistry matters. His collaboration enabled the optimisation of modification procedures, quantification of modification degree, nationwide presentations and the construction of three manuscripts, one of which is published in the International Journal of Biological Macromolecules and two which are currently being drafted. I can't emphasise enough how vital Cormac's input has been to the success of this project.

To my family, who have supported me unconditionally, thank you for always believing in me. I hope you will finally now believe me when I say I'm finished studying (potentially). To Una and Mark, you have both been there for Joshua and me throughout this entire journey and beyond. Your continuing support and love has been the foundation of this success. To my mum, Paulette, you have always encouraged me and made me believe that I could do anything I wanted. It is because of you that I had the confidence to pursue my dreams. Thank you for being my rock.

Finally, to Dean and Joshua. You have bared the brunt of the struggles throughout this PhD between being forced to listen to me recite presentations 30 times, to being interrogated over which blue is the right blue for my poster. You kept me going during Covid when I struggled to find the motivation, and you helped me stay positive when I needed to make up for lost time. Thank you both for your love, understanding and patience. I love you both, always.

All images, unless otherwise stated, were produced using Biorender.com.

ABSTRACT

Peripheral nerve injuries occur as a result of illness or injury, and present a significant healthcare and economic burden. Many of these cases occur in otherwise healthy individuals, in the age range 20-40 years, due to trauma in the work environment. Despite all that is known of this condition, complete functional recovery remains difficult to obtain through current surgical methods.

The aim of this research was to modify hyaluronic acid (HA) to enable 3D printing of hydrogel nerve conduits which could enable full functional recovery of a peripheral nerve injury. An array of compounds were screened in conjunction with HA to assess any potential neurotrophic benefits to their inclusion in the final formulation.

As HA is not conducive to cell attachment, neuronal and glial cell lines were initially used to characterise HA in order to design a testing procedure and acquire a baseline response. HA was then successfully modified with cysteamine HCl and methacrylic anhydride, to produce thiolated HA (HA-SH) and methacrylated HA (HA-MA) respectively, as confirmed by colorimetric and spectroscopic methods. The modification degree was approximately 20% so as not to interfere with the receptor interaction of HA. Modified HA was characterised chemically and biologically to ensure cytocompatibility in neuronal and glial cell lines. UV photo-polymerised hydrogels were created via click chemistry reactions by combining thiolated HA and methacrylated HA in various ratios and their properties were evaluated. Due to the poor mechanical properties of the HA hydrogels, a synthetic polymer, polyethylene glycol dimethacrylate (PEGDMA), was introduced to the matrix. An optimal formulation was discovered and prints were created via stereolithography 3D printing. Direct contact and elution extract testing revealed no significant cytotoxicity over a 24 h period, in contrast to the hydrogels of each of the four polymeric matrices tested (PEGDMA, 50 %wv HA-MA: PEGDMA, 50 %wv HA-SH: PEGDMA and hybrid blend). This would indicate that 3D printing yielded a sample which is representative of the conduit formulation, which is capable of providing biological and physical support to enhance peripheral nerve regeneration.

Through extensive testing of potential neurotrophic compounds, the lead compound Tyrosol failed to produce significant proliferative effects from elution extract testing of 3D printed samples using the resazurin assay. Given its antioxidant status and the significant proliferative effects observed with this compound in direct cell assays, future studies should

refine the test methods in order to evaluate the effective elution concentration of Tyrosol from the final conduit, rather than from a representative sample.

This research could have a significant impact on the future of not only nerve regeneration, but also bioengineering as a whole. This thesis has elucidated the use of click-chemistry reactions to enable highly reliable cross-linking reactions in biological polymers to enable processing which would otherwise be difficult. Further work would involve the ex vivo testing of this formulation in dorsal root ganglion cells before in vivo testing could take place. This formulation could also be tested in other formats such as injectable hydrogels and foams for a number of pathologies

TABLE OF CONTENTS

Candidate's Declaration	i
Dedication	ii
Acknowledgements	iii
Abstract	v
Table of Contents	vii
List of Tables	xiii
List of Figures	xiii
List of Abbreviations	xviii
Chapter 1. Introduction	1
1.1 Thesis Outline	1
1.2 Context	1
1.3 Research questions	5
1.4 Research aim	6
1.5 Research objectives	6
1.6 Justification	7
1.7 Contribution to Existing knowledge	7
Chapter 2. Literature Review	1
2.1 Peripheral nervous system	12
2.2 Injuries to the PNS	15
2.2.1 Mechanisms of peripheral nerve injuries	16
2.2.2 Classification of nerve injuries	17
2.2.3 Wallerian degeneration	18
2.3 Nerve Regeneration	21
2.3.1 Current therapeutic options	21
2.3.1.1 End-to-end repair	22
2.3.1.2 Epineural sleeve repair	23
2.3.1.3 Nerve grafts	23
2.3.1.4 Nerve guidance conduits	24
2.4 Biomaterials	27
2.4.1 Hyaluronic acid	27
2.4.1.1 History	27
2.4.1.2 Physicochemical properties	27
2.4.1.3 Endogenous bioactive properties	31
	vii

2.4.1.4	Synthesis	32
2.4.1.4.1	Microbial Synthesis	32
2.4.1.4.2	Animal Synthesis	33
2.4.1.5	Degradation	34
2.4.1.5.1	Enzymatic degradation	35
2.4.1.6	Functionalisation	35
2.4.1.6.1	Modification of HA via the hydroxyl group	37
2.4.1.6.2	Modification of HA via the carboxyl group	38
2.4.1.6.3	Amidation	39
2.4.1.7	The use of HA for peripheral nerve repair	39
2.5	PEGDMA	41
2.6	Neurotrophic compounds	42
2.6.1	Melatonin	42
2.6.2	Tyrosol	43
2.7	Stereolithography 3D printing	45
Chapter 3.	Materials and methods	44
3.1	Materials	45
3.1.1	Cell lines	45
3.1.1.1	SH-SY5Y cell line	45
3.1.1.2	RT4 D6P2T cell line	46
3.1.2	Investigation into the effect of molecular weight on the cytocompatibility of hyaluronic acid in neuronal and glial cell lines	46
3.1.3	Modification of hyaluronic acid to enable UV photo-crosslinking	47
3.1.4	UV Photo-crosslinking of modified hyaluronic acid	47
3.1.5	Stereolithography 3D printing	47
3.1.6	Identification and incorporation of neurotrophic compounds	47
3.1.7	Tyrosol Drug Delivery	47
3.2	Investigation into the effect of molecular weight on the cytocompatibility of HA	48
3.2.1	Cell Culture	48
3.2.2	Cell propagation	48
3.2.3	Cell Characterisation	49
3.2.4	Cell seeding	50
3.2.5	Plate coating	50
3.2.6	The effect of molecular weight on the cytocompatibility of HA in neuronal and glial cell lines	51

3.2.6.1	Qualitative analysis of the effect of molecular weight on HA coating	51
3.2.6.2	The effect of molecular weight on solution viscosity	51
3.2.6.3	The effect of molecular weight on cell viability	51
3.2.7	Characterisation of LMW HA coating	53
3.2.8	The effect of LMW HA on cell viability and attachment	53
3.3	Modification of HA to enable UV photo-crosslinking	57
3.3.1	Thiolation of HA	57
3.3.2	Methacrylation of HA	57
3.3.3	Chemical characterisation of modified HA	58
3.3.3.1	ATR- FTIR analysis of modified HA	58
3.3.3.2	NMR analysis of modified HA	58
3.3.3.3	Ellmans assay for the quantification of thiols	58
3.3.3.4	Reverse Phase High Performance Liquid Chromatography (RP-HPLC)	59
3.3.4	Biological characterisation of modified HA	60
3.3.4.1	Plate coating	60
3.3.4.2	Resazurin Reduction Assay	60
3.3.4.3	Neutral Red Uptake Assay	60
3.3.4.4	Hyaluronidase degradation of modified HA	61
3.4	UV Photo-crosslinking of modified HA	62
3.4.1	Thiolated HA Hydrogels	62
3.4.2	PEGDMA Hydrogels	62
3.4.3	PEGDHA-MA: HA Hydrogels	62
3.4.4	Methacrylated HA Hydrogels	63
3.4.5	Hybrid Hydrogel System	63
3.4.6	Chemical Characterisation of UV photo-crosslinked hydrogels	63
3.4.6.1	ATR- FTIR analysis UV photo-crosslinked hydrogels	63
3.4.7	Mechanical Characterisation of UV Photo-crosslinked hydrogels	64
3.4.7.1	Swelling Study and Gel Fraction	64
3.4.7.2	Rheology	64
3.4.7.3	Compression	65
3.4.8	Biological Characterisation of UV Photo-crosslinked hydrogels	65
3.4.8.1	Cytocompatibility of UV Photo-crosslinked hydrogels	65
3.4.8.2	Degradation of UV Photo-crosslinked hydrogels	66
2.7.1.1.1	In vitro degradation	66

2.7.1.1.2	Accelerated degradation study	66
3.5	Stereolithography 3D printing of Hyaluronic Acid hydrogels	67
3.5.1	Formlabs 2 SLA printer	67
3.5.2	Identification of optimal photoinitiator	67
3.5.3	3D printing of hydrogel samples	67
3.5.4	Chemical characterisation of 3D printed samples	68
3.5.4.1	ATR-FTIR analysis of 3D printed samples	68
3.5.5	Mechanical testing of 3D printed samples	69
3.5.5.1	Swelling study and Gel fraction	69
3.5.5.2	Rheology	69
3.5.5.3	Compression	70
3.5.6	Biological testing of 3D printed samples	70
3.5.6.1	Cytocompatibility testing of 3D printed samples	70
3.5.6.2	Degradation of 3D printed samples	71
2.7.1.1.3	In vitro degradation	71
2.7.1.1.4	Accelerated degradation study	71
3.6	Identification and incorporation of neurotrophic compounds	72
3.6.1	Selection of drug candidates	72
3.6.2	Bioactivity of neurotrophic compounds	72
3.6.2.1	Resazurin reduction assay of neurotrophic compounds	72
3.6.2.2	BrdU assay	73
3.7	Tyrosol Drug Delivery	75
3.7.1	Tyrosol loaded hydrogels	75
3.7.2	Tyrosol loaded 3D printed samples	76
3.7.3	UV spectroscopy analysis of Tyrosol drug release	77
3.7.4	RP-HPLC analysis of Tyrosol drug release	77
3.8	ISO Standards	78
3.9	Data Management and Statistical Analysis	79
Chapter 4. Investigation into the effect of molecular weight on the bioactivity/ Cytotoxicity of hyaluronic acid in neuronal and glial cell lines		79
4.1	Preface	80
4.2	Results	81
4.2.1	Cell Characterisation assay	81
4.2.2	The use of PDL coating enhances HA cytocompatibility testing	83
4.2.3	Validation of HA plate coating by Alcian Blue	85

4.2.4	The effect of molecular weight on the cytocompatibility of HA	88
4.2.5	Investigation of low molecular weight HA via the MTT Cell Viability Assay	97
4.2.6	Evaluation of the effect of low molecular weight HA via the Resazurin Cell Viability Assay	99
4.2.7	Investigation into the effect of mechanical disruption in the evaluation of HA cytocompatibility in neuronal and glial cell lines using the resazurin reduction assay	101
4.3	Discussion	111
Chapter 5.	Modification of hyaluronic acid to enable UV photo-crosslinking	120
5.1	Preface	121
5.2	Results	123
5.2.1	Thiolation of HA	123
5.2.1.1	¹ H-NMR analysis of HA-SH	124
5.2.1.2	Ellmans assay of HA-SH	125
5.2.2	Methacrylation of HA	127
5.2.2.1	FTIR of HA-MA	128
5.2.2.2	H ¹ NMR analysis of methacrylated HA	129
5.2.2.3	RP-HPLC of HA-MA	130
5.2.3	Cytocompatibility of HA derivatives	132
5.2.4	The effect of modification on hyaluronidase degradation of HA	135
5.3	Discussion	136
Chapter 6.	UV Photo-crosslinking of HA derivatives	139
6.1	Preface	140
6.2	Results	142
6.2.1	ATR-FTIR of photo-polymerised samples	142
6.2.2	Compression testing of photo-polymerised HA hydrogels	143
6.2.3	Rheological characterisation of HA hydrogels	145
6.2.4	Swelling studies of HA hydrogels	149
6.2.5	Degradation of HA Hydrogels	152
6.3	Discussion	154
Chapter 7.	Hybrid hydrogel formulation with tailored degradation profile	154
7.1	Preface	155
7.2	Results	156
7.2.1	ATR-FTIR of PEGDMA and PEGDMA hybrid samples	156
7.2.2	Compression testing	158

7.2.3	Rheology	159
7.2.4	Swelling Studies	162
7.2.5	Degradation of hybrid hydrogels	165
7.2.6	Cytocompatibility testing of hybrid hydrogels	171
7.3	Discussion	174
Chapter 8. Stereolithography 3D printing		174
8.1	Preface	175
8.2	Results	176
8.2.1	ATR-FTIR of 3D printed samples	176
8.2.2	Compression testing of 3D printed samples	177
8.2.3	Rheological characterisation of 3D printed samples	178
8.2.4	Swelling studies	181
8.2.5	Degradation testing of 3D printed samples	182
8.2.6	Cytotoxicity testing of 3D printed samples	187
8.3	Discussion	192
Chapter 9. Neurotrophic compounds for peripheral nerve repair		194
9.1	Preface	195
9.2	Results	196
9.2.1	Initial efficacy screening of potential neurotrophic compounds	196
9.2.2	Proliferative effect of Tyrosol in neuronal and glial cell lines	198
9.2.3	Tyrosol drug dissolution: UV Spectroscopy	200
9.2.3.1	Tyrosol drug loaded samples	201
9.2.4	Tyrosol Drug Dissolution: RP-HPLC	203
9.2.4.1	Detection of tyrosol from 3D prints and hydrogels: RP-HPLC	204
9.2.5	Tyrosol elution from 3D printed formulations	206
9.3	Discussion	209
Chapter 10. Conclusions and Future considerations		206
Chapter 11. References		211
Appendix 1. Journal Publications		i
Appendix 2. Conference Abstracts		vi
Appendix 3. Poster Presentations		ix
Appendix 4. Additional Data		xv

LIST OF TABLES

Table 1. Mechanisms of peripheral nerve injuries and predisposing factors	16
Table 2. Classification of peripheral nerve injuries.....	18
Table 3. FDA approved NGCs available on the market.....	26
Table 4. Molecular weights of endogenous HA and its location in the body.	29
Table 5. Cell Culture Media Composition	48
Table 6. Preparation of Cysteamine Standards.....	59
Table 7. Sample preparation for SLA 3D printing	68
Table 8. Neurotrophic compound concentration in treatment media	73
Table 9. Tyrosol loaded hydrogels	75
Table 10. Tyrosol loaded 3D printed samples	76
Table 11. Polymer ratios for HA hydrogels	140

LIST OF FIGURES

Figure 1. Bands of Bungner.....	2
Figure 2. Comparison of Peripheral Nervous System and Central Nervous System	12
Figure 3. Structure of a peripheral nerve, highlighting the epineurium, perineurium and endoneurium.	13
Figure 4. Anatomy of a peripheral motor nerve..	14
Figure 5. Illustration of the 4 major plexuses of the peripheral nervous system.....	15
Figure 6. Proximal and distal stumps of an injured nerve. Image highlighting the proximal and distal portions of an injured nerve.	19
Figure 7. Epineural and grouped fascicle repair.....	22
Figure 8. Structure of a disaccharide of Hyaluronic acid.	27
Figure 9. Molecular weight dependent applications and biological functions of HA.	30
Figure 10. Overview of HA in intercellular signalling.....	31
Figure 11. Microbial synthesis of HA in Streptococcus species.	33
Figure 12. Animal synthesis of HA	34
Figure 13. Conjugation and crosslinking of HA. Different modification routes for the HA chain include conjugation and crosslinking.....	37
Figure 14. Typical reaction scheme for amidation of HA.	39

Figure 15. Structure of the melatonin molecule.	42
Figure 16. Structure of the Tyrosol molecule.	43
Figure 17. Investigation of MTT attachment assay using parallel TBE assay.	56
Figure 18. Investigation of Resazurin attachment assay using parallel TBE assay.	56
Figure 19. Determination of optimal seeding density in glial and neuronal cell lines for <i>in vitro</i> assay development	82
Figure 20. PDL does not significantly impact the viability of neuronal and glial cell lines.....	83
Figure 21. PDL improves the retention of HA in coated cell culture plates.	86
Figure 22. PDL enhances the homogeneity of HA coatings in tissue culture plates.....	87
Figure 23. 30-50 kDa HA gives optimal cell culture plate coatings for <i>in vitro</i> cell coatings.....	88
Figure 24. Qualitative visual analysis of HA: PDL coatings from 30 to 2200 kDa.	89
Figure 25. Increases in molecular weight corresponded to decreases in the resorufin intensity of SH-SY5Y cells.	90
Figure 26. The number of unattached neuronal cells increases proportionally to concentration and MW.	91
Figure 27. Increases in molecular weight corresponded to decreases in the resorufin intensity in RT4 D6P2T cells.	92
Figure 28. Glial cell detachment increases proportionally to concentration and MW.....	94
Figure 29. The viscosity of HA increases proportionally to MW..	95
Figure 30. The MTT assay detected what appeared to be significant cytotoxicity in neuronal and glial cells exposed to 30-50 kDa HA.....	98
Figure 31. The resazurin assay did not reveal significant toxicity in neuronal cells exposed to 30-50 kDa HA..	99
Figure 32. The resazurin reduction assay did not reveal significant toxicity in glial cells exposed to 30-50 kDa HA.	100
Figure 33. The potent cytotoxicity detected by MTT could not be detected via the resazurin reduction assay.	102
Figure 34. Overestimation of toxicity by MTT is not solely related to mechanical disruption of neuronal cells.	105
Figure 35. Dose-dependent effect of 30-50 kDa HA in neuronal and glial cells at count 1 (20 hour exposure to HA).....	107

Figure 36. MTT significantly increases the detachment of neuronal cells in the presence of HA at count 2 (24 h exposure to HA).....	109
Figure 37. MTT enhances HA toxicity in neuronal cells.	110
Figure 38. Amidation reaction for the production of cysteamine modified HA.	121
Figure 39. ¹ H-NMR spectrum of HA-SH.....	124
Figure 40. Absorption spectrum for Ellmans reagent from 300-700 nm.	125
Figure 41. Ellmans assay for total thiol determination.....	126
Figure 42. FTIR comparison of HA, HA-SH and HA-MA.....	128
Figure 43. ¹ H-NMR analysis of HA-MA..	129
Figure 44. Quantification of MoD of HA-MA.....	130
Figure 45. Cytocompatibility of HA and HA derivatives in neuronal cells..	133
Figure 46. Cytocompatibility of HA and HA derivatives in glial cells.....	134
Figure 47. Modification of HA with thiol accelerates hyaluronidase degradation..	135
Figure 48. Scheme showing the UV photo-crosslinking of HA derivatives to form a HA hydrogel.....	141
Figure 49. ATR-FTIR of UV photo-crosslinked HA hydrogel samples.	142
Figure 50. The compressive strength of HA hydrogels decreases proportional to SH concentration.	143
Figure 51. Rheology of HA-MA.	146
Figure 52. Rheology of HA-MA: HA-SH.	147
Figure 53. Comparison of the swelling characteristics of HA-MA hydrogels with increasing thiol concentration.....	150
Figure 54. Degradation of HA derivative hydrogels.	152
Figure 55. HA Hydrogel Degradation.	153
Figure 56. ATR-FTIR of PEGDMA, 50% PEGDMA: HA-SH and 50% PEGDMA: HA-MA with key peaks noted.....	156
Figure 57. FTIR spectrum of the hybrid blend hydrogel.....	157
Figure 58. The poor compressive strength associated with inclusion of thiol was mitigated insignificantly by addition of 10% PEGDMA in the hybrid blend hydrogel..	158
Figure 59. Rheological analysis of PEGDMA in deionised water hydrogels	160
Figure 60. Rheological comparison between 50 HA-SH: PEGDMA, 50 HA-MA: PEGDMA and hybrid blend hydrogels.	161
Figure 61. Mean swelling ratio and Gel fraction of PEGDMA in water hydrogel samples..	162

Figure 62. Mean swelling ratio and Gel fraction of HA-SH: PEGDMA hydrogel samples.	163
Figure 63. Mean swelling ratio and Gel fraction of HA-MA: PEGDMA hydrogel samples..	163
Figure 64. Mean swelling ratio and Gel fraction of the hybrid blend hydrogel sample vs the other hydrogel formulations	164
Figure 65. <i>In vitro</i> degradation of hybrid blend hydrogels compared with 100 %wv PEGDMA, 50 %wv PEGDMA: HA-MA and 50 %wv PEGDMA: HA-HA-MA: HA-SH.....	165
Figure 66. Accelerated (5 mM NaOH) degradation of hybrid blend hydrogels compared with 100 %wv PEGDMA, 50 %wv PEGDMA: HA-MA and 50 %wv PEGDMA: HA-HA-MA: HA-SH..	166
Figure 67. Accelerated (5 M NaOH) degradation of hybrid blend hydrogels compared with 100 %wv PEGDMA, 50 %wv PEGDMA: HA-MA and 50 %wv PEGDMA: HA-HA-MA: HA-SH.....	166
Figure 68. <i>In vitro</i> (PBS pH 7.4), 5 mM NaOH and 5 M NaOH degradation samples of 100 %wv PEGDMA on day 1 vs day 7.....	167
Figure 69. <i>In vitro</i> (PBS pH 7.4), 5 mM NaOH and 5 M NaOH degradation samples of 50 %wv PEGDMA: HA-MA on day 1 vs day 7..	168
Figure 70. <i>In vitro</i> (PBS pH 7.4), 5 mM NaOH and 5 M NaOH degradation samples of 50 %wv PEGDMA: HA-SH on day 1 vs day 7.....	168
Figure 71. <i>In vitro</i> (PBS pH 7.4), 5 mM NaOH and 5 M NaOH degradation samples of hybrid hydrogels on day 1 vs day 7.....	169
Figure 72. UV cured hydrogels induced significant toxicity in direct contact testing of neuronal and glial cell lines.....	172
Figure 73. Elution assay of hydrogels in neuronal and glial cell lines.....	173
Figure 74. ATR-FTIR of stereolithography 3D printed samples with key peaks highlighted.....	176
Figure 75. Compressive strength and Young's modulus of 3D printed samples	177
Figure 76. Rheological characterisation of 3D printed samples. (a) Amplitude, (b) Frequency and (c) temperature ramp.....	179
Figure 77. Rheological characterisation of 3D printed samples.....	180
Figure 78. Mean swelling ratio and Gel fraction of 3D printed samples..	181

Figure 79. <i>In vitro</i> degradation (pH 7.4) of hybrid blend 3D prints compared with 100 %wv PEGDMA, 50 %wv PEGDMA: HA-MA and 50 %wv PEGDMA: HA-SH.	182
Figure 80. Accelerated (5 mM NaOH) degradation of hybrid blend 3D prints compared with 100 %wv PEGDMA, 50 %wv PEGDMA: HA-MA and 50 %wv PEGDMA: HA-SH.	183
Figure 81. Accelerated (5 M NaOH) degradation of hybrid blend 3D prints compared with 100 %wv PEGDMA, 50 %wv PEGDMA: HA-MA and 50 %wv PEGDMA: HA-SH	184
Figure 82. 100 %wv PEGDMA samples on day 1 and day 7 of the degradation study....	185
Figure 83. 50 %wv PEGDMA: HA-MA samples on day 1 and day 7 of the degradation study..	185
Figure 84. 50 %wv PEGDMA: HA-SH samples on day 1 and day 7 of the degradation study.	186
Figure 85. Hybrid blend 3D printed samples on day 1 and day 7 of the degradation study.	186
Figure 86. Resazurin reduction assay of 3D print leachates in neuronal cells without residual TPO removal.....	188
Figure 87. Resazurin reduction assay of 3D print leachates in neuronal cells without residual TPO removal.....	189
Figure 88. Resazurin reduction assay of 3D print leachates in neuronal cells with residual TPO removal	190
Figure 89. Resazurin reduction assay of 3D print leachates in glial cells with residual TPO removal.....	191
Figure 90. Tyrosol increased the resorufin intensity observed for neuronal cells.....	196
Figure 91. Tyrosol increased the resorufin intensity observed in glial cells in a dose dependent manner.....	197
Figure 92. 1000 nm Tyrosol increases glial cell proliferation.....	198
Figure 93. Standard curve of tyrosol standards in PBS. Standard curve of Tyrosol Abs @ 280 nm vs Tyrosol conc (mM).	200
Figure 94. Cumulative tyrosol drug release from hydrogel samples.....	201
Figure 95. Cumulative tyrosol drug release from 3D printed samples.....	202
Figure 96. Standard curve of tyrosol standards for RP-HPLC.....	203
Figure 97. Interpolated values for the concentration of tyrosol in hydrogel (HG) and 3D printed (3D) samples..	204

Figure 98. Cumulative release profile for tyrosol from different polymer constructs as determined by RP-HPLC.....	205
Figure 99. Elution assay of tyrosol loaded (1 mM) 3D prints in neuronal cells.	207
Figure 100. Elution assay of tyrosol loaded (1 mM) 3D prints in glial cells..	208
Figure 101. MTT assay of glial cells exposed to 8-50 kDa HA of various concentrations.....	xv
Figure 102. MTT assay of neuronal cells exposed to 8-50 kDa HA of various concentrations.....	xvi
Figure 103. MTT assay of glial cells exposed to 30-50 kDa HA of various concentrations.....	xvii
Figure 104. MTT assay of neuronal cells exposed to 30-50 kDa HA of various concentrations.....	xviii
Figure 105. MTT assay of neuronal cells comparing coating times..	xix
Figure 106. MTT assay of neuronal cells after exposure to HA coating with a dry step vs no dry step..	xx
Figure 107. ¹³ C NMR of HA-SH.....	xxi
Figure 108. HH-CoSy NMR of HA-SH	xxi
Figure 109. HMBC NMR of HA-SH	xxii
Figure 110. HSQC NMR of HA-SH	xxiii
Figure 111. DEPT-90 scan of HA-MA	xxiii
Figure 112. HH-CoSy NMR of HA-MA.....	xxiv
Figure 113. HSQC NMR of HA-MA	xxiv

LIST OF ABBREVIATIONS

Hyaluronic Acid	HA
Peripheral nervous system	PNS
Peripheral Nerve Injury	PNI
Poly-D-Lysine	PDL
Kilodalton	kDa

Central nervous system	CNS
Poly (ethylene glycol) dimethacrylate	PEGDMA
Dorsal Root Ganglion	DRG
Ultra Violet	UV
Extracellular Matrix	ECM
Megadalton	MDa
Attenuated Total Reflectance Fourier Transform Infrared Spectroscopy	ATR-FTIR
Stereolithography	SLA
Research Question	RQ
N-Acetyl Cysteine	NAC
Three Dimensional	3D
Bromodeoxyuridine	BrdU
International Organisation for Standardisation	ISO
3-[4,5-dimethylthiazol-2-yl]-2,5 diphenyl tetrazolium bromide	MTT
Synaptophysin	SYN
Growth associated protein	GAP-43
Glial fibrillary acidic protein	GFAP
Tyrosine Hydroxylase	TH
N-Ethyl-N-nitrosourea	ENU
Monoclonal Antibody	mAB
Horse Radish Peroxidase	HRP
Room Temperature	R.T.
High Performance Liquid Chromatography	HPLC

Reverse-phase HPLC

RP-HPLC

Hydrogel

HG

3D print

3D

CHAPTER 1. INTRODUCTION

1.1 THESIS OUTLINE

This thesis is structured to provide a comprehensive understanding of the research project, starting with an introductory chapter that summarises the context and methods employed throughout. This introductory chapter is organized into five subsections, with the intent of offering a clear overview of the project's aims, objectives, and methodology. Subsequent to the introduction, a thorough literature review is presented, which not only encompasses relevant literature, but also critically evaluates the existing body of work in this area. Following the literature review, the materials and methods section delves into the specific techniques and methodologies utilized to achieve the research objectives. In each subsequent chapter, the results of the implemented methods are exhibited, accompanied by a concise paragraph that enables readers to effortlessly interpret the findings within the appropriate context. Each chapter also features a tailored discussion that elaborates on the results in relation to the corresponding work-package. The final chapter, encompassing conclusions and future work, synthesizes the work-package outcomes within a broader context. It provides an interpretation of the results in light of the existing literature and potential future implications, before outlining directions for subsequent research.

1.2 CONTEXT

Peripheral nerve injuries are the most common type of injury to the nervous system and can occur due to illness, malignancy or trauma. It is reported that within the United States, twenty million people currently suffer from peripheral nerve injuries whereas in Europe, there are over 300,000 cases recorded each year (Houshyar et al., 2019). In actuality, the amount is likely to be substantially higher because medical attention is often sought only for moderate to severe injuries. These injuries often result in permanent impairment to muscle function with reduced or no sensation in the affected area.

The peripheral nervous system is made up of thousands of individual nerve fibres called axons which may be myelinated or non-myelinated via Schwann cells. These nerve cells carry signals from the central nervous system (brain and spine) to the limbs of the body. Injury or transection to one of these nerves, results in a reduction of loss of movement and sensation in the affected portion of the body. Following transection of a nerve, a process known as Wallerian degeneration ensues in which regenerating axons are generated toward the distal stump. As the new axon is generated at the proximal stump, Schwann cells

accelerate the degeneration at the distal stump which results in a morphological change in the nerve gap, known as bands of Büngner which are illustrated by Figure 1 below (Panzer et al., 2020).

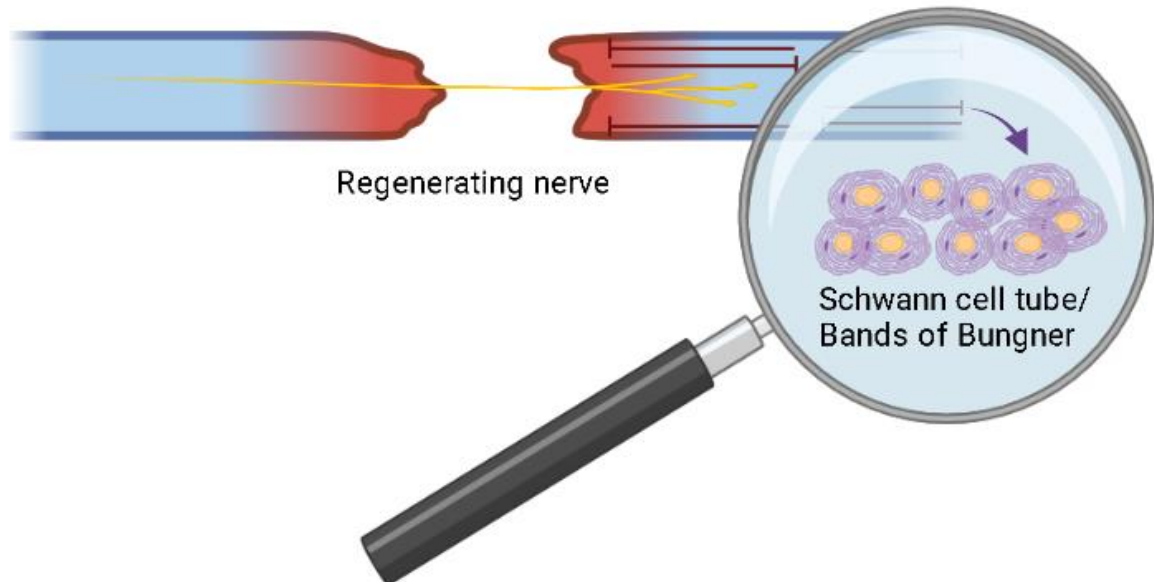


Figure 1. Bands of Bungner (C. Buckley, 2023). Bands of Bungner consist of longitudinally aligned pro-regenerative Schwann cells in a “Schwann cell tube” which serves to guide regenerating axons toward the distal stump.

These bands enable the directing of regenerating axons toward the distal stump. If these regenerating axons reach the distal stump within a favourable amount of time, functional recovery is possible. If not, denervation of Schwann cells occurs and results in the slowing of axonal growth. Therefore, timing is crucial in the event of a peripheral nerve injury. Even in the event of immediate surgical intervention to repair the affected nerve, it is unpredictable as to whether the patient will develop neuropathic pain (Leckenby et al., 2020).

Although peripheral nerves have the ability to regenerate on their own, time constraints, the length of the nerve gap, and the patient's age imply that this regeneration is generally insufficient to accomplish functional recovery, that is, full restoration of movement and feeling in the afflicted area (Vijayavenkataraman, 2020). This is why the advent of surgical procedures to repair the injury site with procedures such as neurorrhaphy came in the 1960s. Current therapeutic options for the treatment of peripheral nerve injuries can be divided

among two categories: surgical and non-surgical. Non-surgical techniques such as electrical stimulation are often chosen, but their success rate has yet to be thoroughly confirmed. As such, only surgical options will be discussed in this section.

Surgical methods are the most commonly utilised treatment for peripheral nerve injuries and the method chosen depends primarily on the length of the nerve gap. For short nerve gap (<1cm) direct end-to-end suturing (neurorrhaphy) is often employed, but in the event of a longer nerve gap this method would lead to excess tension resulting in poor outcome. Similarly, fibrin glue has been used in the same manner as suturing and has produced similar results to suturing but limited human trials have been conducted to date (Masgutov et al., 2019).

The most commonly employed surgical method for medium to large nerve gap is nerve grafting, namely allograft, nerve transfer and autograft (Contreras *et al.*, 2023). Autografts consist of transplanting a healthy nerve from one area of the body to an injured area of the same body, whereas allografts involve the transplanting of a donor nerve from a different body, usually a cadaver. Autografts are considered the gold standard in therapeutic options for peripheral nerve repair and for this reason, only autografts will be discussed in this section, the other techniques are discussed in detail in chapter 2. Autografts, or autogenous nerve grafting, refers to the transplantation of a donor nerve such as the sural nerve to the affected site within the same body. This method has boasted the highest success rate of all afore mentioned techniques. As the donor nerve is from the same body as the affected site, immunological issues are negated and no immune suppressing drugs are required, unlike other techniques such as allografts. However, the donor nerve is most often a fully functioning sensory nerve used to replace a damaged nerve, resulting in sensory loss at the donor site. In addition to this, scarring at the donor site and the formation of a neuroma are common disadvantages seen with this method. A neuroma is a non-cancerous growth of nerves which can occur anywhere in the body and typically causes pain and burning sensations. Perhaps the biggest disadvantage after donor site morbidity however, is the lack of supply of donor nerves as there are very few expendable sensory nerves in the human body (Katiyar et al., 2020). To overcome the many disadvantages of autografts, while still attempting to maintain or surpass the efficacy of such techniques, nerve guidance conduits were created.

Tissue engineering is a relatively recent concept, with the first mention of the term being traced back to a proposal of a research centre, submitted by Y.C. Fung in 1985, and named “Center for the Engineering of Living Tissues”. This proposal was refused at the time by the National Science Foundation (Wang & Yang, 2019). Nerve guidance conduits are tissue engineering structures consisting of biopolymers, natural or synthetic or a combination of the two. They are designed to provide the necessary biological, mechanical and sometimes electrical cues necessary to initiate nerve regeneration. In doing so, the limitations posed by the aforementioned technologies are overcome such as donor site morbidity and supply issues. Conduits work by bridging the gap providing directionality as well as the necessary cues to align the regenerating axon toward the distal stump, thus speeding up the process and reducing the possibility of Schwann cell denervation. Compounds can also be used to further support or enhance the regeneration of axons.

The properties of an ideal conduit include but are not limited to, a biomimetic architecture, structures which serve to align axons, sufficient mechanical support and permeability, conductivity, flexibility and the ability to biodegrade within an acceptable length of time without the production of harmful degradation products. Despite many conduits having made it to market such as Axogen™, no conduit possesses all of the necessary qualities to be considered “ideal” and to surpass the efficacy of autografts (Mauch et al., 2019). In order to optimise the biological and mechanical properties of a conduit, the choice of biomaterial is crucial. For this reason, hyaluronic acid (HA) was selected as the primary biomaterial for the construction of a nerve guidance conduit.

HA is a structurally simple glycosaminoglycan consisting of two sugars, (1→4)-β linked D-Glucuronic and (1→3)-β linked N-acetyl-D-Glucosamine, which alternate throughout a linear chain and offer alternating hydrophobic and hydrophilic disaccharide faces, thus producing an amphiphilic ribbon like structure (Delfi *et al.*, 2021). A major component of the extracellular matrix (ECM), HA, a viscous polymer, is extruded as it is synthesized and exists in the body in various molecular weights ranging from 10^3 (serum) to 10^7 Da (eye vitreous humor) (Snetkov et al., 2020). Many proteoglycans such as aggrecan interact with HA resulting in molecular complexes which occupy a large volume and are responsible for the gel state of the matrix and the stabilisation of the structure of the ECM (Abatangelo et al., 2020). Additionally, HA has the ability to form a pericellular coat around cells, functioning as a signalling molecule interacting with its binding proteins and regulating cell adhesion, migration and proliferation. HA is an endogenous polymer and is naturally

degraded in the body by endogenous hyaluronidases and excreted. This feature makes it a polymer that is frequently employed in the cosmetics and aesthetics industry. Due to its viscoelastic properties, physiological activity and biocompatibility of the polymer, HA is an ideal candidate for a nerve guidance conduit. However, it is this ease in biodegradation which limits the applications of native HA. Modification of the polysaccharide can provide resistance to enzymatic degradation while also providing the necessary architecture for cross-linking and conjugation.

1.3 RESEARCH QUESTIONS

The successful production and consequent safety and efficacy testing of a HA nerve guidance conduit would have a number of significant impacts in biomedical and tissue engineering research. Most notably, patient recovery from peripheral nerve injuries would be significantly improved. Additionally, it provides the base research in utilising low-medium molecular weight HA in peripheral nerve repair, a concept not previously explored. This thesis aspired to create a HA only conduit, through UV photo-crosslinking of thiolated and methacrylated HA. This type of thiolene reaction is highly selective and resistant to water and oxygen. The aim of this thesis was to develop a novel formulation to enable stereolithography 3D printing of hyaluronic acid hydrogel nerve conduits. To that effect, the key research question of this thesis was:

Q. Can a 3D printed hydrogel nerve guidance conduit be fabricated from hyaluronic acid which is inherently bioactive?

The core research question can be broken into five sub-questions and thus, five key workpackages. These sub-questions are as follows:

RQ1. Does low molecular weight HA induce changes in the metabolic activity of neuronal or glial cell lines?

RQ2. What effect, if any, does modification have on the biological and physicochemical effects of HA?

RQ3. Can modification and UV photo-crosslinking be efficiently optimised to produce a hydrogel with a sufficient degree of cross-linking?

RQ4. Can this formulation be optimised to enable stereolithographic (SLA) 3D printing?

RQ5. Can a neurotrophic compound be identified which could be added to the polymer matrix to improve the bioefficacy of the conduit formulation for 3D printing?

Initially, various molecular weights of hyaluronic acid were screened for cytocompatibility. Once the optimal molecular weight was selected, this polymer was modified to introduce thiol and methacrylate groups to separate disaccharides to enable photo-crosslinking. Following confirmation and classification of the modified hyaluronic acid, UV photo-crosslinked hydrogels were produced and characterised in terms of their physicochemical and biological characteristics. This formulation was optimised to improve mechanical performance and this hybrid formulation was then 3D printed. The produced 3D prints were extensively characterised. Finally, potential neurotrophic compounds were screened for inclusion in the conduit and the lead compound, tyrosol, was selected for inclusion and therefore tested extensively in hydrogel and 3D printed sample format.

1.4 RESEARCH AIM

Since the emergence of a paper entitled “Hyaluronic acid enhances peripheral nerve regeneration *in vivo*” (Wang *et al.*, 1998), there has been increasing interest in the use of HA for peripheral nerve repair. However, much of the research to date has focused on high molecular weight HA. This has left quite a significant gap in the knowledge regarding low molecular weight HA and the properties that can be exploited in this less viscous, easier to manipulate form of HA. It is important, not only in the context of patient care but also to discover the advantages and limitations in the use of low molecular weight HA so that further research can be carried out in this area. Additionally, traditional modification and analysis procedures are laborious and cannot be carried out safely without degradation of the endogenous polymer, thus this project aims to produce a streamlined method for the reproducible production of thiolated and methacrylated HA for 3D printing.

1.5 RESEARCH OBJECTIVES

In an effort to answer the research questions and aim mentioned previously, the research compiled below sought to:

1. Establish the effect of low-medium molecular weight HA in neuronal and glial cell lines through a series of bioassay techniques

2. Obtain baseline biological and chemical responses of HA using traditional instruments and compare against their modified counterparts to establish a modification procedure which can provide the desired characteristics
3. Optimise the cross-linking efficacy of HA through various optimisations of photo initiators, polymer ratios and additives
4. Develop a formulation suitable for stereolithography 3D printing of HA
5. Elucidate potential regenerative properties of a variety of compounds for inclusion in the conduit

1.6 JUSTIFICATION

The overall goal of this research was to enable UV photo-crosslinking of HA to allow for a greater range of uses in bioengineering. This cross-linking would facilitate a tailoring of the properties of the engineered structure based on monomer concentration. Additionally, the mechanical strength of the structure could be altered in similar manner. This research is necessary due to the lack of an ideal therapy for peripheral nerve injuries and the lack of multidisciplinary research in this area.

1.7 CONTRIBUTION TO EXISTING KNOWLEDGE

Dissemination of research and knowledge contributions can be found in Appendix 1 and Appendix 2, however, a summary of the contribution to knowledge that has been made by this research can be found below:

Journal Publications

- **Buckley, Ciara,** Murphy, Emma J., Montgomery, Therese R., Major, Ian (2022) ‘Hyaluronic Acid: A Review of the Drug Delivery Capabilities of This Naturally Occurring Polysaccharide’, *Polymers*, 14(17), p. 3442. Available at: <https://doi.org/10.3390/polym14173442>. (*Impact Factor 4.967*)
- Buckley, J. *et al.* (2022) ‘An assessment of the transparency of contemporary technology education research employing interview-based methodologies’, *International Journal of Technology and Design Education*, 32(4), pp. 1963–1982. Available at: <https://doi.org/10.1007/s10798-021-09695-1>. (*Impact factor 2.209*)

- Murphy, E.J. et al. (2023) ‘Polysaccharides—Naturally Occurring Immune Modulators’, *Polymers*, 15(10), p. 2373. Available at: <https://doi.org/10.3390/polym15102373>. (*Impact Factor 4.967*)
- Buckley, C. et al. (2023) ‘Modification of hyaluronic acid to enable click chemistry photo-crosslinking of hydrogels with tailorable degradation profiles’, *International Journal of Biological Macromolecules*, 240, p. 124459. Available at: <https://doi.org/10.1016/j.ijbiomac.2023.124459>. (*Impact Factor: 8.025*)
- Buckley, J. et al. (2023) ‘How transparent are quantitative studies in contemporary technology education research? Instrument development and analysis’, *International Journal of Technology and Design Education* [Preprint]. Available at: <https://doi.org/10.1007/s10798-023-09827-9>.

Presentations

September 2018

Buckley, C; Major, I; Montgomery, T.R; 2018. Investigation of the bioactivity of hyaluronic acid (HA) vs. hot melt extruded HA in neuronal and Schwann cell lines. SURE Network undergraduate conference. Athlone: SURE Network.

March 2021

Buckley, C; Major, I; Montgomery, T.R; Biomaterials that heal: Hyaluronic acid for peripheral nerve repair, *AIT 3MT competition 2021* (Winner of both the popular vote and judges vote in the final)

May 2021

Buckley, C; Major, I; Montgomery, T.R; Biomaterials for peripheral nerve repair: The effect of low molecular weight hyaluronic acid on neuronal and glial cell lines, *Shannon Region Postgraduate Research Conference*.

October 2021

Buckley, C; Major, I; Montgomery, T.R; A day in the life of a postgraduate student, *SURE Network undergraduate conference- Postgraduate Panel*, Galway- Mayo institute of technology, online.

October 2021

Buckley, C; Major, I; Montgomery, T.R.; SURE alumni video interview

Posters

April 2019

Buckley, C; Major, I; Montgomery, T.R.; The modification of hyaluronic acid (HA) with n-acetyl cysteine (NAC) to enable 3D printing of a robust nerve guidance conduit for peripheral nerve repair, BNA Festival of Neuroscience 2019.(Conference proceedings 2019). *Brain and Neuroscience Advances*, 3, p.239821281985549. DOI: <https://doi.org/10.1177%2F2398212819855490>

May 2019

Buckley, C; Major, I; Montgomery, T.R.; ‘The effect of low molecular weight hyaluronic acid on neuronal and glial cell lines’, AIT Research Seminar 2019.

November 2019

Buckley, C; Major, I; Montgomery, T.R.; ‘The modification of hyaluronic acid with N-acetyl cysteine for stereolithography 3D printing of hydrogel nerve conduits’, *AIT Research Seminar 2019*.

June 2020

Buckley, C; Major, I; Montgomery, T.R.; ‘Modification of hyaluronic acid for stereolithography 3D printing of hydrogel nerve conduits’, *AIT Research Seminar 2020*. (Winner of best poster in biosciences and best poster overall)

April 2021

Buckley, C; Major, I; Montgomery, T.R.; ‘Modification of hyaluronic acid for stereolithography 3D printing of hydrogel nerve conduits’. ‘BNA 2021 Festival of Neuroscience Poster abstracts’ (2021) *Brain and Neuroscience Advances*, 5, p. 23982128211035064. doi:[10.1177/23982128211035062](https://doi.org/10.1177/23982128211035062).

September 2021

Buckley, C., Major, I. and Montgomery, T.R. (2021) ‘A cautionary note on the utility of MTT in toxicity screening’, *Toxicology Letters*, 350, p. S108. Available at: [https://doi.org/10.1016/S0378-4274\(21\)00500-2](https://doi.org/10.1016/S0378-4274(21)00500-2).

July 2022

Buckley, C., Major, I. and Montgomery, T.R (2022) 'A novel hyaluronic acid based hydrogel for the enhancement of peripheral nerve regeneration', *Federation of European Neuroscience Societies (FENS) Forum 2022*.

CHAPTER 2. LITERATURE REVIEW

In this section of the thesis, a review of the relevant literature was conducted to define the context of the research in terms of background and current state of the art, as well as to identify the research gap. Furthermore, this review takes an in-depth view of the materials and processes used throughout this thesis. In order to do this, the background and context was discussed in terms of the peripheral nervous system, disorders of the peripheral nervous system, cell types of the peripheral nervous system and the translation of these into bench models and current therapeutic options. Having established the pitfalls of current therapies, the use of biological and inert materials in peripheral nerve regeneration is discussed in depth. And finally, fabrication methods using these polymers are discussed.

2.1 PERIPHERAL NERVOUS SYSTEM

The peripheral nervous system (PNS) is responsible for the transfer of signals between the brain and the limbs and organs of the body, and is composed of all nerves and ganglia which exist outside of the brain and spinal cord as illustrated by Figure 2 below (Varier *et al.*, 2022). Peripheral nerves convey neural signals from the sense organs and sensory receptors in the organism inward to the central nervous system (CNS) and from the CNS outward to the muscles and glands of the body (Mai and Paxinos, 2011).

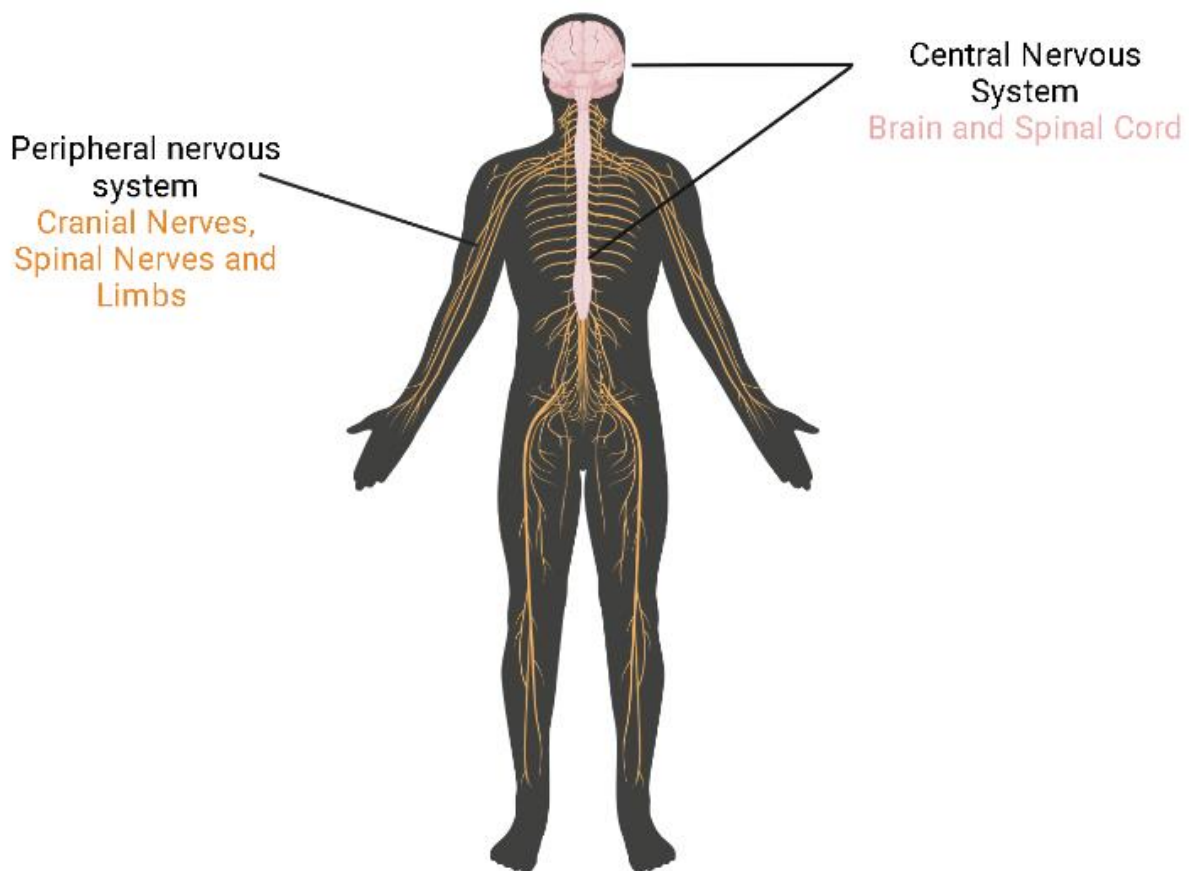


Figure 2. Comparison of Peripheral Nervous System and Central Nervous System (C. Buckley 2023). Image denotes the CNS consisting of the brain and spinal cord in pink. The PNS which consists of cranial and spinal nerves, and the nerves throughout the limbs, is denoted in yellow.

Peripheral nerves consist of nerve fibre bundles and surrounding connective tissue sheaths including blood vessels. The individual nerve fibres and the supporting Schwann cells are

surrounded by a loose connective tissue, the endoneurium. The perineurium is a dense connective tissue which surrounds a fascicle consisting of a bundle of nerve fibres. The epineurium, which is the outermost layer of connective tissue sheaths the entire nerve fascicles (Figure 3).

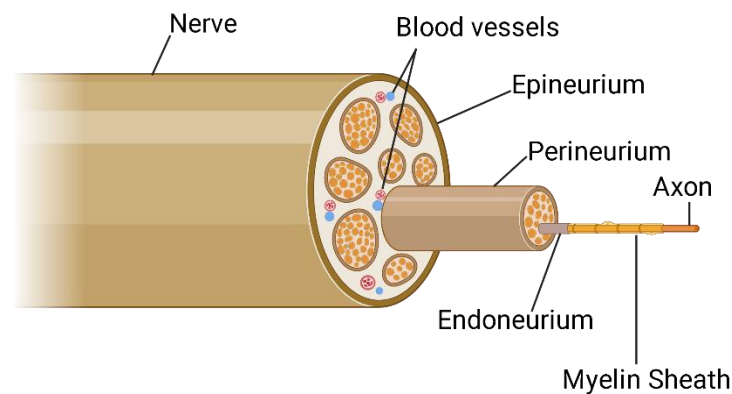


Figure 3. Structure of a peripheral nerve, highlighting the epineurium, perineurium and endoneurium (C. Buckley, 2023).

The CNS consists of the brain and the spinal cord and comprises both grey matter and white matter. Within grey matter is neuronal cell bodies, dendrites, axon terminals, synapses and glial cells. White matter contains bundles of axons, most of which are myelinated, and oligodendrocytes. The nerves which comprise the CNS are very well protected by structures such as the skull and the spinal column. Therefore, injuries to the CNS are much less common than PNS injuries, which is a key factor as to why the CNS mostly lacks the ability to self-regenerate nerves after injury unlike the PNS (Hoda, 2019).

At the core of each nerve is the axon, a thin tube of axoplasm extending from the cell body to the target organ. Axons can be either myelinated or unmyelinated. Unmyelinated axons are partially sheathed by the Schwann cell membrane whereas myelinated axons are

enveloped in compacted spirals of Schwann cell membrane which forms a sheath as illustrated in Figure 4 below. This myelin sheath is composed in segments known as internodes, each one being derived from a single Schwann cell. Between internodes, a small gap of unsheathed axon can be observed. This gap is known as the node of Ranvier, and is vital for the flow of ions necessary for action potential (Bosch-Queralt, Fledrich and Stassart, 2023).

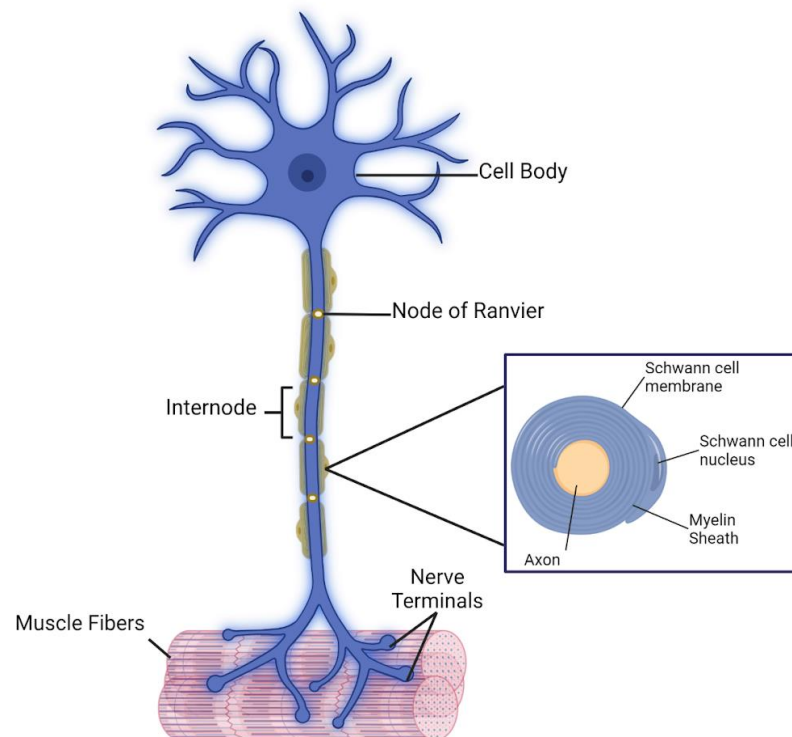


Figure 4. Anatomy of a peripheral motor nerve. Structure showing the extension of a single myelinated axon from the cell body to the target organ, initiating contact at the neuromuscular junction. Internodes are shown with intermittent gaps, or nodes of Ranvier (C. Buckley, 2023).

2.2 INJURIES TO THE PNS

Injuries to the peripheral nervous system may occur due to trauma, illness or malignancy and can result in gaps or erosion within the nerve that ultimately limit or stop function in that specific area. These injuries are reported in 15-40% of all trauma cases worldwide (Dai and Li, 2015) and are commonly associated with chronic pain and contribute largely to the healthcare burden due to difficulty in treatment and economic cost. It is estimated that peripheral nerve injuries (PNI) affect approximately 1 million people across Europe and the US per annum, with only 25% of those who undergo surgery, the gold standard treatment option, regaining full function (Eleftheriadou *et al.*, 2020).

While regeneration is far more common in the PNS than the CNS as mentioned previously, the success of such regeneration is variable with outcomes dependant on the severity and site of the injury (Zheng and Tuszynski, 2023). Upper extremity injuries appear much more common than lower extremity injuries, making up approximately two-thirds of reported injuries. Of the four PNS plexuses, or nerve networks, illustrated in Figure 5 below- cervical, brachial, lumbar and sacral- the brachial plexus is the most commonly affected (Kouyoumdjian, 2006).

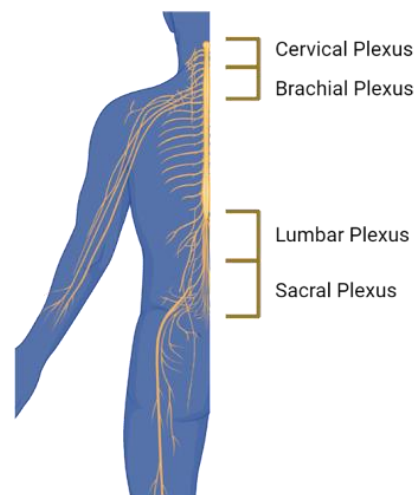


Figure 5. Illustration of the 4 major plexuses of the peripheral nervous system (C. Buckley, 2023)

In this section, the mechanisms by which nerve injuries occur, the characterisation of such injuries and different types of degeneration will be discussed.

2.2.1 Mechanisms of peripheral nerve injuries

There are multiple mechanisms that could lead to a peripheral nerve injury along with a multitude of predisposing factors which could lead a person to be more likely to develop a peripheral nerve injury. The most common mechanisms are summarised in Table 1 below.

Table 1. Mechanisms of peripheral nerve injuries and predisposing factors

Mechanism	Predisposing factors
Direct nerve injury	From surgical methods, trauma from needles (Hewson, Bedfordth and Hardman, 2018)
Stretch and Compression	Insufficient padding, use of tourniquets (Masri <i>et al.</i> , 2020), use of surgical retractors (Jellish and Oftadeh, 2018)
Ischemia	Use of tourniquets, prolonged immobility, presence of haematoma surrounding a nerve, local anaesthetic drugs (Brull <i>et al.</i> , 2015)
Toxicity of injected solution	Axonal damage from local anaesthetics, highly concentrated solutions. Prolonged exposure (Hogan, 2008)
Double crush syndrome	Patients with diabetes mellitus or rheumatoid arthritis at a greater risk of permanent injury due to the disease causing a pre-existing injury (Cohen <i>et al.</i> , 2016)
Unknown factors	-

In addition to those mechanisms listed in the table above, a combination of these factors could also lead to a permanent nerve injury. Patients who smoke and/ or suffer from conditions such as hypertension, diabetes mellitus may experience changes in the microvascular system which render those patients more susceptible to a PNI. These patients may also be more likely to undergo surgery where both surgical factors and anaesthetic factors lead to an increased risk of a permanent PNI. Additionally, perioperative factors such as dehydration, hypoxia or electrolyte disturbances have all been implicated in the development of PNIs.

2.2.2 *Classification of nerve injuries*

The classification system most commonly used in clinical settings are Seddon's characterisation of nerve injuries which were founded by Sir Herbert Seddon in 1942 and the later adapted version by Sunderland in 1978 (Hussain *et al.*, 2020). Seddon characterised nerve injuries into three sub categories- Neurapraxia, Axonotmesis and Neurotmesis. Neurapraxia is where there is no anatomical disruption but where there is a transient conduction block along a nerve. This type of injury is usually as a result of a blunt injury. No Wallerian degeneration occurs but there is often a loss in movement or motor function with some residual sensory or autonomic function and recovery is usually complete within days to weeks. Axonotmesis is characterised by axonal damage with surrounding connective tissues remaining intact, whereas the nerve trunk and associated connective tissues are destroyed in neurotmesis (Althagafi and Nadi, 2023).

The classification of nerve injuries by both Seddon and Sunderland are summarised in Table 2 below.

Table 2. Classification of peripheral nerve injuries

Seddon	Sunderland	Pathophysiology
Neuropraxia (Nerve compression injury)	Type I	Local demyelination, intact nerve (Zhang and Xing, 2018)
Axonotmesis (Nerve crush injury)	Type II	Axonal damage with intact endoneurium. Wallerian degeneration due to axoplasmic flow disruption (Dubový, 2011).
	Type III	As per type II with the addition of endoneurial injury (Sumarwoto, Poetera and Abimanyu, 2021)
	Type IV	As per type II with endoneurial and perineurial damage but intact epineurium (Abrahão <i>et al.</i> , 2021)
Neurotmesis (Nerve transection injury)	Type V	Complete transection of entire nerve trunk (Matos Cruz and De Jesus, 2023).

2.2.3 Wallerian degeneration

After the occurrence of any nerve injury greater than and including axonotmesis (type II), a complex process ensues which involves the axon, its cell body, cellular connections and the surrounding connective tissues (Rodriguez-Collazo and Laube Ward, 2021). Wallerian degeneration occurs in grade II to grade V injuries (Li *et al.*, 2023) and are divided into what occurs in the distal portion and what occurs in the proximal portion. The distal and proximal stumps in relation to a nerve gap are illustrated by Figure 6 below.

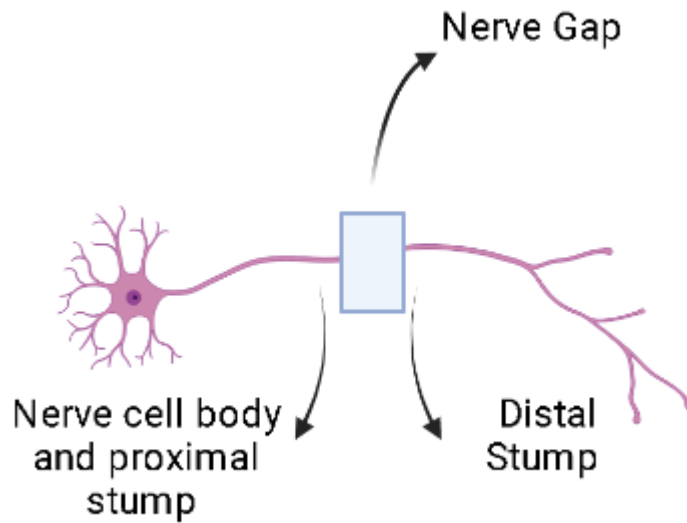


Figure 6. Proximal and distal stumps of an injured nerve. Image highlighting the proximal and distal portions of an injured nerve.

Distal

The first sign of changes after a nerve injury occur in the axon distal injury site, where the retrograde and anterograde signal flow is disturbed. As the axonal plasma membrane integrity is compromised, there is an influx of extracellular ions such as calcium and sodium which in turn activates a cascade reminiscent of apoptosis (Menorca, Fussell and Elfar, 2013). The recruitment of leukocytes follows injury and instigates the cytokine-mediated signalling cascade and alteration in the neighbouring non-neuronal cells (Mahar and Cavalli, 2018). Following this, synthesis of ECM molecules, neurotrophins, chemokines, proteolytic enzymes and interleukins commences. Wallerian degeneration of the axonal portion takes approximately 1 week in total and by day 3, Schwann cells have begun retracting from the node of Ranvier (Coleman and Höke, 2020). Activated Schwann cells and macrophages begin digesting myelin. It is at this point that there is a stark switch from neuronal degradation at the distal end to neuronal regeneration from the proximal stump. The upregulation of c-Jun protein production signals for Schwann cells to transition from myelin-producing to repair cells (Blom, Mårtensson and Dahlin, 2014). The proliferation of Schwann cells facilitates the sprouting of new nerve branches from the injured terminus and initiates regeneration.

Proximal

Depending on the severity of the injury, a limited amount of breakdown extends up from the proximal end of the axon as far as the first node of Ranvier. In the case of a very proximal injury, apoptosis of the cell body may occur but a process known as chromatolysis is more common. Chromatolysis is characterised by the break down and dispersion of the rough endoplasmic reticulum, displacement of the cell nucleus and increased expression of transcription factors which alter the gene expression from axonal maintenance to protein synthesis (Menorca, Fussell and Elfar, 2013; Elsayed *et al.*, 2019). This process can result in nerve repair or apoptosis.

2.3 NERVE REGENERATION

The PNS possesses the unique ability to self-regenerate (Snider *et al.*, 2002). Following injury, the cell membrane seals off each end of the cut axon which allows for the formation of a growth cone. This growth cone enables the extension of filopodial sprouts into the narrow gap between the distal and proximal stumps (Sarnat, 2023). The Schwann cells contained within these sprouts then undergo mitotic division to form perineurial tubes which bridge the gap. Each tube is surrounded by a basal lamina which contains various neurotrophic compounds and extends distally to the location of the original nerve terminal.

The extension of growth cones into the gap occurs through a combination of chemoattraction to neurotrophic factors following contact with a perineurial tube. These growth cones contain actin, a structural protein. Axons elongate and migrate forward through contact, trailed by neurotubules (Bayır *et al.*, 2022). Neurotubules contain the protein tubulin which stiffens the trailing axon. Later, the axon is infiltrated with neurofilaments which act as a permanent cytoskeleton (Fader *et al.*, 2022). The perineurial tubes upregulate neurotrophin synthesis in order to guide the growing axon to its target (Som, Miles and Bakst, 2019).

The basal lamina is crucial to the regeneration of axons as it contains neurotrophic compound such as glycoproteins, laminin, and fibronectin (Yang *et al.*, 2021). These substances are critical for guiding the axonal outgrowth. If a growing axon does not reach its appropriate ending, it will eventually degenerate (Wareham, Risner and Calkins, 2020). This is a key reason as to why intervention or scaffolding is generally required. Regeneration without intervention generally takes place at a rate which is too slow to achieve full functional recovery. In the majority of cases, severe injuries require immediate surgical intervention, and therefore they will be the focus of this section.

2.3.1 Current therapeutic options

Despite all that is known of the pathophysiology of PNI and regeneration, peripheral nerve repair still poses a significant challenge for reconstructive surgeons. The preferred method of repair is direct repair when the gap is small and the ends can be approximated with minimal tension (Bhandari, 2019). This type of repair has been found to be more successful in nerves which are purely motor or purely sensory (Narayan, Arumugam and Chittoria, 2019), and have minimal involvement of intraneural connective tissue. To achieve optimal regeneration, the nerve stumps must be perfectly aligned without tension and have been repaired non-traumatically- that is, with the minimum amount of tissue damage and sutures.

In the case of nerve gaps which cannot be approximated and coaptated without tension, nerve grafts such as autografts or allografts are used. However, all of these approaches have significant drawbacks, such as donor site morbidity and the necessity for immunosuppression, which will be described in further depth in the next section. To overcome these issues, conduit repair was researched as a way to provide an optimal environment for axonal outgrowth, support the growth of Schwann cells, and provide neurotrophic stimulation. This section will first discuss methods of direct repair, followed by nerve grafts and finally, conduit repair.

2.3.1.1 End-to-end repair

End-to-end nerve repair techniques include epineural repair, group-fascicular repair, and fascicular repair. Epineural repair is a technique commonly used following a sharp nerve injury without nerve tissue loss (Raut and Johnson, 2023). In this type of repair, 4-8 sutures or fibrin glue are placed in the epineurium sheath to align and obtain continuity of the nerve without tension. Correct positioning is confirmed via continuity of structures such as blood vessels within the epineurium (Khan and Perera, 2020).

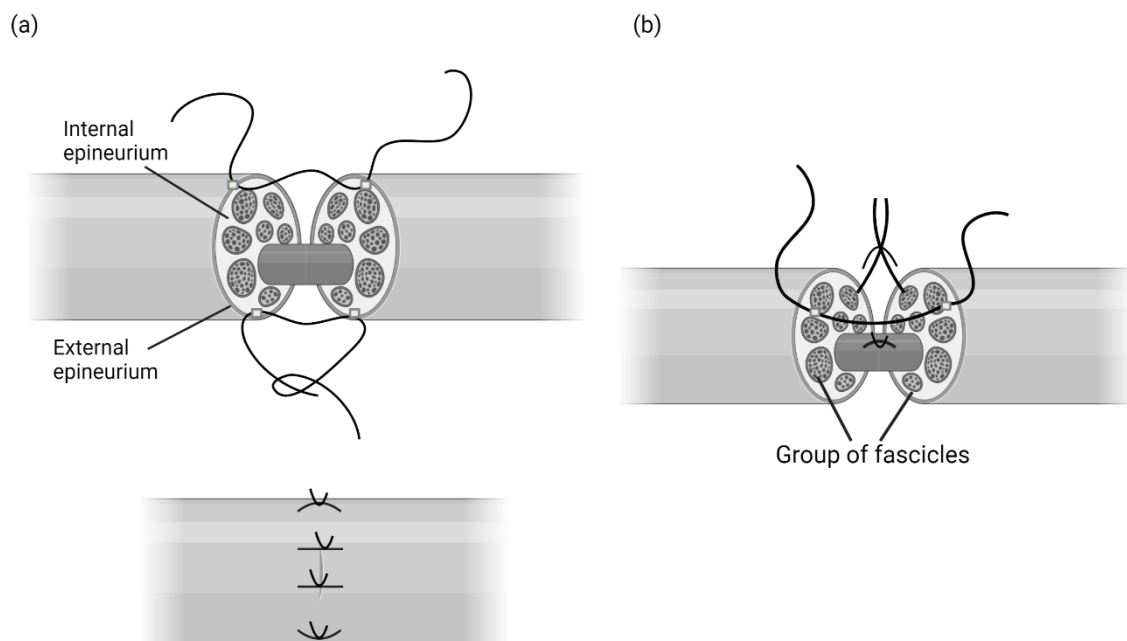


Figure 7. Epineural and grouped fascicle repair. Epineural repair (a) sutures are passed through the internal and external epineurium of the proximal and distal stump. Grouped

fascicle repair (b) sutures are passed through the interfascicular epineurium (C. Buckley, 2023).

In grouped fascicle repair, the epineurium is retracted before approximating corresponding groups of fascicles with 2-3 sutures penetrating the interfascicular epineurium (Krauss, Weber and Mackinnon, 2022). Scar tissue formation is impeded by limiting the number of sutures and the degree of tension on the wound. Fascicular repair requires the placing of sutures through the perineurium and the separation of fascicles. This method is no longer commonly used as it requires 2-3 sutures per fascicle which encourages scar tissue formation (Cho *et al.*, 2020).

2.3.1.2 *Epineural sleeve repair*

A potentially better alternative to end-to-end repair is epineural sleeve neurorrhaphy. This method involves rolling back the epineurium of the distal end and resecting a 2-mm nerve segment. The newly created epineural sleeve is pulled over the proximal end and sutured. This method has been shown to have improved functional recovery when compared against end-to-end repair as it enables the guidance of neurons to their targets and prevents neuroma formation (Ioncioaia, 2023).

In addition to end-to-end repair and epineural sleeve repair, there have been studies which discussed the promising research into end-to-side repair which could be utilised in cases where the proximal stump was not available or the nerve gap was of significant distance (Guionneau *et al.*, 2020).

2.3.1.3 *Nerve grafts*

Nerve grafts are the most common therapeutic method used for medium and large nerve gaps. Nerve grafts are subdivided into autografts, allografts and nerve transfers. Autografts involve removing a less vital nerve such as the sural nerve and transplanting it into the affected area on the same body. Autografting has long been considered the gold standard for peripheral nerve repair but there are several disadvantages with this procedure (Fadia *et al.*, 2020). The donor nerve is usually a sensory nerve, the loss of which results in sensory loss, injury site scarring and neuroma formation. In addition, limited supply is a major issue. Despite this gold standard method being purported to offer the best result over others, successful recovery post-surgery is found to be about 50% (Vijayavenkataraman, 2020).

Allografts overcome the supply issue by using donor nerves from cadavers or a tissue bank, this has the added benefit of avoiding donor site morbidity. However, the patient is required

to undergo a temporary period of immunosuppressant therapy to allow for the foreign tissue to be accepted by the body. The associated morbidity of this immunomodulatory therapy is the major disadvantage to allografts (Nassimizadeh, Nassimizadeh and Power, 2019).

Finally, nerve transfers refer to the repair of a distal injury by utilising a proximal foreign nerve with redundant nerve function. This method is well established in the treatment of brachial plexus injuries, but standard procedures need to be established for other areas of the peripheral nervous system (Sneiders *et al.*, 2019). Donor site morbidity still remains an issue in this case, as well as pre-existing injury to the donor nerve.

As no current method provides an ideal solution, nerve guidance conduits have been postulated as the solution.

2.3.1.4 *Nerve guidance conduits*

PNI presents a significant healthcare challenge, for which nerve guidance conduits (NGCs) have arisen as a promising approach which offers an alternative to autografts and reducing donor site morbidity. These NGCs provide a protective environment which bridges the gap between the distal and proximal ends, facilitating axonal regeneration and potentially re-establishing nerve function.

In nerve regeneration, cell-cell and cell-ECM interactions play a crucial role. For this reason, nerve guidance conduits need to possess ECM like qualities (Chelyshev, Kabdesh and Mukhamedshina, 2022) and be biocompatible, biodegradable, flexible and mechanically stable in order to ensure it's not immunogenic and that it will perform biologically. Nerve conduits are tubular structures which guide the regenerating axons to the distal nerve stump. First generation synthetic nerve conduits generally consisted of medical grade silicone due to the flexibility and accessibility of the material (Gaudin *et al.*, 2016). However, modern nerve conduits consist of biodegradable materials such as collagen or polyurethanes which ensure mechanical stability, prevent scar tissue formation, and promote cell adhesion and migration.

The key principles of NGCs are physical support, axonal guidance and biomaterial selection. NGCs act as a bridge between severed ends of the nerve, and therefore need to be physically capable of maintaining the spatial orientation and prevent the formation of neuromas (Yang *et al.*, 2022). Axonal guidance is vital as the axon will degenerate if it is not effectively guided within a reasonable timeframe. In order to achieve this, many topographical measures can be implemented such as micro or nano-engineering grooves or fibres to the inner surface

of the conduit to guide axons across the injury site (Zheng *et al.*, 2022). Biomaterial choice is responsible for the biocompatibility, biodegradability and mechanical strength of the conduit which are all vital for the success of nerve regeneration. However, many biomaterials can provide the biological cues for nerve regeneration, but fall short in terms of mechanical strength (Tian *et al.*, 2022).

NGCs can be classified into three categories based on their composition: synthetic, biological and hybrid conduits. Synthetic conduits are made up of biocompatible synthetic polymers such as polylactic acid (PLA) or polyglycolic acid (PGA). The use of these polymers is attractive due to the control precision offered over their physical and mechanical properties, degradation rates and ease in manufacturing (Kang, Lee and Gwak, 2022). Biological conduits are conduits made of biological polymers such as HA or collagen. These polymers offer a biomimetic scaffold which closely resembles native tissues. However, they often lack in their mechanical strength (Kumar *et al.*, 2022).

To overcome this deficit, hybrid conduits offer a combination of synthetic and biological, harnessing the positive qualities of each.

Recent advances in NGCs have focused on enhancing the regenerative properties of these scaffolds through incorporation of bioactive molecules, cell based approaches, 3D printing and electrical stimulation. Bioactive molecules such as growth factors and neurotrophins can enhance axonal outgrowth and modulate immune responses which creates a more favourable microenvironment for nerve regeneration (Yao *et al.*, 2022). Cellular approaches such as cell laden conduits, utilising Schwann cells or neural stem cells, can significantly aid in regeneration by promoting axonal regeneration, myelination and functional recovery (Chen *et al.*, 2023).

There has been a shift toward patient centred and patient specific approaches in recent years and 3D printing can facilitate this by enabling precise fabrication of NGCs with patient-specific dimensions and architectures which can vastly improve patient outcomes (Venkata Krishna and Ravi Sankar, 2023). Finally, electrical stimulation has been shown to be capable of further enhancing regeneration by promoting neurite outgrowth and functional recovery (Hasiba-Pappas *et al.*, 2023).

A number of nerve conduits have already been granted FDA approval, some of which are outlined in Table 3 below, and this list is constantly expanding.

Table 3. FDA approved NGCs available on the market.

Product	Material	Reference
VersaWrap Nerve Protector	Calcium Alginate and HA	(Hones <i>et al.</i> , 2023)
NeuroShield™	Chitosan	(Parker <i>et al.</i> , 2021)
Reaxon Plus	Chitosan	(Jiang <i>et al.</i> , 2019)
NeuroFlex™ (Flexible Collagen Nerve Cuff)	Bovine-derived Collagen Type I	(Meek and Coert, 2008)
Reinforced Flexible Collagen Nerve Cuff	Bovine-derived Collagen Type I	(Gao <i>et al.</i> , 2023)
AxoGuard™ Nerve Connector	Porcine small intestine	(Ducic, Safa and DeVinney, 2017)
Nerbridge™	Porcine-derived collagen/PGA	(Nakamura <i>et al.</i> , 2020)
CovaOrthonerve Resorbable Collagen Membrane	Porcine-derived Collagen	(Parker <i>et al.</i> , 2021)
NeuraGen	Collagen Type I	(Mathot <i>et al.</i> , 2020)
NeuroMatrix™	Collagen Type I	(Giusti <i>et al.</i> , 2014)
Neurotube	PGA	(Hsu, Chang and Yen, 2017)

Ultimately, NGCs are a promising candidate for PNI and recent advances in biomaterial incorporation, bioactive molecules and advanced manufacturing techniques have substantially improved their regenerative potential. However, further research and investment is required to improve their long-term stability and clinical outcomes.

2.4 BIOMATERIALS

2.4.1 Hyaluronic acid

Hyaluronic acid (HA) is a naturally occurring glycosaminoglycan which is found throughout the human body in the vitreous humour, joints, umbilical cord, connective tissue and skin. This widely available polysaccharide has found a number of applications from cosmetics and food supplements, to wound healing and drug delivery. Section 2.4.1 will discuss HA in terms of its history, physicochemical properties, biological properties, synthesis and degradation, functionalisation and applications in nerve repair.

2.4.1.1 History

HA was first discovered in 1934 when Karl Meyer and his colleague John Palmer isolated a previously unknown material from the bovine vitreous body. This novel substance was named after identifying the two sugar molecules which made up the material, one of which was uronic acid. The “hyal” portion came from the word hyaloid which refers to the glassy-like appearance of the vitreous body hence the combination was called hyaloid + uronic acid or hyaluronic acid (Selyanin *et al.*, 2015). HA was first identified as an acid and is most commonly referred to as an acid, but HA behaves more like the salt, sodium hyaluronate in physiological conditions. For this reason, Endre Balazs coined the name hyaluronan in 1986 (Balazs, Laurent and Jeanloz, 1986), which captured the various forms of HA while conforming to the international polysaccharide nomenclature- the acid and the salt.

2.4.1.2 Physicochemical properties

HA, shown in Figure 8 below, is an anionic polymer which is made up of disaccharides of D- glucuronic acid and N-acetyl-D-glucosamine, with β (1, 4) and β (1, 3) glycosidic bond linkages.

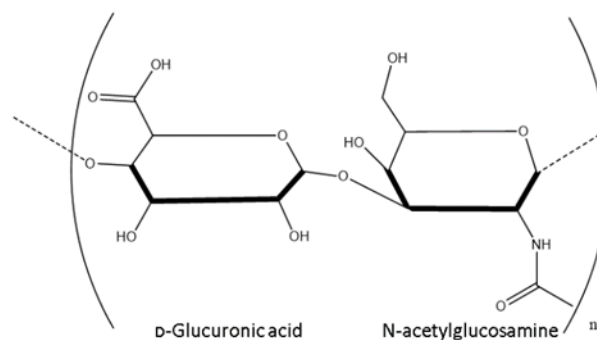


Figure 8. Structure of a disaccharide of Hyaluronic acid (C.Buckley, 2023).

The chains of hydrogen bonds in the HA molecule gives rise to the unique physicochemical properties which HA is so well-known for such as its viscoelastic properties. In the form of an elongated chain, HA in aqueous solution exhibits the highest viscosity. In this respect, HA concentration and viscosity are directly proportional, that is, as the concentration of HA in aqueous solution increases, so too does the viscosity due to chain weaving and the formation of 3-Dimensional matrices. This occurrence is the foundation of gelation, however this viscosity can be modulated, to enable the use of concentrated solutions, through the use of viscosity modifiers such as salts as demonstrated by Selyanin et al, (2015).

Molecular weight (MW) is the principal determinant for the biological functions of HA. The average MWs of human endogenous HA is summarised in Table 3 below. While it typically exists as a high molecular weight polymer, of over 10^6 Daltons (Da), it can be cleaved by an enzyme, hyaluronidase, in the body to obtain molecules of much lower MWs. The biological functions include control of tissue hydration, supramolecular assembly of proteoglycans in the ECM, and multiple roles in receptor-mediated cell detachment, mitosis and migration.

Table 4. Molecular weights of endogenous HA and its location in the body.

Tissue	Concentration ($\mu\text{g/ml}$)	Molecular weight (kDa)	Comment
Umbilical cord	4100	500	(Balazs <i>et al.</i> , 1967)
Synovial fluid	1400-3600	6000-7000	(Bjelle, Andersson and Granath, 1983; Tammi <i>et al.</i> , 1994)
Dermis	200-500	>1000	(Papakonstantinou, Roth and Karakiulakis, 2012; Garg and Hales, 2004)
Epidermis	100	>1000	(Papakonstantinou, Roth and Karakiulakis, 2012; Garg and Hales, 2004)
Thoracic lymph	0.2-50	1400	(Tengblad <i>et al.</i> , 1986; Laurent <i>et al.</i> , 1987; Harrer <i>et al.</i> , 2021)
Urine (excreted)	0.1-0.3	4-12	(Turathum, Gao and Chian, 2021)

Figure 9 below highlights the dependence that commercial HA applications have on MW also. HA exceeding 1000 kDa is primarily useful in the surface hydration of cells and has applications in ophthalmology, wound healing and cosmetics. HA holds applications in wound healing between 10 kDa and 1000 kDa, whereas oligosaccharides with an MW of ≤ 10 kDa have been found to promote the proliferation of fibroblasts, and angiogenesis.

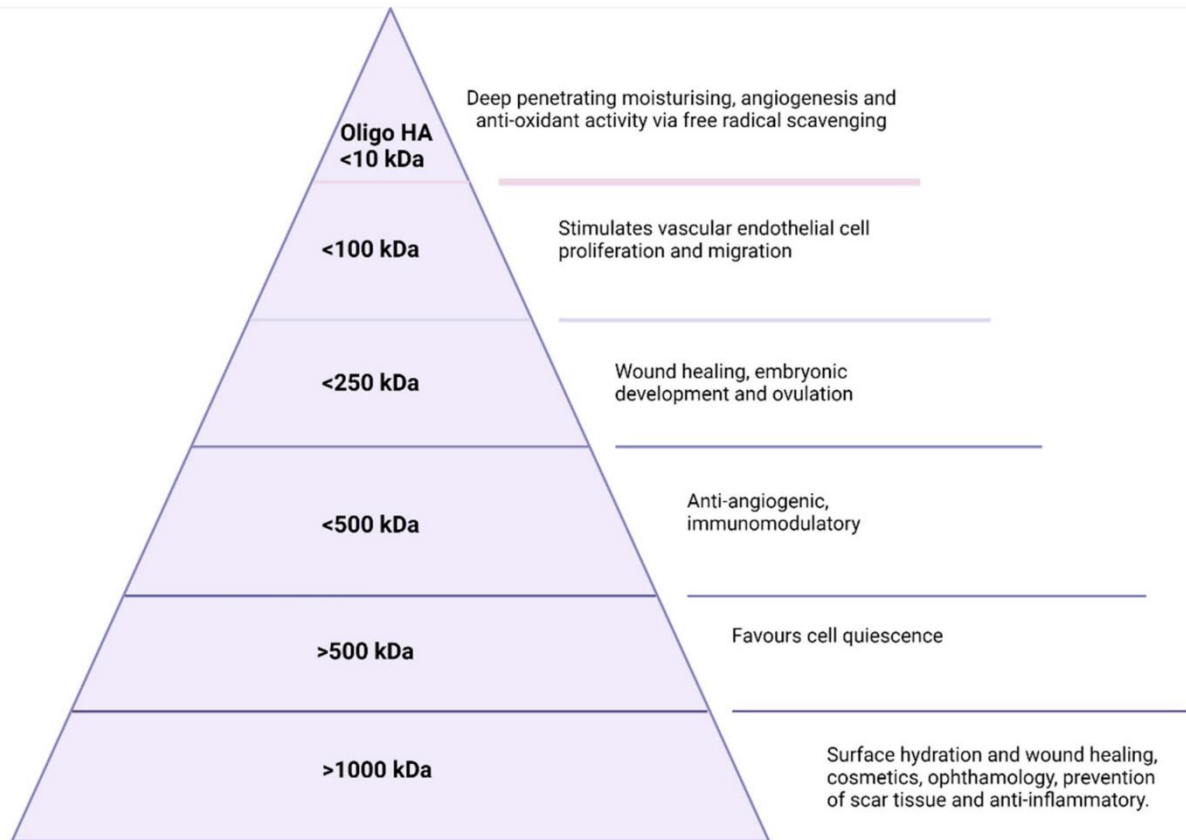


Figure 9. Molecular weight dependent applications and biological functions of HA (C. Buckley et al., 2022).

2.4.1.3 Endogenous bioactive properties

In the body, HA interacts with a multitude of molecules and receptors and conducts numerous functions throughout the ECM via specific and non-specific interactions. Some of the most commonly known receptors that HA interacts with are Neurocan, the receptor for hyaluronan-mediated motility (RHAMM), GHAP (glial HA binding protein), CD44, Aggrecan, and TSG6 (TNF-stimulated gene 6) (Vasvani, Kulkarni and Rawtani, 2020; Rangasami *et al.*, 2021). CD44 is arguably the most biologically relevant receptor due to its multifunctional cell surface conjugated protein that is present in an abundance of cell varieties. These cell surface binding proteins possess key residues which allow for wrapping around and securing the HA polymer chain to the CD44 receptor.

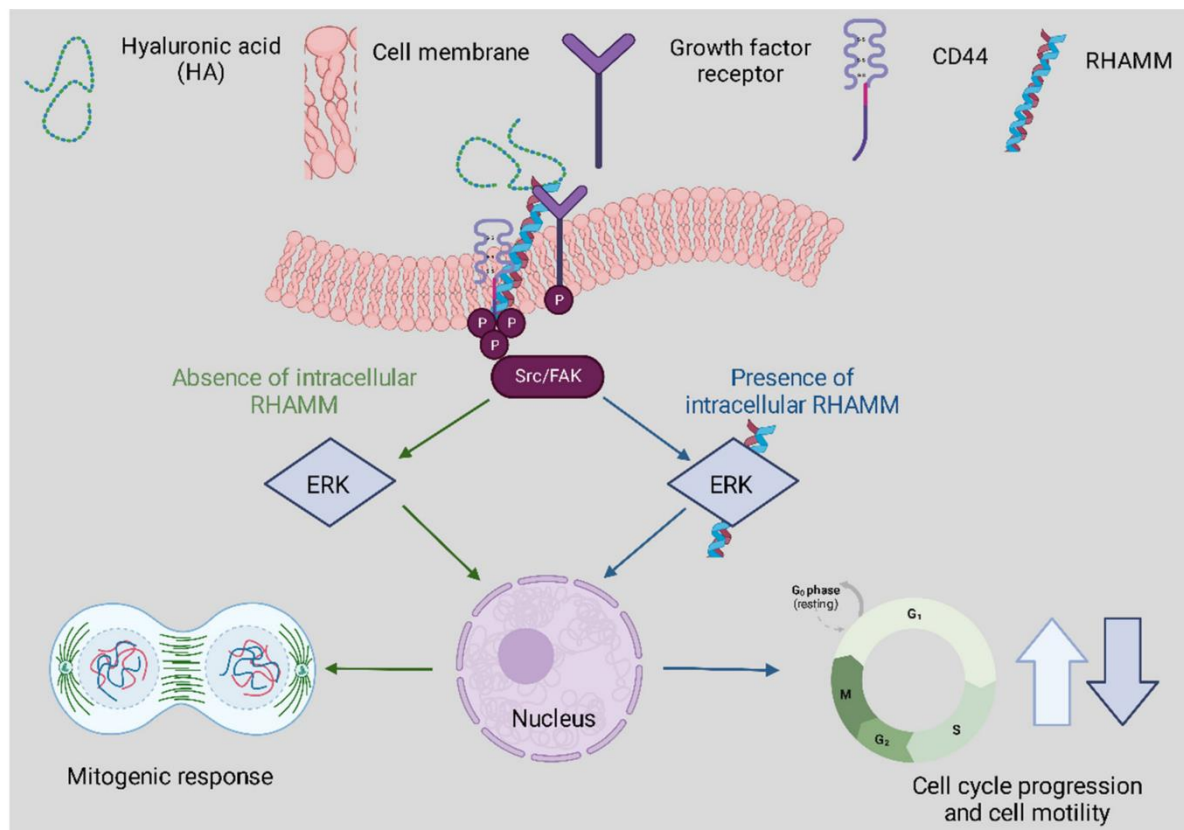


Figure 10. Overview of HA in intercellular signalling (C. Buckley et al., 2022). The track denoted in green highlights extracellular signalling involving CD44-HA mediated pathways. The blue track is for intracellular RHAMM signalling. Cell surface RHAMM interacts with CD44, HA, and growth factor receptors (GFR) to activate protein tyrosine kinase signalling cascades that activate the ERK1/2 MAP kinase cascade in a c-Src/FAK/ERK1/2 dependent manner (depicted in green track). In the absence of intracellular RHAMM, this signalling

can stimulate the transcription of mitogenic effectors to regulate a mitogenic response (cell proliferation/random motility). In the presence of intracellular RHAMM (blue track), MEK-1/p-ERK1/2 also binds to a number of protein partners that allows activated RHAMM to enter the nucleus to regulate functions of microtubule dynamics via centrosome structure/function, and cell cycle progression. Activated RHAMM also controls the expression of genes involved in cell motility. Overall, the effect of HA is pro-proliferation and the development of cellular infrastructure whilst providing critical immune support.

The interaction between HA and its primary receptors, CD44 and RHAMM, is responsible for many functions within tissues. CD44 expression is a known activation marker that aids in classifying memory and effector T cells. It can also assist in early T cell signaling as it is bound to the lymphocyte-specific protein kinase (Rangasami *et al.*, 2021). CD44 also contributes to cell adhesion interactions and proliferation as illustrated in Figure 10 above (Schumann *et al.*, 2015). Despite the binding of HA to CD44, it has been evidenced that HA degradation can trigger inflammation through toll-like receptors such as TLR2 and TLR4 in macrophages and nerve fiber cells (Hanoux *et al.*, 2018). Both TLR and HA are vital components of the innate immune system.

2.4.1.4 *Synthesis*

HA is unique in that it is one of the only mucopolysaccharides not synthesised by the Golgi apparatus. Instead, it is synthesized at the plasma membrane. HA conducts a plethora of physiological functions in both humans and animals despite its relatively simple elongated structure. HA can be isolated from animal sources such as rooster comb, or certain bacteria such as *Streptococcus*. However, HA extracted from these sources results in purification issues due to the inherent variability within animals and the presence of endotoxins in *Streptococcus* species. The primary sources of commercial HA for industry are either animal or microorganism derived.

2.4.1.4.1 **MICROBIAL SYNTHESIS**

Three distinct genes are required to synthesise HA in bacteria species- *HasA*, *HasB* and *HasC*. In the first stage of the biosynthesis of HA, glucose is converted to glucose-6-phosphate, the most vital precursor in this pathway, via the enzyme hexokinase as illustrated in Figure 11 below. Following this initial stage, glucuronic acid and N-acetyl glucosamine can be produced by two distinct routes (Weigel and DeAngelis, 2007; Weigel, Hascall and

Tammi, 1997; Vigetti *et al.*, 2014; Yao *et al.*, 2021). Despite this well-defined biosynthesis pathway in bacteria such as the *Streptococcus* genus, the endotoxin produced by *Streptococcus* would render the HA produced unsuitable for human use. Additionally, the expensive growth media necessary and difficulty in controlling the fermentation process make this genus less than ideal.

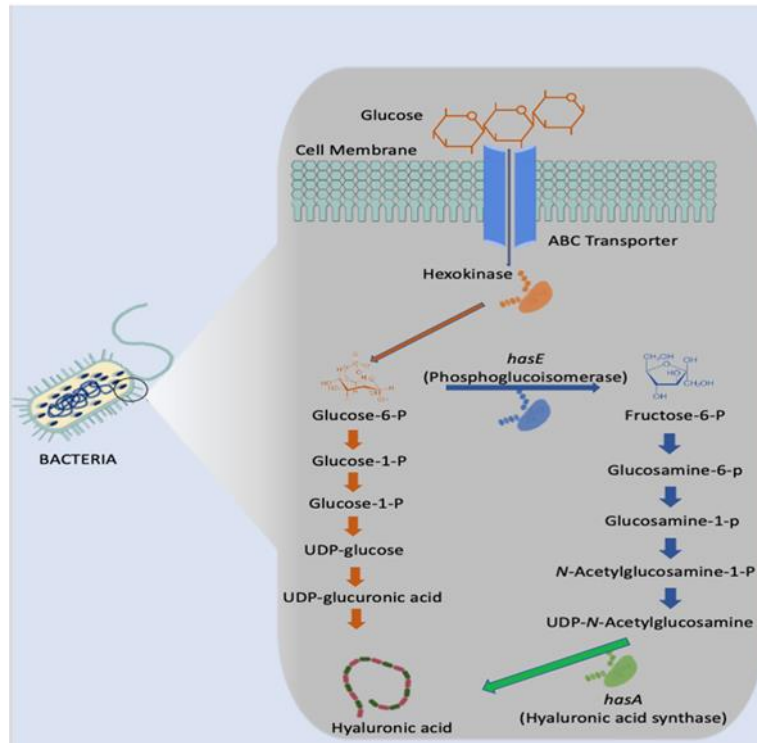


Figure 11. Microbial synthesis of HA in *Streptococcus* species (C. Buckley et al., 2022).

However, not all bacterial strains possess these caveats. To overcome the issues with *Streptococcus* production of HA, other strains which are generally regarded as safe (GRAS) have been investigated and engineered for HA production. One such strain is *Lactococcus lactis*, which was engineered by Sheng et al. (2015) using the HA biosynthesis operon and the *lacF* selectable marker.

2.4.1.4.2 ANIMAL SYNTHESIS

Vertebrates contain three different *has* isozymes- *has1*, *has2* and *has3*, which are responsible for HA synthesis during embryonic development, morphogenesis, wound healing, ageing and cancer progression. HA synthases serve to lengthen the polysaccharide by repeated addition of glucuronic acid and N-acetyl-D-glucosamine groups as illustrated in Figure 12

below. The size of the HA produced is dependent on the kinetic profile of the *has* protein. *Has1* and *has2* proteins are moderately active and implicated in the synthesis of high MW HA, whereas *has3* proteins are highly active and produce low MW HA.

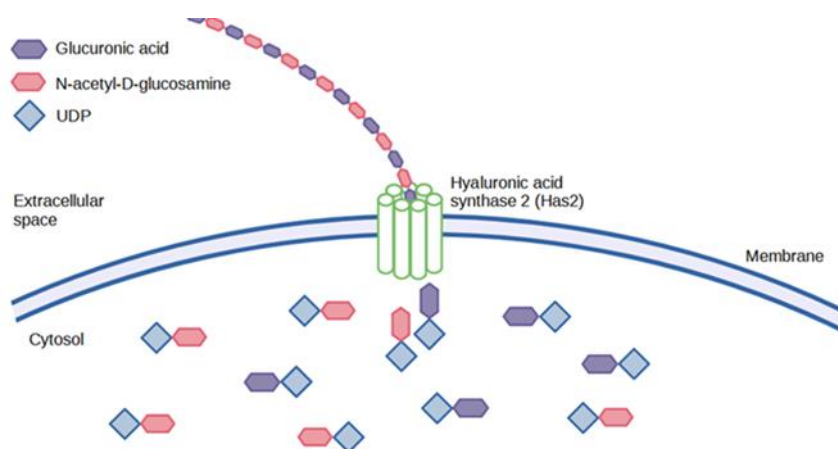


Figure 12. Animal synthesis of HA (C. Buckley et al., 2022). HA is synthesised by three HASes at the plasma membrane using uridine diphosphate (UDP) bonded glucuronic acid and N-acetylglucosamine as substrates.

Due to the high MW which can be obtained from HA extracted from animals, rooster comb still remains an important product. However, the harsh extraction process often results in poor yield and polydispersity of molecular weights. This occurs due to the grinding, acid treatments and organic extractions necessary for HA extraction. In addition, contaminating proteins are a significant issue in the isolation of HA from animals. Hyaluronidase, an enzyme specific to HA, may be bound to the polymer in animal tissues. If this enzyme is present, it could illicit an immune response in the body if not completely removed from the end product. There is also the potential for nucleic acid contamination or the spread of animal prions which could result in infectious disease spread. For these reasons, the advantages of animal extracted HA such as molecular weight are negated by the high cost, labour intensive processes involved. Therefore, biotechnological solutions are the preferred route of commercial HA synthesis if possible.

2.4.1.5 Degradation

As previously mentioned in section 2.4.1.4, there exists an enzyme, hyaluronidase (HYAL), which is specific for HA. Endogenous human HA is primarily degraded by this enzyme

family but may also be initiated by free radical degradation. This process occurs due to oxidative stress induced by free radicals or pro-oxidants which cause organic damage to molecules or cells. Free radical degradation, in particular, has been implicated in HA degradation in ageing or arthritis. These free radicals initiate degradation via non-specific scission of the glycosidic bond, and the concentration of free radicals is directly proportional to the extent of HA degradation. The half-life of HA in human tissue ranges from three to five minutes in blood to approximately 70 days in the eye's vitreous body. This turnover rate is controlled by localised degradation or tissue release from the lymph system.

Extracellularly, a multitude of mechanisms can be used to produce smaller HA fragments. This is of importance as smaller HA fragments are preferred for use in cancer treatments as a drug delivery system (Luo, Dai and Gao, 2019), as an antioxidant or in cosmetics. Medium chain HA, however, can be useful in wound repair and regeneration. Extracellular methods to produce smaller fragments of HA include chemical degradation, physical force, free-radical cleavage, pH, temperature, ultra-sonic stresses and, of course, enzymatic degradation.

2.4.1.5.1 ENZYMATIC DEGRADATION

The HYAL family of enzymes mentioned in the previous section are responsible for the enzymatic degradation of HA. Six of these enzymes have been identified in humans: HYAL1, HYAL2, HYAL3, HYAL4, PH20 and HYALP1. These enzymes serve to cleave the large molecule into smaller oligosaccharides. β -D-glucuronidase and β -N-acetylhexosaminidase then further degrade the fragments by removing non-reducing sugars from the terminal ends. The small fragments of HA produced by this process have been shown modulate gene expression in many cell types. Due to their small size, they could invoke an inflammatory response through interaction with toll-like receptors (TLR) such as TLR-2, TLR-4 and CD44, which induce NF- κ B activation that, in turn, is responsible for inflammatory mediator transcription such as TNF- α and Il-1 β . Despite this, there is growing research into using these oligosaccharides of HA (<10 kDa) to modulate inflammatory response. Wang et al., (2020) demonstrated how these oligos could be used as an agent for reconstructing cardiac function against myocardial infarction.

2.4.1.6 Functionalisation

Native HA has found a broad range of applications in areas such as ophthalmology and cosmetics due to its unique physicochemical characteristics. Additionally, HA can be modified to expand the capabilities of this polysaccharide and allow for cross-linking and

engineering, to tailor the degradation profile *in vivo*, to improve cell attachment or to enable conjugation.

The relatively simple structure of HA allows for ease of modification of its two main functional groups- the hydroxyl and the carboxyl groups. Additionally, further synthetic modifications may be performed following the deacetylation of the acetamide group, which can allow for the recovery of amino functionalities. Regardless of which functional group is to be modified, there are two routes for modification; crosslinking or conjugation. These modification methods are illustrated in Figure 13.

Conjugation is a form of modification which involves the grafting of a molecule onto the HA chain via covalent bond. Crosslinking, on the other hand, involves the formation of a matrix of polyfunctional compounds which cross chains of native or conjugated HA via two or more covalent bonds. Crosslinking can be performed on either native HA or conjugated HA. This is of particular interest in the area of bioconjugation. For the purpose of this thesis, conjugation of the HA molecule enabled photo-crosslinking of the HA molecule.

Bioconjugation is the act of conjugating peptides or proteins to a natural polymer to increase efficacy. Previously, this has been done using polyethene glycol (PEG). PEGylation was found to increase the effectiveness of drugs by reducing renal clearance, enzymatic degradation and immunogenicity *in vivo*. However, repeated injection of PEGylated liposomes has been found to cause long-term cycle decline via accelerated blood clearance. For this reason, HA is now under investigation as a plausible alternative.

Conjugation allows for crosslinking with a variety of molecules to enable a range of functions from drug carriers to 3D printing of specific architecture for bioengineering purposes. The crosslinking of HA allows for fine-tuning of many characteristics, such as mechanical, rheological and swelling properties, and protects the polymer from enzymatic degradation to allow for longer residence time at the required treatment site. The onset of processes such as bioconjugation and crosslinking has enabled new applications in medicine, aesthetics, and bioengineering to treat a range of different illnesses and injuries. The different approaches and applications of functionalisation have been discussed in great detail by Sanjay Tiwari and Pratap Bahadur (2019), so only a brief overview of hydroxyl and carboxyl group chemical modifications will be discussed in this literature review.

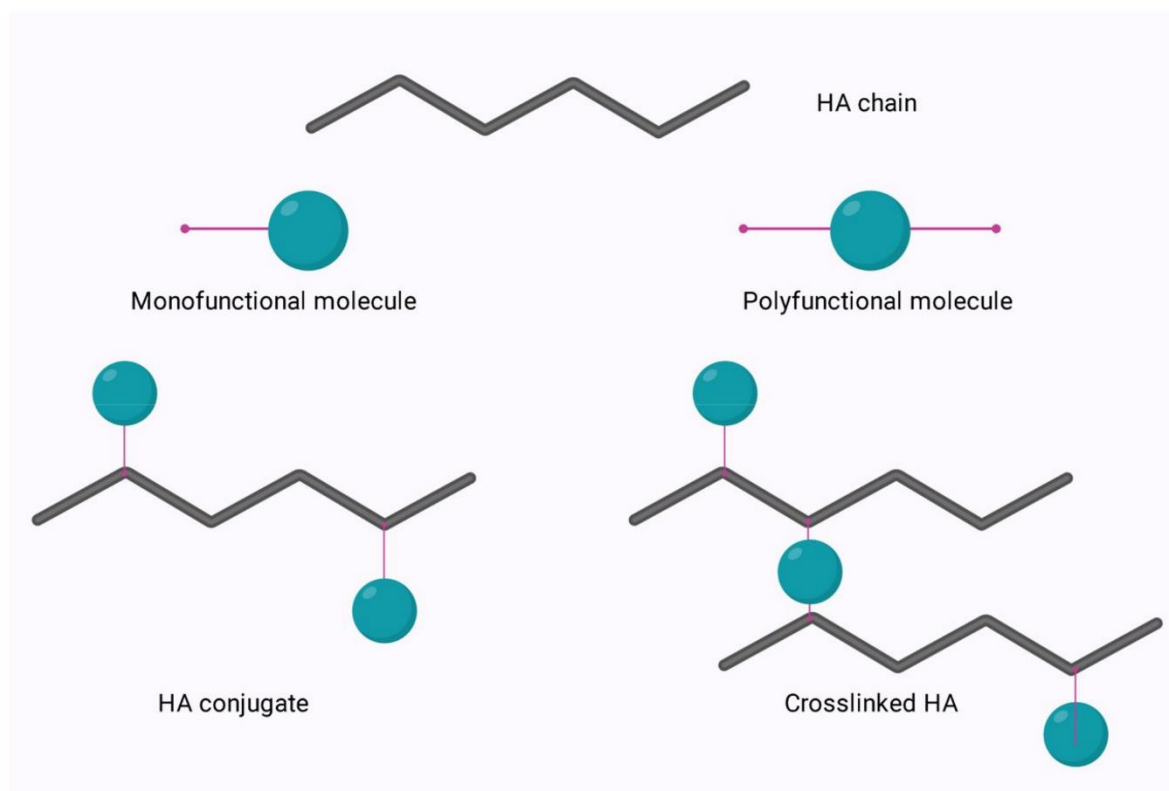


Figure 13. Conjugation and crosslinking of HA (C. Buckley et al., 2022). Different modification routes for the HA chain include conjugation and crosslinking.

2.4.1.6.1 Modification of HA via the hydroxyl group

By selecting the hydroxyl moiety for modification and retaining the original state of the carboxyl group, the recognition of the HA molecule by degradative enzymes is preserved. Each disaccharide unit of HA is made up of four hydroxyl groups, one amide group and one carboxyl group. One of the most highly marketed HA derivatives, butanediol-diglycidyl ether (BDDE) HA, is produced in an alkaline aqueous solution through simple synthetic procedures involving the hydroxyl group (Tiwari and Bahadur, 2019). A similar method is utilised throughout this thesis in which methacrylic acid was reacted with HA in alkaline solution. Additionally, divinyl sulfone (DVS) or ethylene sulfide can be used to form other ether derivatives in water in the same manner (Andrade del Olmo *et al.*, 2021). Many HA hydrogels have been created utilising this method for applications such as bone tissue engineering, wound healing and drug delivery (Singh, Rai and Prakash Tewari, 2023).

A novel HA drug delivery system targeting tumour cells was created when performing a dimethylaminopyridine (DMAP)-catalysed esterification reaction between butyric anhydride and low molecular weight (LMW) sodium hyaluronate in dimethylformamide (DMF). Other modification methods involve isourea coupling and periodate oxidations. However, both of these methods are performed in harsh conditions and may compromise the integrity and biocompatibility of the HA.

2.4.1.6.2 Modification of HA via the carboxyl group

The main modifications of the carboxylic group of HA are esterification, carbodiimide mediated, 1-ethyl-3-[N,N-dimethylaminopropyl]-carbodiimide (EDC)/ N-hydroxysuccinimide (NHS) modification, EDC/ hydrazide modification and finally thiol modification (Kwon *et al.*, 2019). Esterified HA is usually prepared by first preparing the quaternary salt of HA followed by reacting with an esterifying reagent. The insolubility of HA is proportional to the degree of esterification obtained. Two of the best characterised esterified HA derivatives are ethyl and benzyl esters of HA, named HYAFF® 7 and HYAFF® 11, respectively (Campoccia *et al.*, 1996; Turner *et al.*, 2004). These derivatives were created for tissue engineering applications.

Another option for modification is carbodiimide mediated whereby a carbodiimide activates the carboxyl group of the HA under acidic conditions. This activation allows for nucleophilic attack of the carboxylate anion to produce O-acylisourea, which the nucleophiles can capture. The most common nucleophilic agents are primary amines despite the low percentage in the nucleophilic amine state at equilibrium (Turner *et al.*, 2004). One of the biggest pitfalls of this method is the formation of the stable intermediate N-acylurea from O-acylisourea, which can happen within seconds when using viscous macromolecules, thus out-competing the exogenous amines (Lai, 2012).

To combat this, a two-step procedure utilising EDC and NHS was created, which was more efficient and increased the yield of modified products. However, the degree of substitution is poor, generally below 20%. This is preferable to most biological investigations so as not to interfere with CD44 interaction (Zhao *et al.*, 2006; D'Este, Eglin and Alini, 2014; Khunmanee, Jeong and Park, 2017; Thirumalaisamy *et al.*, 2021). Following chemical conjugation, various crosslinking methods can be employed to allow for use in multiple applications, from tissue engineering to wound healing and aesthetics.

2.4.1.6.3 Amidation

As previously mentioned, carbodiimide modifications are one of the most common modifications performed, typically using EDC due to its water solubility. In this reaction using EDC, the carboxylic acid moieties are activated by EDC, which forms an O-acyl isourea intermediate. In the second step of the reaction, a nucleophilic attack of the amine to the activated HA occurs, forming an amide bond as shown in Figure 14 below. However, the formation of the stable N-acyl urea by-product may occur due to the reaction of the O-acyl isourea with water (Huang and Huang, 2018). If this occurs, no further reaction with the amine takes place. For this reason, many researchers use catalysts such as 4-dimethylaminopyridine (DMAP) in an attempt to push the reaction forward and reduce the amount of N-acyl urea formed (Siengalewicz, Mulzer and Rinner, 2014). This method was used throughout this thesis.

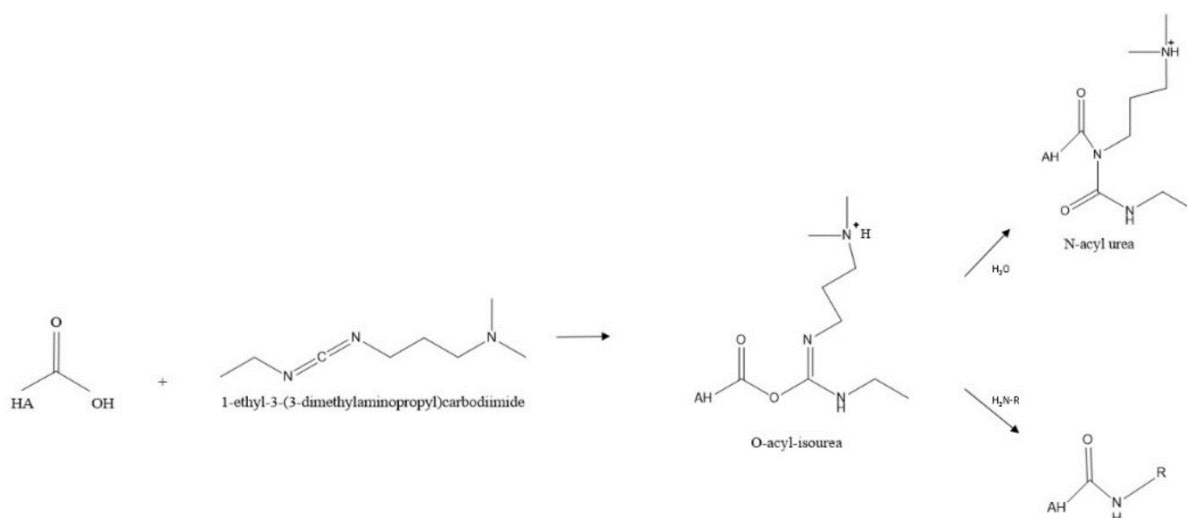


Figure 14. Typical reaction scheme for amidation of HA (C. Buckley et al., 2022).

There are more variants of this carbodiimide-mediated amidation, such as the use of biscarbodiimides as the reactive reagent, as opposed to only an activator or adding NHS to prevent the formation of the stable unreactive by-product N-acyl urea, all of these have been discussed in detail by Schanté et al., (2011).

2.4.1.7 The use of HA for peripheral nerve repair

As has been outlined throughout this literature review, the interest in HA for bioengineering applications has risen exponentially in the last decade as it is a component of the ECM and

has undisputed water binding properties which aid in the regeneration of a variety of wounds or malaises within the human body (Chaala *et al.*, 2023). As HA is highly hydrophilic, it has low cell adhesion potential, however this can be modulated by the addition of proteins or polyelectrolytes which have been shown to enhance Schwann cell growth and proliferation on HA (Entekhabi *et al.*, 2021). Despite the low cell adhesion properties of HA *in vitro*, it has been shown to prevent the formation of glial scarring (Jabbari, Babaeipour and Saharkhiz, 2023) which would impede the growth of regenerating axons. Hydrogels of HA are of particular interest in nerve repair due to the hydrated lattice structure which resembles the ECM of cells. However, the low mechanical properties of these hydrogels have been of concern. There is now emerging research of exosome laden HA hydrogels from mesenchymal stem cells which utilises this low mechanical strength of HA hydrogels for the benefit of peripheral nerve repair (Liu *et al.*, 2022).

Alternatively, the mechanical properties of HA hydrogels can be increased by utilising various techniques such as stereolithography 3D printing, which produces a tighter cross-linked network structure and therefore, better mechanical properties, or by combining HA with polymers possessing greater mechanical properties (Talaie *et al.*, 2023). In one study by Entekhabi *et al.*, (2021), an inner sponge composed of HA was then encased in PCL nanofibers for the purpose of peripheral nerve regeneration. Their study showed that by encasing the HA sponge in PCL fibres, the compressive strength and modulus were increased. Ultimately, HA is an easily manipulated, biodegradable, tuneable and biocompatible polymer that can be used for a multitude of applications from peripheral nerve repair, to drug delivery, vaccine adjuvants, wound repair and cosmetic applications. This thesis utilises HA for the purposes of developing a photo-crosslinked hydrogel and 3D printed hydrogel which could sustain neuronal and glial cells, possess tailorable degradability and deliver neurotrophic drug compounds which enhance nerve repair *in vivo*.

2.5 PEGDMA

PEGDMA is a synthetic polymer which has found increasing use in bioengineering due to the ability to fine tune the material properties of this polymer through manipulation of monomer molecular weight, water content and monomer concentration. Additionally, PEGDMA has a slow degradation rate (Li *et al.*, 2023) which can be utilised in tissue engineering as rapid degradation can lead to inflammation and insufficient tissue repair.

PEGDMA is a derivative of Poly (ethylene glycol) (PEG) which has been used consistently across a range of applications. Of particular interest, is photo-crosslinkable PEG as this can be pre-cured or cured in situ with the aid of biocompatible photoinitiators and UV light (Ma *et al.*, 2022). This enables the localised delivery of therapeutic or mechanical agents and therefore, reduced systemic side effects (Andrade del Olmo *et al.*, 2022). The selection of PEGDMA in this study was based off the body of research available on PEG as there has not been a significant body of work published on PEGDMA to date. PEG is a synthetic material with a vital role in tissue engineering as it is generally considered non-toxic, non-immunogenic and is easily cleared from the body (Tzagiollari *et al.*, 2022). PEG is water soluble and can be easily modified using photoreactive groups such as methacrylates (to produce PEGDMA) or bioactive compounds such as growth factors. Additionally, when cross-linked, PEG based hydrogels show impressive mechanical properties which could modulate the poor mechanical properties generally associated with HA hydrogels (Abrego *et al.*, 2022).

Due to the resistance of PEGDMA hydrogels to degradation, they may impart resistance to a HA based hydrogel to degradation. As shown in a study by Khetan and Corey, (2019), PEGDMA was combined with methacrylated HA for the purpose of increasing the ability of hydrogels to withstand degradation for the purpose of extending shelf-life of cryopreserved tissue engineering products. Shelf-life is an important consideration for any product which could potentially be marketed. This study purported PEGDMA as having excellent biocompatibility and the ability to maintain cells embedded in its matrix. Their study ultimately showed that this polymer matrix system could be utilised for long term storage of tissue engineered constructs for “off-the-shelf” applications due to the excellent ability of PEGDMA to withstand degradation.

2.6 NEUROTROPHIC COMPOUNDS

The inclusion of neurotrophic compounds is vital in nerve regeneration for neural development, survival, outgrowth, and branching of neurons (Pandey and Mudgal, 2022). However, many of the best known factors are expensive which can hinder upscaling of production of nerve conduits. These factors include nerve growth factor (NGF), brain-derived neurotrophic factor (BDNF), neurotrophin-3 (NT-3) and NT-4/5. Additionally, the *in vivo* response to these growth factors can vary significantly depending on the delivery method. Many of these growth factors have short half-lives and therefore, require sustained drug release over the life time of the conduit which can add another layer of difficulty in design and production (Baazaoui and Iqbal, 2022).

To counteract some of these issues, alternative compounds were investigated which were shown to portray neurotrophic like characteristics but are regularly accessible and stable in the body.

2.6.1 Melatonin

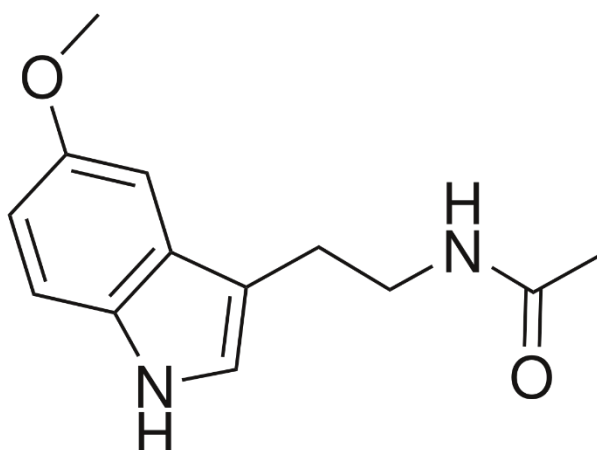


Figure 15. Structure of the melatonin molecule (C. Buckley, 2023).

Following nerve injury, the body begins the process of self-regeneration. However, it is pertinent that this is done as quickly and efficiently as possible as any delay can lead to scarring and neuroma formation, and thus, insufficient recovery. For this reason, many researchers have turned to investigating neurotrophic compounds to support nerve regeneration in the body. One such compound is melatonin, a potent anti-oxidant of which interest has surged among researchers. Melatonin is one of the primary hormones of the

pineal gland and is responsible sleeping and waking regulation. It is for this reason that melatonin is commonly used as a treatment for insomnia. It has been speculated that melatonin could be an effective neuroprotective agent and has been shown to promote axonal regrowth and sprouting in a study by Edizer *et al.*, (2019) and Turgut and Kaplan, (2011).

In a study by Wongprayoon and Govitrapong, (2015), 100 nM melatonin was found to attenuate neuro-inflammation in SH-SY5Y cells. This neuro-inflammation was induced by methamphetamine via the MT2 receptor, a receptor with high affinity for melatonin. In this study, cells were pre-treated with melatonin prior to methamphetamine exposure to evaluate the neuroprotective effects of melatonin. This neuro-protective response was also found to be inhibited by pre-inhibition with luzindole, an agonist of the melatonin MT1 and MT2 receptors. Another study by Stazi *et al.*, (2021), found significant increase in axon length post transection injury when treating rat primary cerebellar granular neurons (CGN) with 10 nM melatonin. The authors also found significant increases in Schwann cell proliferation.

2.6.2 Tyrosol

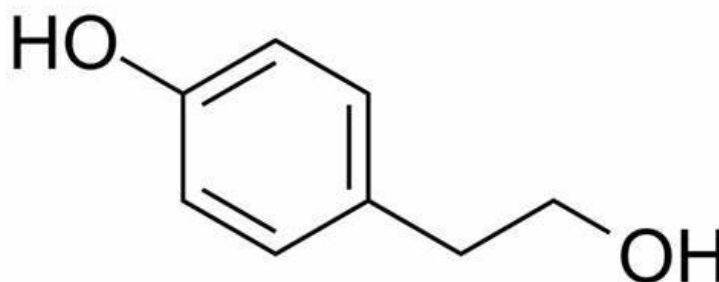


Figure 16. Structure of the Tyrosol molecule (C. Buckley, 2023).

Very little research is available on tyrosol, however, there is a growing body of work on hydroxytyrosol. Hydroxytyrosol (HT) is a phenolic compound that is found in olive oil and has gained traction in recent years as being the main reason for the cardio and neuroprotective effects of olive oil. This compound has been reported to possess anti-oxidant, anti-cancer, anti-inflammatory and neuroprotective properties. A study by Ristagno *et al.*, (2012) showed the neuroprotective effects of HT in diabetic neuropathy, where thermal response latency was significantly improved. Thermal response latency indicates the

protection of small sensory fibres against diabetes. Kamil *et al.*, (2020) demonstrated the proliferative capacity of HT in Schwann cells exposed to low doses (approximately 70 and 140 nM). It was hypothesized that tyrosol may possess similar capabilities to hydroxytyrosol, especially as tyrosol is a constituent of rhodiola. Rhodiola has been reported to have neuroprotective effects and is used as an adaptogen. It is clear from the literature that salidroside, a key component of rhodiola, has been found to have neuroprotective effects but there is little data on the molecule of which it is a glucoside- tyrosol. Liu *et al.*, (2017) reported how 0.2 mM salidroside resulted in significantly increased growth and proliferation of Schwann cells. Based on the data available for hydroxytyrosol and salidroside, a concentration range for tyrosol was developed for initial screening.

2.7 STEREOLITHOGRAPHY 3D PRINTING

Stereolithography (SLA) 3D printing is a vat photo-polymerisation technique which uses light irradiation in the form of a laser to initiate photo-polymerisation in a vat of resin to produce solid, intricate objects with high spatial resolution. Using this technique, it is possible to achieve layer thicknesses as low as 1 μm . This technique is now well established in many industries from automotive to jewellery making, however, it is only in recent years that it is really showing its potential in the medical and pharmaceutical fields with potential to establish itself in personalised medicine, drug elution and surgical tools (Lakkala *et al.*, 2023). SLA requires the generation of reactive species upon exposure to the laser irradiation, therefore for polymers like HA and PEGDMA, a photoinitiator is required to enable polymerisation. These photoinitiators are reactive species which generate free radicals capable of attacking and modifying the functional groups of monomers, forming a polymer. In a study by Hossain Rakin *et al.*, (2021) methacrylated hyaluronic acid (HA-MA) was synthesized and 3D printed using SLA. In their study, they found that the polymerisation and mechanical properties increased with increasing degree of modification. Therefore, it is vital to ensure that enough reactive functional groups are present for SLA.

CHAPTER 3. MATERIALS AND METHODS

3.1 MATERIALS

3.1.1 Cell lines

In this project, two continuous cell lines were utilised due to time and resource limitations. These cell lines were chosen as the best representative cultures available at that time to provide insight into responses in human neuronal cells, SH-SY5Y, and rat Schwann cells, RT4 D6P2T. Although there are significant limitations associated with the use of a continuous cell lines over a primary cell line, there is justification for the use of secondary cell lines in initial biocompatibility screening. The two chosen cell lines will be discussed in further detail below.

3.1.1.1 SH-SY5Y cell line

The SH-SY5Y cell line is a well-characterised and widely used cell line as an *in vitro* model for neurodegeneration, neurotrauma, developmental neurotoxicity and neurite outgrowth in neurobiological research. This cell line was originally derived from a neuroblastoma tumour of a 4 year old female suffering from bone marrow metastasis. The parent line, SK-N-SH, was sub-cloned three times to produce SH-SY5Y cells (Dravid *et al.*, 2021).

When used in the undifferentiated state, as was done in this project, SH-SY5Y express markers indicative of immature neurons and grow as a culture of both floating epithelial-like cells and adherent neuroblast-like cells (Kovalevich, Santerre and Langford, 2021). They proliferate rapidly and appear non-polarized with few, short processes. However, they possess the ability to be differentiated using a variety of methods to produce specific neuron sub-types such as adrenergic, cholinergic, and dopaminergic neurons (Kovalevich and Langford, 2013). Fully differentiated SH-SY5Y cells have been demonstrated to express numerous markers of mature neurons such as growth-associated protein (GAP-43) and synaptophysin (SYN), and to lack expression of glial markers such as glial fibrillary acidic protein (GFAP). This indicates that differentiation results in a homogenous neuronal population.

As SH-SY5Y cells were utilised undifferentiated in this study, care was taken to ensure only neuroblast-like cells were used to provide the best possible model of neurotoxicity. These neuroblast-like cells have been shown to possess tyrosine hydroxylase (TH) and dopamine- β -hydroxylase which would be characteristic of catecholaminergic neurons. Whereas the epithelial-like counterparts do not. Numerous studies have evaluated the use

of undifferentiated SH-SY5Y cells and highlighted their utility in Parkinson's disease research (Jiang *et al.*, 2019) and neurotoxicity studies (Amar, Donohue and Gust, 2023).

Despite the limitations associated with the use of a secondary cell line, there is ethical justification in utilising a secondary cell line for initial screening stages of a project. Additionally, the use of SH-SY5Y provides a human cell line indicative of early immature neuron responses. This cell line was used for screening of compounds for nerve conduit development by other researchers also who utilised SH-SY5Y and the 3-[4,5-dimethylthiazol-2-yl]-2,5 diphenyl tetrazolium bromide MTT assay to determine biocompatibility (Stocco *et al.*, 2021).

3.1.1.2 RT4 D6P2T cell line

RT4 D6P2T, a rat neural Schwannoma cell line, was used as a glial cell model for this project. This cell line was derived from an N-ethyl-N-nitrosourea (ENU) induced rat peripheral neurotumour (RT4). The RT4-AC cell line was subsequently isolated and developed a distinct cell type, RT4-D, which was later subcloned to produce the D6P2T variant (Xia *et al.*, 2023). This cell line has been well-established as a suitable glial cell model due to the expression of myelin proteins and S100 protein which are glial cell specific. This expression has been shown to be superior in the RT4 D6P2T cell line than other glial cell models (Hai *et al.*, 2002).

Human dorsal root ganglion (DRG) would be the ideal cell type to use in this study as they carry the sensory messages from various receptors such as pain and temperature at the periphery towards the CNS for a response. However, these cells are very expensive and can be difficult to purify the culture of contaminating cells (Zuchero, 2014). For this reason, many studies have made use of the RT4 D6P2T cell line as a model for the peripheral nerve regeneration (Lizarraga-Valderrama *et al.*, 2021; Abu-Niaaj, Harris and Pixley, 2020).

3.1.2 Investigation into the effect of molecular weight on the cytocompatibility of hyaluronic acid in neuronal and glial cell lines

Dulbecco's modified eagle medium (DMEM) high glucose (4500 mg/L) with sodium bicarbonate, Penicillin-Streptomycin (10,000 units penicillin and 10mg/ml Streptomycin), L-glutamine (200 mM), Fetal Bovine Serum, Dimethyl Sulfoxide (DMSO), Trypan Blue, Non-essential amino acids (NEAA), 3-(4,5-Dimethylthiazol-2-yl)-2,5-Diphenyltetrazolium Bromide (MTT), Resazurin Sodium salt, Dulbecco's Phosphate buffered saline (PBS),

poly-D-lysine 30,000- 70,000 gmol⁻¹ (PDL), Alcian Blue (8GX), glacial acetic acid, guanidine hydrochloride and trypsin-EDTA all from Sigma Aldrich Ltd. Hyaluronan sodium salt 8,000- 50,000 Da and 30,000- 50,000 Da was purchased from Glentham Ltd. Hyaluronan sodium salt 300,000-500,000 Da, 1,000,000- 1,250,000 Da and 2,000,000- 2,200,000 Da were purchased from Contipro. T75 and T25 vented cell culture flasks, 96 well, 48 well, 24 well, 12 well and 6 well tissue culture plates, and 50 ml falcon tubes were all purchased from Sarstedt and provided by the BRI, TUS.

3.1.3 Modification of hyaluronic acid to enable UV photo-crosslinking

Formamide, dimethyl formamide, 4-dimethylaminopyridine (DMAP), N,N'-Dicyclohexylcarbodiimide (DCC) and 1-Ethyl-3-(3-dimethylaminopropyl) carbodiimide (EDC) were purchased from Glentham Ltd. Folins ciocalteau, dialysis tubing, sodium chloride, hydrochloric acid, methacrylic anhydride, Ellmans reagent (DNTB) were purchased from Merck, Ireland.

3.1.4 UV Photo-crosslinking of modified hyaluronic acid

Polyethyleneglycol dimethacrylate (PEGDMA) 400 was purchased from Polysciences. Irgacure 2959 was purchased from Merck. The UV curing system used was from Dr. Gröbel UV-Elektronik GmbH, Ettlingen, Germany. Carbazole, sodium tetraborate, sodium carbonate, methacrylic acid, concentrated sulfuric acid, acetic acid, molecular grade ethanol, Neutral Red reagent and sodium hydroxide pellets were purchased from Merck, Ireland.

3.1.5 Stereolithography 3D printing

Form 2 resin tanks were purchased from Formlabs. Diphenyl (2,4,6-trimethylbenzoyl) phosphine Oxide (TPO) was purchased from TCI chemicals. Methanol was purchased from Merck Ireland.

3.1.6 Identification and incorporation of neurotrophic compounds

Melatonin and Tyrosol (2-(4-Hydroxyphenyl) ethanol were purchased from Glentham UK. BrdU Cell Proliferation Assay was purchased from Merck Ireland.

3.1.7 Tyrosol Drug Delivery

Phosphoric acid solution 49.5- 50.5 %, acetonitrile and clear glass HPLC vials were purchased from Merck Ireland.

3.2 INVESTIGATION INTO THE EFFECT OF MOLECULAR WEIGHT ON THE CYTOTOXICITY OF HA

3.2.1 Cell Culture

Two cell lines were used during this investigation, SH-SY5Y, a neuroblastoma cell line, and RT4-D6P2T, a glial cell line. Through method development it was determined that cell performance is largely dependent on propagation, confluence and passage number.

To ensure reproducibility, a cell bank of SH-SY5Y and RT4-D6P2T cells was established from passage 35 and passage 19 respectively.

Table 5. Cell Culture Media Composition

	Propagation media	Resuscitation media	Freezing media	Cytotoxicity testing media	Differentiation media
DMEM high glucose	√	√	-	√	√
l-glutamine	0.584 g/L	0.584 g/L	-	0.584 g/L	0.584 g/L
Pen/ Strep	10 mL/L	10 mL/L	-	10 mL/L	10mL/L
FBS	10% v/v	15% v/v	10% v/v	10% v/v	0.1% v/v
NEAA (for SH-SY5Y)	1% v/v (for SH-SY5Y only)	1% v/v (SH-SY5Y only)	-	1% v/v (SH-SY5Y only)	1% v/v (SH-SY5Y only)
DMSO	-	-	10%	-	-

3.2.2 Cell propagation

Cells frozen at 2×10^6 /vial at passage 35 and 19 (SH-SY5Y/RT4 D6P2T respectively) were thawed by adding 1ml warm propagation media to each vial. Frozen medium was removed by suspending the contents of one vial in 10 ml of propagation medium in a 50 ml falcon tube. Thawed cells were centrifuged at $400 \times g$ for 5 min. The cell pellets were then resuspended in resuscitation medium and seeded at 10^6 /T-75 flask. Flasks were incubated at

37 C and 5% CO₂ for 2–3 days before splitting to ensure cells were free of DMSO. Both cell lines were allowed a 7 day recovery period prior to assaying.

3.2.3 Cell Characterisation

Optimal seeding density of both cell lines was determined via the 3-[4,5-dimethylthiazol-2-yl]-2,5 diphenyl tetrazolium bromide MTT assay. T75 flasks were cultured to 70% confluence before seeding 96 well plates at cell densities of 0.5 x 10⁴, 1 x 10⁴, 0.5 x 10⁵, 1 x 10⁵, 0.5 x 10⁶ and 1 x 10⁶ cells/ml. In order to assess cell viability and cell density, cells were counted during each passage. After centrifuging, the supernatant was discarded and pelleted cells were re-suspended in 10 ml propagation media and triturated to ensure a single cell suspension. 200µl of cell suspension was combined with 300µl sterile PBS and 500µl 0.4% Trypan blue. 10µl of this solution was loaded into each counting chamber of a clean haemocytometer. Cells were counted in five squares, including only edge cells on the top and left of individual quadrants, in triplicate. The cell density was then calculated by using the formula below:

$$\text{Total number of cells/ml} = \frac{(\text{Total cell count}) \times 5}{15} \times 10^4 \text{ cells/ml}$$

Where:

“10⁴” refers to 10,000 cells/ml

“5” refers to the dilution factor of cells to 0.4% Trypan Blue

“15” refers to the total number of squares counted over three separate counts

The result from this formula was given in no. of cells/ml and thus could be diluted to give the appropriate seeding density required.

After counting, cell viability was calculated by the following formula:

$$\text{Cell Viability} = \frac{\text{Total no. live cells}}{\text{Total no. cells counted}} \times 100$$

For validation purposes, cells with a viability less than 90% were not used in cytotoxicity assays.

3.2.4 Cell seeding

Confluent cells (70-80%) in T-75 flasks were detached using a trypsin–EDTA solution. Propagation medium was then added to neutralize the trypsin, before pelleting the cells by centrifugation at 400 x g for 5 min. Supernatants were removed, and cell pellets were re-suspended in propagation medium and counted using a haemocytometer. Cell densities were adjusted to 0.5×10^6 cells/ml for SH-SY5Y and 0.25×10^6 cells/ml for RT4 D6P2T as this was determined optimal through the cell characterisation assays. Cells were seeded into tissue culture plates and incubated overnight at 37°C and 5% CO₂ to allow for attachment. Cell viability was determined to be consistently over 90% in a standard trypan blue exclusion method prior to the seeding of cells. Exposure to test substances occurred either during the overnight attachment period, or following the overnight attachment period depending on the nature of the substance to be tested.

3.2.5 Plate coating

A 0.1mg/ml solution of poly-D-lysine (PDL) was prepared and sterile filtered. PDL was used as a diluent for the preparation of various HA solutions after evaluating the benefits of PDL on coating homogeneity vs water (Figure 22). The coating was qualitatively analysed using the Alcian Blue assay (Figure 21). 24 well tissue culture plates were coated by pipetting 300µl of HA/ modified HA solution into designated wells and incubating overnight at room temperature (R.T) protected from light. After overnight incubation, the solution was removed from the plates and the plates were allowed to dry for 30 mins within the laminar flow hood. The plates were then washed 2x with sterile water. The plates were allowed to fully dry prior to seeding with cells or qualitative analysis via Alcian Blue Assay.

A 1% w/v solution of Alcian blue (8GX) was prepared in 3% v/v acetic acid (pH 2.5). HA solutions were prepared in PDL and placed in designated wells for coating and standards. Coated wells were prepared as previously described, whereas standards were prepared by pipetting the HA solution into each well and proceeding with the assay without removal or washing of HA solutions. 300 µl of this Alcian Blue solution was added to each test well and incubated at 37 °C for 30 mins. After 30 mins, the plates were washed 2x with sterile PBS and dried at R.T. for 30 mins before solubilising with 6M guanidine HCl for 72 h in a stirring incubator at 70 rpm, 37 °C. The solubilised dye was placed in a 96 well plate in duplicate and the plates were then read in a UV-Vis plate reader at 620 nm.

3.2.6 The effect of molecular weight on the cytocompatibility of HA in neuronal and glial cell lines

3.2.6.1 Qualitative analysis of the effect of molecular weight on HA coating

Having established that PDL was necessary to ensure homogenous HA coating of the tissue culture wells, a range of HA molecular weights were screened in order to select the optimal molecular weight as a lead candidate for inclusion into the hydrogel conduit. HA of various molecular weight ranging from 30 kDa to 2200 kDa were dissolved in 0.1 mg/ml PDL and used to coat 24 well tissue culture plates as outlined previously. The plates were then stained with Alcian Blue, solubilised and analysed as outlined in 3.3.5 above. Following qualitative analysis of the effect of molecular weight on HA coatings, the viscosity of the different molecular weight solutions was analysed using a TA instruments discovery hybrid rheometer (HR30).

3.2.6.2 The effect of molecular weight on solution viscosity

1 % w/v HA solutions of various MW (30-50, 300-500, 1000-1250 and 2000-2200 kDa) were prepared in 0.1 mg/ml PDL and stirred at 550 rpm for 2h protected from light. To assess the effect of molecular weight on solution viscosity, samples were analysed using a TA instruments HR30 rheometer fitted with a 20 mm cone geometry. Samples were analysed under shear rates of 1 to 1000 $1.s^{-1}$ to analyse and compare the effect of shear stress on the viscosity of the samples. Axial force was constrained to $0.1 \pm 0.01N$.

3.2.6.3 The effect of molecular weight on cell viability

The effect of molecular weight on cell viability of neuronal and glial cells exposed to HA was assessed using the resazurin reduction assay. 24 well tissue culture plates were coated in various molecular weight HA solutions as outlined in section 3.2.5. Neuronal and glial cells were seeded at cell densities of 0.5×10^6 and 0.25×10^6 cells/ml respectively. The cells were allowed to adhere to the coated plates overnight in a $37^\circ C$, 5 % CO_2 incubator. After overnight incubation, cell viability was assessed using the modified resazurin reduction assay (ii) and the trypan blue assay.

(i) Resazurin reduction assay

The resazurin reduction assay works on the principle that actively metabolising viable cells will convert resazurin to the fluorescent resorufin which can then be detected at an excitation and emission of 530/ 590. Through optimisation it was determined that a four hour incubation with resazurin was sufficient for sensitivity without over saturation. Resazurin

working solution was prepared by first preparing a 0.5 %wv stock solution of resazurin in sterile 1X PBS and sterile filtering through a 0.2 µm filter. This solution was diluted in fresh culture media as required. The resazurin reduction assay was conducted by removing spent media from cells before adding the working solution of resazurin in media (0.02 %wv) to cells and incubating for a period of 4 hours. Where necessary, after 4 hours the supernatant was transferred to 96 well plates before reading the fluorescent intensity at 530/ 590 ex/ em.

(ii) Modified resazurin reduction assay

The modified resazurin assay works in the same manner as the traditional resazurin assay with the addition of media removal steps. Media removal steps were introduced prior to the addition of resazurin and after 4 hour incubation in order to replicate the mechanical disruption of an MTT assay. The justification for this was that it was noted that when cells were seeded onto the surface of HA coated plates, they did not spread and adhere as expected and instead stayed rounded. However, these cells still metabolised resazurin to resorufin and therefore were deemed viable. The modified resazurin was used in order to quantify these cells as a function of dye exposure.

Cells were seeded on HA-PDL coated plates and placed in the incubator to adhere overnight at 37 °C, 5% CO₂. After overnight incubation, spent media was removed and placed into eppendorfs for counting. A working stock of resazurin in media (0.02 %wv) was placed in each well at a volume suitable for the tissue culture plate used, and the cells were incubated for a further 4 hours. Total exposure time to HA coatings was 24 hours as outlined in ISO 10993-5. After incubation, the supernatant from each well was removed and centrifuged to enable counting of cells. The supernatant was then placed in a 96 well plate and the fluorescent intensity was detected at 530/ 590 ex/em.

(iii) Trypan Blue Exclusion (TBE) Assay

The TBE assay uses trypan blue to evaluate viability through the integrity of the cell membrane. In viable cells, trypan blue cannot penetrate the cell wall and therefore no uptake of dye is observed. However, as cell viability decreases, so too does the integrity of the cell membrane and thus, uptake of trypan blue increases. This can then be quantified through cell counting. At media removal stages of the MTT and resazurin reduction assay, the cells which were in suspension from each well, due to lack of adhesion to HA, were stored in labelled eppendorfs maintaining replicates. To 0.2 ml of each cell solution, 0.3 ml PBS and 0.5 ml 0.4 %wv Trypan Blue was added and immediately pipetted to a haemocytometer for

counting. Counts were performed in triplicate and the cell density and viability were calculated as outlined in section 3.2.3 above.

3.2.7 Characterisation of LMW HA coating

24 well tissue culture plates were coated as outlined in 3.3.5 above. Briefly, a 1 % w/v solution of 30-50 kDa HA was prepared in 0.1 mg/ml PDL. 0.3 ml HA solution of various concentration (0, 0.001, 0.01, 0.05, 0.1, 0.5, 1 % w/v) was pipetted into individual wells of the tissue culture plates. In the case of coatings, the plates were incubated overnight at R.T. protected from light before washing the plates 2x with sterile water. In the case of standards, the HA solution remained in the well and alcian blue solution was added into the well in conjunction with the HA solution. The Alcian blue assay was then conducted as outlined in section 3.3.5.

3.2.8 The effect of LMW HA on cell viability and attachment

In this section, the MTT and resazurin reduction assay were used to determine the effect of LMW HA on cell viability and attachment.

The MTT assay is a commonly used colorimetric assay to measure cell viability and assess cytotoxicity. This assay was first developed by Tim Mosmann in 1983 (Mosmann, 1983) and relies upon the conversion of the yellow tetrazolium salt into insoluble formazan crystals by mitochondrial enzymes in metabolically active cells (Gonzalez and Tarloff, 2001; Fedotcheva and Beloborodova, 2022). The purple formazan crystals can then be detected spectrophotometrically.

The resazurin reduction assay also relies upon enzymatic conversion by mitochondrial enzymes to convert resazurin to the fluorescent resorufin (Lavogina *et al.*, 2022). However, a key difference is that this conversion does not involve crystal formation and can be detected in the media without the need for various wash steps and solubilisation.

(i) MTT cell viability assay

The MTT assay was initially employed as a method of quantifying cell viability through metabolic activity as the production of formazan is directly proportional to metabolic activity of the cells. MTT reagent was prepared and filter sterilised to give a final concentration of 0.5 mg/ ml in cell culture media. Spent media from each well was removed and replaced with this working solution of MTT. The plates were incubated for 4 h at 37 °C. After 4 h, the media was removed and the formazan was solubilised with the addition of DMSO. The

plates were placed in a stirring incubator at 70 rpm, 37 °C for 15 mins to ensure complete solubilisation before reading the absorbance at 540 nm in a microplate reader. Where necessary, solubilised formazan was transferred to 96 well plates before reading the absorbance.

(ii) MTT Attachment assay

After 20 h exposure to HA coated plates, media from each well was removed to labelled eppendorfs in triplicate, to maintain replicates, and pelleted by centrifugation at 1000 rpm and 4 °C for 5 minutes (Count 1, Figure 17). Propagation media containing 1X MTT was added to each well of one 24 well plate, while propagation media alone was added to each well of the other 24 well plate. Both plates were returned to the incubator at 37 °C and 5% CO₂.

The eppendorfs were retrieved and the supernatant discarded. The pellet was re-suspended in 200 µl propagation media. Each Eppendorf was counted using a haemocytometer by adding 300 µl PBS and 500 µl trypan blue. The number and viability of cells counted after exposure to various concentrations of HA were recorded.

After 24 h exposure to HA (inclusive of 4 h MTT incubation), media from each well of the 2 plates was removed to labelled eppendorfs in triplicate and pelleted by centrifugation at 1000 rpm and 4 °C for 5 minutes (Count 2, Figure 17). In the case of the MTT dye exposed plate, DMSO was added to each well and the plate was placed in a shaking incubator for 15mins to allow for complete solubilisation of the formazan crystals. In the control plate (no MTT), 300 µl trypsin-EDTA was added to each well for 3 minutes before quenching with propagation media and removing to labelled eppendorfs in triplicate and pelleted by centrifugation at 1000rpm and 4°C for 5 minutes (Count 3, Figure 17). The eppendorfs were then counted as outlined in section 3.2.3.

After complete solubilisation of the formazan, the 24 well plate was read in a spectrophotometer at 540 nm with a background measurement of 630 nm.

This procedure was performed for both cell lines and a minimum of N=3 was obtained for each cell line.

(iii) Resazurin Attachment Assay

After 20 h exposure to HA coated plates, media from each well was removed to labelled eppendorfs in triplicate and pelleted by centrifugation at 1000 rpm and 4 °C for 5 minutes

(Count 1, Figure 18). Propagation media containing 1X Resazurin was added to each well of one 24 well plate, while propagation media alone was added to each well of the other 24 well plate. Both plates were returned to the incubator at 37 °C and 5% CO₂.

The eppendorfs were retrieved and the supernatant discarded. The pellet, if present, was re-suspended in 200µl propagation media. Each Eppendorf was counted using a haemocytometer by adding 300µl PBS and 500µl trypan blue. The number and viability of cells counted after exposure to various concentrations of HA were recorded.

After 24 h exposure to HA (4 h Resazurin incubation), media from each well of the 2 plates was removed to labelled eppendorfs in triplicate and pelleted by centrifugation at 1000 rpm and 4 °C for 5 minutes (Count 2, Figure 18). In the case of the resazurin dye exposed plate, the supernatant from centrifugation was read in a fluorescent plate reader at ex/em 530/590. It had previously been confirmed than centrifugation does not affect the fluorescence of the resorufin formed. In the control plate (no resazurin), trypsin-EDTA was added to each well for 3 minutes before quenching with propagation media and removing to labelled eppendorfs in triplicate and pelleted by centrifugation at 1000rpm and 4°C for 5 minutes (Count 3, Figure 18). All eppendorfs were then counted as outlined in section 3.2.3.

This procedure was performed for both cell lines and a minimum of N=3 was obtained for each cell line.

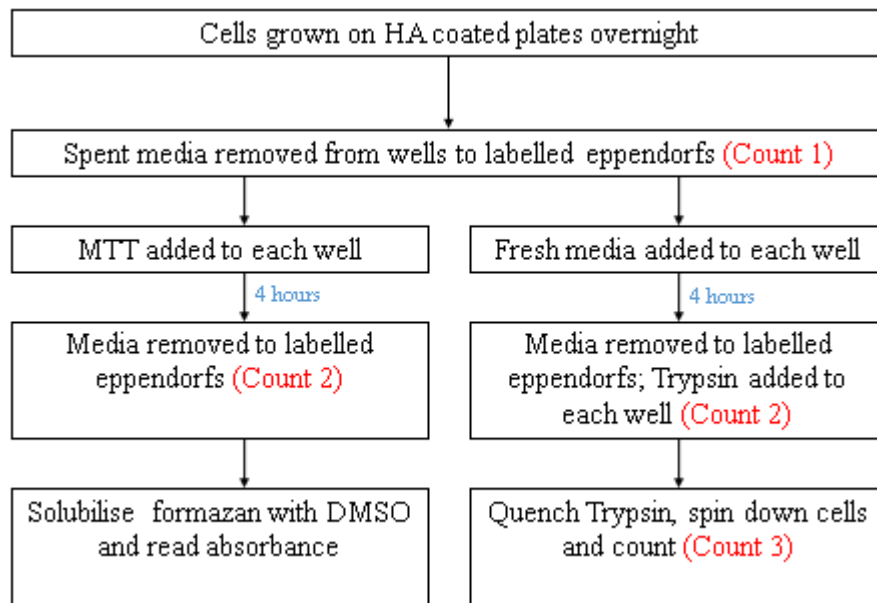


Figure 17. Investigation of MTT attachment assay using parallel TBE assay. Flowchart outlining the main assay steps in the parallel assay streams. Assays were conducted in 24 well tissue culture plates with SH-SY5Y and RT4 D6P2T cell lines and a minimum of N=3 was obtained for each cell line.

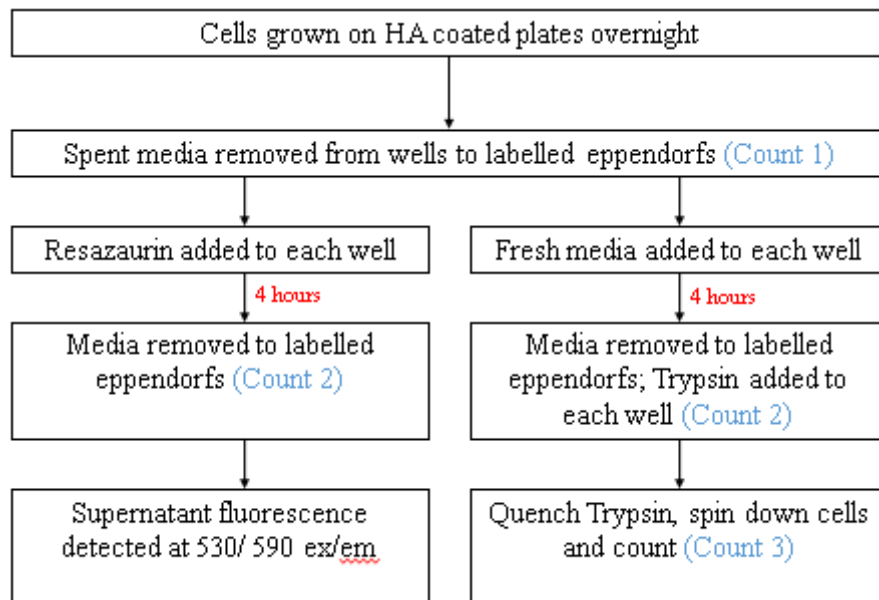


Figure 18. Investigation of Resazurin attachment assay using parallel TBE assay. Flowchart outlining the main assay steps in the parallel assay streams. Assays were conducted in 24 well tissue culture plates with SH-SY5Y and RT4 D6P2T cell lines and a minimum of N=3 was obtained for each cell line.

3.3 MODIFICATION OF HA TO ENABLE UV PHOTO-CROSSLINKING

3.3.1 *Thiolation of HA*

A 4 %w/v solution of 30-50 kDa HA was prepared in deionised water and placed on ice. Molar equivalents of EDC HCl and DMAP were added to the HA solution and the solution was left stirring on ice for 1 hour to enable activation of the carboxylic acid moiety. After 1h, a 2 molar excess solution of cysteamine HCl in formamide was added to the HA solution under nitrogen. The reaction was allowed to proceed overnight protected from light. After 24 hours, the HA-SH solution was dialysed using dialysis tubing (MWCO 12-14 kDa) vs 100 mM NaCl with water changes every 4 hours for 48 hours. For the final water change, the pH of the dialysis solution was reduced to pH 2.5 to disassociate the HA- dialysis tubing complex that could form. Following dialysis, the dialysate was vacuum filtered using a Buchner funnel and the filtrate was decanted into 100 ml round bottom flasks for freeze drying. Once decanted, the round bottom flasks were sealed with parafilm and placed at -20 °C for 48 hours to ensure samples were completely frozen. After 48 hours, samples were freeze dried using a lyophiliser. Freeze dried samples were recovered and quantified before storing protected from light at -20 °C until needed.

3.3.2 *Methacrylation of HA*

A 4 %wv solution of 30-50 kDa HA was prepared in deionised water and stirred until completely dissolved. Through optimisation it was determined that a 20 fold molar excess of methacrylic anhydride produced HA that was approximately 20 % modified as determined via NMR and HPLC. Therefore, a 20 fold molar excess of methacrylic anhydride was slowly added to the HA solution while stirring. The pH was adjusted to 8.5 and the reaction was allowed to proceed overnight. After 24 hours, the resulting solution HA-MA was dialysed using dialysis tubing (MWCO 12-14 kDa) vs basic water (pH 8.0) with four hourly water changes for 24 hours, followed by dialysis vs deionised water (pH 5) with water changes every 4 hours for a further 24 hours with the final four hour dialysis vs acidic water (pH 2.5). Following dialysis, the dialysate was vacuum filtered using a Buchner funnel and the filtrate was decanted into 100 ml round bottom flasks for freeze drying. Once decanted, the round bottom flasks were sealed with parafilm and placed at -20 °C for 48 hours to ensure samples were completely frozen. After 48 hours, samples were freeze dried using a lyophiliser. Freeze dried samples were recovered and quantified before storing protected from light at -20 °C until needed.

3.3.3 Chemical characterisation of modified HA

3.3.3.1 ATR- FTIR analysis of modified HA

Attenuated total reflectance Fourier transform infrared spectroscopy (ATR-FTIR) was used to characterise spectrum changes arising from changes in the chemical structure of the HA molecule. Samples were analysed post lyophilisation using a Perkin Elmer Spectrum One (Perkin Elmer, Waltham, MA, USA) fitted with a universal ATR sampling accessory. Samples were tested in triplicate on three separate batches of modified materials (N=3). All data was recorded at R.T. in the spectral range of 4000- 650 cm^{-1} , utilising 15 scans per sample cycle and a fixed universal compression force of 80 N. Subsequent analysis was carried out using Spectragryph spectrum analysis software.

3.3.3.2 NMR analysis of modified HA

Nuclear Magnetic Resonance spectroscopy was conducted using a Bruker Avance III 500 MHz NMR spectrometer. All spectra were recorded at 25°C. Samples for NMR were dissolved in D₂O at ambient temperature to >10mg/ 0.5ml for ¹³C-NMR, and diluted to ~1-2 mg/mL for ¹H-NMR. ¹H-spectra and ¹H-spectra with water suppression were recorded. For the purposes of purity checking and spectral assignment, ¹³C/DEPT-90/DEPT-135/HH-CoSy/HSQC/HMBC spectra were also obtained.

3.3.3.3 Ellmans assay for the quantification of thiols

The Ellmans assay was employed as outlined by Qie et al. (2021) to determine the total thiol content of the HA-SH sample after lyophilisation, with some modifications. The Ellmans assay is a colorimetric assay which is based on the reaction between a thiol group and 5,5'-dithio-bis(2-nitrobenzoic acid) (DNTB), also known as Ellmans reagent. This reaction produces a TNB chromophore which has a lambda max of 412 nm (Rahman et al., 2006). The rate of formation of the TNB product is directly proportional to the concentration of thiol in the sample. The concentration of thiol in the HA-SH sample was determined from the linear equation or regression curve generated from a series of thiol standards, in this case cysteamine HCl. This method only detects free thiol in the samples and therefore in order to calculate the total thiol content, disulphide bonds formed in the product required cleaving via 8M urea during the Ellmans assay. A set of cysteamine standards were prepared in reaction buffer (TGE buffer, pH 8.0, or TGE buffer with 8M urea) as per Table 6 below. A solution of 250 μl Ellmans (4 mg/ml in TGE buffer) in 12.5 ml reaction buffer was prepared and 250 μl was placed in each well of a 96 well plate. 25 μl of sample was added in triplicate, the plate was mixed and incubated for 15 minutes at R.T. The absorbance was read at 412

nm and the concentration of thiol (mM) was interpolated from the standard curve. Total thiol content was obtained by adding the interpolated concentration (mM) of HA-SH in TGE buffer (free thiol) and HA-SH in 8M Urea (bound thiol).

Table 6. Preparation of Cysteamine Standards

Standard	Vol. of Reaction buffer (ml)	Amount of Cysteamine (MW= 113.61)	Final Concentration (mM)
A	3	0.0005 g	1.5
B	0.0831	0.417 ml of Standard A	1.25
C	0.167	0.334 ml of Standard A	1
D	0.25	0.25 ml of Standard A	0.75
E	0.334	0.167 ml of Standard A	0.5
F	0.417	0.083 ml of Standard A	0.25
G	0.5	0 ml	0 (blank)

3.3.3.4 Reverse Phase High Performance Liquid Chromatography (RP-HPLC)

The degree of methacrylation was determined by RP-HPLC as previously described by Oudshoorn et al., (2007). In order to determine the effect of methacrylic anhydride starting concentration on the degree of substitution obtained, HA-MA was synthesized with different molar equivalents of methacrylic anhydride: 1X, 10X and 30X. These samples were then analysed as follows. HA-MA (15 mg) was dissolved in NaOH (aq. 0.02 M, 10 mL) and incubated at 37 °C for 30 min to enable hydrolysis of bound methacrylate groups from the polymer. A series of dilutions (1:2, 1:5 and 1:10) were prepared from this mixture in eluent and twenty microlitres in triplicate were then injected onto a column (XBridge BEH C18, 4.6 mm × 150 mm, 1.5 µm, 130Å, Waters Corp.). Analysis was performed on Nexera-*i* system (Shimadzu Corp.) equipped with a LC-2040 pump, LC-2040 auto-sampler and a PDA detector model SPD-M40. The elution was performed in isocratic mode at a flowrate of 1 mL min⁻¹ with the mobile phase consisting of acetonitrile: water (15:85) adjusted to pH 2 with orthophosphoric acid. Peak areas from chromatograms obtained at 210 nm were analysed on LabSolutions software (Shimadzu Corp.) and subsequently used to quantify the degree of substitution of methacrylated hyaluronic acid.

3.3.4 Biological characterisation of modified HA

3.3.4.1 Plate coating

24 well tissue culture plates were coated using the procedure as outlined in section 3.3.5. Briefly, 1 % wv solutions of HA-MA and HA-SH were prepared in 0.1 mg/ml PDL and dilutions were prepared to achieve concentrations of 0, 0.001, 0.01, 0.1, 0.5 and 1 % wv. 0.3 ml of each solution was pipetted into individual wells and the plate was incubated overnight at R.T, protected from light. After 24 hours, the solution from each well was removed and the plates were allowed to dry for 1 hour before washing 2x with sterile water. The plates were allowed to dry for a further 30 mins before seeding with cells or being wrapped with parafilm and stored at 4 °C.

3.3.4.2 Resazurin Reduction Assay

Neuronal and glial cells were seeded on either HA-SH or HA-MA coated plates at a cell density of 0.5×10^6 cells/ml (SH-SY5Y) or 0.25×10^6 cells/ml (RT4 D6P2T). The cells were allowed to adhere overnight at 37 °C and 5% CO₂ before assaying with resazurin. Resazurin working solution was prepared as outlined in section 3.2.6.3 (ii) and this solution was added to cells after 20 hour exposure to the modified HA coatings. The cells were incubated with 1X resazurin solution for four hours (total of 24 hour exposure to modified HA coatings) before detecting the fluorescent signal emitted from the resorufin at ex/em 530/ 590. Tissue culture plates were read directly after confirming that the coating did not interfere with the fluorescence signal.

3.3.4.3 Neutral Red Uptake Assay

The neutral red uptake assay relies upon the uptake of the supravital dye neutral red (3-amino-7-dimethylamino-2-methyl-phenazine hydrochloride) by viable cells. The binding of this weak cationic dye occurs in lysosomes (Ates *et al.*, 2017). Neutral red assay in both uptake and release methodologies have found utility in many biomedical and environmental applications (Repetto, del Peso and Zurita, 2008).

A neutral red stock solution was prepared by dissolving 40 mg/ml neutral red dye in 10 ml 1X PBS. This solution was sterile filtered and stored at R.T, protected from light. To prepare a working solution, the stock solution was diluted 1: 100 the day before use in sterile culture medium and stored overnight at 37 °C as outlined in a method by Repetto *et al.*, (2008).

Cells were seeded as described before in section 3.3.4.2 on HA derivative coated plates. The cells were allowed to adhere overnight at 37 °C and 5% CO₂. After overnight incubation,

spent media was removed from each well before adding 0.004 %wv neutral red in fresh media. Neutral red dye (300 µl) was added to each well and the plate was incubated for a further 4 hours (24 hours total exposure time). After incubation, the cells were washed with sterile PBS and a solution of 1 %wv glacial acetic acid in 50 %vv ethanol was added to each well to extract the dye. This dye was then detected at 540 nm in a UV-Vis plate reader.

Data was analysed using GraphPad Prism V8.01.

3.3.4.4 *Hyaluronidase degradation of modified HA*

24 well tissue culture plates were coated in either HA, HA-SH or HA-MA respectively by dissolving the HA or HA derivative in 0.1 mg/ml PDL and coating each well with 0.3ml of this solution. After washing and drying the coated plates as outlined in section 3.3.5, a control solution (PBS) or 0.4-1 IU hyaluronidase was added to each well and aliquots were collected every 15 minutes to monitor the degradation of HA. The aliquots were collected by removing the entire solution from the well to eppendorfs, maintaining replicates, before replacing with fresh control solution or enzyme. These samples (in triplicate) were then put through a carbazole assay (N=2) to quantify the uronic acid present in each sample. The carbazole assay is a colorimetric method of quantification of uronic acid which is a component of hyaluronic acid (Li et al., 2020). In this way, this assay can measure the relative amount of HA in a sample. A negative control of PDL without HA was used to provide a baseline control of uronic acid detected in the carbazole assay. In this study, the carbazole assay was used to quantify the amount of HA degraded from the coating via hyaluronidase in order to evaluate the differences in degradability between unmodified, thiolated and methacrylated HA. This study was developed on the basis of previous studies which have utilised hyaluronidase and carbazole in similar manners to monitor the degradation of HA (Li *et al.*, 2019; Sciabica *et al.*, 2023).

3.4 UV PHOTO-CROSSLINKING OF MODIFIED HA

UV Photo-crosslinking of all samples took place in a custom silicon mould placed in a UV curing system (Dr. Grobel U-Electronik GmbH) with a spectral range of between 315–400 nm at an average intensity of 10–13.5mW/cm².

3.4.1 *Thiolated HA Hydrogels*

HA-SH solutions of between 1 %wv and 5 %wv were prepared by dissolving lyophilised HA-SH in deionised water and stirring until a homogenous solution was obtained. To this, a methanolic stock of Irgacure 2959 was added to a final concentration of 0.1 %wv per hydrogel. The solution was stirred for a further 30 mins to ensure homogeneity before pipetting into a silicone mould and curing in the UV curing system for 10 mins, after which it was determined whether polymerisation had occurred or not. In the case of un-polymerised samples, residence time in the UV curing system was increased up to a maximum of 30 mins to observe if gelation would occur with longer exposure time. After removal, the hydrogels were blotted free of un-polymerised monomer and used for testing within 72 hours.

3.4.2 *PEGDMA Hydrogels*

PEGDMA hydrogels were prepared by preparing solutions of 100, 75, 50 and 25 %wv PEGDMA in deionised water. The solutions were stirred until homogenous before adding methanolic stock of Irgacure 2959 to a final concentration of 0.1 %wv per hydrogel. The solutions were pipetted into a silicone mould and placed in the UV curing system for 10 mins, after which it was determined whether polymerisation had occurred or not. After removal, the hydrogels were blotted free of un-polymerised monomer and used for testing within 72 hours.

3.4.3 *PEGDHA-MA: HA Hydrogels*

PEGDHA-MA: HA hydrogels were prepared by first preparing a 5 %wv solution of HA-SH or 5 %wv HA-MA and stirring at 750 rpm until dissolved. Once dissolved, hydrogel solutions of PEGDHA-MA: HA concentrations 80, 75, 60, 50, 40, 25, 20 %wv were prepared from the 5 %wv HA-SH and HA-MA stock solution and stirred until homogenous. A methanolic stock of Irgacure 2959 was added to a final concentration of 0.1 %wv. This solution was pipetted into silicone moulds before curing in the curing system for 10 mins, after which it was determined whether polymerisation had occurred or not. In the case of un-polymerised samples, residence time in the UV curing system was increased up to a maximum of 30 mins to observe if gelation would occur with longer exposure time. After

removal, the PEGDHA-MA: HA-SH and PEGDHA-MA: HA-MA hydrogels were blotted free of un-polymerised monomer and used for testing within 72 hours.

3.4.4 *Methacrylated HA Hydrogels*

Methacrylated HA hydrogels were prepared by preparing a 5 %wv stock solution of HA-MA in deionised water and stirring at 750 rpm until dissolved. Hydrogels solutions of various concentration, 100, 75, 50, and 25 %wv were prepared using deionised water as a diluent and stirred until homogenous. Methanolic stock of Irgacure 2959 was then added to a final concentration of 0.1 %wv and stirred for a further 30 mins before pipetting the solution into a silicone mould and placing into the UV curing system for 10 minutes, after which it was determined whether polymerisation had occurred or not. After removal, the cured samples were blotted free of un-polymerised monomer and used for testing within 72 hours.

3.4.5 *Hybrid Hydrogel System*

Hybrid hydrogel systems were prepared by first preparing both the synthetic and natural parts. PEGDMA was stirred at 700 rpm before adding methanolic stock of Irgacure 2959 to a final concentration of 0.1 %wv per hydrogel. In parallel, a 5 %wv stock solution of both HA-SH and HA-MA were prepared and stirred until completely dissolved. Hydrogel solutions were prepared by mixing the polymer solutions in a ratio of 50 (HA-SH): 40 (HA-MA): 10 (PEGDMA) which was determined to be optimal formulation via optimisation. This solution was pipetted into the silicone mould before placing in the UV curing system for 10 mins, after which it was determined whether polymerisation had occurred or not. In the case of un-polymerised samples, residence time in the UV curing system was increased up to a maximum of 30 mins to observe if gelation would occur with longer exposure time. After removal, the hydrogels were blotted free of un-polymerised monomer and used for testing within 72 hours.

3.4.6 *Chemical Characterisation of UV photo-crosslinked hydrogels*

All testing was completed on hydrogels within 72 hours of curing to ensure reproducibility and stability.

3.4.6.1 *ATR- FTIR analysis UV photo-crosslinked hydrogels*

Attenuated total reflectance Fourier transform infrared spectroscopy (ATR-FTIR) was used to characterise spectrum changes arising from changes in the chemical structure of any of the polymers used which would indicate polymerisation. Samples were analysed post UV-

curing using a Perkin Elmer Spectrum One (Perkin Elmer, Waltham, MA, USA) fitted with a universal ATR sampling accessory. Samples were tested in triplicate on three separate batches of hydrogels (N=3). All data was recorded at R.T. in the spectral range of 4000- 650 cm⁻¹, utilising 15 scans per sample cycle and a fixed universal compression force of 80 N. Subsequent analysis was carried out using Spectragryph spectrum analysis software.

3.4.7 Mechanical Characterisation of UV Photo-crosslinked hydrogels

3.4.7.1 Swelling Study and Gel Fraction

Swelling experiments were performed on hydrogel samples in Dulbecco's PBS (pH 7.4). After curing, samples were placed in triplicate in a petri dish and immersed in 30 ml PBS at 37°C until equilibrium weight had been reached. The samples were blotted free of solution, and allowed to equilibrate at R.T. for 5 minutes before weighing. After recording the swollen weight (W_s), the hydrogels were placed in a 37°C vacuum oven at 200 mbar pressure and dried to equilibrium dry weight. The mean swelling ratio of samples were calculated using the formula provided by (Park et al., 2009):

$$\text{Mean Swelling Ratio } (Q) = \left(\frac{W_s - W_d}{W_s} \right) \times \frac{100}{1}$$

Following this, the equilibrium water content of the sample was calculated using the following equation as detailed by (Killion et al., 2011; Burke et al., 2019):

$$\text{Equilibrium Water Content } (EWC) = \left(\frac{W_s - W_d}{W_d} \right) \times \frac{100}{1}$$

Finally, the gel fraction of each gel was calculated using an equation as described by (Killion, 2013):

$$\text{Gel Fraction} = \left(\frac{W_d}{W_{redry}} \right) \times \frac{100}{1}$$

Where W_s , W_d and W_{redry} refer to the weights of the hydrogels in the swollen state (W_s), dry state (W_d) and post re-drying (W_{redry}). Re-drying refers to hydrogels which were dried post polymerisation before swelling in PBS to equilibrium and finally vacuum drying once again to equilibrium dry weight.

3.4.7.2 Rheology

Rheological analysis was performed using an advanced rheometer AR1000 (TA instruments) fitted with a Peltier temperature control to investigate the comparative strength

of samples. Samples were tested in quintuplicate, using individual samples, within 72 hours of preparation using a 20mm parallel steel plate with samples in the equilibrium swollen state. Amplitude sweeps were performed at a constant frequency of 1 Hz with percentage strain ranging from 1×10^{-4} to 1×10^1 . Dynamic frequency sweeps were performed at a constant strain of 0.01% (linear viscoelastic region) with frequency ranging from 1.0×10^{-2} to 1.0×10^2 Hz. Temperature ramps were performed between 4 and 37 °C in 2 °C increments with a soak time of 30 seconds. Prior to testing, samples were cut using a steel bore to 20 mm and blotted free of liquid using filter paper to minimise slippage. The compression load was constrained to 5 ± 0.2 N during testing and the mean \pm SD of the storage and loss modulus under dynamic conditions were reported.

3.4.7.3 Compression

Compression testing was carried out using a screw-driven mechanical testing machine (Lr10K, Lloyd Instruments, Bognor Regis, UK) fitted with a 2.5 kN load cell (N=5). Samples were swollen to equilibrium in phosphate buffered saline (PBS) (pH 7.4) prior to testing and an unconfined compression was carried out at a speed of 1 mm/min using samples that were 20 mm in diameter and 1.8 mm in height. A pre-load of 5 N was employed before compressing samples to 70 % strain. Stress-strain curves were generated from which Young's modulus was calculated based on the linear portion of the graph. The stress at limit was calculated based on the load at the compressive limit of each sample.

3.4.8 Biological Characterisation of UV Photo-crosslinked hydrogels

3.4.8.1 Cytocompatibility of UV Photo-crosslinked hydrogels

The cytocompatibility of UV photo-crosslinked hydrogels was evaluated by both direct contact and elution.

For direct contact, hydrogel samples were prepared in triplicate and cured in 12 well plates and then dried in a vacuum oven overnight. The samples were then sterilised under a UV lamp for 15 mins prior to swelling hydrogel samples in sterile media at 37°C. After swelling overnight, the spent media was removed and cells were seeded at a density of 0.5×10^6 cells/ml for SH-SY5Y and 0.25×10^6 cells/ml for RT4 D6P2T cells. The cell laden hydrogels were incubated overnight at 37°C before assaying using the resazurin reduction assay.

The elution assay was performed by placing 20 mm hydrogel samples in 6 well plates before drying in a vacuum oven at 37°C overnight. The dried samples were sterilised under UV light for 15 mins before swelling the samples in sterile supplemented cell culture media. The

samples were incubated overnight at 37°C in an incubator to allow the hydrogels to swell. Once swollen, the media from each sample was removed and placed in labelled containers to be used as treatment media. SH-SY5Y and RT 4 D6P2T cells were seeded in a 96 well plate and allowed to adhere overnight before removing the spent media and replacing with the treatment media described earlier. The cells were returned to the incubator for 20 hours before assaying using the resazurin reduction assay (Total exposure to treatment media was 24 hours).

3.4.8.2 Degradation of UV Photo-crosslinked hydrogels

The degradability of UV Photo-crosslinked hydrogels was evaluated in physiological, and accelerated conditions.

2.7.1.1.1 In vitro degradation

The degradation of UV photo-crosslinked hydrogels under physiological conditions was evaluated by placing samples of 20 mm diameter in a 6 well tissue culture plate in quintuplicate and submerging each hydrogel in Dulbecco's PBS (pH 7.4). The plates containing the hydrogels were incubated at 37°C and weights and images were recorded every 24 hours for 7 days. Images were captured using a Canon 450 D SLR camera.

2.7.1.1.2 Accelerated degradation study

Hydrogel samples of 20 mm diameter were placed in a 6 well plate as outlined previously, in quintuplicate. Hydrogel samples were submerged in either 5 mM or 5 M NaOH, and weights and images were recorded every 24 hours for 7 days or until the sample had completely degraded.

3.5 STEREOLITHOGRAPHY 3D PRINTING OF HYALURONIC ACID HYDROGELS

3.5.1 Formlabs 2 SLA printer

The form 2 SLA printer from Formlabs is a SLA printer with self-heating tank and a 405 nm violet laser. The maximum build volume possible is 145 x 145 x 175 mm and has a layer thickness range of 25 to 100 microns. The printer was used in open mode with no cartridge and polymer solution was poured directly into the form 2 resin tank. The resin tank blocks light and is made from shatter resistant polycarbonate. Prints were designed on Preform software and the generated computer aided drawing (CAD) file was uploaded to the Form 2 printer prior to printing. All prints were produced on the platform without supports.

3.5.2 Identification of optimal photoinitiator

When producing the UV photo-cured hydrogels, Irgacure 2959 was utilised which has been exhaustively tested for cytotoxicity and has been proven as non-cytotoxic at concentrations not exceeding 0.1 %wv. For this reason, initial trials attempted to use this photoinitiator in concentration ranges from 0.1 %wv up to 5 %wv. However, Irgacure 2959 is most efficiently activated using a 365 nm and therefore, sufficient curing wasn't observed. Diphenyl (2,4,6-trimethylbenzoyl)phosphine oxide (TPO) is a photoinitiator with a longer than usual absorption peak with a wavelength of maximum absorption (λ_{max}) of approximately 425nm. This made TPO a much more suitable photoinitiator for 3D printing, however, it is soluble only in organic solvents. After many trials, it was found that the best result was produced by first preparing a methanolic stock of TPO and diluting it to a final concentration of 1 %wv in the polymer solution.

3.5.3 3D printing of hydrogel samples

Solutions were prepared of polymer or polymer blends as outlined in Table 7 below. These solutions were stirred until dissolved using a hot plate and magnetic stir bar. Once dissolved, the solutions were mixed to create blends and stirred until homogenous. Methanolic stock of TPO was added to the solutions of lone polymer or blends to a final concentration of 1%wv before stirring for a further 30 mins to ensure complete dispersion. The solution was then poured into the resin tank of the Form2 printer and the uploaded CAD file was selected. The printed samples were cured post-printing in a UV curing chamber for 10 mins before rinsing uncured monomer and blotting dry. These samples were used within 72 hours of printing.

Table 7. Sample preparation for SLA 3D printing

	PEGDMA	HA-SH	HA-MA	TPO
100% PEGDMA	49.5 g	-	-	1 %wv
50 % HA-SH 50% PEGDMA	24.75 g	24.75 g	-	1 %wv
50 % HA-MA 50 % PEGDMA	24.75 g	-	24.75 g	1 %wv
50 % HA-SH 40 % HA-MA 10 % PEGDMA	4.95 g	24.75g	19.8 g	1 %wv

3.5.4 Chemical characterisation of 3D printed samples

3.5.4.1 ATR-FTIR analysis of 3D printed samples

ATR-FTIR was used to characterise spectrum changes arising from changes in the chemical structure of the polymers used which would indicate polymerisation. Samples were analysed post 3D printing using a Perkin Elmer Spectrum One (Perkin Elmer, Waltham, MA, USA) fitted with a universal ATR sampling accessory. Samples were tested in triplicate on three separate batches of printed samples (N=3). All data was recorded at R.T. in the spectral range of 4000- 650 cm⁻¹, utilising 15 scans per sample cycle and a fixed universal compression force of 80 N. Subsequent analysis was carried out using Spectragryph spectrum analysis software.

3.5.5 Mechanical testing of 3D printed samples

3.5.5.1 Swelling study and Gel fraction

Swelling experiments were performed on 3D printed samples in Dulbecco's PBS (pH 7.4). After curing, samples were placed in triplicate in a petri dish and immersed in 30 ml PBS at 37°C until equilibrium weight had been reached. The samples were blotted free of solution, and allowed to equilibrate at R.T. for 5 minutes before weighing. After recording the swollen weight (W_s), the hydrogels were placed in a 37°C vacuum oven at 200 mbar pressure and dried to equilibrium dry weight. The mean swelling ratio of samples were calculated using the formula provided by Park et al., (2009):

$$\text{Mean Swelling Ratio (Q)} = \left(\frac{W_s - W_d}{W_s} \right) \times \frac{100}{1}$$

Following this, the equilibrium water content of the sample was calculated using the following equation as detailed by (Killion et al., 2012; Burke et al.):

$$\text{Equilibrium Water Content (EWC)} = \left(\frac{W_s - W_d}{W_d} \right) \times \frac{100}{1}$$

Finally, the gel fraction of each gel was calculated using an equation as described by (Killion et al, 2013):

$$\text{Gel Fraction} = \left(\frac{W_d}{W_{redry}} \right) \times \frac{100}{1}$$

Where W_s , W_d and W_{redry} refer to the weights of the hydrogels in the swollen state (W_s), dry state (W_d) and post re-drying (W_{redry}). Re-drying refers to hydrogels which were dried post polymerisation before swelling in PBS to equilibrium and finally vacuum drying once again to equilibrium dry weight.

3.5.5.2 Rheology

Rheological analysis was performed using an advanced rheometer AR1000 (TA instruments) fitted with a Peltier temperature control to investigate the comparative strength of samples. Samples were tested in quintuplicate, using individual samples, within 72 hours of preparation using a 20mm parallel steel plate with samples in the equilibrium swollen state. Amplitude sweeps were performed at a constant frequency of 1 Hz with percentage strain ranging from 1×10^{-4} to 1×10^1 . Dynamic frequency sweeps were performed at a constant strain of 0.01% (linear viscoelastic region) with frequency ranging from 1.0×10^{-2} to 1.0×10^2 Hz. Temperature ramps were performed between 4 and 37 °C in 2 °C increments

with a soak time of 30 seconds. Prior to testing, samples were cut using a steel bore to 20 mm and blotted free of liquid using filter paper to minimise slippage. The compression load was constrained to 5 ± 0.2 N during testing and the mean \pm SD of the storage and loss modulus under dynamic conditions were reported.

3.5.5.3 *Compression*

Compression testing was carried out using a screw-driven mechanical testing machine (Lr10K, Lloyd Instruments, Bognor Regis, UK) fitted with a 2.5 kN load cell (N=5). Samples were swollen to equilibrium in phosphate buffered saline (PBS) (pH 7.4) prior to testing and an unconfined compression was carried out at a speed of 1 mm/min using samples that were 20 mm in diameter and 1.8 mm in height. A pre-load of 5 N was employed before compressing samples to 70 % strain. Stress-strain curves were generated from which Young's modulus was calculated based on the linear portion of the graph. The stress at limit was calculated based on the load at the compressive limit of each sample.

3.5.6 *Biological testing of 3D printed samples*

3.5.6.1 *Cytocompatibility testing of 3D printed samples*

The cytocompatibility of 3D printed samples was evaluated via the elution assay. The elution assay was performed by placing 20 mm hydrogel samples in 6 well plates and submerging in methanol for 30 mins, followed by washing 2x in deionised water before drying in a vacuum oven at 37°C and 200 mbar pressure overnight. Submerging in methanol was deemed necessary after initial experiments revealed unexpected cytotoxicity which was determined to be due to unreacted photo-initiator. Thus, by submerging in methanol, any unreacted TPO can be effectively removed from the matrix prior to testing. The dried samples were sterilised under UV light for 15 mins before swelling the samples in sterile supplemented cell culture media. The samples were incubated overnight at 37°C in an incubator to allow the hydrogels to swell. Once swollen, the media from each sample was removed and placed in labelled containers to be used as treatment media. SH-SY5Y and RT 4 D6P2T cells were seeded in a 96 well plate and allowed to adhere overnight before removing the spent media and replacing with the treatment media described earlier. The cells were returned to the incubator for 20 hours before assaying using the resazurin reduction assay as outlined in section 3.2.6 (Total exposure to treatment media was 24 hours).

3.5.6.2 *Degradation of 3D printed samples*

The degradability of 3D printed samples was evaluated in physiological, and accelerated conditions.

2.7.1.1.3 *In vitro degradation*

The degradation of 3D printed samples under physiological conditions was evaluated by placing samples of 20 mm diameter in a 6 well tissue culture plate in quintuplicate and submerging each hydrogel in Dulbecco's PBS (pH 7.4). The plates containing the 3D prints were incubated at 37°C and weights and images were recorded every 24 hours for 7 days. Images were captured using a Canon 450 D SLR camera.

2.7.1.1.4 *Accelerated degradation study*

3D printed samples of 20 mm diameter were placed in a 6 well plate as outlined previously, in quintuplicate. 3D prints were submerged in either 5 mM or 5 M NaOH, and weights and images were recorded every 24 hours for 7 days or until the sample had completely degraded.

3.6 IDENTIFICATION AND INCORPORATION OF NEUROTROPHIC COMPOUNDS

3.6.1 Selection of drug candidates

A comprehensive literature review was conducted to identify compounds which could potentially possess neurotrophic ability. This literature review was conducted by using search terms such as “neurotrophic”, “Nerve + Regeneration + drug” and many other terms and combinations of terms. These terms were used to search databases such as PubMed, science direct and Google Scholar. Connected papers was then used to expand the scope.

3.6.2 Bioactivity of neurotrophic compounds

After identifying melatonin and tyrosol as lead drug candidates, a series of assays were conducted to identify any potential proliferative or cytotoxic effects associated with their inclusion. Melatonin was dissolved in DMSO and diluted in cell culture media to obtain a 1 μ M stock solution. The concentration of DMSO did not exceed 0.00005 %v/v, however, a vehicle control was included to verify that there was no toxicity associated with the vehicle concentration. Therefore, all assays included a vehicle control, a negative control (media only, no cells) and a positive control (media only, with cells). This solution was stored at -20 °C until needed. Similarly, tyrosol was dissolved in cell culture media at a concentration of 1 μ M and stored in at -20 °C until needed. No significant difference was detected between the vehicle control and positive controls when assayed with resazurin and analysed using one-way ANOVA. Therefore, all data is represented as % cell viability of the positive control. Before use, the solutions were sterile filtered through a 0.2 μ M filter.

3.6.2.1 Resazurin reduction assay of neurotrophic compounds

24 tissue culture were seeded with SH-SY5Y and RT4 D6P2T cells at cell densities of 0.5×10^6 and 0.25×10^6 cells/ml respectively. These cells were allowed to adhere overnight in propagation media at 37 °C and 5% CO₂. After overnight incubation, treatment media containing either melatonin or tyrosol was added to each well in triplicate as per Table 8 below.

Table 8. Neurotrophic compound concentration in treatment media

Melatonin (nM)	Tyrosol (nM)
0	0
10	0.1
25	1
50	10
75	100
100	1000
125	10000

Cells were exposed to the treatment media for 20 hours prior to the addition of resazurin to the cell culture media. The plate was then incubated for a further 4 hours (24 hour total exposure time). Finally, the conversion of resazurin to resorufin was detected at ex/em 530/590 and the data was analysed using GraphPad Prism V8.01.

3.6.2.2 *BrdU assay*

The bromodeoxyuridine (BrdU) assay is an assay that detects 5-bromo-2'-deoxyuridine (BrdU) incorporated into cellular DNA during cell proliferation using an anti-BrdU antibody. When cells are cultured with labelling medium that contains BrdU, this pyrimidine analogue is incorporated in place of thymidine into the newly synthesized DNA of proliferating cells. After removing labelling medium, cells are fixed and the DNA is denatured with fixing/denaturing solution. Then a BrdU mouse monoclonal antibody (mAb) is added to detect the incorporated BrdU. Anti-mouse IgG, horse radish peroxidase (HRP)-linked antibody is then used to recognize the bound detection antibody. HRP substrate TMB is added to develop colour. The magnitude of the absorbance for the developed colour is proportional to the quantity of BrdU incorporated into cells, which is a direct indication of cell proliferation.

This assay was conducted by seeding both cell lines at a density of 0.1×10^6 cells/ml into labelled wells of a 96 well plate. These cells were allowed to adhere overnight at 37 °C and 5 % CO₂. The following day, BrdU reagent was diluted 1: 2000 in fresh media and 20 µl of this solution was pipetted into each well to be labelled. BrdU was allowed to incorporate

into cells overnight in the incubator. On day 3, the contents of the wells were emptied by inverting the plates over clean paper towels. 200 µl of fixative/ denaturing solution was added to each well and the plate was incubated for 30 mins at R.T. The contents of each well were removed by pipetting before adding 100 µl 1X Anti-BrdU antibody to each well. The plate was incubated at R.T. for 1 hour. The plate was washed 3x with 1X wash buffer. 100µl of peroxidase goat anti-mouse IgG horse radish peroxidase (HRP) conjugate was added to each well and the plate was again incubated at R.T for 30 mins. The plate was washed a further 3x with 1X wash buffer before flooding the entire plate with deionised water and removing by inversion on paper towels. While protecting the plate from light, 100µl of substrate solution was added to each well and incubated for 15 mins at R.T. After 15 mins, 100 µl of stop solution was added in the same order the substrate solution was added in. The absorbance was read at dual wavelengths of 450 nm – 540 nm in a UV-Vis plate reader within 30 mins of adding the stop reagent.

Data was analysed using GraphPad Prism V8.01.

3.7 TYROSOL DRUG DELIVERY

3.7.1 Tyrosol loaded hydrogels

Tyrosol loaded hydrogels were prepared by first preparing either a 10 mM (UV Spectrophotometric) or 1000 mM (Reverse-phase (RP)-HPLC) solution of tyrosol in PBS (pH 7.4) in a volumetric flask. This solution was mixed by inversion until fully dissolved. Polymer solutions were prepared as outlined in Table 9 below:

Table 9. Tyrosol loaded hydrogels

	Tyrosol	PEGDMA	HA-SH	HA-MA	Irgacure 2959
100%	600 μ l	5.34 g	-	-	0.1 % wv
PEGDMA					
50 % HA-SH 50%	600 μ l	2.67 g	2.67 g	-	0.1 % wv
PEGDMA					
50 % HA-MA 50 %	600 μ l	2.67 g	-	2.67 g	0.1 % wv
PEGDMA					
50 % HA-SH 40 % HA-MA 10 %	600 μ l	0.534 g	2.67 g	2.136 g	0.1 % wv
PEGDMA					

The hydrogel solutions were stirred until homogenous before pipetting into a silicone mould and placing in a UV curing chamber for 10 mins as outlined in section 3.4. On removing the samples from the UV curing chamber, the samples were rinsed briefly and blotted dry with filter paper to remove uncured monomer solution. The samples were used for testing within 72 hours of curing.

3.7.2 Tyrosol loaded 3D printed samples

Tyrosol loaded 3D prints were prepared by first preparing either a 10 mM or 1000 mM solution of tyrosol in PBS (pH 7.4) in a volumetric flask. This solution was mixed by inversion until fully dissolved. Polymer solutions were prepared as outlined in Table 10 below:

Table 10. Tyrosol loaded 3D printed samples

	Tyrosol	PEGDMA	HA-SH	HA-MA	TPO
100%	5 ml	44 g	-	-	1 %wv
PEGDMA					
50 % HA-SH	5 ml	22 g	22 g	-	1 %wv
50% PEGDMA					
50 % HA-MA	5 ml	22 g	-	22 g	1 %wv
50 % PEGDMA					
50 % HA-SH	5 ml	4.4 g	22 g	17.6 g	1 %wv
40 % HA-MA					
10 % PEGDMA					

The polymer solutions were stirred until homogenous before adding to the resin tank of a SLA 3D printer as described in section 3.6.3. On removing the samples from the 3D printer, the samples were placed in a UV curing chamber to post-cure for 10 mins before being rinsed briefly and blotted dry with filter paper to remove uncured monomer solution. The samples were used for testing within 72 hours of curing.

3.7.3 *UV spectroscopy analysis of Tyrosol drug release*

A series of standards was prepared in PBS to provide values within the linear absorbance range. This concentration range was 310 nM up to 3100 nM tyrosol in PBS. After obtaining a repeatable standard curve, individual hydrogels of 100 % PEGDMA, 100 % HA-MA and the hybrid hydrogel of 50 HA-SH: 40 HA-MA: 10 PEGDMA (% wv) containing 10,000 nM tyrosol per hydrogel were placed in solutions of 10 ml PBS. Samples were taken at regular intervals, with complete solution changes each time. Samples were read using a quartz cuvette in a UV spectrophotometer at 280 nm which was auto zeroed on air. Tyrosol is a phenolic compound which explains its lambda max of 280 nm. Blank readings were obtained for PBS alone, these blank readings were subtracted from the sample values prior to plotting the data.

3.7.4 *RP-HPLC analysis of Tyrosol drug release*

The concentration of tyrosol was determined by RP-HPLC. Samples were prepared by UV photo-polymerisation or stereolithography as outlined in sections 3.7.1 and 3.7.2 above. The supernatants were injected neat and 1 microliter in triplicate was injected onto a column (XBridge BEH C18, 4.6 mm × 150 mm, 1.5 μm, 130Å, Waters Corp.). Analysis was performed on Nexera-*i* system (Shimadzu Corp.) equipped with a LC-2040 pump, LC-2040 autosampler and a PDA detector model SPD-M40. The elution was performed in isocratic mode at a flowrate of 1 mL min⁻¹, 60°C, with the mobile phase consisting of acetonitrile: water (15:85) adjusted to pH 2 with orthophosphoric acid. Peak areas from chromatograms obtained at 274 nm were analysed on LabSolutions software (Shimadzu Corp.) and subsequently used to quantify the release of tyrosol from photo-polymerised hydrogels and 3D printed samples.

3.8 ISO STANDARDS

The International Organisation for Standardisation (ISO) standards are an internationally recognised set of guidelines and criteria which are developed and maintained by the ISO, who are an independent non-governmental organisation. These guidelines provide specifications and guidelines which strive to ensure consistency, quality and safety across a variety of different industries worldwide.

The primary advantages of utilising ISO standards are the assurance of quality and consistency, and ensure interoperability and compatibility. In terms of this project, using ISO standardised approaches helps enable the replicability and reproducibility of the experiments contained herein. Detailed below is the ISO standards used within this research project and a brief overview of the guidelines pertaining to the standard.

3.8.1 ISO 10993-5: 2009 Section 8.3 Test by direct contact

This ISO standard sets out guidelines for the qualitative and quantitative testing of specimens for evaluation of cytotoxicity. This set of guidelines states that test specimens should be placed on the cell layer, however, it also specifies that where appropriate, cells can be seeded to the surface of the sample. This was the method utilised in this project in order to prevent unnecessary physical trauma to the cells. ISO 10993-5: 2009 also states that the cells must be incubated with the test specimen for a minimum of 24 hours and that a minimum of 3 replicates should be used (ISO, 2009).

3.8.2 ISO 10993-5: 2009 Section 8.2 Test on extracts

Leachates from the hydrogel and 3D printed samples were tested using the guidance outlined in ISO 10993-5: 2009 section 8.2. This standard specifies that where monolayer cultures are used, the medium should be discarded before adding the extract in diluent (ISO, 2009). In this project, cell culture medium was used as the diluent for extracted leachates. As before, cells were incubated with the treatment for 24 hours as stated in the guidelines and a minimum of 3 replicates were used. If cytotoxic leachates were detected, ISO standard 10993-17:2002 would have been utilised which outlines criteria for the testing and handling of leachates (ISO, 2002).

3.9 DATA MANAGEMENT AND STATISTICAL ANALYSIS

Data management is a critical aspect of scientific research as it contributes significantly to the integrity, accessibility and usability of data. An effective data management system encompasses a multitude of practices such as data collection, organisation, storage, sharing and analysis. The integrity of the data relies upon the development of robust protocols for data documentation, ensuring data is accurately and comprehensively recorded.

Throughout this project, data was first recorded in laboratory notebooks and USB keys. Data was labelled and organised by work-package and date. The data was promptly extracted into raw data tables in Microsoft excel where primary analysis was completed. The procedures and any protocol deviations were transcribed into a Microsoft word document. All documents were stored in designated folders on the universities secure OneDrive cloud storage, where access was controlled by the account holder (me). Therefore, there were no GDPR concerns over data storage.

Statistical analysis of the data was completed using GraphPad Prism® Version 8.01 which was kindly provided by Dr. Therese Montgomery. Normality of the data was determined using the Anderson-Darling test for normality. Where appropriate, one-way or two-way ANOVA was utilised to identify statistical significance in treated populations. The statistical significance was accepted at $P \leq 0.05$. All graphs and associated metadata were uploaded to the university managed OneDrive cloud storage weekly and also stored on a USB key.

**CHAPTER 4. INVESTIGATION INTO THE EFFECT OF
MOLECULAR WEIGHT ON THE BIOACTIVITY/
CYTOTOXICITY OF HYALURONIC ACID IN
NEURONAL AND GLIAL CELL LINES**

4.1 PREFACE

Despite the body of work that already exists for HA, much of this has focused on the effects of HMW HA *in vitro* and *in vivo*. There are also significant studies on very low MW HA which show the pro-inflammatory effects of LMW HA, however, these tend to use oligo HA <10 kDa. In this study we examined a range of HA MWs in order to determine which MW gave the most favourable outcomes in neuronal and glial cell populations. The MW examined were 30-50, 300-500, 1000-1250 and 2000-2200 kDa. First, MTT assays were completed to establish a baseline density curve for both cell lines in order to select a seeding density which would provide a 70% confluent culture after 24 h incubation. Following this, 24 h exposure HA assays were conducted using MTT and resazurin in both cell lines. Given the viscous nature of HA, modified assay methodologies were employed to ensure the robustness of the testing procedure. These methods were validated and proven to be robust and repeatable and serve to aid in the testing of viscous water-soluble polysaccharides.

HA was proven to be non-conducive to cell adhesion and therefore was combined with PDL to ensure even direct contact of cells with the HA surface. Despite this, cell loss during media removal steps still proved to be a significant issue, particularly in the case of the MTT assay. This response was investigated thoroughly and MTT was ruled out as an appropriate assay medium for this particular system.

This chapter provided a baseline response to enable the further testing of HA, HA hydrogels and HA 3D prints.

4.2 RESULTS

4.2.1 Cell Characterisation assay

In order to determine the optimal seeding density for the testing of HA, it was necessary to perform a characterisation assay via the MTT assay as outlined in section 3.2.7. In doing this, it would be possible to identify a seeding density which would produce wells of approximately 70 % confluence after overnight incubation in both cell lines. Many cell lines grow at different rates and therefore baseline characteristic is a vital component of *in vitro* method development.

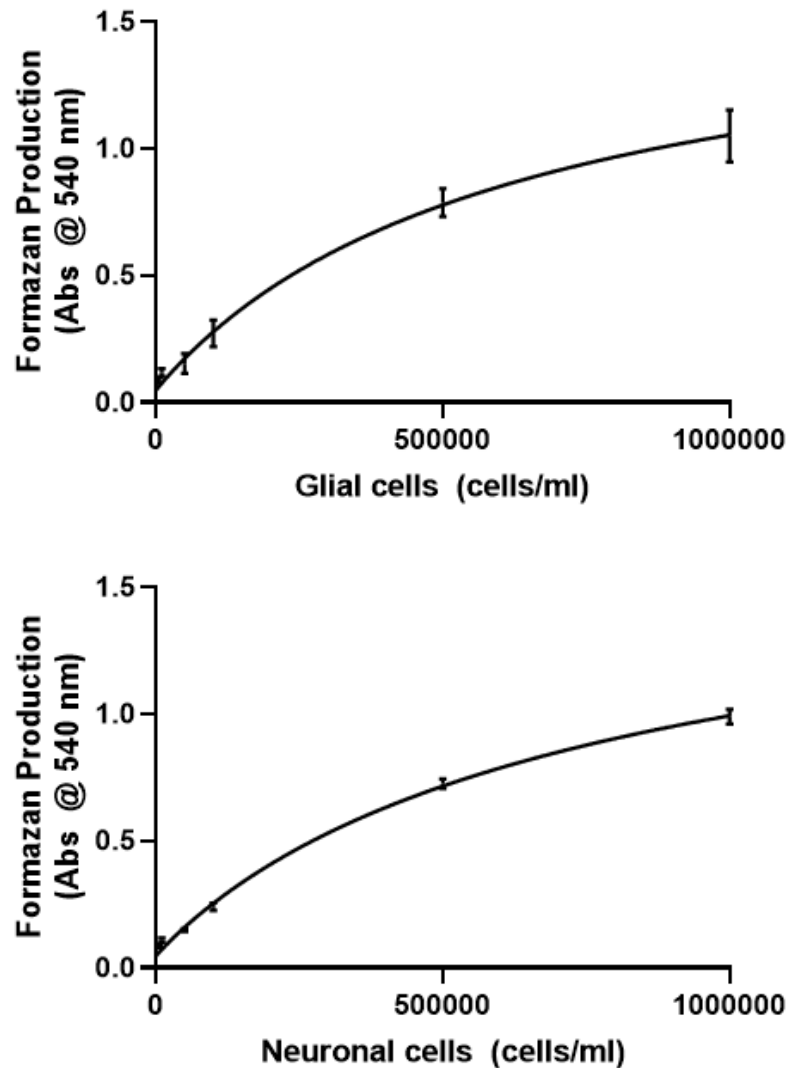


Figure 19. Determination of optimal seeding density in glial and neuronal cell lines for *in vitro* assay development. Optimal seeding density was determined in glial and neuronal cells via the MTT assay. Cells were seeded at various densities and allowed to adhere overnight before assaying. It was determined that an initial seeding density of 0.5×10^6 cells/ml for SH-SY5Y cells and 0.25×10^6 cells/ml for RT4 D6P2T cells produces wells which are approximately 70% confluent and produce an absorbance reading of approximately 0.8 AU – 1.0 AU after overnight incubation. This seeding density was used for all 24 h HA experiments outlined in this chapter. Data shown is the mean \pm SEM of 3 independent experiments (N=3), conducted in triplicate (n=3). Data was analysed using GraphPad Prism V8.01.

4.2.2 The use of PDL coating enhances HA cytocompatibility testing

PDL is a commonly used surface coating for cell culture plates and can be used to increase cell attachment to the surface of polymers. It was for this reason that PDL was chosen as the diluent for the HA polymer samples to be tested. Before introducing another variable, however, it was necessary to rule out any toxicity or interference associated with the use of PDL itself. Plates were coated as outlined in section 3.2.5. Cells were then seeded on coated and uncoated plates in parallel at a density of 0.5×10^6 cells/ml for SH-SY5Y cells and 0.25×10^6 cells/ml for RT4 D6P2T cells. No cytotoxicity was detected in the presence of PDL and there was no significant difference when comparing with a negative control of an uncoated tissue culture well.

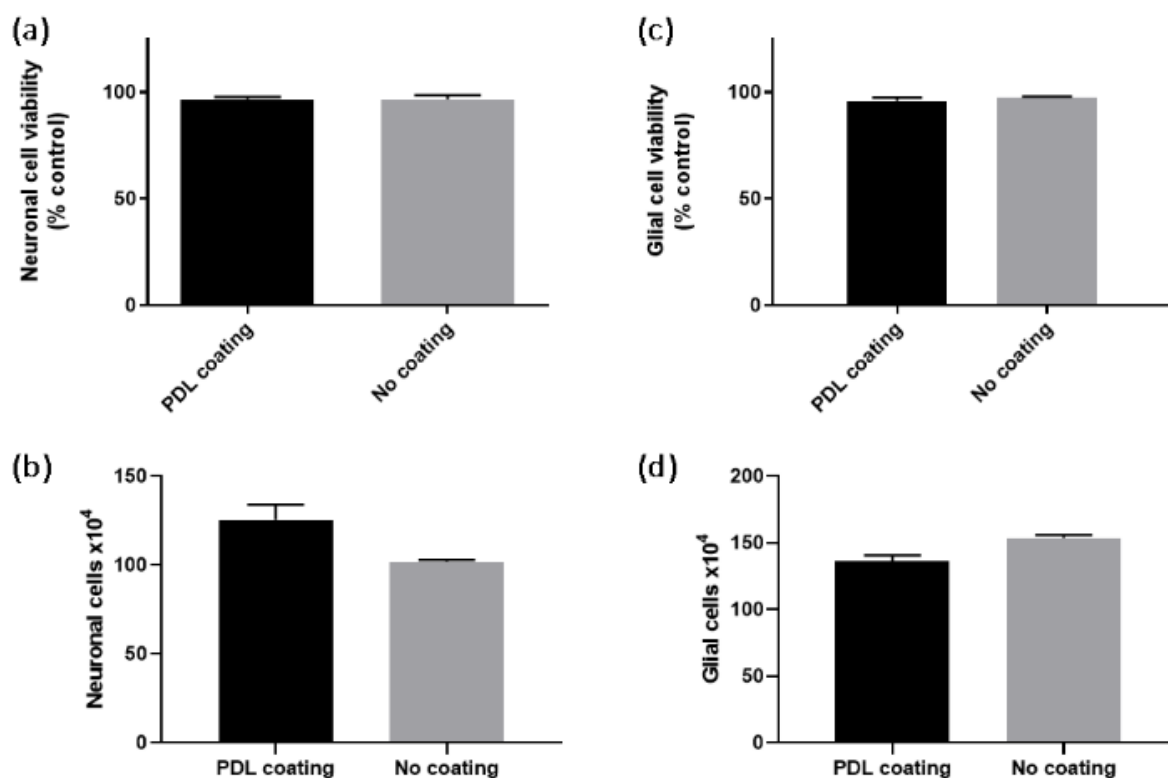


Figure 20. PDL does not significantly impact the viability of neuronal and glial cell lines. The effect of PDL on SH-SY5Y (a-b) and RT4 D6P2T (c-d) cell lines was evaluated using the MTT assay and the TBE assay. No significant effect was observed ($P > 0.05$) when comparing the viability and number of cells grown on PDL vs no PDL using two-way ANOVA with Tukey posttests. Neuronal and glial cells were seeded at a cell density of 0.5×10^6 cells/ml and 0.25×10^6 cells/ml respectively on coated and uncoated 24 well cell culture plates in parallel. After overnight incubation at 37 °C, MTT and trypan blue assays

were employed. Data presented is the mean \pm of 3 independent experiments (N=3), conducted in triplicate (n=3). Data was analysed using GraphPad Prism V8.01.

4.2.3 Validation of HA plate coating by Alcian Blue

HA is a highly viscous polymer and as such, it was not appropriate to add it to the surface of adherent cells. Therefore, various concentrations and molecular weights of HA were dissolved in either PDL or water and used as cell culture plate coatings for the cells to grow on. HA is not conducive to cell attachment so it was intended that PDL would aid in the attachment of cells to the substrate to ensure full contact for the determination of cytocompatibility. The quality and homogeneity of the coatings were assessed via the Alcian Blue assay.

Alcian Blue is a polyvalent basic dye which binds to acid mucins (Repellin *et al.*, 2023). The presence of copper in the dye gives a blue colour which can be used to semi-quantitatively determine the presence of HA in the coating after the series of wash steps.

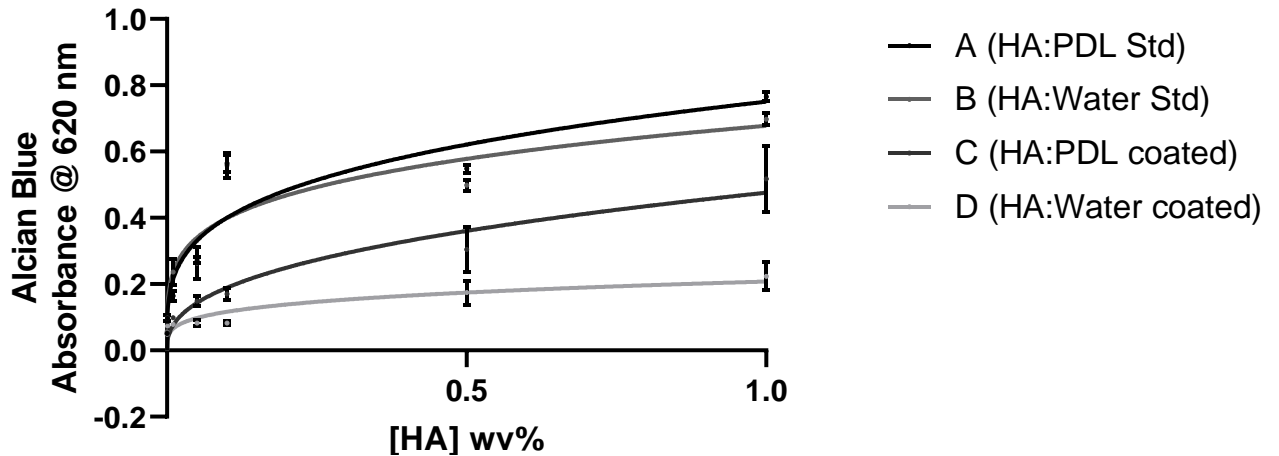


Figure 21. PDL improves the retention of HA in coated cell culture plates. Comparison between HA coatings in PDL vs sterile water. (a) HA in PDL Standard, (B) HA in water standard, (C) HA in PDL coated and (D) HA in water coated, where standard (Std) refers to the coating solution remaining in the well rather than removed for washing and coated refers to the removal and subsequent washing of the wells before solubilisation. In all instances, 30-50 kDa HA was used. PDL was found to increase the retention of HA in the wells of a 24 well cell culture plate but this was not found to be significant ($P > 0.05$) when compared using two-way ANOVA with Tukey posttests. When imaging, it became evident that PDL allowed for a smoother and more uniform coating as seen by Figure 22 below and such, HA was dissolved in PDL for subsequent experiments. Data shown is the mean \pm SEM of 4 experiments (N=4), conducted in triplicate (n=3). Data was analysed using GraphPad Prism V8.01.

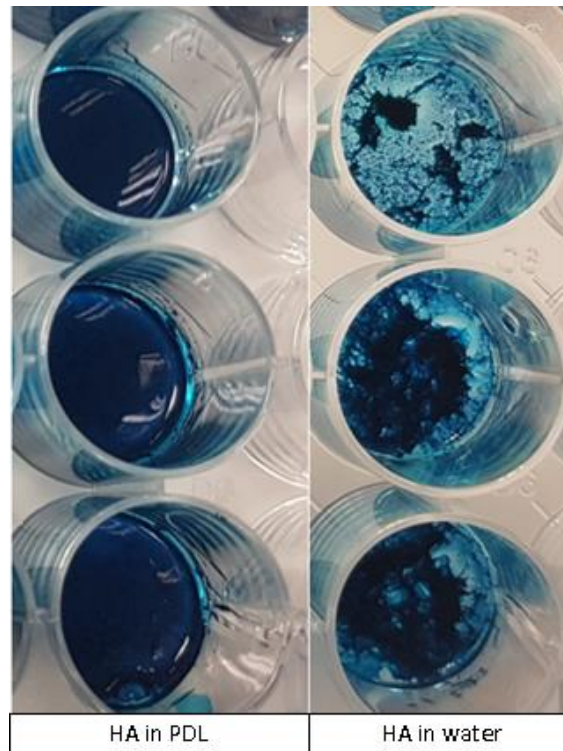


Figure 22. PDL enhances the homogeneity of HA coatings in tissue culture plates. In the case of water as the 30-50 kDa HA coating diluent (right), aggregates can be observed leading to an uneven coated surface which would make equal direct contact exposure to cells impossible. In Figure 22, the HA in PDL coating is observed as a homogenous coated surface (Left). These images were taken using a Canon 450D DSLR camera after washing 2x with sterile water and before solubilisation with 6M guanidine HCl.

4.2.4 The effect of molecular weight on the cytocompatibility of HA

After establishing that PDL was necessary to ensure a homogenous coating of HA, it was necessary to evaluate the impact of molecular weight on the coating before testing the impact of molecular weight on cytocompatibility. The effect of molecular weight on HA coatings was evaluated using Alcian Blue dye where the intensity of the dye is directly proportional to the concentration of HA.

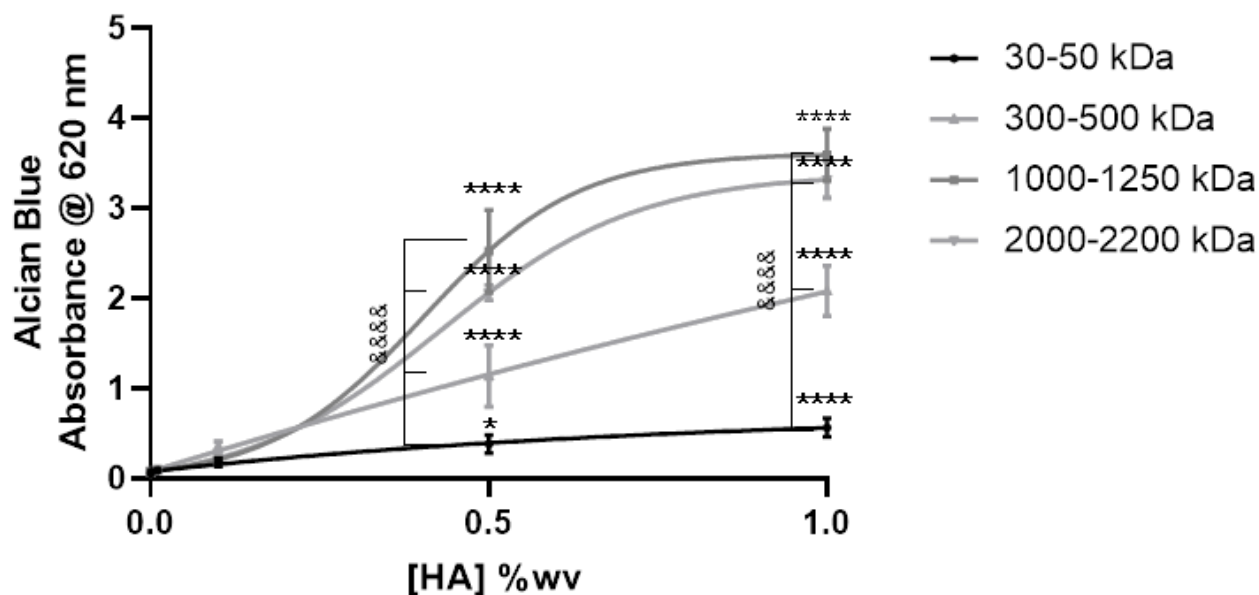


Figure 23. 30-50 kDa HA gives optimal cell culture plate coatings for *in vitro* cell coatings. Data is the mean \pm SEM of 5 independent experiments (N=5), conducted in triplicate (n=3). * $P < 0.05$, **** $P < 0.0001$ vs control (0 %wv HA of given MW) when compared using one-way ANOVA with Tukey posttests. &&&& $P < 0.0001$ vs 30-50 kDa HA when compared using two-way ANOVA with Tukey posttests. Data was analysed using GraphPad Prism V8.01.

As can be seen in Figure 23, as the molecular weight increased, the absorbance deviated further from linearity. This is further evidenced by the lack of significant variation between results up to 0.5 %wv, after and including this concentration however, there was a significant variation between 30-50 kDa and the other concentrations. This is due to the increased viscosity observed with increasing molecular weight which caused unreliable over-retention of HA coatings.

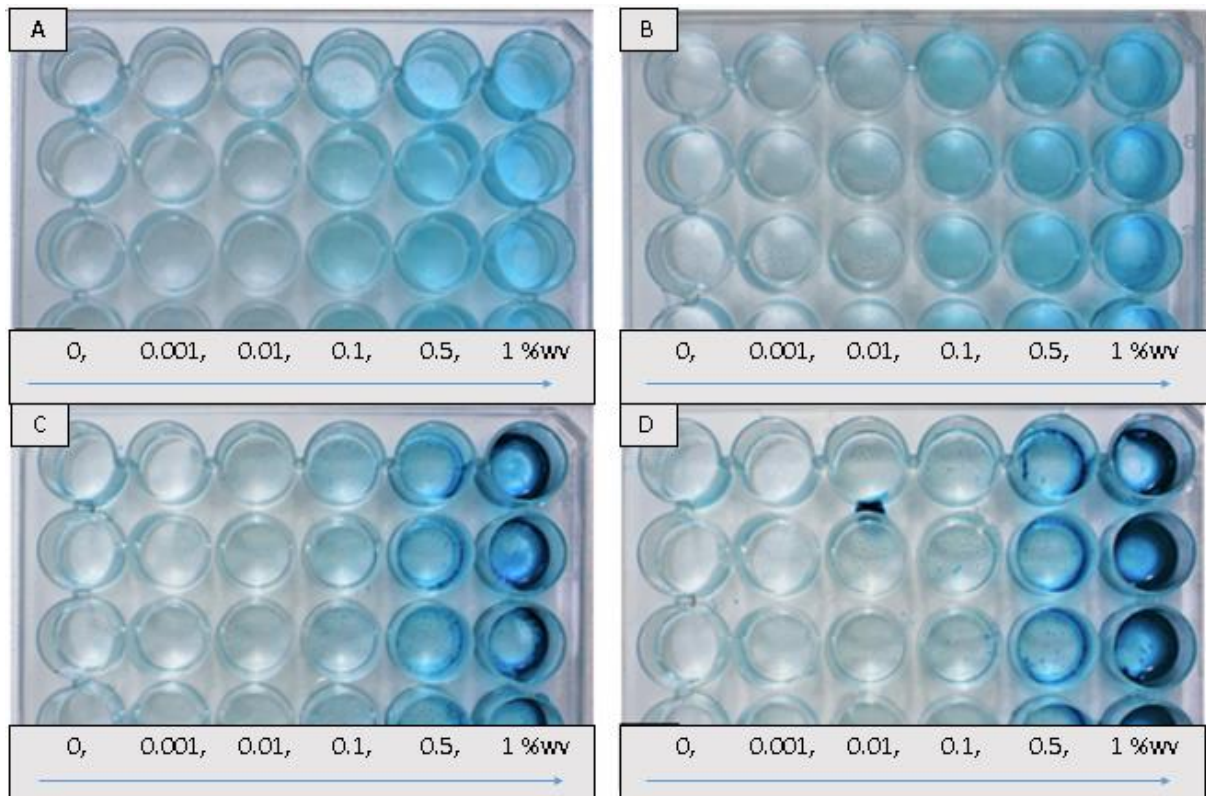


Figure 24. Qualitative visual analysis of HA: PDL coatings from 30 to 2200 kDa. Images A-D in Figure 24 portray the alcian blue – HA complexes formed across various concentrations in 30-50kDa (A), 300-500kDa (B), 1000-1250kDa (C) and 2000-2200kDa (D) respectively. These images were taken using a Canon 450D DSLR camera after washing 2x with sterile PBS and before solubilisation with 6M guanidine HCl.

Following analysis of the coatings, the various molecular weights of HA were screened in neuronal and glial cell lines to visualise the effect of molecular weight on cell viability. This was done by coating as detailed in section 3.2.5 and then seeding cells on top of the coated plates. The modified resazurin reduction assay (Section 3.2.6.3) was utilised to analyse cell health at various time-points of the assay. These time-points involved after 20 h incubation of cells with the HA coating, prior to addition of resazurin, and also at 24 h, after 4 h incubation with resazurin (As illustrated in Figure 18).

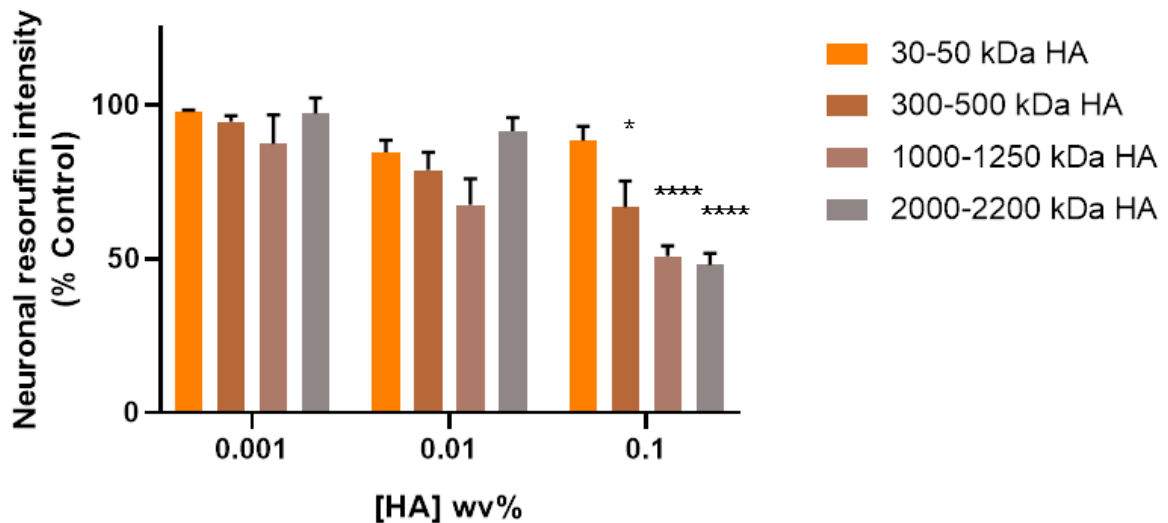


Figure 25. Increases in molecular weight corresponded to decreases in the resorufin intensity of SH-SY5Y cells. Neuronal cells were seeded at a seeding density of 0.5×10^6 cells/ml and incubated on coated HA plates for 24 h (inclusive of 4 h resazurin incubation). The fluorescent intensity of resorufin was detected at 530/590 ex/em. Control is equal to cell viability on 0 %wv HA (PDL only) for each individual molecular weight. Data is the mean \pm SEM of 4 independent experiments (N=4), conducted in triplicate (n=3). **** $P < 0.0001$, * $P < 0.05$ vs 30-50 kDa HA coating when compared using two-way ANOVA with Tukey posttests. Data was analysed using GraphPad Prism V8.01.

The cells removed from each well in the media removal steps of the modified resazurin assay (Figure 18) were collected in individual eppendorfs to maintain replicates. 0.2 ml of each cell suspension was combined with 0.3 ml PBS and 0.5 ml 0.4 %wv Trypan Blue solution. The TBE assay relies upon the principle that viable cells have a membrane which is impermeable to Trypan Blue. Therefore, the dye provides a medium by which visualisation of cells is easier for counting, and also a method for quantifying live and dead cells. Dead or compromised cells can be identified and quantified by their uptake of Trypan Blue.

Initially, 0.5×10^6 neuronal cells/ml were seeded in each well (0.3 ml per well). After overnight incubation on HA coated plates (20 h), spent media was removed from each well

and counted as outlined in section 3.2.6.3 (iii). Figure 26 below illustrates the total number of cells counted $\times 10^4$ in each MW condition. Also illustrated is the proportion of those cells which were deemed live or dead. This assay served to highlight that although a significant portion of the seeded cells were not attached, the majority of these cells remained viable. However, the number of unattached cells increased proportionally to MW and concentration.

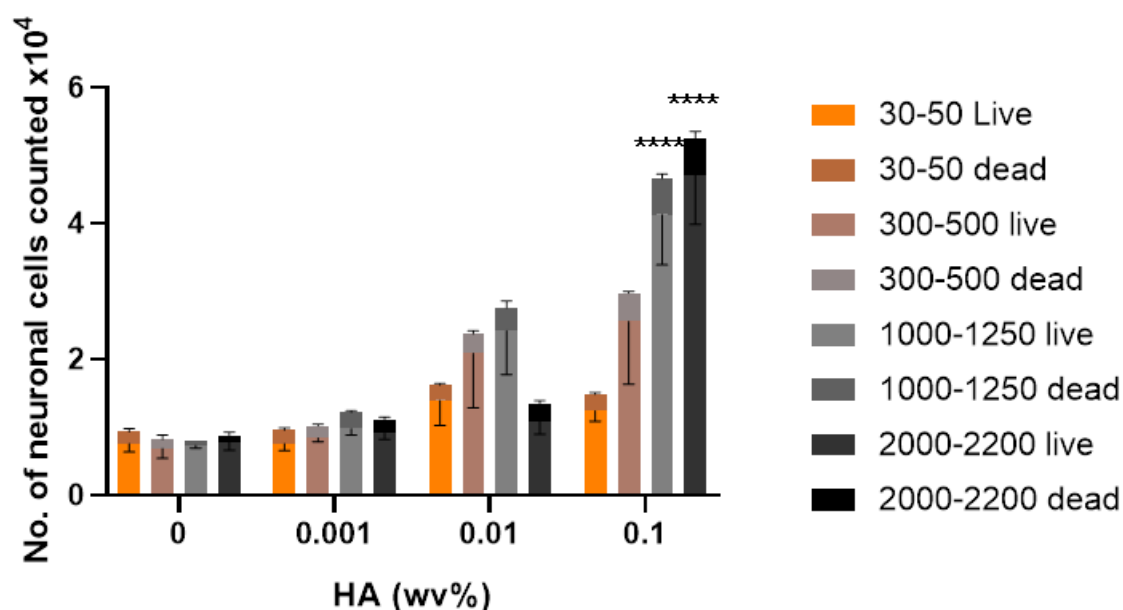


Figure 26. The number of unattached neuronal cells increases proportionally to concentration and MW. Graph represents the number of unattached neuronal cells counted after 24 h exposure (inclusive of 4 h resazurin assay) to various molecular weights of HA from 30-50 kDa HA to 2000-2200 kDa HA. Initial seeding density was 0.5×10^6 cells/ml (150,000 cells/well). Data is the mean \pm SEM of 3 independent experiments (N=3), conducted in triplicate (n=3). **** $P < 0.0001$, *** $P < 0.001$ vs cells exposed to 30-50 kDa HA when compared using two-way ANOVA with Tukey posttests. Data was analysed using GraphPad Prism V8.01.

The modified resazurin and TBE assays were repeated in glial cells to determine whether the response obtained was neuronal specific. Assays were conducted in parallel to ensure against environmental factors between days. This was done by coating as detailed in section 3.2.5 and then seeding glial cells on the surface of the coated plates. The modified resazurin reduction assay (Section 3.2.6.3) was utilised to analyse cell health at various time-points of the assay. These time-points involved after 20 h incubation of cells with the HA coating, prior to addition of resazurin, and also at 24 h, after 4 h incubation with resazurin (As illustrated in Figure 18).

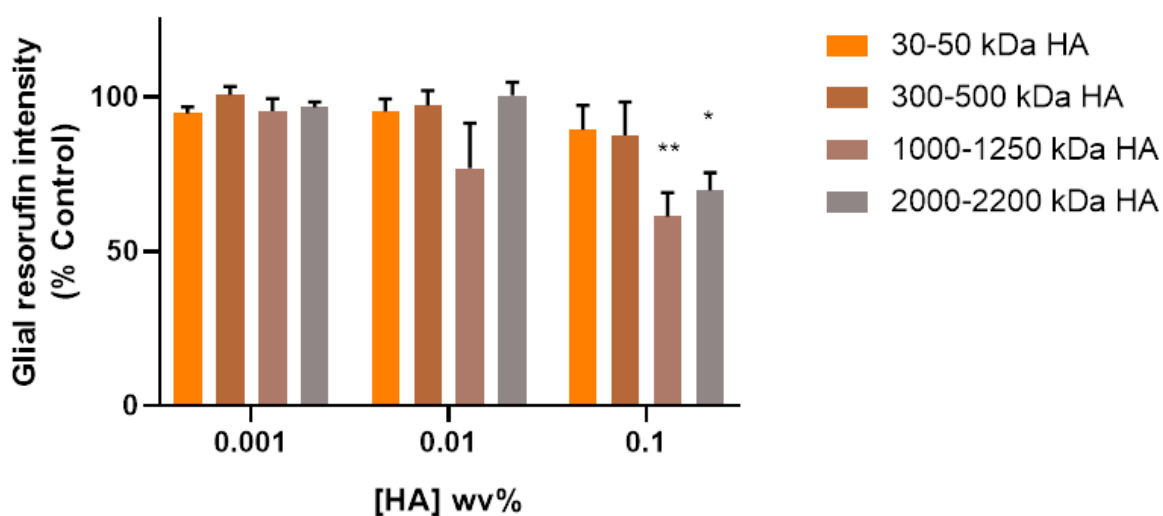


Figure 27. Increases in molecular weight corresponded to decreases in the resorufin intensity in RT4 D6P2T cells. Glial cells were seeded at a seeding density of 0.25×10^6 cells/ml and incubated on coated HA plates for 24 h (inclusive of 4 h resazurin incubation). The fluorescent intensity of resorufin was detected at 530/590 ex/em. Control is equal to resorufin intensity on 0 %wv HA (PDL only). Data is the mean \pm SEM of 4 independent experiments (N=4), conducted in triplicate (n=3). $**P < 0.01$, $*P < 0.05$ vs 30-50 kDa HA coating when compared using two-way ANOVA with Tukey posttests. Data was analysed using GraphPad Prism V8.01.

The cells removed from each well in the media removal steps of the modified resazurin assay (Figure 18) were collected in individual eppendorfs to maintain replicates. 0.2 ml of each cell suspension was combined with 0.3 ml PBS and 0.5 ml 0.4 %wv Trypan Blue solution.

Initially, 0.25×10^6 glial cells/ml were seeded in each well (0.3 ml per well). After overnight incubation on HA coated plates (20 h), spent media was removed from each well and counted as outlined in section 3.2.6.3 (iii). Figure 28 below illustrates the total number of cells counted $\times 10^4$ in each MW condition. Also illustrated is the proportion of those cells which were deemed live or dead. This assay served to highlight that although a significant portion of the seeded cells were not attached, the majority of these cells remained viable. However, the number of cells in suspension increased proportionally to MW and concentration.

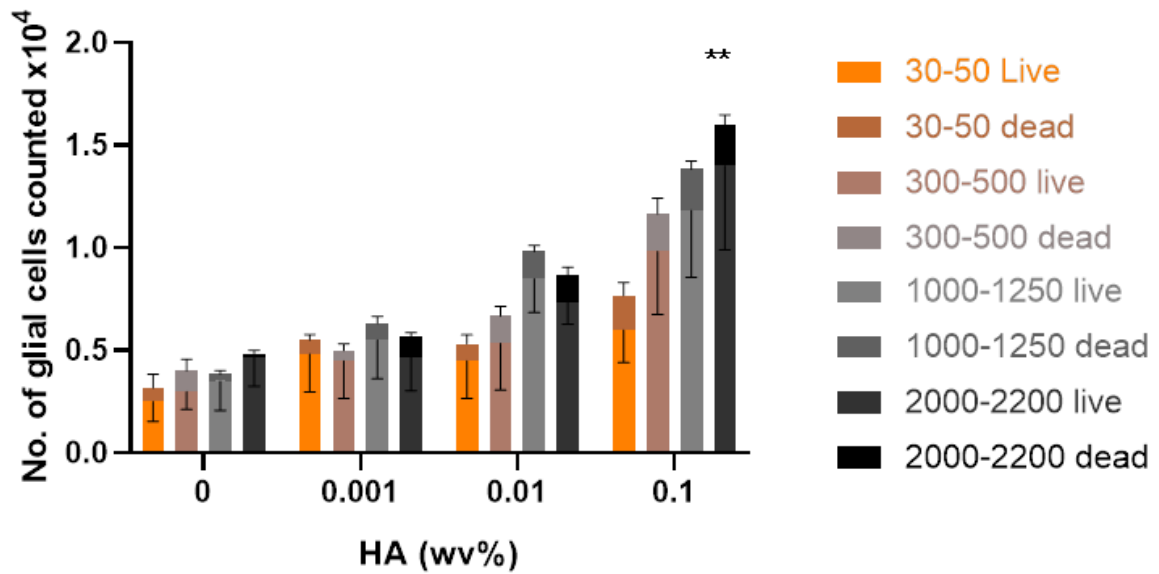


Figure 28. The number of unattached glial cells increases proportionally to concentration and MW. Graph represents the number of unattached glial cells counted after 24 h exposure (inclusive of 4 h resazurin assay) to various molecular weights of HA from 30-50 kDa HA to 2000-2200 kDa HA. Initial seeding density was 0.25×10^6 cells/ml (150,000 cells/well). Data is the mean \pm SEM of 3 independent experiments (N=3), conducted in triplicate (n=3). ****P < 0.0001, ***P < 0.001 vs cells exposed to 30-50 kDa HA when compared using two-way ANOVA with Tukey posttests. Data was analysed using GraphPad Prism V8.01.

It was evident that increased MW resulted in decreased cell attachment, and it was postulated that this was due to the increasing viscosity in the higher MW HA samples. Figure 29 below illustrates the results of frequency sweeps which evaluate the rheological properties of a material in response to increasing shear. These frequency sweeps were performed on 1 %wv solutions of HA in PDL to replicate the plate coating solutions used.

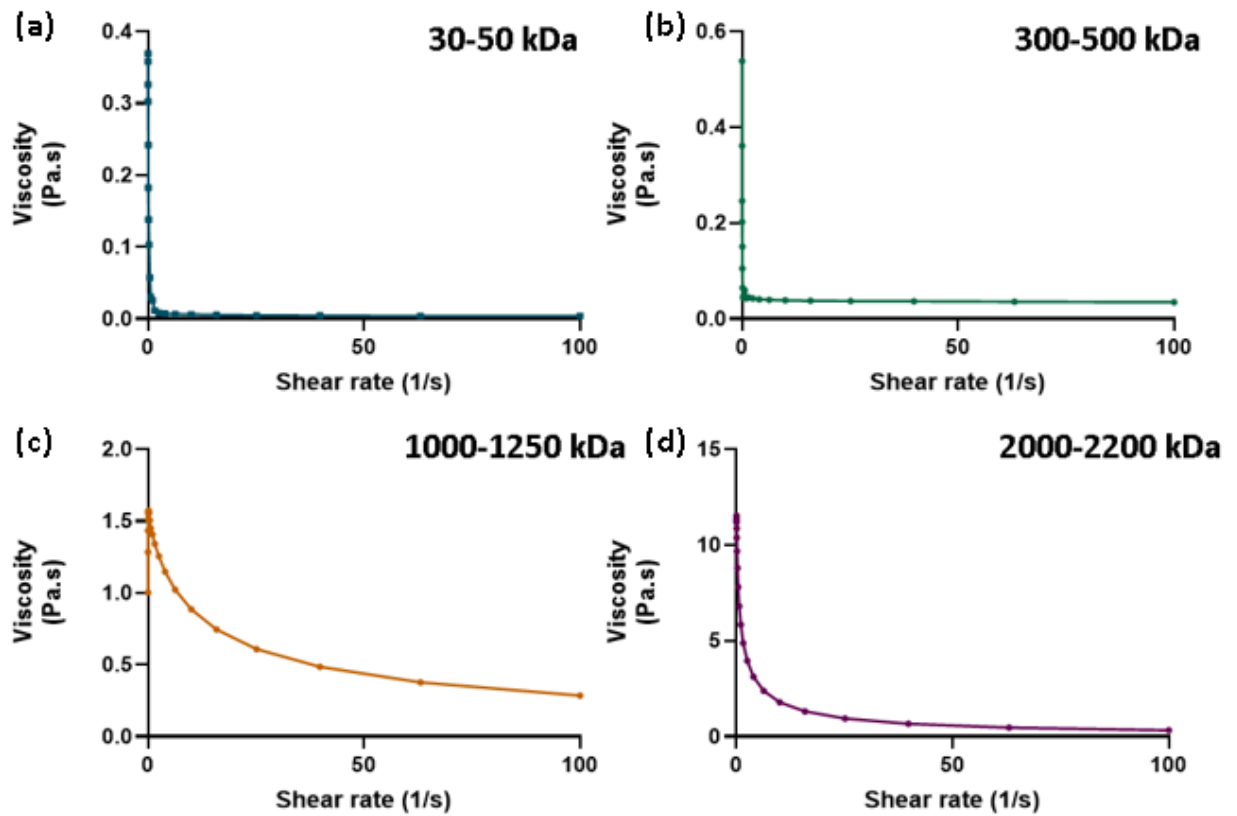


Figure 29. The viscosity of HA increases proportionally to MW. Viscosity and shear-thinning behaviour of HA MWs (a) 30-50 kDa, (b) 300-500 kDa, (c) 1000-1250 kDa and 2000-2200 kDa, was determined using a TA instruments rheometer in frequency sweep mode. Tests were performed on 1 %wv HA in PDL solutions. Data is the mean \pm SD of 1 experiment (N=1), performed in triplicate (n=3).

As Figures 25-28 above show, cell attachment decreased in a proportional manner to the MW of HA, thus imitating cytotoxicity. However, when these cells were collected and analysed using the TBE assay, they were mostly alive. The unattached cells were collected after 24 h exposure to the HA coating (4 h resazurin exposure) and were harvested by removing spent media from each well and spinning down in a centrifuge. Cells were then re-suspended in trypan blue for counting and the resorufin supernatant was read in a fluorescent plate reader.

It was postulated that the increased viscosity observed with increased molecular weight was preventing cell attachment, producing what initially appeared to be a cytotoxic effect. The viscosity of each HA solution was analysed as a function of shear rate using a rheometer, which confirmed that 30-50 kDa possessed the lowest viscosity. This correlation between viscosity and attachment led to the decision to proceed with 30-50 kDa HA for further investigations as this would allow for greater contact for *in vitro* testing.

4.2.5 Investigation of low molecular weight HA via the MTT Cell Viability Assay

The MTT assay is a colorimetric assay based on the conversion of tetrazolium dye to the insoluble formazan by mitochondrial dehydrogenases (Macedo *et al.*, 2022). The rate of conversion is directly comparable to the mitochondrial activity of the cell line. This is one of the most commonly utilised reagents for the evaluation of toxicity in continuous cell lines. This method was employed to evaluate the effect of 30-50 kDa HA in neuronal and glial cell lines.

Neuronal and glial cell lines were seeded on 30-50 kDa HA coated 24 well plates and incubated for 20 h before MTT reagent was added to each well as discussed in detail in section 3.2.6.3. Prior to the addition of MTT, spent media from each well was removed which introduced a mechanical disruption step due to the removal and replacement of media at the 20 h time point. After addition of MTT, plates were returned to the incubator for 4 h at 37 °C and 5 % CO₂. After 4 h MTT incubation, the insoluble formazan crystals were solubilised in DMSO and the absorbance intensity was detected at 540 nm.

Figure 30 below shows a significant decrease in the cell viability in both cell lines exposed to concentrations of HA exceeding 0.01 % wv. However, cell viability in the glial cell lines remained above 70 % when expressed as % control of the 0% HA (PDL only) control. In contrast, the cell viability of neuronal cells grown on 1 % wv 30-50 kDa HA was found to be 10 % viable when compared to the control population. This resulted in an apparent LC₅₀ of 0.019 % wv HA in neuronal cells.

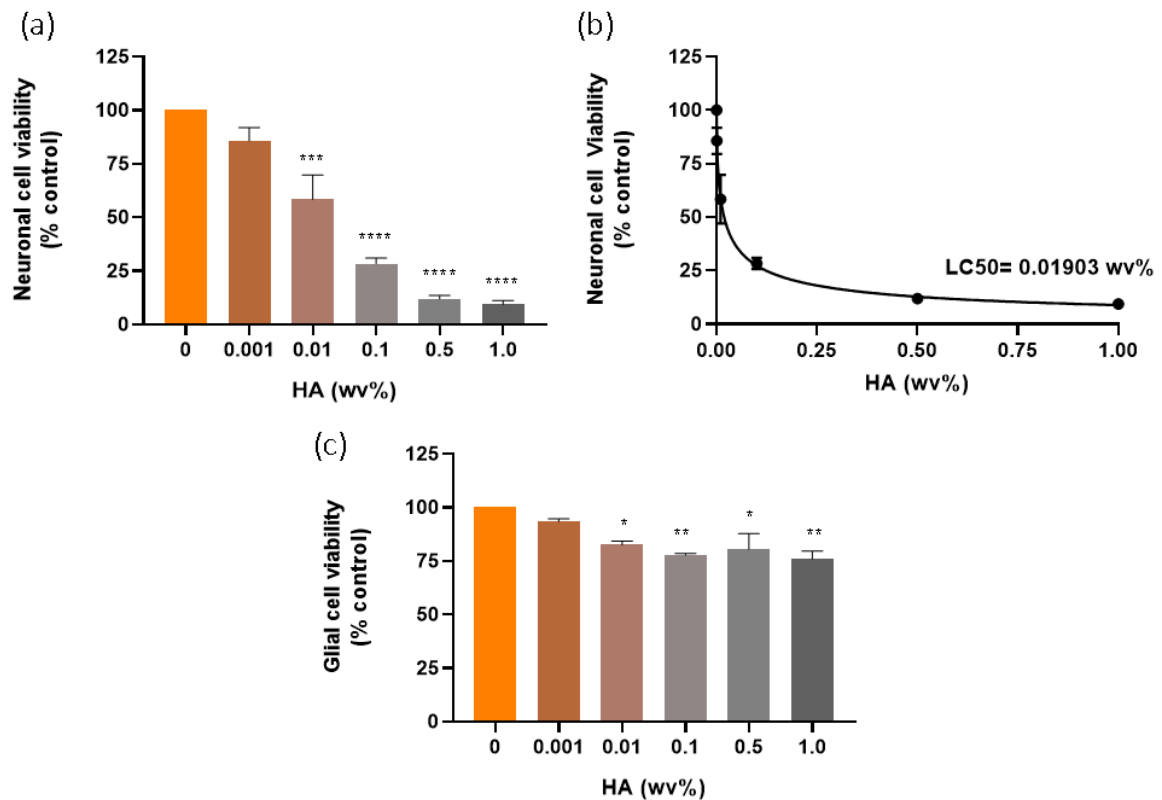


Figure 30. The MTT assay detected what appeared to be significant cytotoxicity in neuronal and glial cells exposed to 30-50 kDa HA. (a) Neuronal cells displayed a dose dependent decrease in cell viability at concentrations greater than 0.01 %wv HA. Neuronal cell viability is expressed as % of a 0 %wv HA control (PDL only) in order to determine the vehicle independent effect of 30-50 kDa HA. (b) The concentration which was determined to be lethal to 50 % of the cell population (LC50) was found to be 0.019 %wv in neuronal cells. (c) Glial cells also exhibited what appeared to be significant cytotoxicity at concentrations exceeding 0.01 %wv HA but not to the same extent as neuronal cells. Glial cell viability is expressed as a % of the 0% HA (PDL only) control. Data is the mean \pm SEM of 4 independent experiments (N=4), conducted in triplicate (n=3). * $P < 0.05$, ** $P < 0.01$, *** $P < 0.001$, **** $P < 0.0001$ vs control (PDL only) when compared using two way ANOVA with Tukey posttests in GraphPad Prism V8.01.

4.2.6 Evaluation of the effect of low molecular weight HA via the Resazurin Cell Viability Assay

Due to the extent of apparent toxicity observed in SH-SY5Y, the resazurin assay was chosen to confirm the results shown in Figure 30, as it works on a similar method of action. The non-fluorescent oxidised blue resazurin dye is reduced to the fluorescent resorufin in the media by the mitochondrial respiration of cells. The amount of resorufin detected is directly proportional to the number of living cells. Plates were coated using a solution of 30-50 kDa HA in PDL as per section 3.2.5 and cells were exposed to the HA coating for a total of 20 hours prior to the addition of resazurin and further incubation for 4 h (24 h total exposure). In this assay, resazurin was added directly to the media in the each well, rather than removing and replacing the media in each well.

The perceived toxicity observed in the MTT assay could not be replicated using the resazurin reduction assay as per Figure 31. One hypothesis for this was that through the normal sequence of a MTT assay, there are many wash steps through which cells can be lost. Conversely, no media removal step was included in the resazurin reduction assay and thus, it was hypothesised that this was where cells were being lost and appearing as significant cytotoxicity.

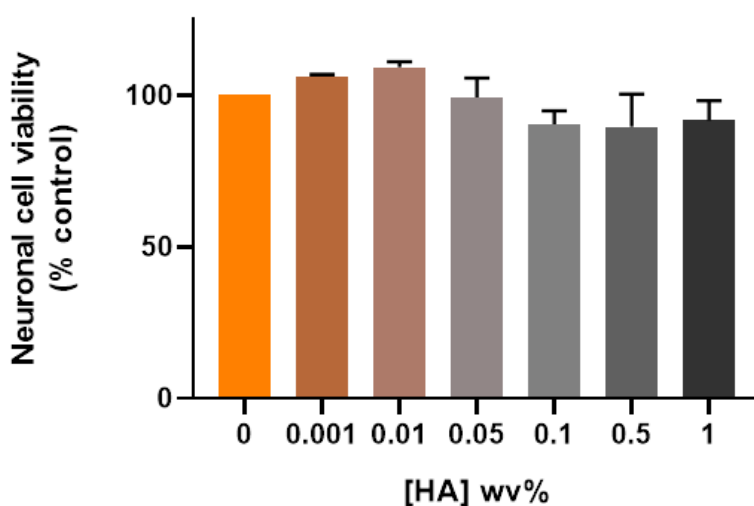


Figure 31. The resazurin assay did not reveal significant toxicity in neuronal cells exposed to 30-50 kDa HA. No cytotoxicity was observed in neuronal cells grown on HA coated plates for 24 h (inclusive of 4h resazurin assay). Data is the mean \pm SEM of 2 independent experiments (N=2) performed in triplicate (n=3). $P > 0.05$ vs 0% HA (PDL only) control using one-way ANOVA with Tukey posttests in GraphPad Prism V8.01.

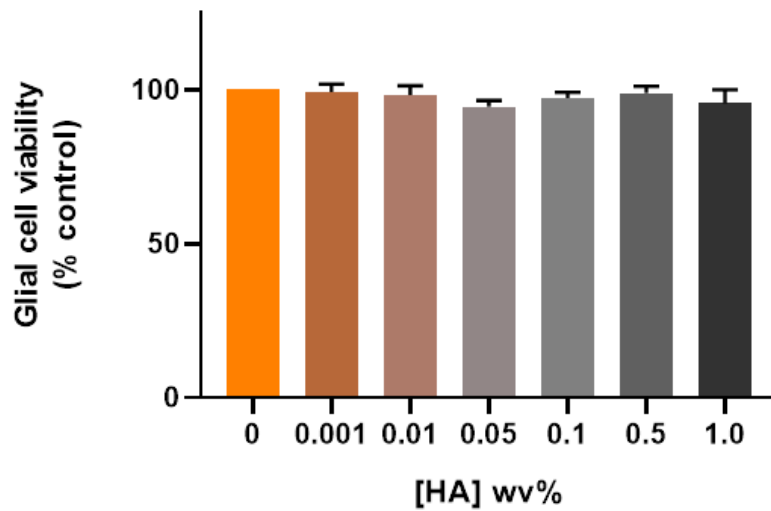


Figure 32. The resazurin reduction assay did not reveal significant toxicity in glial cells exposed to 30-50 kDa HA. No cytotoxicity was observed in glial cells grown on HA coated plates for 24 h (inclusive of 4h resazurin assay). Data is the mean \pm SEM of 2 independent experiments (N=2) performed in triplicate (n=3). $P > 0.05$ vs 0% HA (PDL only) control using one-way ANOVA with Tukey posttests in GraphPad Prism V8.01.

4.2.7 Investigation into the effect of mechanical disruption in the evaluation of HA cytocompatibility in neuronal and glial cell lines using the resazurin reduction assay

Due to the discrepancy in the results between MTT and resazurin when assessing the cytocompatibility of HA, further investigation was necessary. Both assays rely on a similar method of action (MOA), however, there are distinct differences in how the assays are conducted which were initially thought to be the cause of the discrepancy. These differences are highlighted in the methods and detailed diagrams of section 3.2.8.

Figure 33 below is a comparative figure which shows the stark contrast between the potency of cytotoxicity detected via the MTT assay and the resazurin reduction assay. In the MTT assay, media is removed prior to the addition of the tetrazolium dye, and again after incubation before solubilisation of the formazan crystals. In contrast, no media removal steps were utilised in the resazurin assay, with resazurin dye being added directly to the media at the 20 h time point. This difference in methodology was thought to be responsible for the significant difference between results obtained in the two assays which rely upon similar principles. A modified version of the resazurin assay was then developed (Figure 34) in order to determine the effect of mechanical disruption on cells during the assays and whether this was the cause of the enhanced perceived toxicity observed by MTT.

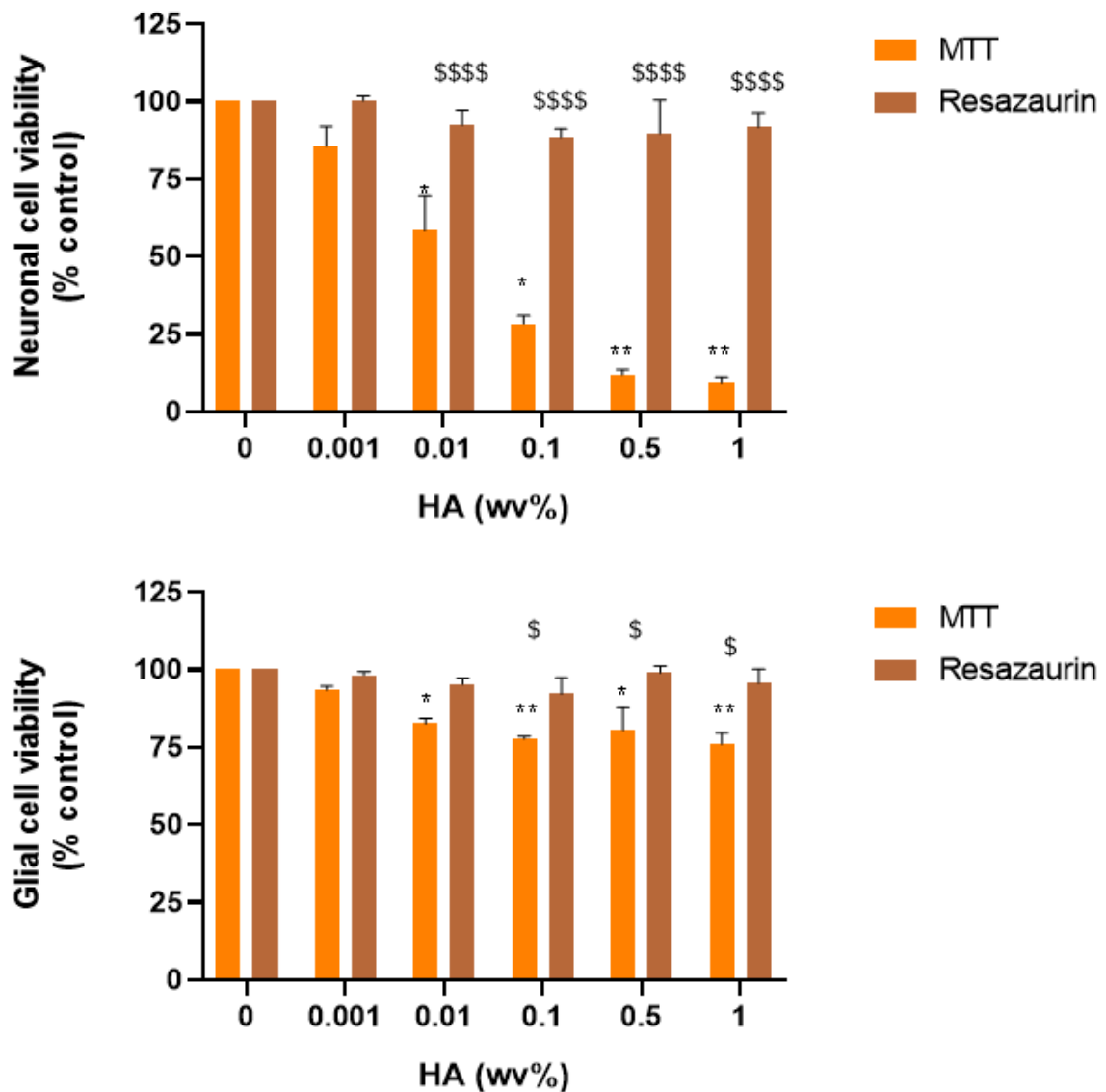


Figure 33. The potent cytotoxicity detected by MTT could not be detected via the resazurin reduction assay. Neuronal and glial cell lines were seeded on 30-50 kDa HA coated plates and incubated for a period of 24 h, inclusive of the assay incubation time. The absorbance (MTT)/ fluorescent (resazurin) intensity was detected at 540 nm (MTT)/ 530/ 590 ex/m (Resazurin). Cell viability is expressed as % of 0% HA control (PDL only). Data is expressed as the mean \pm SEM of 3 experiments (N=3), performed in triplicate (n=3). *P < 0.05, **P < 0.01, ***P < 0.001, ****P < 0.0001 vs 0% HA control when compared using one-way ANOVA with Tukey posttests. \$P < 0.05, \$\$\$P < 0.01 vs Resazurin when compared using two-way ANOVA with Tukey posttests in Graphpad Prism V8.01.

Figure 33 clearly highlights differences in the cytotoxicity representation by MTT and resazurin. This difference was particularly evident in neuronal cells which showed significant differences in results by MTT and resazurin at concentrations exceeding 0.05 %wv HA. A similar response was observed in glial cells at concentrations exceeding 0.1 %wv, however the result was not to the same degree of significance as observed in neuronal cells. This result indicates a potential neuronal sensitivity to HA and MTT, potentially through a synergistic effect.

In order to investigate the effect of mechanical disruption and elucidate whether this was responsible for the difference in metabolic activity response observed, a modified resazurin reduction assay was developed which included two media removal steps at 20 h and 24 h (see section 3.2.6.3 for method) to replicate the mechanical disruption of cells in the procedure of the MTT assay. The results showed a dose-dependent decrease in neuronal cell viability as shown in Figure 34 with a significant reduction in resorufin above 0.1 %wv 30-50 kDa HA (* $P < 0.05$, ** $P < 0.01$ vs. control). The decrease in neuronal cell viability with the modified resazurin reduction assay was significantly different from the results obtained with MTT ($P < 0.05$, $P < 0.01$, $P < 0.001$, $P < 0.0001$ vs. MTT). There was no significant difference between the resorufin intensity between resazurin and modified resazurin when analysed using two-way ANOVA with Tukey Posttests ($P > 0.05$). However, although not significant, there was an evident difference between the traditional and modified resazurin assays. Whilst there was a significant decrease in the metabolic activity observed at concentrations above 0.5 %wv 30-50 kDa HA in the modified resazurin assay, the magnitude of the decrease was still significantly more pronounced at these concentrations in the MTT assay. These results show that the decreased cell viability observed with the MTT assay was not solely related to mechanical disruption, although it is a factor in the cell loss.

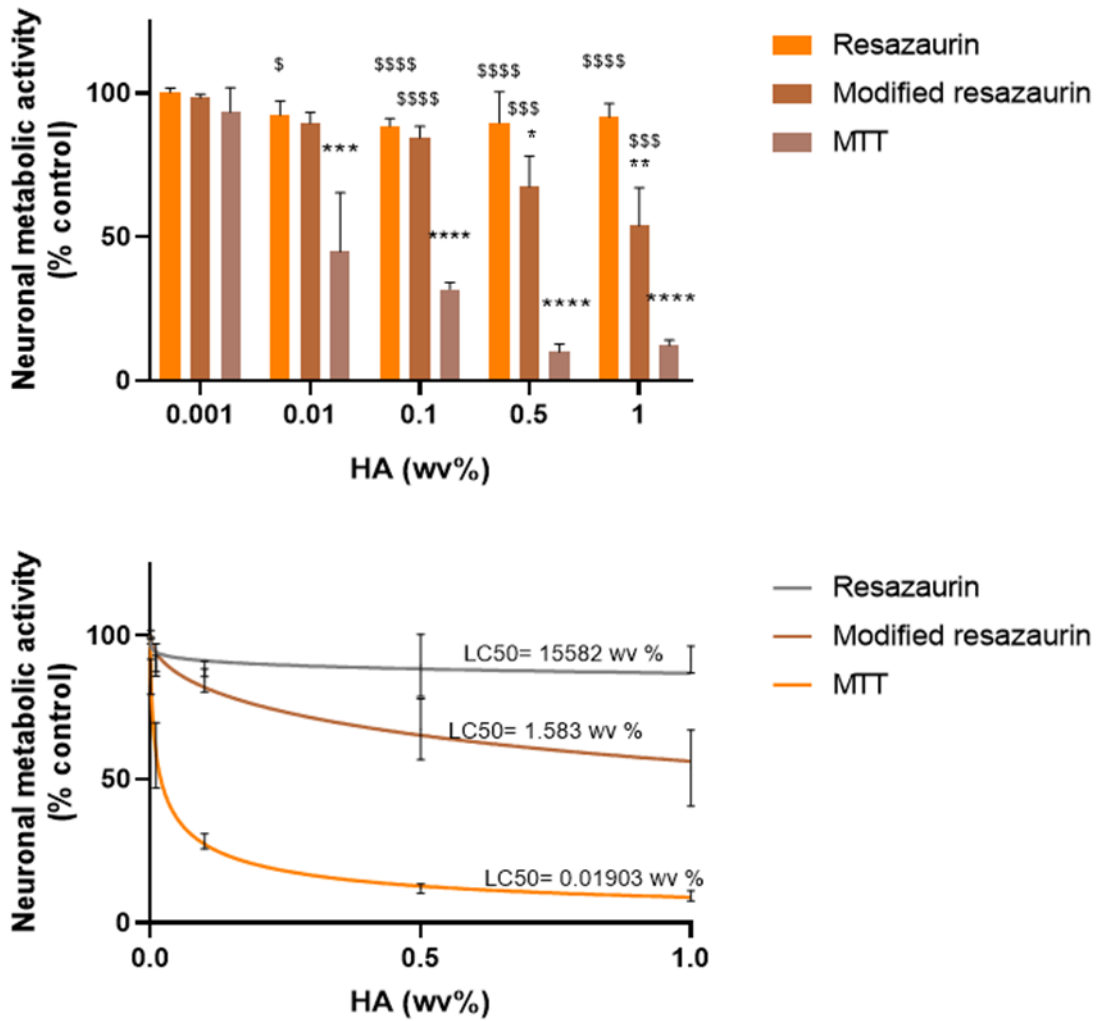


Figure 34. Overestimation of toxicity by MTT is not solely related to mechanical disruption of neuronal cells. Cell viability after 24 h exposure to 30-50 kDa HA (inclusive of 4 h assay incubation) is expressed as % of 0 % HA (no PDL) control. Data shown is the mean \pm SEM of 4 independent experiments (N=4), conducted in triplicate (n=3). * $P < 0.05$, ** $P < 0.01$, *** $P < 0.001$, **** $P < 0.0001$ vs control, $^{\$}P < 0.05$, $^{\$ \$ \$}P < 0.001$, $^{\$ \$ \$ \$}P < 0.0001$ vs MTT when compared using two-way ANOVA with Tukey posttests.

Having determined that mechanical disruption resulted in a significant decrease in metabolic activity in the modified resazurin assay, it was then necessary to evaluate whether the removed cells were in fact dead or simply in suspension and to elucidate if there was synergistic toxicity emanating from the use of either MTT or resazurin, even after accounting for equal mechanical disruption through wash steps. To achieve this, MTT (see Figure 17 for method details) and resazurin (see Figure 18 for method details) attachment assays were developed with TBE assays in parallel to quantify the number of cells removed at each media removal step, and analyse their viability. These methods consisted of three counts; count 1 occurred in all conditions after 20 h 30-50 kDa HA exposure before the addition of assay dye. Count 2 occurred after 4 h assay incubation (24 h total HA exposure time) in all conditions. Count 3 only occurred in the TBE stream (right hand side stream of Figure 17 and Figure 18), and this occurred after the addition of trypsin to each well.

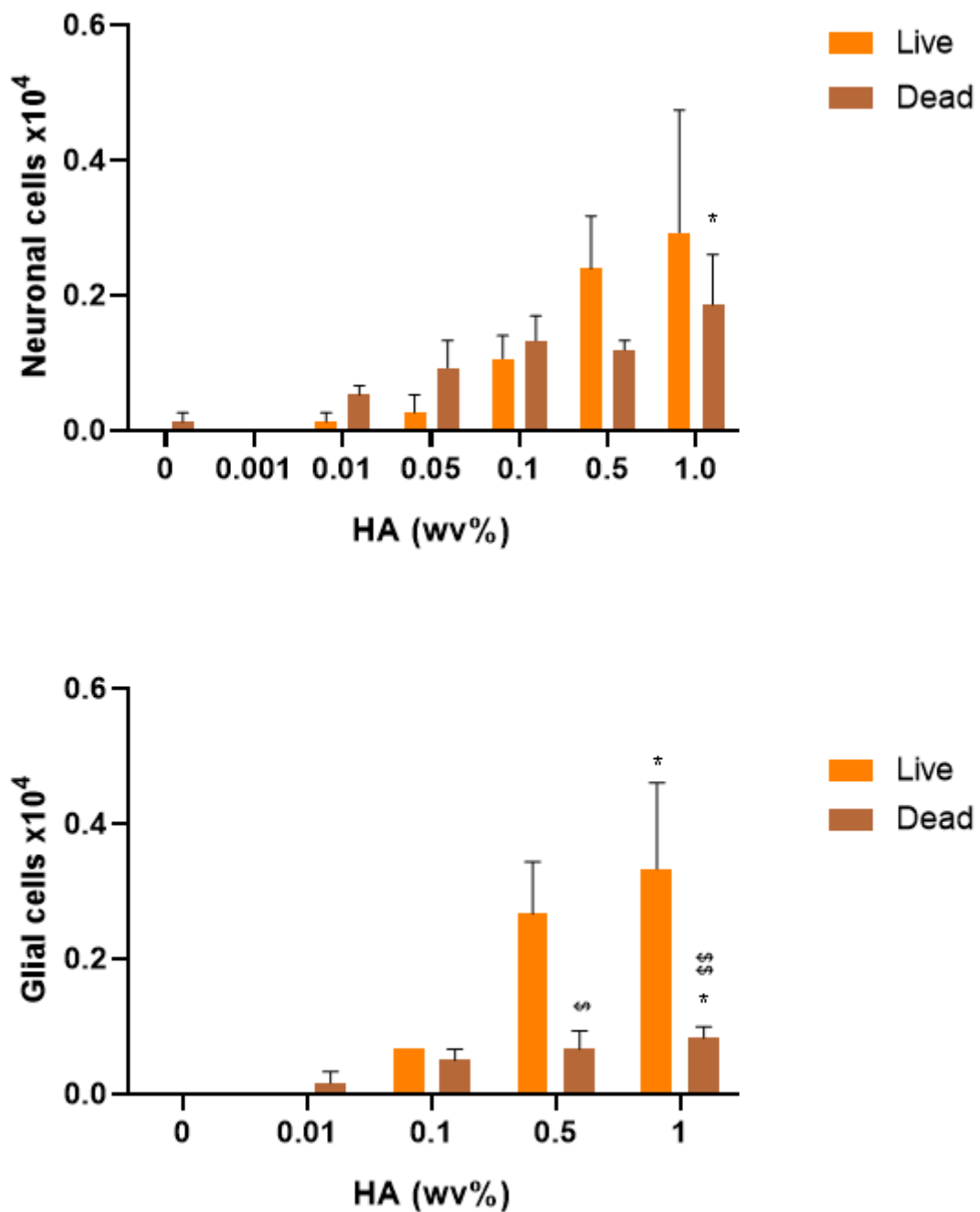


Figure 35. Dose-dependent effect of 30-50 kDa HA in neuronal and glial cells at count 1 (20 hour exposure to HA). Data shown is the mean \pm SEM of 5 independent experiments (N=5), conducted in triplicate (n=3). * P < 0.05 vs control, $^{\$}$ P < 0.05, $^{\$}$ P < 0.01 vs live when compared using two-way ANOVA with Tukey posttests in GraphPad Prism V8.01.

Figure 35 shows the effect of 30-50 kDa HA after 20 h exposure in both neuronal and glial cells where less than 4,000 unattached cells were counted out of an initial 150,000 cells which were seeded into each well. Therefore, approximately 2.7% (when compared to total number of cells initially seeded) of total cells were unattached after 20 h exposure to LMW HA. In neuronal cells, no significant difference was observed when comparing the number of live vs dead cells but a significant difference was detected in glial cells ($^{$$}P > 0.05$). However, after the addition of MTT, the number of unattached cells rose to approximately 80000 (Figure 36 neuronal) and 60000 (Figure 36 glial) respectively in a dose-dependent manner ($^{****}P < 0.0001$ vs. control). This result significantly differed from the number of unattached cells obtained during the resazurin or TBE assay (Figure 36) ($^{$$$$}P < 0.0001$). Of the large proportion of cells that had detached from each well, 10% of these cells were determined unviable by TBE at the highest HA concentration. Additionally, MTT significantly increased the number of live cells detached when compared against both the resazurin reduction assay and the TBE assay ($^{\$}P < 0.05$, $^{$$}P < 0.01$, $^{$$$}P < 0.001$, $^{$$$$}P < 0.0001$ vs. resazurin/ TBE). No significance, $P > 0.05$, was noted when comparing the number of dead cells counted in each treatment (Figure 36), however, there was a significant increase in the number of dead cells detected by TBE at 1 %wv HA ($^{*}P < 0.05$) in neuronal cells.

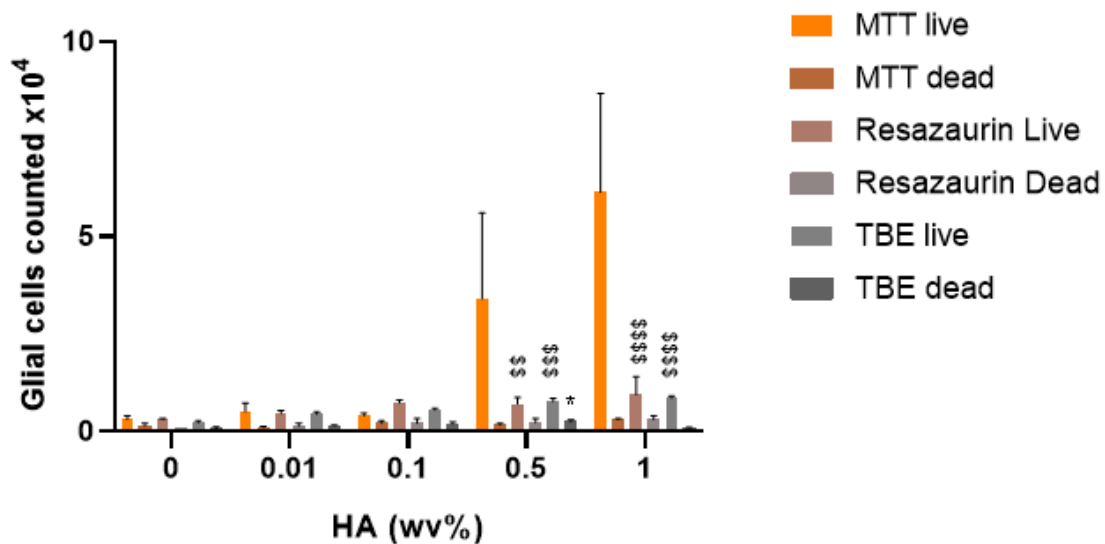
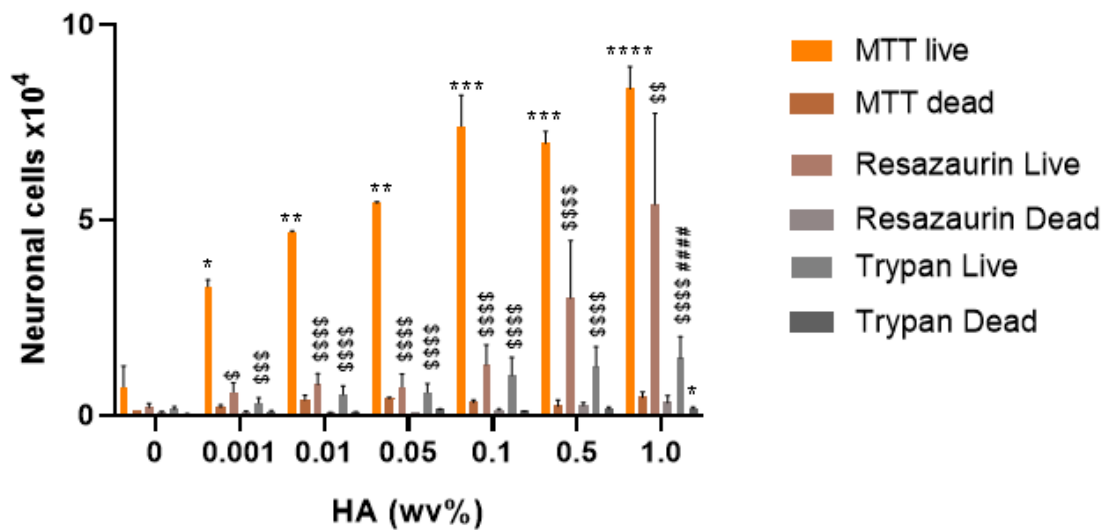


Figure 36. MTT significantly increases the detachment of neuronal cells in the presence of HA at count 2 (24 h exposure to HA). Graphs show neuronal and glial cell detachment after 24 h HA exposure (inclusive of 4 h assay incubation). Data shown is the mean \pm SEM of 3 independent experiments (N=3), conducted in triplicate (n=3). * $P < 0.05$, ** $P < 0.01$, *** $P < 0.001$, **** $P < 0.0001$ vs control, $^{\$}P < 0.05$, $^{\$\$}P < 0.01$, $^{$$$}P < 0.001$, $^{$$$$}P < 0.0001$ vs live when compared using two-way ANOVA with Tukey posttests in GraphPad Prism V8.01.

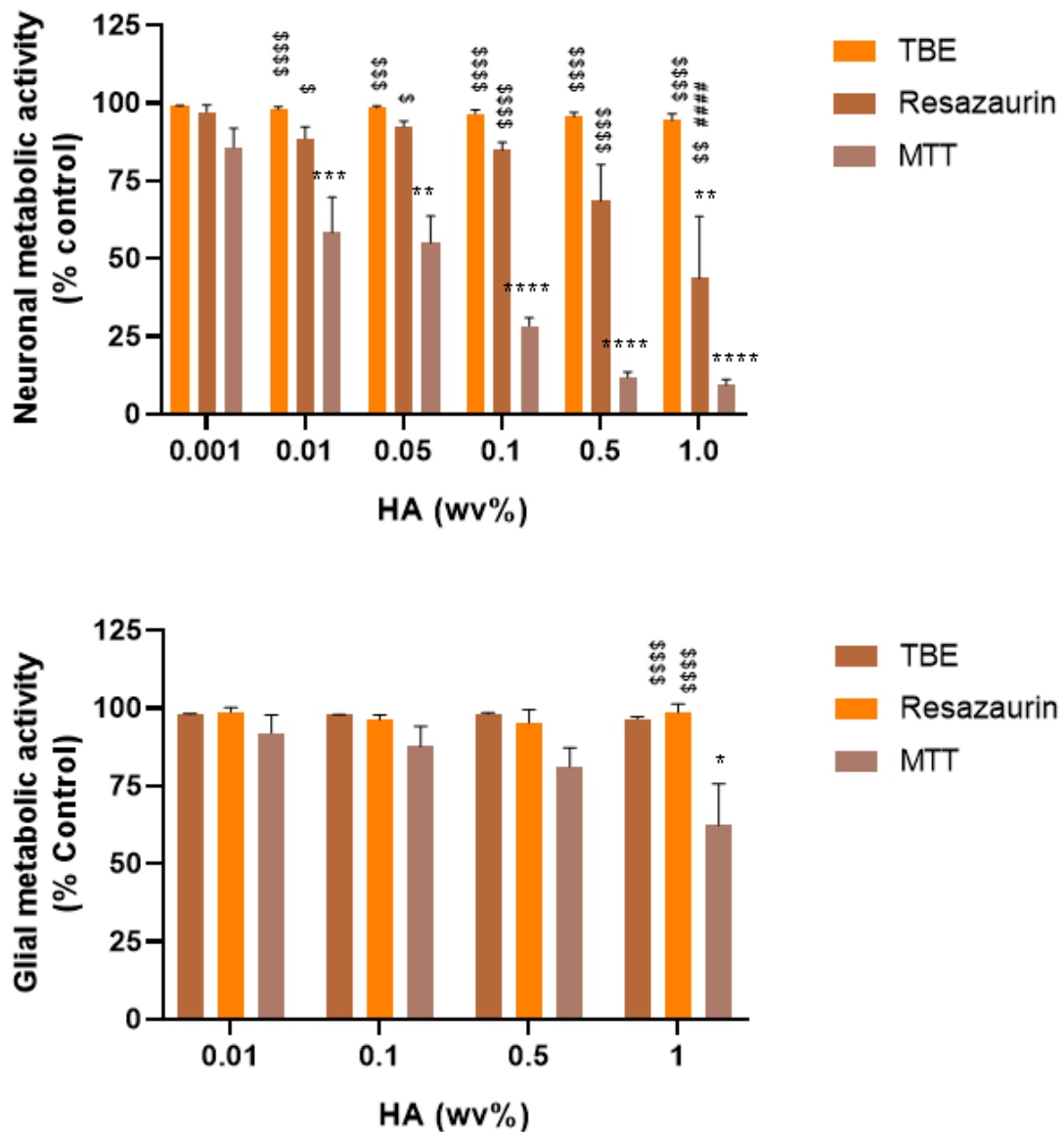


Figure 37. MTT enhances HA toxicity in neuronal cells. Graphs illustrate the cell viability at Count 3. Data was obtained by detecting absorbance intensity of solubilised formazan for MTT, fluorescent intensity of resorufin for Resazaurin reduction assay and the number of cells counted after trypsin for the TBE assay. All data is expressed as a % of the 0 % HA control. Data shown is the mean \pm SEM of 3 independent experiments (N=3), conducted in triplicate (n=3). * $P < 0.05$, ** $P < 0.01$, *** $P < 0.001$, **** $P < 0.0001$ vs control, \$ $P < 0.05$, \$\$ $P < 0.01$, \$\$\$ $P < 0.001$, \$\$\$\$ $P < 0.0001$ vs MTT when compared using two-way ANOVA with Tukey posttests in GraphPad Prism V8.01.

4.3 DISCUSSION

Chapter 4 was concerned with the initial screening and characterisation of low and high MW HA, and optimisation of testing methods. Because of the unique physicochemical properties of HA, it presents unique challenges when faced with the prospect of *in vitro* testing. It was for this reason that it was decided that a coating procedure would be utilised to overcome the viscosity issue while still ensuring direct contact as outlined in ISO 10993-5:2009 for the biological evaluation of medical devices. Once cell characterisation was completed and a cell density selected, plate coatings were analysed using either PDL or deionised water as a diluent for HA. This evaluation took place by using Alcian Blue which complexes with HA to produce a qualitative result which can be interpreted as semi-quantitative by solubilising the coloured complex formed. Both the qualitative and quantitative data was used to inform the decision on diluent as despite no significant difference being observed between samples in water vs PDL, qualitative analysis revealed very different results. The addition of PDL to the HA solutions allowed for a smooth, continuous and homogenous HA coating of the cell culture plate, most likely due to alteration of surface tension and interfacial adhesion. When the plates were coated using HA and water, however, aggregates were observed within the well which would significantly bias the reading of cytotoxicity studies. As a result, all HA studies following were performed using a solution of HA in PDL and using this to coat plates in the desired concentrations. This allowed for consistency and replicability across all results enabling the comparison and contrasting of results when new variables were introduced.

Once the methodology was validated, it was necessary to screen a variety of HA molecular weights. HA is available in MWs ranging from oligo sizes (5-10 kDa) up to very high MW (>2000 KDa) and the literature outlines very different effects on the body depending on the MW used. HA in MWs ranging from 30-50 kDa up to 2000-2,200 KDa were screened in neuronal and glial cell lines to evaluate the viscosity of coatings and MW dependent cytotoxicity. Alcian Blue analysis demonstrated that as the MW and viscosity increased, so too did the coating retention after washing. The resazurin assay then revealed that decreased cell attachment was observed that was directly proportional to increasing MW. The combination of this qualitative and quantitative analysis led to the hypothesis that increased MW was responsible for the increased viscosity and therefore increased retention of coating. This additional retained coating could prevent cell attachment. To confirm this, trypan blue was utilised to analyse the number and viability of cells lost as a result of detachment. The results of this series of assays showed that increased MW led to decreased attachment of

both neuronal and glial cells but the cells remained viable. On the basis of these data, it was determined that 30-50 kDa would be chosen for additional testing as this had the least impact on cellular attachment.

Cytocompatibility testing of 30-50 kDa HA was undertaken using the MTT assay which relies upon the metabolic conversion of the soluble tetrazolium dye to insoluble formazan within the cell which is directly proportional to the rate of metabolic processes and therefore can be used as an indicator of cell viability via metabolic activity. Tissue culture plates were coated with 30-50 kDa HA and cells were seeded on the HA surface and allowed to grow for 20 h prior to the removal of spent media and addition of MTT dye and incubation for a further 4 h. This media removal step introduces a level of mechanical disruption to the cells. After 4 h, the media containing MTT was removed before the addition of DMSO to solubilise the formazan. MTT revealed significant perceived toxicity that hadn't been observed in the resazurin molecular weight screen, particularly in the case of the neuronal cells. This result could not be repeated with a standard resazurin assay and therefore it was postulated that the result was as a result of mechanical forces within the standard procedure of an MTT assay. To test this, it was necessary to design a new assay, the modified resazurin assay, which could account for and mimic the cell loss observed at each wash stage of an MTT assay. The method flowchart for both attachment assays can be seen in Figures 17 and 18, section 3.2.8. Throughout these assays, the cell loss at each wash stage was quantified using trypan blue to determine the live dead cell ratio of the unattached cell populations. By utilising these attachment assays, it could be concluded that MTT was causing significant cell loss in the presence of HA, particularly in the case of neuronal cells. This result could not be replicated with either resazurin, modified resazurin assay or the trypan blue exclusion assay. However, the modified resazurin assay did show significantly decreased metabolic activity via resorufin vs control, although this was determined not to be significant in comparison to the traditional resazurin assay. This is indicative of the role mechanical disruption plays in cell loss, but does not account for the degree of cell loss observed. This has highlighted the need for a battery approach when evaluating the cytocompatibility of materials.

It is theorised that a synergistic effect occurred between HA and MTT which would account for the increased cell loss observed with MTT vs the modified resazurin assay. Although significant cell loss was observed with the modified resazurin assay, significantly greater cell loss was observed with MTT. In a paper by Lü *et al.*, (2012), the authors showed that the metabolism and exocytosis of MTT could activate apoptosis related factors in SH-SY5Y

and cause physical damage to cells. In this study, the authors showed that MTT could induce cell death and that this response was time dependent. This cell death occurred due to the increased plasma permeability and exocytosis of intracellular granules and subsequent formation of formazan crystals. Additionally, numerous studies have found interactions between drug substances and MTT which may result in overestimation of toxicity (Asuzu *et al.*, 2022; Hassan *et al.*, 2022). However, it was determined through this study that although the cells were unattached, they largely remained viable. This would indicate that the synergistic effect between MTT and HA impacted the cell adhesion of SH-SY5Y in a manner that was neuron specific.

Overall, this chapter has provided insight into the utility of PDL to obtain smooth, homogenous and continuous coatings for direct contact testing of neuronal and glial cell lines. Additionally, MWs of HA ranging from 30 kDa to 2200 kDa were screened, and 30-50 kDa was found to be the lead compound for further evaluation. This decision was made due to the reduced viscosity observed in Figure 29, which would allow for ease in manufacturing later, as well as enabling greater cell adhesion as shown in Figures 25-28. Additionally, traditional assays were utilised and modified to enable accurate capturing of the cell viability in the presence of 30-50 kDa HA. These modified assays allowed for the accounting of mechanical disturbance of cells while avoiding the other potential issues with MTT such as synergistic effects with the HA.

**CHAPTER 5. MODIFICATION OF HYALURONIC ACID
TO ENABLE UV PHOTO-CROSSLINKING**

5.1 PREFACE

HA has the potential for utility in a variety of industries due to its unique physicochemical properties. However, the native structure of HA is not conducive to cell attachment in *in vitro* model systems or ease in cross-linking. Therefore, the purpose of this section was to develop a method of modification of the HA molecule which would enable highly reliable click chemistry cross-linking to occur.

The first method was to modify HA using a thiol containing compound. N-acetyl cysteine was the first compound chosen due to the associated anti-oxidant activity of the drug. However, the degree of modification (MoD) obtained in first tests was unsatisfactory, thus it was decided to use a thiol molecule with a simpler structure to prevent steric hindrance. The compound chosen for further testing was cysteamine HCl to produce thiolated HA (HA-SH). The reaction undertaken was an amidation reaction as shown in Figure 38 and consistently produced a MoD of $20 \pm 9\%$.

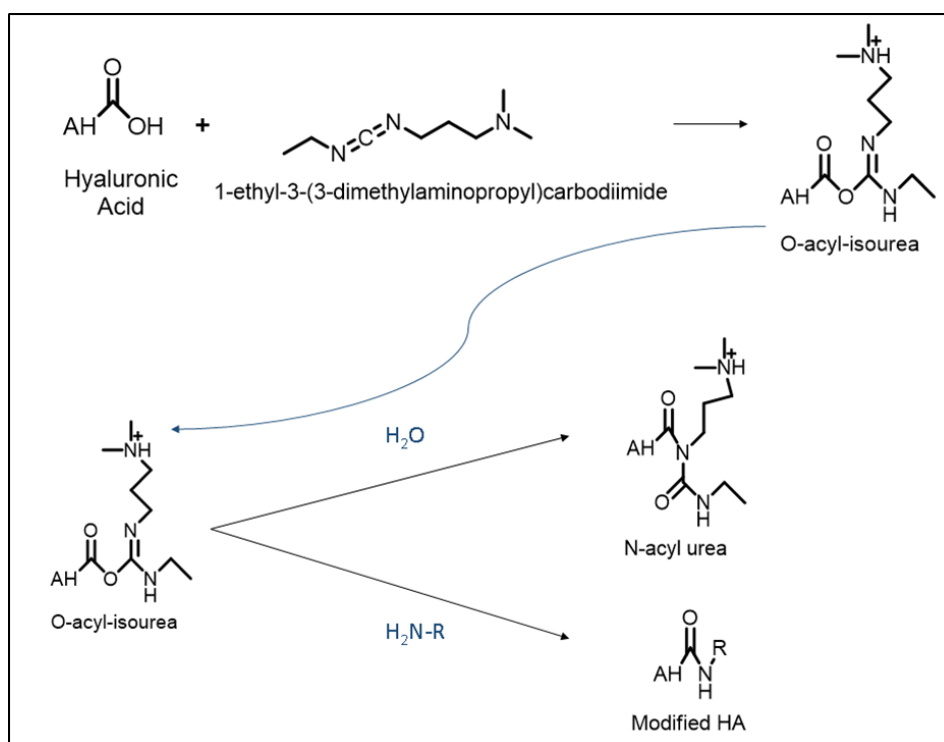


Figure 38. Amidation reaction for the production of cysteamine modified HA. Reaction scheme example of an amidation reaction for the production of HA-SH. Highlighted is the potential formation of the stable N-acyl urea.

Thiolated HA will not photo-crosslink with itself as it requires an alkene bond and therefore it was necessary to introduce another functional group to enable photo-crosslinking between HA molecules. For this purpose, HA was modified with methacrylic anhydride to produce methacrylated hyaluronic acid (HA-MA). Various molar equivalents of methacrylic anhydride were trialled in the reaction to determine the ratio of reactants that would consistently produce a MoD of approximately 20%.

The HA derivatives were extensively characterised for their physicochemical and biological properties before utilising these compounds in UV photo-crosslinking reactions which are outlined in chapter 6.

5.2 RESULTS

5.2.1 Thiolation of HA

Thiolated HA (HA-SH) was produced via a carbodiimide mediated substitution reaction and the subsequent product was extensively dialysed, filtered and lyophilised to obtain a fluffy white spongy material which flaked. 30-50kDa HA was selected as the optimal molecular weight to modify due to the results shown in chapter 4, and the lower viscosity when compared to its higher molecular weight counterparts. In order to confirm thiolation of the HA molecule and calculate the degree of modification (MoD), many methods were utilised such as FTIR, the Ellmans assay and H^1 -NMR. The thiol bearing HA shows little change in the FTIR, however, the signal resulting from the thiol SH is likely broadened by the polymeric nature of the sample and while the C-S is in the fingerprint region ($400-1500\text{ cm}^{-1}$). Therefore, NMR and the Ellmans assay were used for qualitative and quantitative analysis of the thiolated product.

5.2.1.1 $^1\text{H-NMR}$ analysis of HA-SH

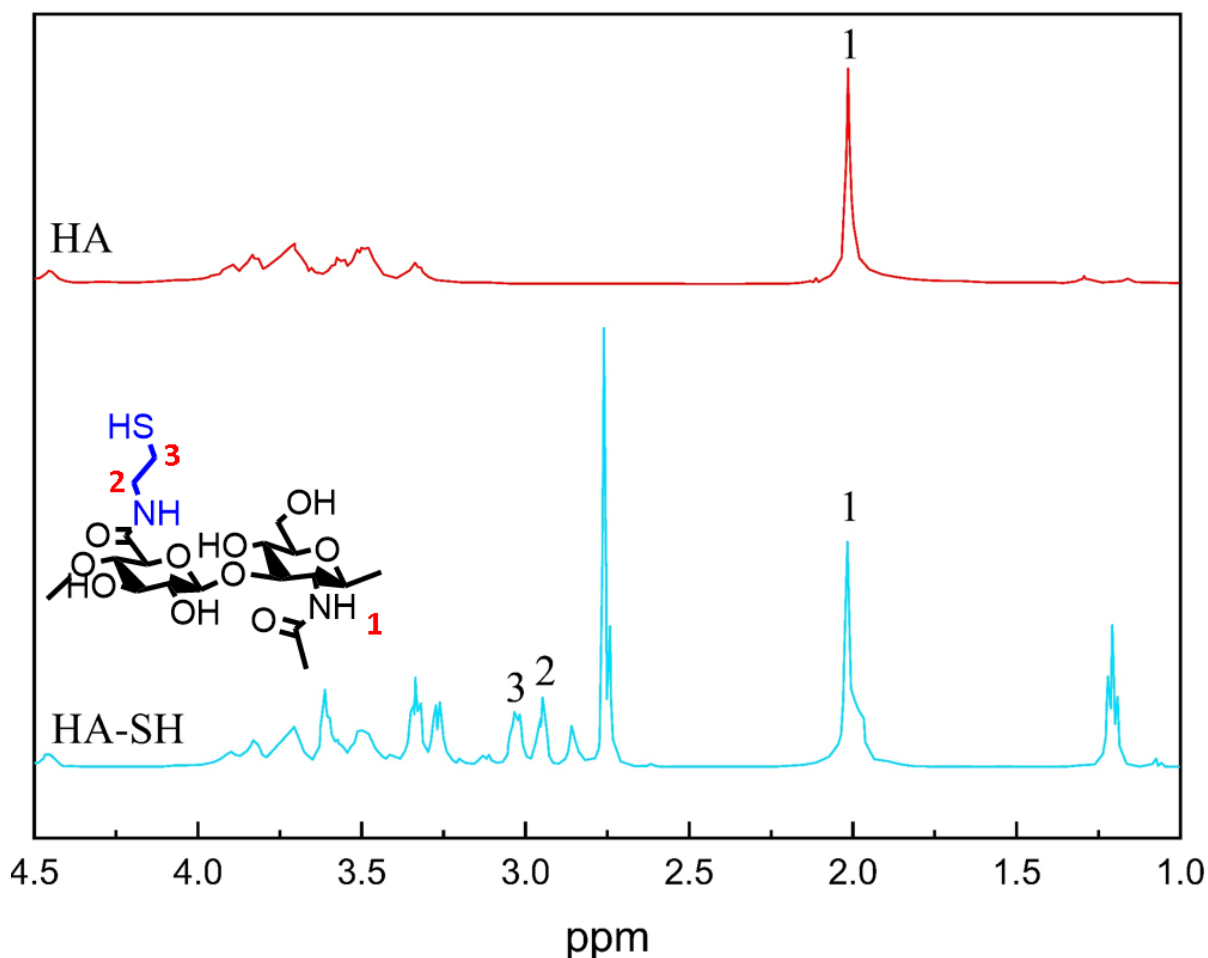


Figure 39. $^1\text{H-NMR}$ spectrum of HA-SH. Spectrum of HA and HA-SH spectrums with water suppression and key peaks labelled which correspond to labelled functional groups on the displayed HA-SH structure.

$^1\text{H-NMR}$ analysis of the modified compound revealed the methylene protons of cysteamine at 2.9 ppm and 3.04 ppm as seen in the HA-SH spectrum above. The degree of thiolation was calculated through integration of the peaks relative to the N-acetyl peak of HA, which is labelled as (1) in Figure 39 above. The degree of modification was calculated to be approximately 27.7% ($N=3$). For the purposes of purity checking and spectral assignment, $^{13}\text{C/DEPT-90/DEPT-135/HH-CoSy/HSQC/HMBC}$ spectra (not shown) were also obtained.

5.2.1.2 Ellmans assay of HA-SH

The concentration of both free and bound thiol was calculated via the Ellmans assay in the HA-SH sample. This assay provides a colorimetric response proportional to the concentration of thiol in the sample and the addition of 8M urea enables cleavage of disulphide bonds and calculation of the bound thiol in the sample. Therefore, total thiol can be calculated, from which the degree of modification can be calculated. An absorption spectrum was obtained for Ellmans reagent to determine the λ_{max} of the Ellmans reagent as shown in Figure 40 below.

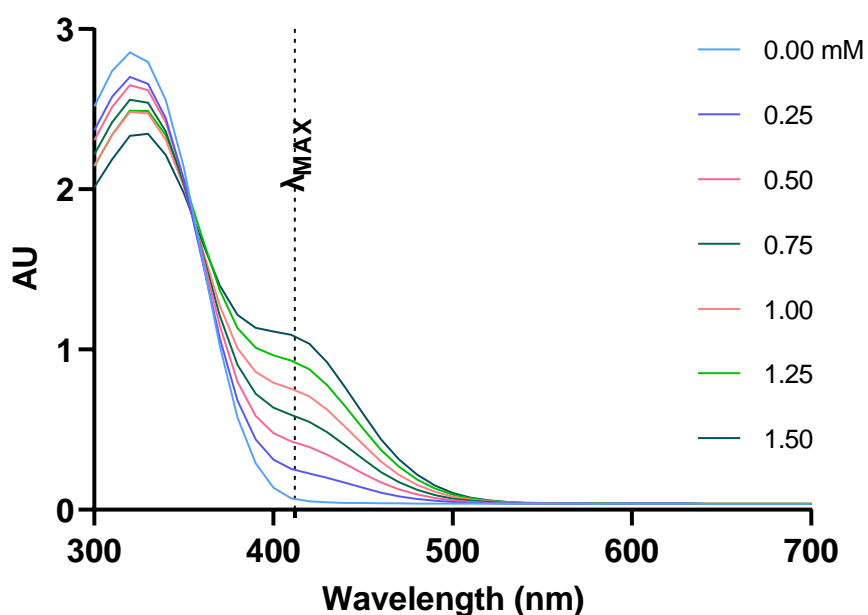
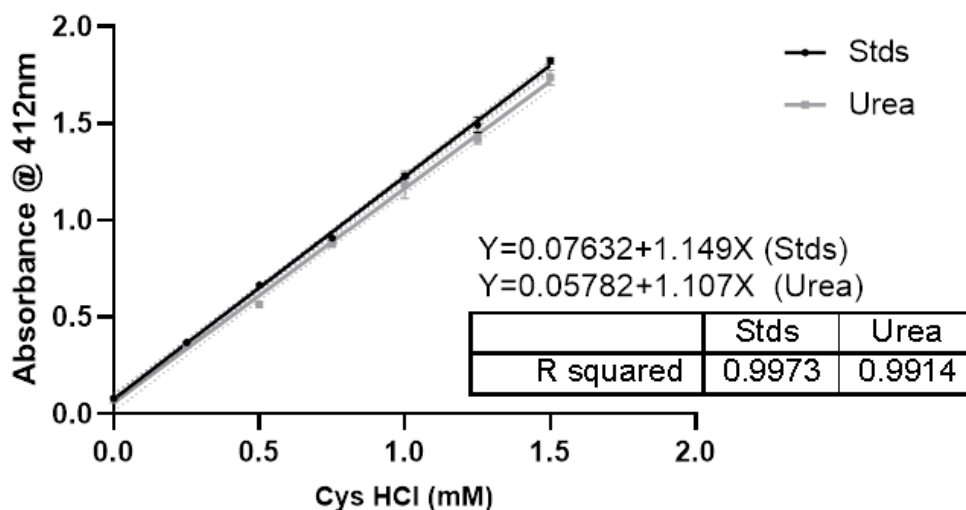


Figure 40. Absorption spectrum for Ellmans reagent from 300-700 nm.

A series of cysteamine standards were assayed to obtain a standard curve from which experimental samples could be tested against. Figure 41 below illustrates the cysteamine standard curve with the values obtained for the experimental samples. The experimental samples were tested for free thiol (Stds) and bound thiol (Urea), and from these values the total thiol content of each sample could be calculated. A total thiol concentration of 0.515 mM was obtained (N=5).



	X (Interpolated)	Stds (Entered)	Urea (Entered)
HA-SH	0.290	0.410	
HA		0.075	
HA-SH	0.225		0.307
HA	0.013		0.072

Total thiol (HA-SH): 0.515 mM

Figure 41. Ellmans assay for total thiol determination. Total thiol content of each sample was determined for each HA-SH and HA by combining the free thiol content in TGE buffer (Std) with the thiol detected from the cleavage of disulphide bonds (Urea). Unmodified HA was analysed as a control. Data is the mean \pm 5 independent experiments (N=5), conducted in triplicate (n=3). Data was analysed using GraphPad Prism V8.01.

The Ellmans assay consistently produced a degree of modification of approximately 22%. This was calculated based on the total number of HA monomers available for modification. This value was within the range of the 20% that was aimed for so as not to hinder the functionality of the HA receptors such as CD44.

5.2.2 *Methacrylation of HA*

Methacrylated HA (HA-MA) was prepared by reacting a 2 %wv solution of HA in deionised water with a 10-fold molar excess of methacrylic anhydride (MA). The molar excess was elucidated through a series of reactions utilising different molar equivalents and the degree of modification (MoD) was quantified via ¹H-NMR and Reverse-phase HPLC. Using a 10 molar excess of methacrylic anhydride produced the optimal MoD, approximately 20%, to enable cross-linking without sacrificing the bioactivity of the polymer. The reaction was continuously adjusted to pH 8-9 with 5M NaOH to drive the reaction forward. Once the reaction had completed, the solution was dialysed as before against basic water (pH 10) for 24 hours with water changes every 4 hours followed by 24 hours against acidified water with 4 hourly water changes. The resulting dialysate was vacuum filtered before lyophilisation and storage at -20°C until needed.

5.2.2.1 FTIR of HA-MA

ATR-FTIR analysis was completed on the HA derivatives in lyophilised powder form. In all spectra, the characteristic OH peak is visible at 3298.8 cm^{-1} along with N-H stretching arising from the N-acetyl side chain of HA. The peaks appearing at approximately 1030 cm^{-1} can be attributed to the C-OH whereas the peaks identified at 1605 and 1405 cm^{-1} can be attributed to the asymmetric (C = O) and symmetric (C-O) stretching modes of the planar carboxyl groups in HA.

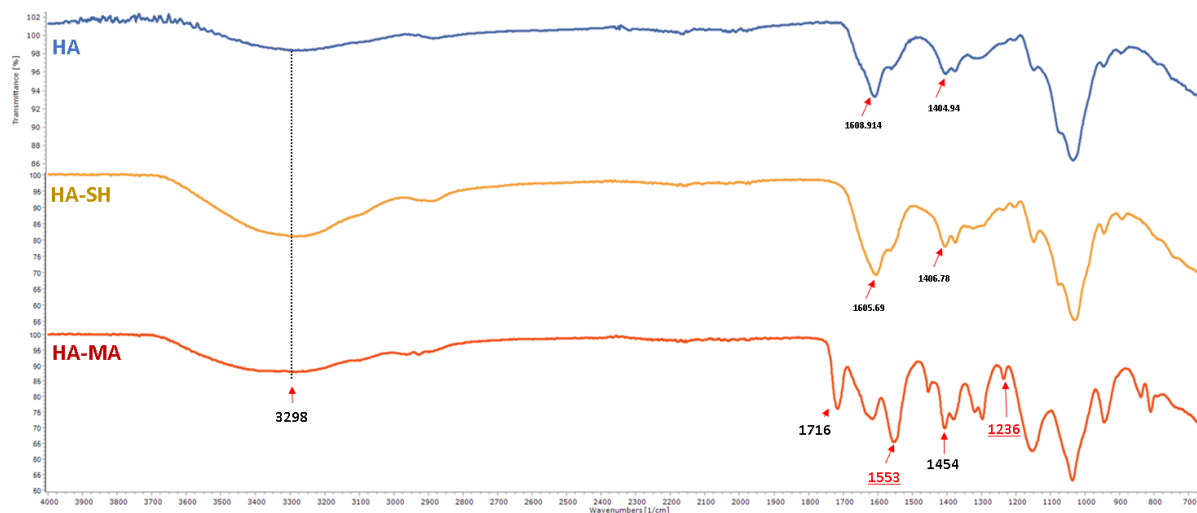


Figure 42. FTIR comparison of HA, HA-SH and HA-MA. ATR-FTIR analysis was completed in triplicate on lyophilised samples of HA (blue), HA-SH (yellow) and HA-MA (red). The main identifying peaks are labelled.

The thiol bearing HA shows little change in the FTIR however, the signal resulting from the thiol SH is likely broadened by the polymeric nature of the sample and while the C-S is in the fingerprint region ($400\text{-}1500\text{ cm}^{-1}$). The presence of a peak at 1716 cm^{-1} arises from the methacrylic ester carbonyl vibration, confirming successful methacrylation of the HA. The peaks denoted in red highlight the peaks that disappear when cross-linked as will be highlighted later in the document.

5.2.2.2 ^1H NMR analysis of methacrylated HA

^1H -NMR analysis of the lyophilised HA-MA product revealed the vinyl protons of methacrylate at approximately 5.9 ppm and 6.1 ppm. It also appeared that there was some contaminants in the product and therefore, an extra dialysis against basic water was introduced to the methodology to ensure all unreacted methacrylic acid was removed prior to drying. The MoD of HA-MA was determined relative to the N-acetyl peak as before.

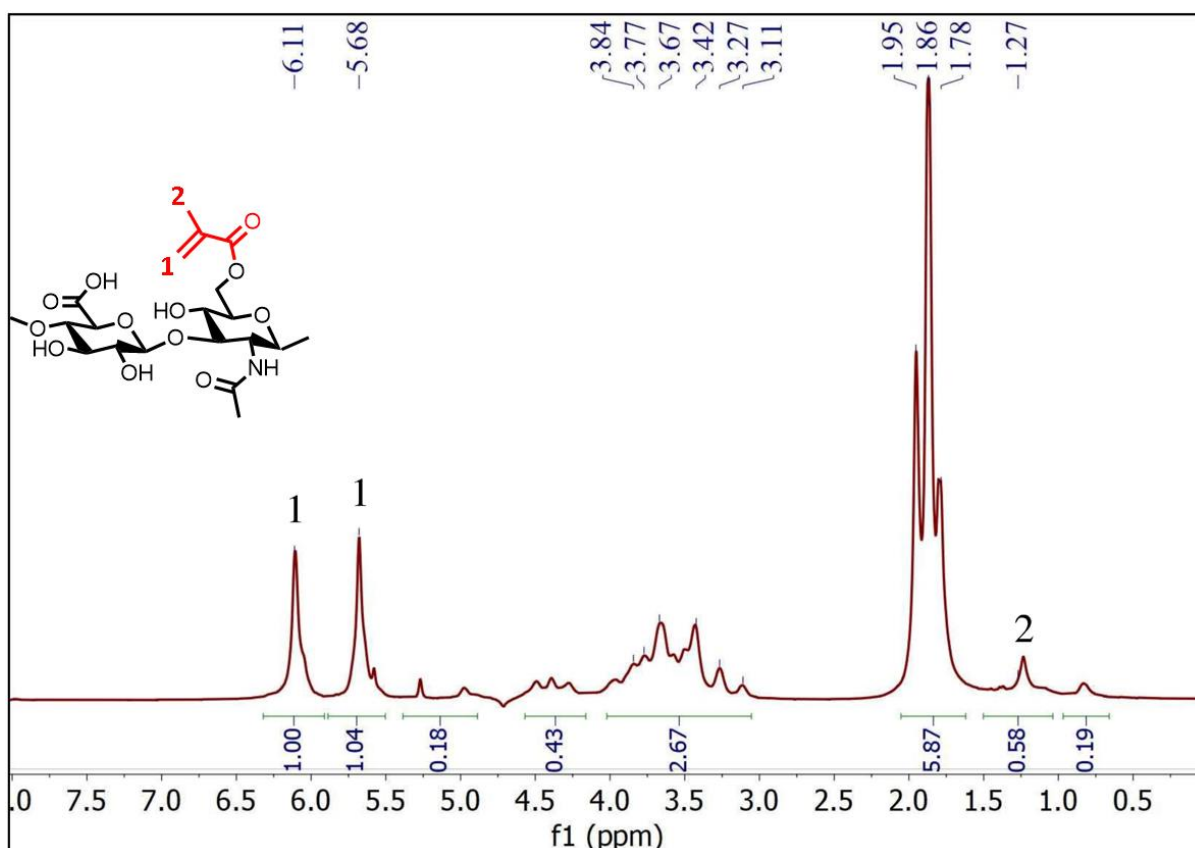


Figure 43. ^1H -NMR analysis of HA-MA. Spectrum shows HA-MA with main peaks labelled and their corresponding functional groups on the attached chemical structure.

The MoD was determined by ^1H -NMR for HA-MA was approximately 20%. This value is in agreement with the target MoD of 20% to enable continuation of receptor interactions.

5.2.2.3 RP-HPLC of HA-MA

RP-HPLC was employed to confirm the MoD obtained via the integrals of NMR. This was done by first obtaining a standard curve of methacrylic acid standards before then running samples prepared by reacting 1X, 10X and 30X molar equivalents of methacrylic acid with HA.

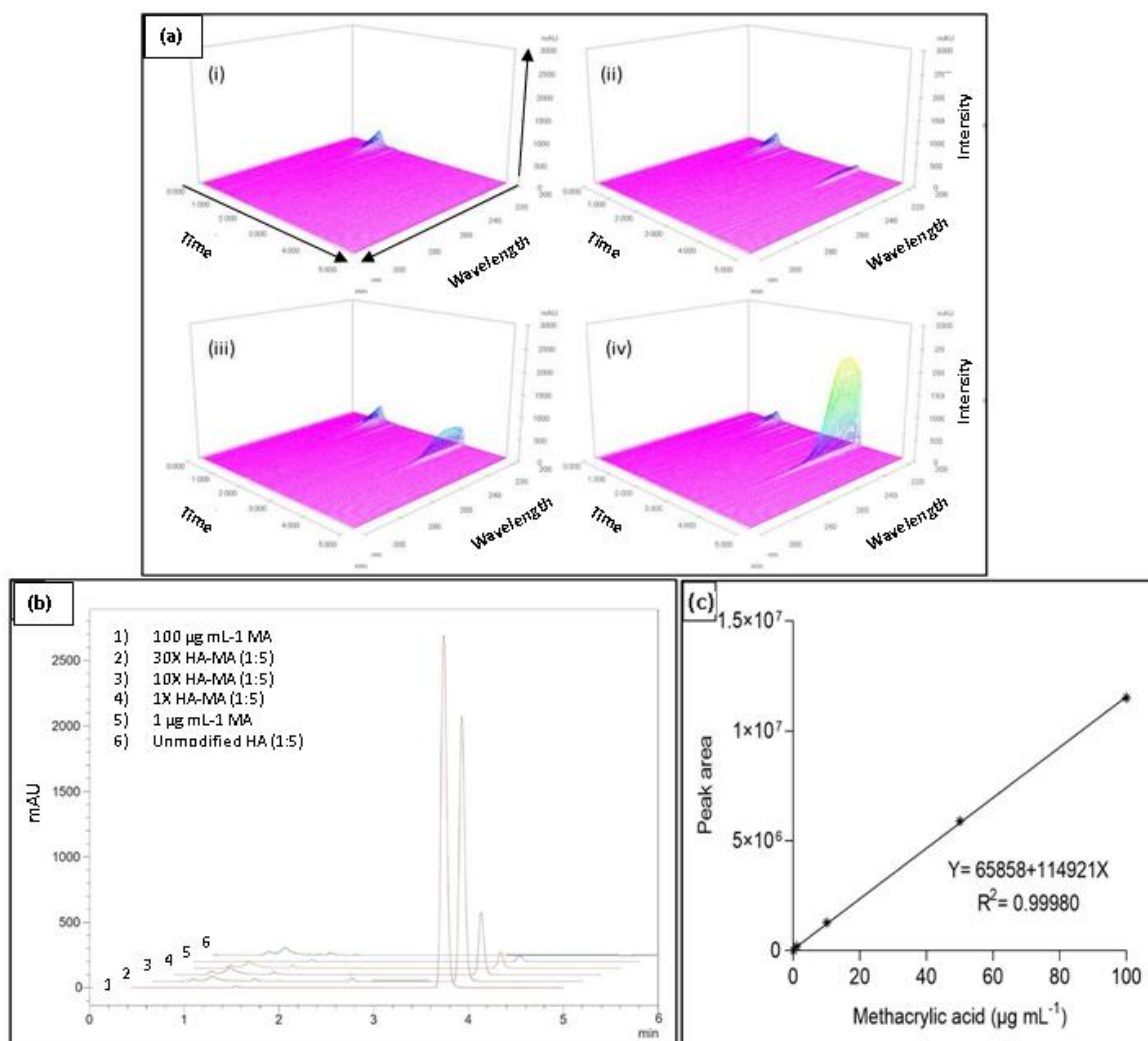


Figure 44. Quantification of MoD of HA-MA. (a) 3D chromatograms of 1:5 diluted samples of (i) HA, (ii) 1X HA-MA, (iii) 10X HA-MA and (iv) 30X HA-MA. (b) Chromatogram overlay of samples at 210 nm. (c) Calibration curve of methacrylic acid standards (0.05- 100 µg/ ml).

Figure 44 above shows the 3D chromatograms (a) of diluted samples of unmodified HA (i), 1X HA-MA (ii), 10X HA-MA (iii) and 30X HA-MA (iv) where the fold number refers to the molar equivalents used during the modification process. Also shown in Figure 44 is the chromatogram overlays of samples (b) and the calibration curve of methacrylic acid samples (c) from which the degree of substitution of HA-MA was calculated. Due to increased reactivity, as a result of lower steric hindrance, the primary alcohol at C6 of the N-acetylglucosamine moiety undergoes modification chemoselectively. It was found that using a 1 molar equivalent of methacrylic anhydride resulted in 6 % of primary hydroxyls modified, a 10-fold molar excess of methacrylic anhydride resulted in 25 % and a 30-fold excess of methacrylic anhydride resulted in 124 % of primary hydroxyls modified. The degree of substitution (DS) of HA-MA was calculated using the formula below as adapted from Eyley, Klug and Diephuis, 1947:

$$DS = \frac{MW_{HAU} \times m_{MA}}{MW_{MA} - m_{net} \times m_{MA}}$$

Where:

MW_{HAU} : Molecular weight of anhydrodisaccharide unit of hyaluronic acid.

m_{MA} : Mass of methacrylic acid in sample of modified hyaluronic acid.

MW_{MA} : Molecular weight of methacrylic acid.

m_{net} : Net increase in mass of anhydrodisaccharide unit for each methacrylate group substituted.

These results agreed with the degree of modification calculated via NMR and on this basis, a 10-fold excess of methacrylic anhydride was used for subsequent modifications.

5.2.3 Cytocompatibility of HA derivatives

The cytocompatibility of HA-SH and HA-MA was evaluated in neuronal and glial cells. Due to the enhanced cytotoxicity observed via MTT in section 4.2.7, the resazurin reduction assay and neutral red (as outlined in section 3.3.4) uptake assay were employed to assess cell viability in the presence of the lyophilised derivatives. The use of neutral red provided a non-metabolic based method for determining cell viability, without the additional labour of cell counting. In this method, neutral red uptake was used to evaluate cell viability via membrane integrity (Asuzu *et al.*, 2022). The plates were coated as outlined in section 3.2.5 in either HA, HA-MA or HA-SH, utilising PDL as a diluent. The cells were exposed to the HA or HA derivative for 20 h before the addition of assay dye (24 h total exposure time). The neutral red assay is independent of cell metabolism and works on a similar basis to trypan blue in that it is dependent on cell membrane integrity, therefore it was useful as a component of the battery testing approach.

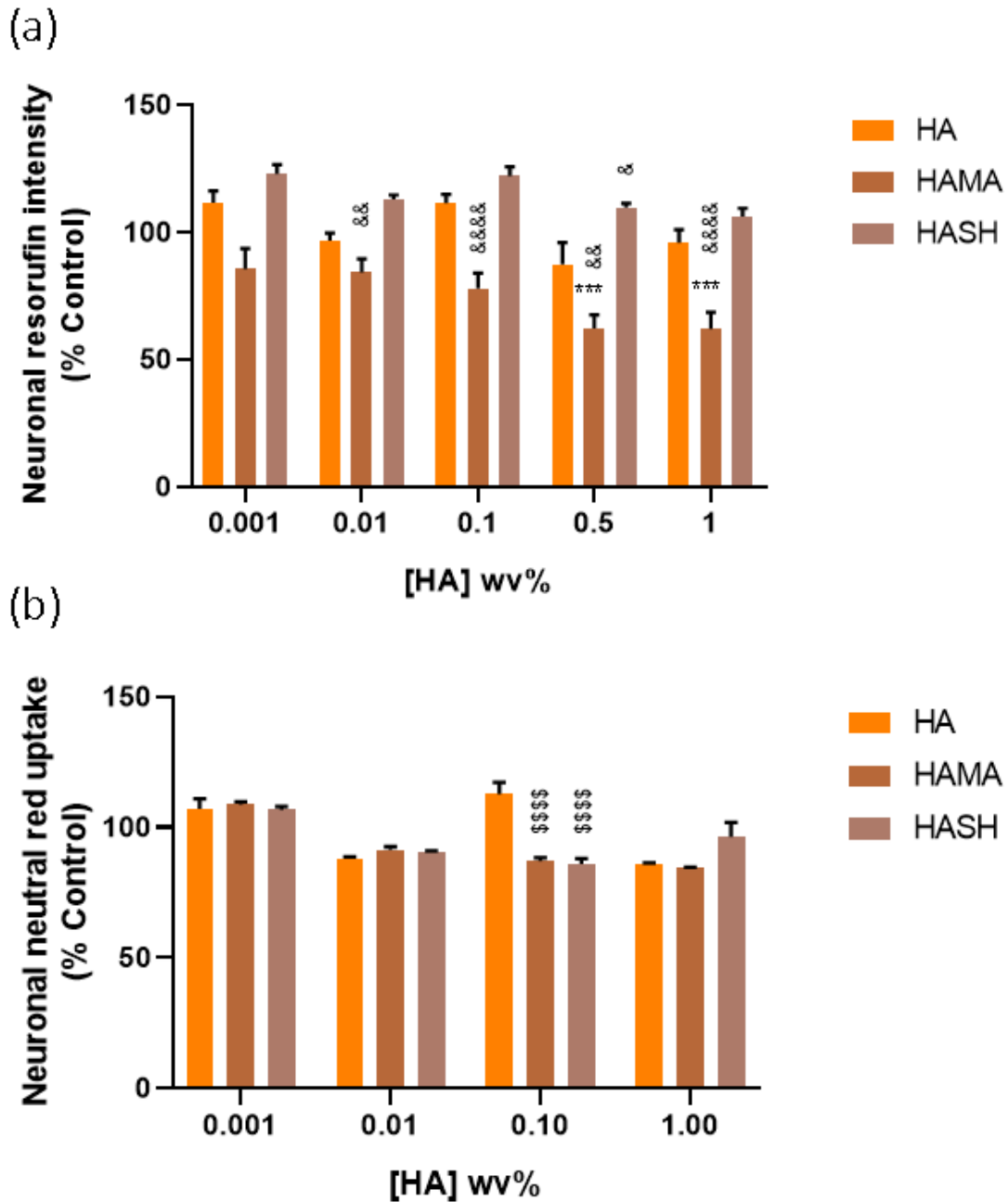


Figure 45. Cytocompatibility of HA and HA derivatives in neuronal cells. Resazurin reduction (a) and neutral red uptake (b) assay of neuronal cells after 24 h exposure (inclusive of 4 h assay incubation) to HA, HA-MA and HA-SH. Data represents mean \pm SEM of three independent experiments (N=3), conducted in triplicate (n=3). *** $P < 0.001$ vs control (HA control (0 % wv) refers to 0.1 mg/ml PDL.); $^{\&}P < 0.05$, $^{\&\&}P < 0.01$, $^{\&\&\&}P < 0.001$, $^{\&\&\&}P$ vs native HA equivalent when compared using two-way ANOVA with Tukey post-tests in GraphPad Prism V8.01.

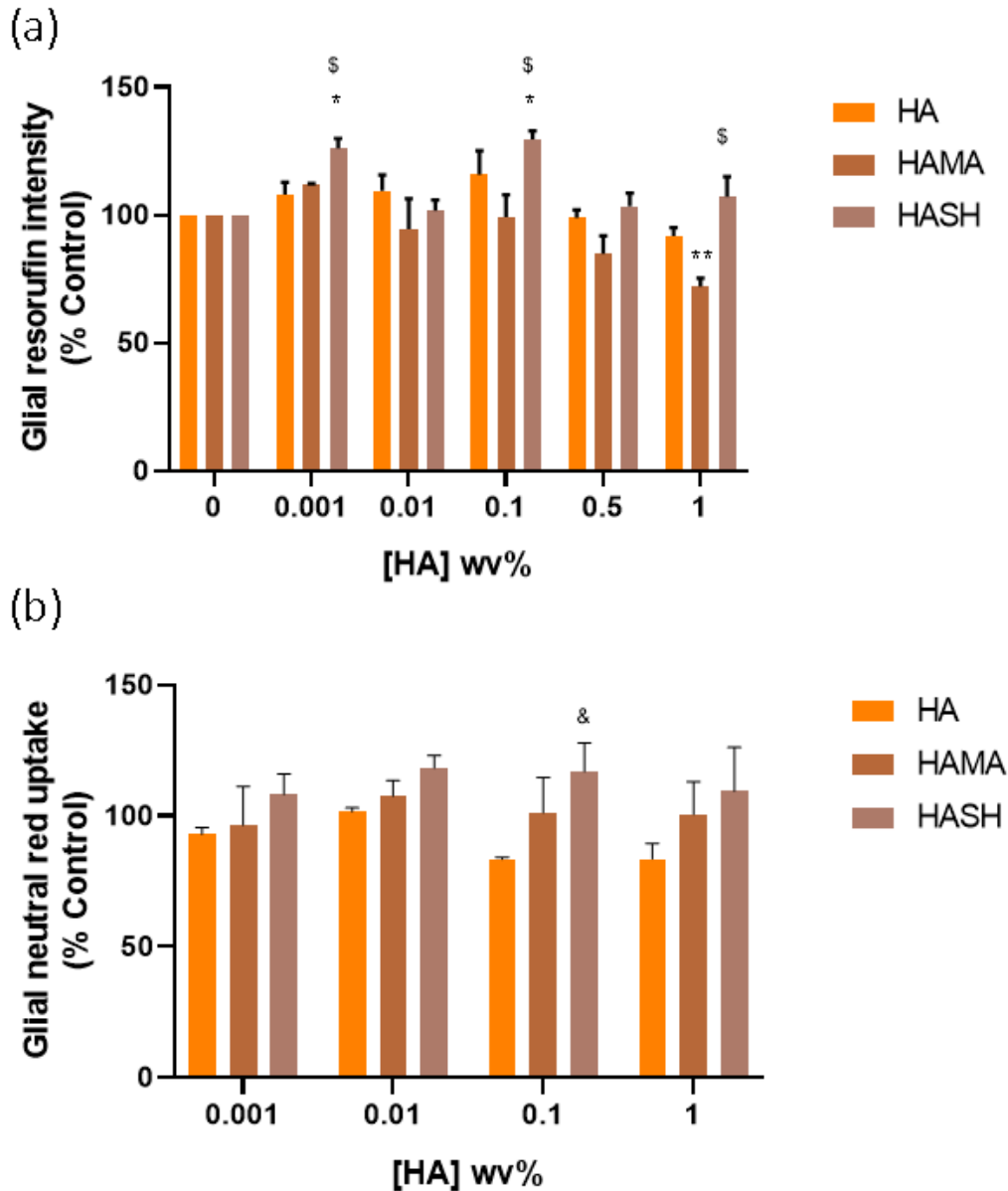


Figure 46. Cytocompatibility of HA and HA derivatives in glial cells. Resazurin reduction (a) and neutral red uptake (b) assay of glial cell viability after 24 h exposure to HA, HA-MA and HA-SH. Data represents mean \pm SEM of three independent experiments (N=3), conducted in triplicate (n=3). * $P < 0.05$ vs control (HA control (0 % wv) refers to 0.1 mg/ml PDL.); & $P < 0.05$ vs native HA equivalent when compared using two-way ANOVA with Tukey post-tests in GraphPad Prism V8.01.

5.2.4 The effect of modification on hyaluronidase degradation of HA

In the body, HA would be degraded quickly by the endogenous enzyme hyaluronidase. This could provide a unique challenge in the creation of a medical device due to the lack of control over the degradation time of the HA structure. The purpose of this study was to evaluate how modification had effected the degradation of coated HA and modified HA via hyaluronidase. This was done by using hyaluronidase to degrade the HA or HA derivative coating, releasing uronic acid which was then detected via the carbazole assay.

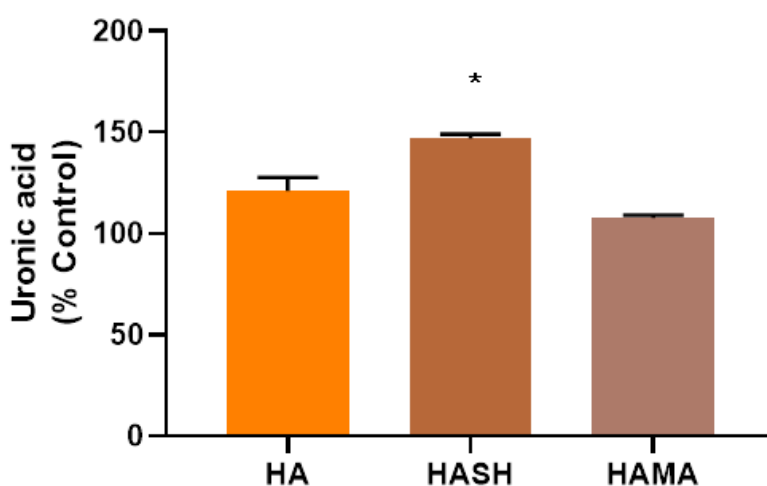


Figure 47. Modification of HA with thiol accelerates hyaluronidase degradation. Graph shows the degradation of HA, HA-SH and HA-MA via hyaluronidase expressed as % control of 0% HA (PDL only). Data is the mean \pm SEM of 3 independent experiments (N=3), conducted in triplicate (n=3). *P < 0.05, **P < 0.01 vs unmodified HA (HA) when compared using two-way ANOVA with Tukey posttests in GraphPad Prism V8.01.

5.3 DISCUSSION

In this chapter, HA-SH and HA-MA were produced and characterised extensively. HA-SH was initially synthesized by modifying 30-50 kDa HA with N-acetyl cysteine (NAC) in the presence of dimethyl formamide (DMF) and formamide. However, it was found early on, that using NAC was producing a MoD of 4-10%. It was hypothesized that this was due to the steric hindrance resulting from the structure of NAC and HA. Additionally, different carbodiimides were trialled such as N,N'-dicyclohexylcarbodiimide (DCC) and 1-ethyl-3-(3-dimethylaminopropyl)carbodiimide hydrochloride (EDC) in the presence and absence of 4-Dimethylaminopyridine (DMAP) which was used as a catalyst to speed up the reaction and prevent the formation of the stable N-acyl urea as outlined in Figure 38. After initial screening trials, the procedure chosen for continuation utilised cysteamine HCl as the thiol containing compound due to its simpler structure. Additionally, the reaction took place in deionised water which served to help protect the chain length of the HA molecule as earlier trials in DMF/ formamide resulted in no product recovered. The product was thought to have been lost to the dialysis due to degradation of the HA chains. Finally, EDC and DMAP were chosen as the carbodiimide/ catalyst system due to the lesser toxicity associated with EDC and easier removal post modification.

HA-MA was produced using a 10X concentration of methacrylic anhydride. This reaction was developed through optimisation of reactant ratios and was driven forward by the continuous stabilisation of pH to approximately pH 8.5 with 5M NaOH.

The HA derivatives were then chemically characterised using ATR-FTIR, ¹H-NMR and RP-HPLC. Figure 39 shows the ¹H-NMR spectrum of HA and HA-SH and identifies the methylene protons of cysteamine HCl. The integrals of the peaks was obtained and it was from this that the MoD was calculated in relation to the N-acetyl peak of HA. The MoD was calculated to be approximately 27.7%. For the purposes of purity checking and spectral assignment, ¹³C/DEPT-90/DEPT-135/HH-CoSy/HSQC/HMBC spectra (Appendix 3) were also obtained.

The FTIR of HA-SH showed little change, potentially due to the broadening of the SH caused by the polymeric nature of the sample. Therefore, the Ellmans assay was employed. The Ellmans assay detects both free and bound thiol groups colorimetrically and the results are depicted in Figure 41. This figure illustrates the linear relationship with a coefficient of determination of 0.99 for both standard curves of standards in both reaction buffer and 8M

urea from which unknowns were measured. In reaction buffer, the concentration of free thiol was calculated to be 0.29 mM, and after treatment with 8M urea the concentration of bound thiol was calculated to be 0.225 mM. Therefore, the total thiol content of the sample was determined to be 0.515 mM. This was calculated to be approximately 22% of available monomers which is quite close to the calculated 27.7% from $^1\text{H-NMR}$.

ATR-FTIR was used for initial chemical characterisation of HA-MA. The presence of a peak at 1716 cm^{-1} arises from the methacrylic ester carbonyl vibration, confirming successful methacrylation of the HA. HA-MA was also characterised via $^1\text{H-NMR}$. Figure 43 shows the spectrum obtained for HA-MA, from which the MoD was calculated to be approximately 20%. This was calculated from the integrals of the vinyl protons in relation to the N-acetyl peak integral. This sample was produced using a 10X molar ratio of methacrylic anhydride. To test the impact of starting molar ratio of reactants, RP-HPLC was employed.

Figure 44 shows the 3D chromatograms and standard curve of 1X, 10X and 30X HA-MA samples in relation to methacrylic acid standards. The correlation between $^1\text{H-NMR}$ and RP-HPLC proved to be very robust with RP-HPLC quantifying the degree of modification to be 25% +/- 3% and $^1\text{H-NMR}$ calculated at 20% +/- 9%, this was not surprising as $^1\text{H-NMR}$ lacks the sensitivity of RP-HPLC.

It has already been established through the literature (Serafin, Culebras and Collins, 2023) and earlier testing in this thesis that native HA is not conducive to cell attachment to *in vitro* testing substrates and decreased cell adhesion is observed with increasing concentration of HA as well as increased methacrylation of HA. Therefore, it was necessary to test the impact that modification had on cytocompatibility. To do this, the HA derivatives were dissolved in 0.1 mg/ml PDL and used to coat tissue culture plates as outlined in section 3.2.5. Cells were then seeded on top of the polymer coating to ensure direct contact. After 24 h exposure, cells were assayed to determine the metabolic activity of cells in the presence of HA or HA derivatives.

Figures 45 and 46 outline the results obtained for neuronal (45) and glial (46) cells as determined by resazurin (a) and neutral red uptake (b). The resazurin reduction assay detected a significant decrease in cell viability vs both the control and native HA in neuronal cells. At concentrations of 0.5 %wv and 1 %wv, there was a significant decrease in neuronal cell viability vs control (0 % HA) in the presence of HA-MA. This decrease was also observed when comparing native HA to HA-MA in neuronal cells at 0.001, 0.1, 0.5 and 1.0

%wv. However, a significant increase in cell viability was observed when comparing HA-SH to HA in neuronal cells at 0.5 %wv. However, these results were not replicated with the neutral red uptake assay. Both assays work on a different mechanism of action which may explain the discrepancy in results with resazurin relying on the metabolic activity of cells, whereas neutral red uptake relies upon the membrane integrity to convey the health of cells. In this manner, the resazurin reduction is more sensitive as it detects even faint metabolic activity in dying or compromised cells whereas neutral red is a strict live dead assay (Shih, 2012).

In glial cells, Figure 46, resazurin (a) revealed a significant increase in cell viability in the presence of HA-SH at concentrations of 0.001 and 0.1 %wv HA-SH vs control (0 % HA). However, when assayed using neutral red, these results were not significant but a similar trend was observed. Neutral red uptake did reveal an increase in glial cell viability vs native HA at a concentration of 0.01 %wv HA-SH which was in agreement with the results obtained in the resazurin reduction assay. In both cell lines, HA-MA caused decreased cell viability when compared with HA-SH and HA. This was not surprising as it has been well documented that methacrylates can induce variable cytotoxic responses in *in vitro* cell models (Sulek *et al.*, 2022). This highlights the necessity of a battery approach in cytocompatibility testing as differing sensitivities of assay methods could have significant implications in the trajectory of a project. Resazurin, due to its method of action, could potentially overestimate viability as at a particular time point, the cells were actively metabolising but it may not reflect the cell health at the end point of the assay. Neutral red uptake assay, however, is a reliable indicator of cell viability (Espíndola *et al.*, 2022).

Finally, Figure 47 illustrates the total uronic acid released over 105 mins from the hyaluronidase degradation of HA and HA derivatives. HA is broken down endogenously in the body by a family of enzymes known as hyaluronidases. This breakdown occurs rapidly and fragments large chain HA into smaller chains which have been shown to be inflammatory. Through modification, this degradation rate can be altered. HA, HA-SH and HA-MA coated plates were prepared as outlined previously. These plates were then treated with hyaluronidase and aliquots were collected at regular time points. The aliquots were tested using the carbazole assay. The carbazole assay is a method used to quantify the amount of HA colorimetrically via uronic acid (Daminato *et al.*, 2022). The theory behind this assay design was that as the enzyme cleaved HA from the coating on the bottom of the plates, uronic acid would be released into the media and could then be quantified. The amount of

uronic acid detected in each sample would reflect the degree to which each HA sample was degraded, or released from the plate coating, by the enzyme in that specific time period. In this manner, it would be clear to see the effect that modification has on the ability of hyaluronidase to cleave HA.

HA-SH was found to degrade significantly faster than native HA when treated with the hyaluronidase enzyme. HA-MA was found to degrade significantly less than native HA when treated with hyaluronidase. This data is indicative that a tailored degradation profile could be obtained by altering the ratio of methacrylation and thiolation in a HA construct.

Overall, this chapter has shown the successful modification of HA with thiol and methacrylate which were completed using mild procedures so as to preserve the integrity of the HA chain (Ding *et al.*, 2022). Many researchers such as Lee *et al.*, (2022) have shown the use of thiolated HA for nerve repair and highlighted the low cytotoxicity associated with its use. There was some concern initially over the use of methacrylate, however, numerous studies stated that grafted methacrylate produced no cytotoxicity (Ventura-Hunter *et al.*, 2022; Li *et al.*, 2022) and therefore it was deemed suitable for inclusion. The modification of HA was necessary in order to facilitate UV cross-linking and subsequently, 3D printing. Having established that HA and HA derivatives were biocompatible, the HA derivatives were analysed for their resistance to degradation. This assay was completed using coated plates and the underlying principle of the assay was that hyaluronidase, as it degrades the HA coating, would release uronic acid from HA, which could then be quantified using the carbazole assay. It was found that HA was more susceptible to hyaluronidase degradation after thiolation which correlates with findings made by Yang *et al.*, (2023) who found that cystamine modified HA coatings on chemotherapy drugs could enable efficient targeting via receptors and release via hyaluronidase degradation of HA. Conversely, methacrylate imparted greater resistance to the HA from degradation. This study has shown that a tailored degradation rate could be obtained by careful consideration of modification degree and polymer ratio. However, it must be noted that this assay was completed in coating format and it would be pertinent to examine this response in context of the final conduit.

CHAPTER 6. UV PHOTO-CROSSLINKING OF HA DERIVATIVES

6.1 PREFACE

Native HA does not have the necessary chemical structure for click chemistry photo-crosslinking reactions to take place. However, by nature these reactions are quick and reliable and serve a variety of purposes in bioengineering. Therefore, HA was modified to introduce the necessary functional groups to enable click chemistry crosslinking to occur. Various blends of HA derivatives, as outlined in Table 11 below, were photo-polymerised after 10 minutes of UV exposure.

Table 11. Polymer ratios for HA hydrogels

Sample	HA-MA	HA-SH	Irgacure 2959
A	100	0	0.1
B	80	20	0.1
C	60	40	0.1
D	50	50	0.1
E	40	60	0.1
F	20	80	0.1
G	0	100	0.1

The reaction scheme for UV photo-polymerisation of thiolated and methacrylated HA is outlined in Figure 48 below. This timing was deemed sufficient for complete polymerisation of samples following several optimisation experiments not shown within this manuscript. Samples F and G were found to insufficiently cross-link within this period of time, and therefore were excluded from further testing. Insufficient cross-linking was determined by the lack of gel formation after the initial 10 minutes of UV-curing time. A further trial of 30 minutes UV-exposure was conducted to assess whether prolonged exposure to UV would enable cross-linking to occur but on removal from the chamber, no gel solids were observed in the silicone mould. As HA remained in the viscous liquid state at these concentrations, they were deemed insufficiently cross-linked. This insufficient polymerisation is thought to be due to insufficient methacrylate moieties for the thiol to react across in an 80MA: 20SH ratio. Polymerisation occurs in this process through free radical chain polymerisation in

which the production of free radicals via the photo-initiator and UV light initiates a polymerisation reaction between the thiol group and methacrylate moiety. 100 % wv HA-SH did not photo-polymerise under UV due to the absence of the methacrylate moiety but the formation of disulphide bonds occurred when the sample was allowed to sit at R.T. for 30 minutes which produced a polymer film (not shown). Following removal from the UV chamber, the hydrogels were rinsed with deionised water and blotted free of solution before storage protected from light. All hydrogels were used within 72 h of photo-polymerisation.

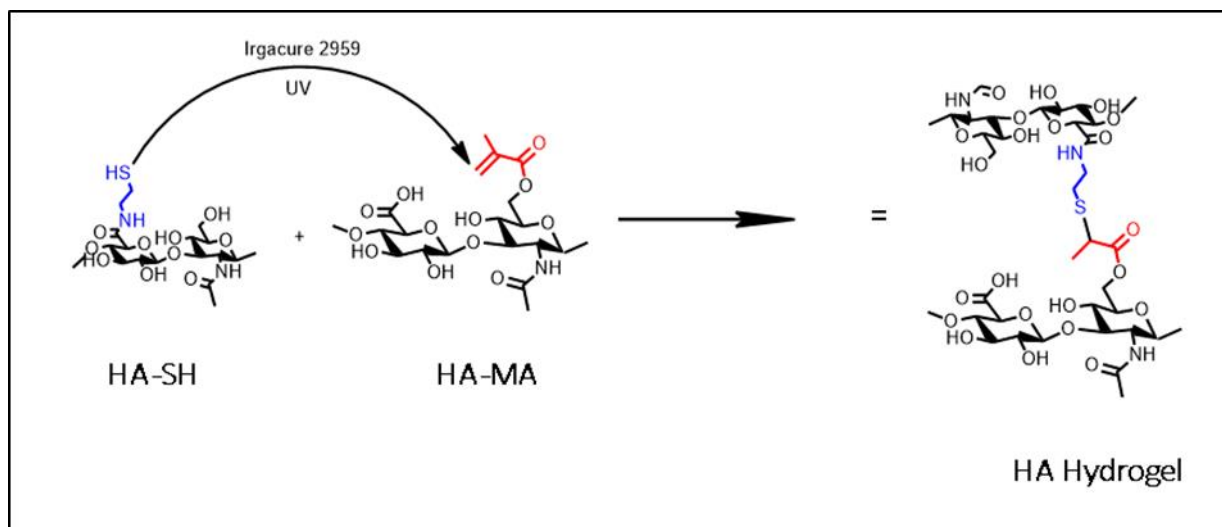


Figure 48. Scheme showing the UV photo-crosslinking of HA derivatives to form a HA hydrogel.

6.2 RESULTS

6.2.1 ATR-FTIR of photo-polymerised samples

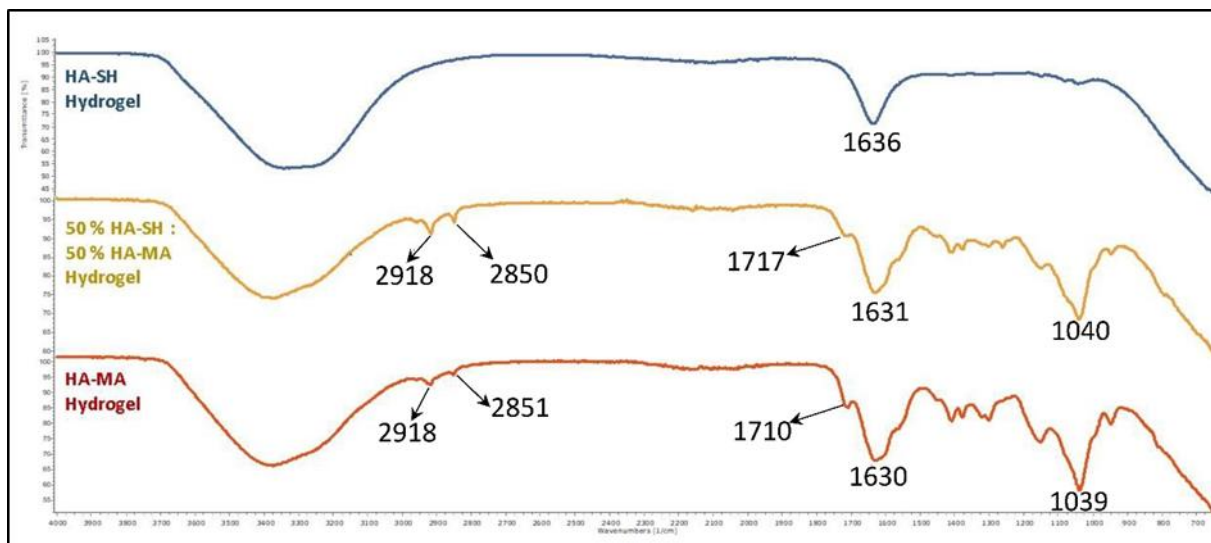


Figure 49. ATR-FTIR of UV photo-crosslinked HA hydrogel samples.

Post-polymerisation, samples for characterisation were dried in a vacuum oven to rid the samples of excess water. FTIR analysis of photo-cured samples revealed a loss of peaks at 1553 and 1236 cm^{-1} (highlighted in Figure 36 above) which arise from the C=C stretching and C-O stretching of methacrylate which can be seen in Figure 49. This confirms polymerisation has taken place. Generally, the broad absorption band at 3700-3200 cm^{-1} corresponds to the vibrations from O-H stretching.

6.2.2 Compression testing of photo-polymerised HA hydrogels

Compressive strength of a polymer dictates the force a hydrogel can withstand which is an important parameter for the design of medical devices or many other bioengineering applications. The ideal scenario would present a polymer blend with sufficient strength to withstand compressive forces *in vivo* while still retaining the elasticity necessary to facilitate regeneration of tissues. Figure 50 below illustrates the compressive strength at limit and the Young's modulus for each hydrogel. The compressive strength of each sample decreased with increasing concentration of thiols showing the decrease in stiffness of all hydrogels proportional to thiol concentration. The Young's modulus, which is the gradient of the line in a stress strain plot, remained relatively constant across the 80:20, 60:40 and 50:50 [MA]:[SH] HA blends.

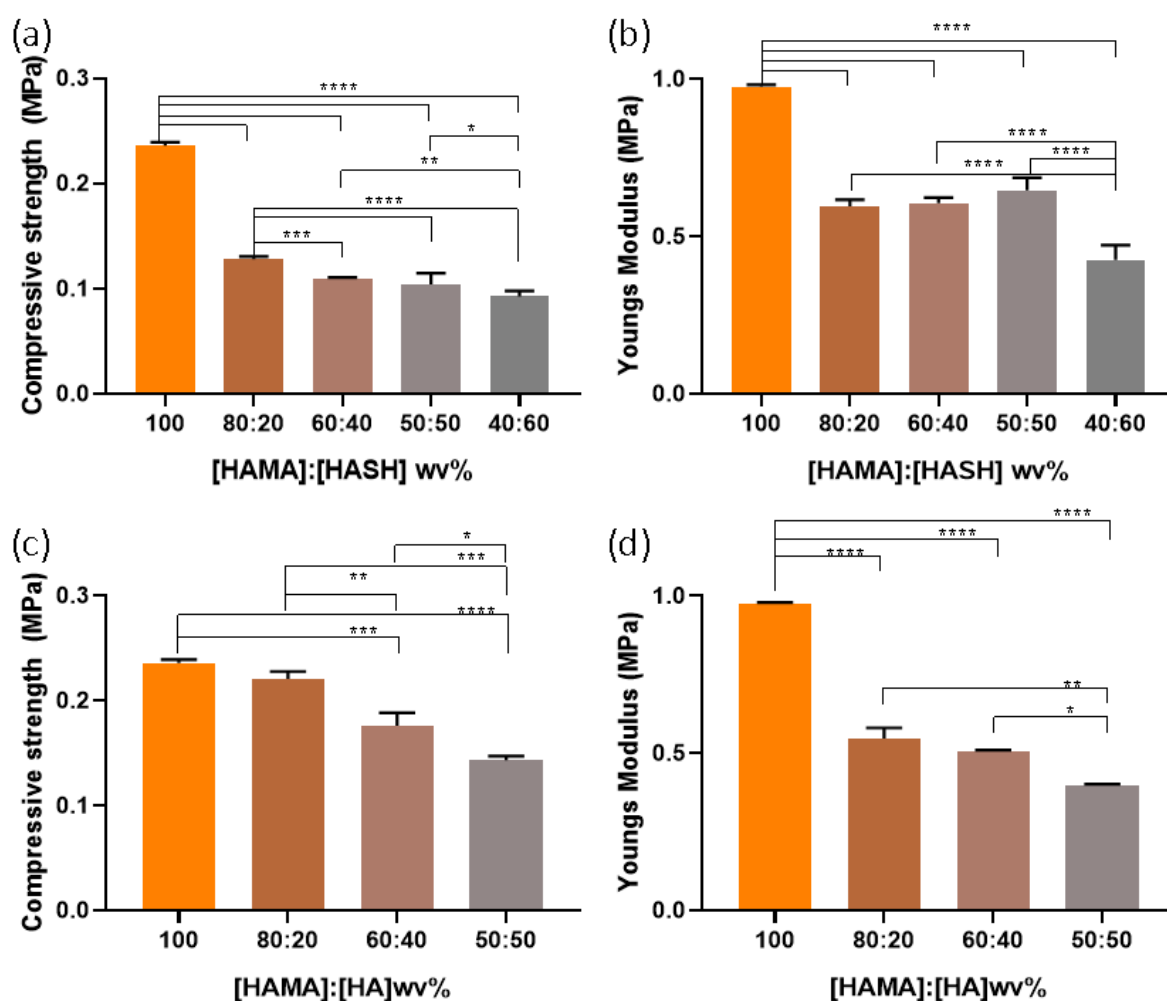


Figure 50. The compressive strength of HA hydrogels decreases proportional to SH concentration. The compressive properties of HA derivative hydrogels showing (a/c) the

compressive strength of HA-MA: HA-SH blends and HA-MA: unmodified HA control blends and (b/d) the Young's modulus of same. Data is the mean \pm SEM of 5 independent experiments (N=5), conducted in triplicate (n=3). *P < 0.05, **P < 0.01, ***P < 0.001, ****P < 0.0001 when comparing different conditions using one-way ANOVA with Tukey post-tests in GraphPad Prism V8.01.

Increases in thiol concentration proportionally increases the elasticity of a hydrogel as is made evident by Figure 50 (a-b) which clearly shows a deficit in compressive strength relative to thiol concentration. This could be due to the reduced bond strength observed with increased thiol concentration as has been reported in literature when cross-linking with methacrylate (Sara Howe et al., 2018). Interestingly, this decrease in compressive strength is greater with the introduction of thiol than the control (c-d) which was HA-MA in various ratios with unmodified HA. The unmodified HA should not crosslink and therefore the sample should be cross-linked HA-MA with unmodified HA molecules existing within the cross-linked network. In all cases, 100 % HA-MA had a compressive strength of approximately 0.24 MPa, however, an introduction of 20 % thiol reduced the compressive strength observed to approximately 0.12 MPa. Conversely, replacing the thiol content with unmodified HA resulted in a reduction of compressive strength of 0.02 MPa which is a difference of 0.1 MPa from the introduction of thiol. The Young's modulus shown in (b) and (d) highlight the greater elasticity in the matrix of thiol containing hydrogels as Figure (d) shows a proportional decrease to the lower concentrations of methacrylate in the matrix, whereas (b) shows a steady Young's modulus across concentrations up to 40 %wv methacrylate where a stark decrease is observed. In order to perfect the balance between a flexible hydrogel and a hydrogel with sufficient compressive strength for specific bioengineering applications, the ratio of thiol to methacrylate in the HA hydrogel could be fine-tuned or alternatively a co-polymer could be used with higher compressive strength as noted by Singh et al, (2023) .

6.2.3 *Rheological characterisation of HA hydrogels*

Rheological characterisation of the hydrogels is shown below in Figure 51 and Figure 52. The storage modulus of a hydrogel shows the ability of a hydrogel to store strain energy and is directly related to the cross-linking density of a polymer. Figure 52 (g-i) below shows that as the thiol concentration increases, so too does the storage modulus and in turn, the degree of crosslinking, up to a ratio of 50:50. This is due to the formation of thiolene bonds between the methacrylate and thiols. This is especially evident when comparing Figure 51 (a-f) with Figure 52 (g-i). Figures (a-c) show samples of HA-MA hydrogels prepared with deionised water in place of thiol, whereas in samples (d-f), samples were prepared as a blend of HA-MA and unmodified HA in various ratios. This was done in order to have a suitable control to compare the thiolene methacrylate hydrogels as confirmation of the presence of thiolene bonds.

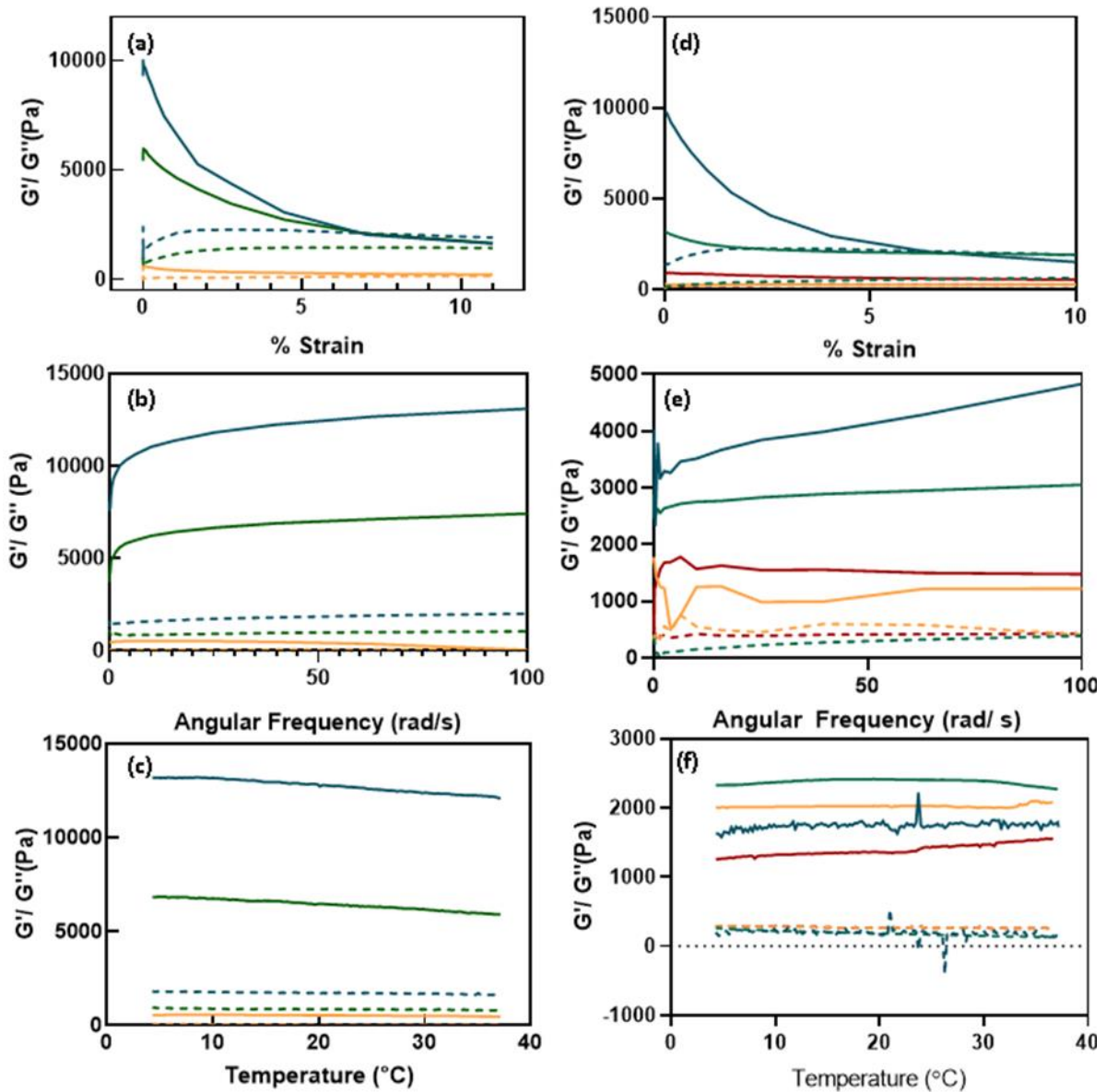


Figure 51. Rheology of HA-MA. (a-c) Rheological characterisation of HA-MA derivative blends with deionised water. (d-f) Rheological characterisation of HA-MA and unmodified HA blends. (a/d) Amplitude sweep, (b/e) Frequency sweep and (c/f) Temperature ramp of HA derivative hydrogels.

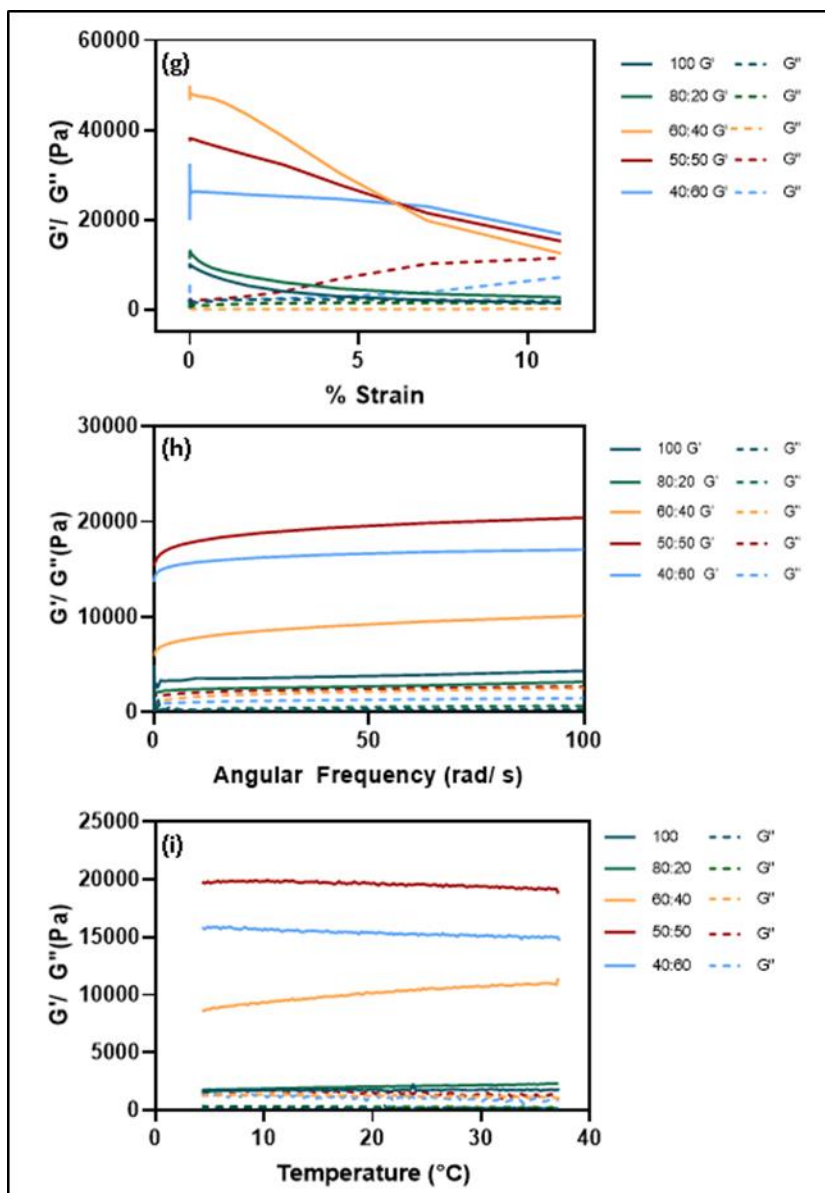


Figure 52. Rheology of HA-MA: HA-SH. (g-i) Rheological characterisation of HA-MA and HA-SH. (g) Amplitude sweep, (h) Frequency sweep and (i) Temperature ramp of HA derivative hydrogels.

It is evident when comparing these graphs that the thiol imparted better mechanical properties on the hydrogels than deionised water or unmodified HA, i.e. in Figure 51 (a), 60:40 HA-MA: deionised water had a storage modulus of less than 1000 Pa, whereas in Figure 52 (g) 60: 40 HA-MA: HA-SH had a storage modulus of almost 50000 Pa. This indicates that thiolene linkages are present, resulting in a more elastic hydrogel. All samples

remained stable across a temperature range of 4-37 °C showing that the storage modulus of the material would not be affected through storage or physiological temperature exposure. This is an important characteristic for a potential medical device formulation. Also shown in Figure 51 and Figure 52 is the evolution of the viscous or dissipative (G'') modulus as a function of strain, frequency and temperature. As expected, in all cases, hydrogels displayed a gel-type mechanical spectra ($G' > G''$). However, a cross-over modulus was observed in (a) at a strain of approximately 7.8 % and (d) at approximately 5.5 % strain in the case of 100 %wv HA-MA and 80 %wv HA-MA where the hydrogel began to show more viscous like characteristics as the % strain increased.

Typically, in viscoelastic samples it would be expected that the storage moduli of samples would be equal to the Young's moduli of samples, however, when comparing Figure 45 (a-c) with Figure 51 (d-f) and Figure 52 (g-i), the opposite is true in terms of this material. 100 %wv HA-MA hydrogels showed a higher Young's modulus than thiol containing samples in compression testing but performed worse in rheological analysis. This may be due to the increased elasticity imparted by the thiolene bonds due to the decrease in bond strength in the thiolene network versus the methacrylate network.

6.2.4 Swelling studies of HA hydrogels

The degree to which a hydrogel swells is due to how tightly networked the polymer matrix is after photopolymerisation (Dave and Gor, 2018). Significant increase in weight due to swelling would indicate a greater amount of space between polymer chains, as would be expected with high molecular weight molecules such as HA. The degree of swelling of a medical device must be carefully monitored and should be within expected and defined parameters, therefore it is a vital investigation. The mean swelling ratio (Q) shown in Figure 53 increased with increasing thiol content in the hydrogels. This is in contrast to what was expected as increased cross-linking density in hydrogels would typically result in less swelling. However, this was non-significant and the slight increase in swelling could be attributed to the enhanced degradation observed in thiolene hydrogels as illustrated in Figure 54 and Figure 55 below. The gel fraction of hydrogels initially decreased when comparing 100 %wv HA-MA to the 80: 20 %wv HA-MA: HA-SH blend, however, this was non-significant and the gel fraction remained consistent across all other concentrations, further

confirming the presence of cross-linked network between the HA-MA and HA-SH components.

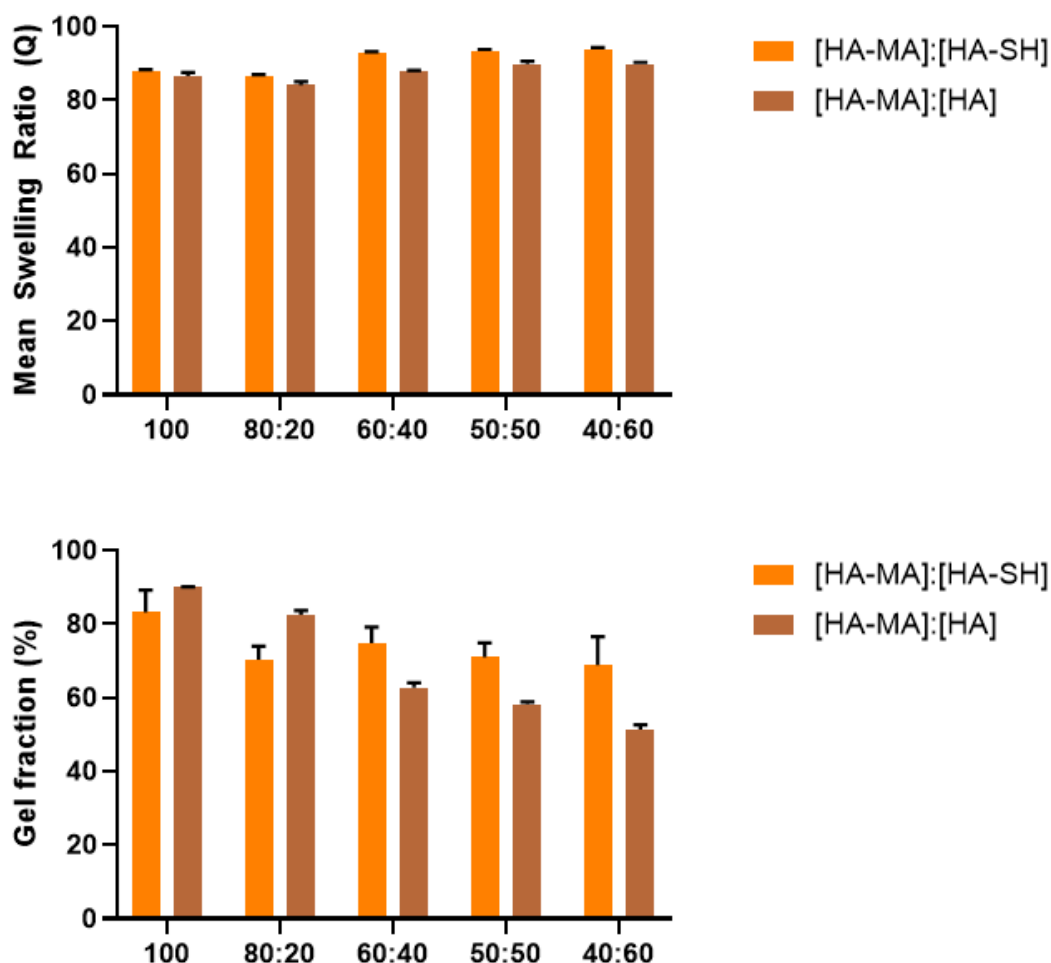


Figure 53. Comparison of the swelling characteristics of HA-MA hydrogels with increasing thiol concentration. Data shown is the mean \pm SEM of 5 independent experiments (N=5), conducted in triplicate (n=3). No significance ($P > 0.05$) was detected between concentrations when comparing HA hydrogels with various ratios of methacrylate: thiol using one-way ANOVA with Tukey post-tests. No significance ($P > 0.05$) was detected when comparing [HA-MA]: [HA-SH] vs [HA-MA]: [HA] using two-way ANOVA with Tukey posttests in GraphPad Prism V8.01.

No significant differences were observed when comparing the Q ratio between HA-MA: HA-SH hydrogels and the control HA-MA: HA hydrogels. However, in both cases an increase in swelling was observed across concentrations. This swelling was not significant when comparing across concentration. The control hydrogels (HA-MA: HA) showed

decreases in the gel fraction % proportional to the decrease in HA-MA concentration. This is in contrast to the HA-MA: HA-SH hydrogels which showed an initial decrease in gel fraction before stabilising across the concentration ranges 80:20 to 40:60 %wv.

6.2.5 Degradation of HA Hydrogels

In order to replicate the conditions of degradation in a variety of conditions, HA hydrogels were exposed to various conditions such as (a) pH 7.4 buffer (physiological pH), (b) 5 mM NaOH (mildly accelerated), (c) 5 M NaOH (accelerated). Hydrogels were weighed and imaged daily to analyse the extent of degradation in each condition.

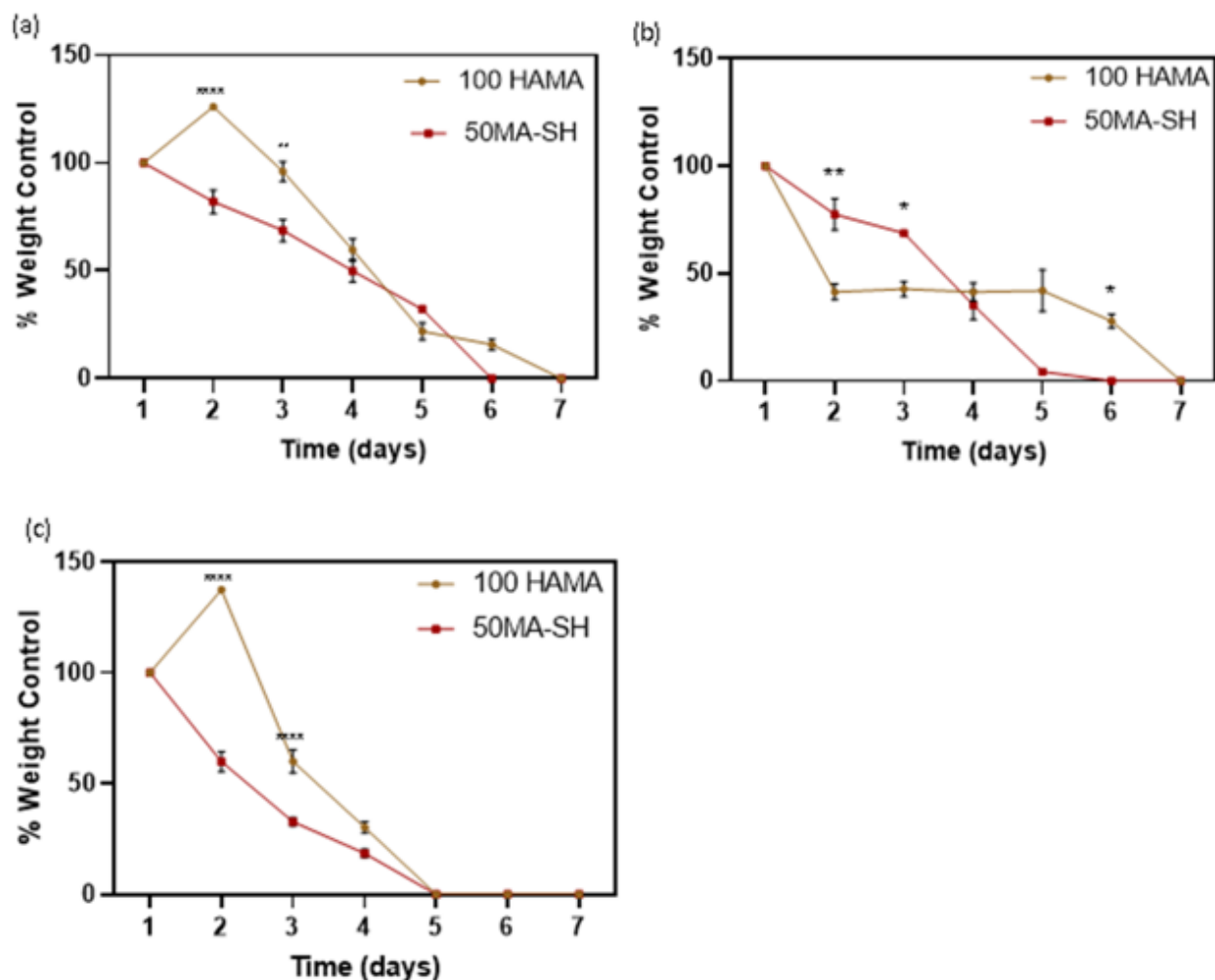


Figure 54. Degradation of HA derivative hydrogels. Degradation was performed in pH 7.4 (a), 5 mM NaOH (pH 11.7) (b), 5 M NaOH (pH 13.7) (c). Control refers to starting weight of hydrogels in their equilibrium swollen state. Data is the mean \pm SEM of 2 independent experiments (N=2), performed in triplicate (n=3). * $P < 0.05$, ** $P < 0.01$, **** $P < 0.0001$ vs 100 HA-MA (a, b, c) or native HA equivalent (d) when compared using two-way ANOVA with Tukey post-tests in GraphPad Prism V8.01.

In all cases, the addition of thiols resulted in a decrease in resistance to degradation as shown in Figure 54. In pH 7.4, there were significant differences between the rates of degradation when comparing HA-MA and the HA-MA: HA-SH blend at day 2 and day 3 ($****P < 0.0001$ and $**P < 0.01$ respectively), however, after this point no significant difference was observed. Similar observations were made with 5 mM NaOH and 5 M NaOH.

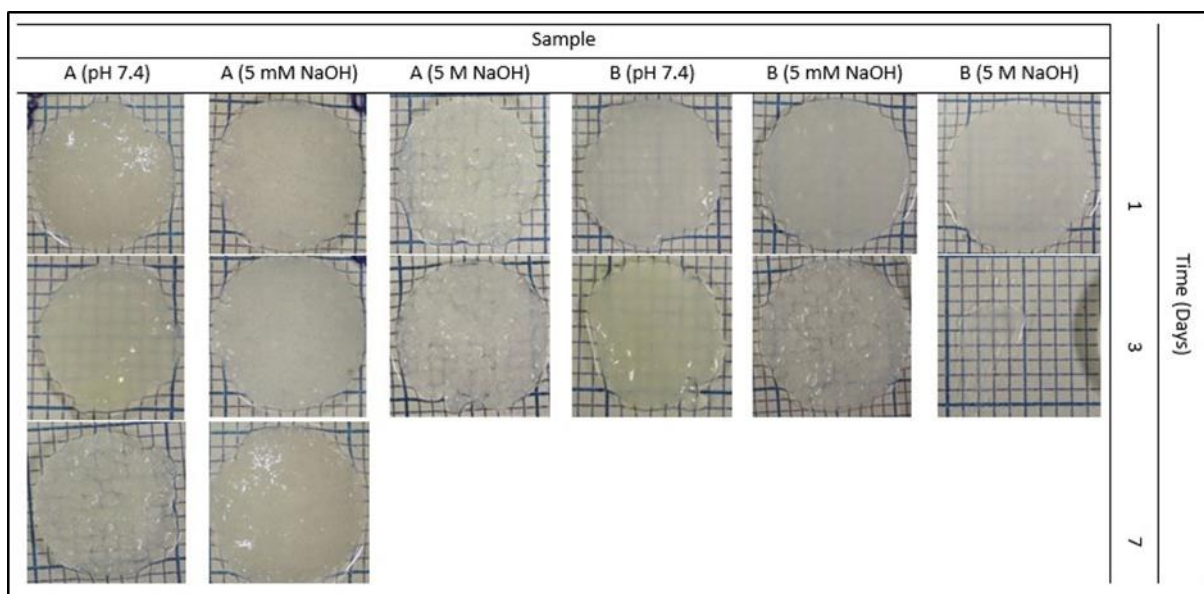


Figure 55. HA Hydrogel Degradation. HA-MA (A) and 50% HA-MA: HA-SH hydrogels (B) after exposure to pH 7.4, 5 mM NaOH or 5 M NaOH. Images were captured using a Canon 450D DSLR camera and used unedited.

This finding is consistent with the images of HA-MA hydrogels vs 50% HA-MA: HA-SH hydrogels taken at days 1, 3 and 7 as shown in Figure 55, where it can be seen that a higher methacrylate concentration imparts a greater resistance to degradation. By day 7, only the HA-MA hydrogel in 5M NaOH had completely degraded, whereas all 50 % HA-MA: HA-SH hydrogels had degraded completely.

6.3 DISCUSSION

HA hydrogels were successfully produced via a cross-linking reaction between thiolated HA (HA-SH) and methacrylated HA (HA-MA). This production of a novel HA hydrogel has a variety of applications from wound healing to ophthalmology, however, the HA only hydrogel proved to have insufficient compressive strength for a nerve conduit. Kwan *et al.*, (1992) states that a native nerve has a compressive strength of 0.5- 13 MPa and therefore, a NGC should be equal to or greater than that of a native nerve. The highest compressive strength observed was approximately 0.24 MPa in the 100 % wv HA-MA sample and this decreased proportionally to increasing thiol concentration. Therefore, in order for this formulation to function for nerve repair, a constituent with greater mechanical properties would need to be included.

In terms of rheological properties, however, an increased storage modulus was observed in samples containing thiol with the highest storage modulus being observed in the 60:40 % wv HA-MA: HA-SH hydrogel sample. This is hypothesized to be due to increased cross-linking being HA-SH and the enhanced viscoelasticity imparted by the thiol containing HA. This enhanced viscoelasticity is a good quality for NGCs as it enables greater resilience to the forces and movement within the human body. HA-MA hydrogels containing unmodified HA were used as a control to confirm that this effect was due to the inclusion of thiol.

The HA-SH containing hydrogels experienced increased swelling with increasing thiol concentration which is contradictory to what would be expected but this increase was found to be insignificant when analysed using one-way ANOVA with Tukey posttests. The slight increase could be attributed to the faster rate of degradation in thiol containing samples as has been noted in the literature (Hao *et al.*, 2014).

This is confirmed by the results shown in section 6.2.5 where it is evident that the inclusion of thiol significantly increased the rate of degradation compared to 100 % wv HA-MA hydrogels. This quality would enable the tuning of degradation rates by altering the concentration of thiol in the sample.

Due to the less than ideal mechanical properties of the HA hydrogels, it was decided to investigate the inclusion of a synthetic polymer with better mechanical properties into the matrix. However, many synthetic polymers have long degradation times in the body. With the discovery that degradation can be altered proportionally to thiol concentration, this long

degradation time can be attenuated to enable the development of a hybrid hydrogel with a tuneable degradation profile.

**CHAPTER 7. HYBRID HYDROGEL FORMULATION
WITH TAILORED DEGRADATION PROFILE**

7.1 PREFACE

Due to the decreased compressive strength observed in HA hydrogels with increasing thiol concentration, it was necessary to include a compound which would improve the mechanical properties of the hydrogels. PEGDMA is a synthetic polymer which has been shown to be bio-inert in the literature (Johannsmeier *et al.*, 2019) and impart impressive mechanical strength (Bharadwaz, Dhar and Jayasuriya, 2023) when cross-linked. PEGDMA was initially fully characterised alone to establish a baseline of parameters prior to combining it into hybrid hydrogel systems. Then, HA-SH and HA-MA were UV photo-crosslinked with PEGDMA in various ratios as outlined in chapter 5. The produced hydrogels were exhaustively characterised in order to narrow down the selection to final formulation candidates. The aim of this section was to identify a formulation which would possess the improved cytocompatibility and degradability of a HA hydrogel but with the improved mechanical properties imparted by PEGDMA.

7.2 RESULTS

7.2.1 ATR-FTIR of PEGDMA and PEGDMA hybrid samples

PEGDMA was analysed alone and in combination with either HA-SH or HA-MA to view the effect of the modified HA on the PEGDMA sample. FTIR was performed to analyse the chemical effects post curing.

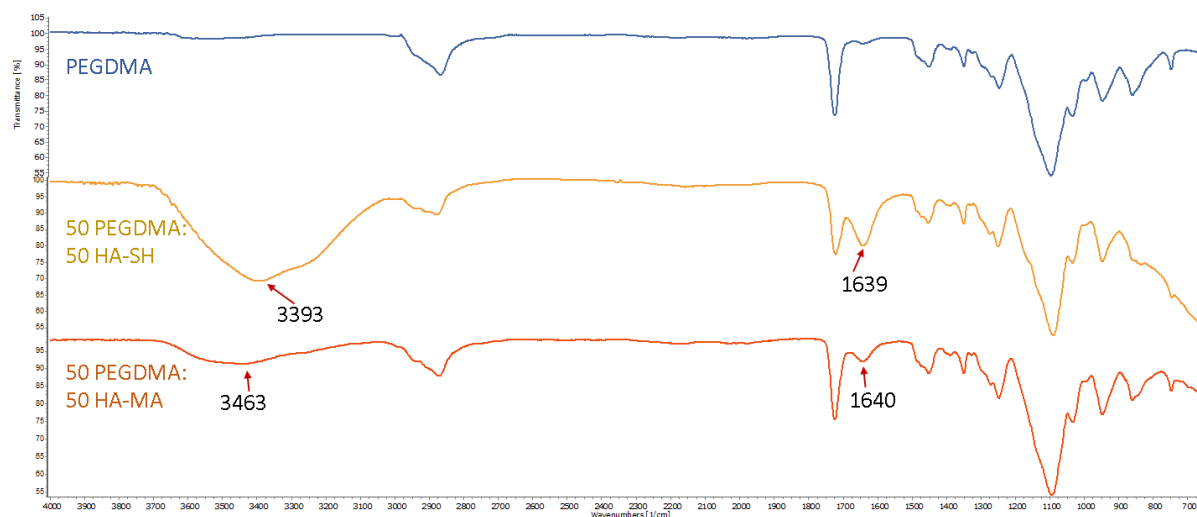


Figure 56. ATR-FTIR of PEGDMA, 50% PEGDMA: HA-SH and 50% PEGDMA: HA-MA with key peaks noted.

Post-polymerisation, samples for characterisation were dried in a vacuum oven to rid the samples of excess water. FTIR analysis of photo-cured samples as shown in Figure 56 revealed a loss of peaks at 1553 and 1236 cm^{-1} (highlighted in Figure 36 above) which arise from the C=C stretching and C-O stretching of methacrylate in HA-MA. This confirms polymerisation has taken place. Generally, the broad absorption band at 3700-3200 cm^{-1} corresponds to the vibrations from O-H stretching in HA. PEGDMA dominates the spectra in all cases with only the peaks at approximately 3400 cm^{-1} and 1640 cm^{-1} indicating the presence of HA in the polymer matrix.

Following a battery of initial trials where various ratios were composed of HA-SH, HA-MA and PEGDMA, an ideal formulation of 50% HA-SH, 40% HA-MA and 10% PEGDMA was decided upon. From this point forth, this ideal formulation will be referred to as the “hybrid blend”. When analysed via FTIR, the characteristic peaks at 3400 cm^{-1} and 1640 cm^{-1} can be clearly identified.

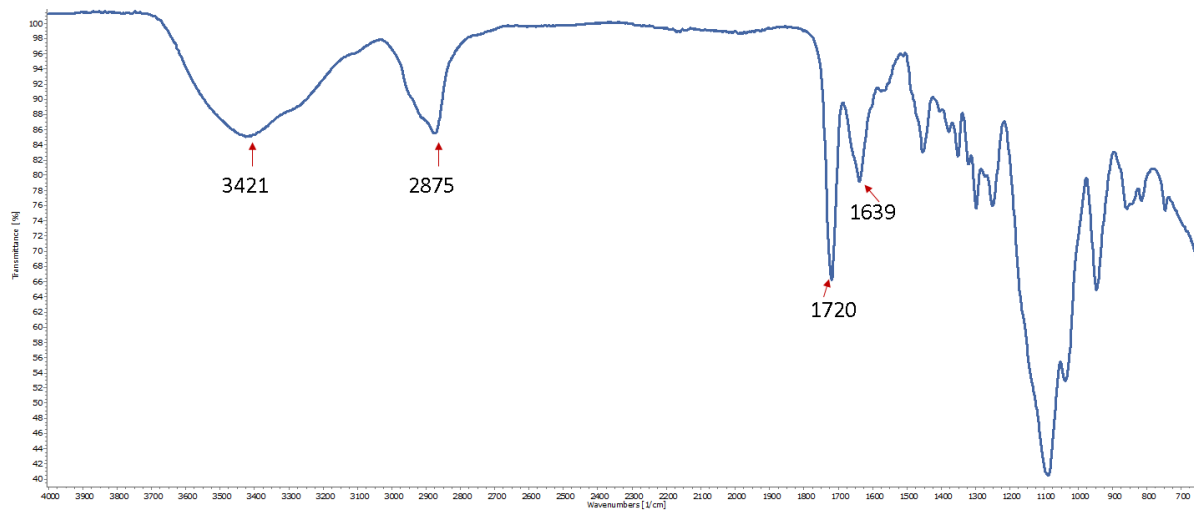


Figure 57. FTIR spectrum of the hybrid blend hydrogel. ATR-FTIR spectrum of the hybrid hydrogel composed of 50 % HA-SH: 40 % HA-MA and 10 % PEGDMA, with key peaks noted.

7.2.2 Compression testing

Due to the poor mechanical properties observed in the HA-MA: HA-SH hydrogels, it was decided to trial the inclusion of PEGDMA to determine the effect PEGDMA would have on mechanical strength of a hydrogel. Hydrogels were prepared as before and UV photopolymerised in a UV chamber before swelling to equilibrium and testing. PEGDMA had significantly better compressive properties than HA as can be seen in Figure 58 below.

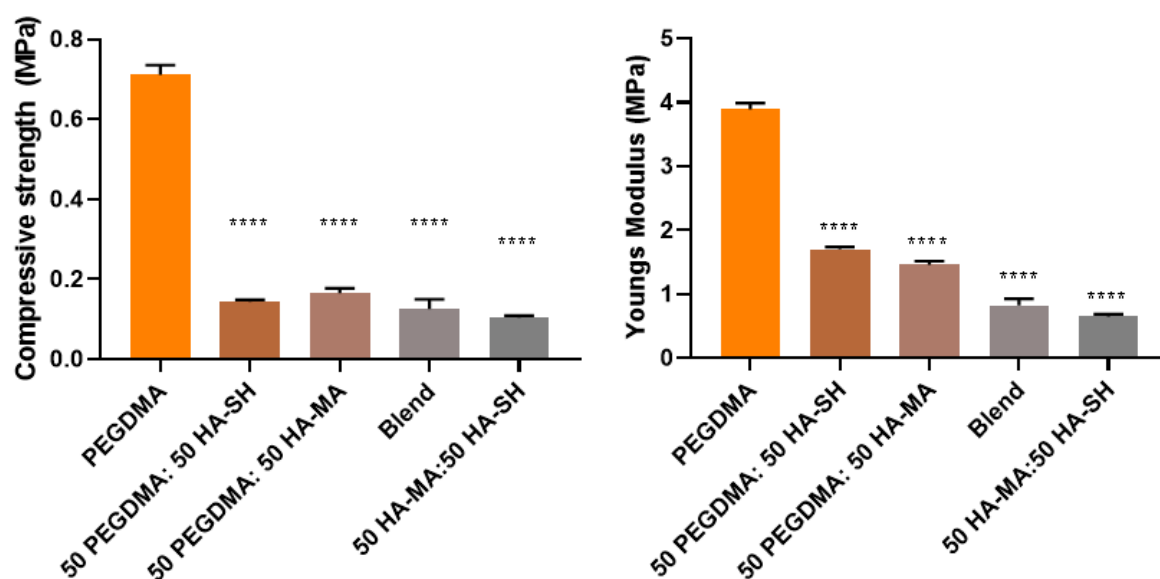


Figure 58. The poor compressive strength associated with inclusion of thiol was mitigated insignificantly by addition of 10% PEGDMA in the hybrid blend hydrogel. Blend refers to the hybrid blend formulation of 50% HA-SH: 40% HA-MA and 10% PEGDMA. **** $P < 0.0001$ when comparing vs PEGDMA using one-way ANOVA with Tukey posttests in GraphPad Prism V8.01.

As can be seen in Figure 58, the hybrid hydrogel blend performed better than the 50% HA-MA: HA-SH hydrogel, although this result was not significant. Only the 100 %wv PEGDMA sample met the criteria of a compressive strength greater than 0.5 MPa.

7.2.3 Rheology

PEGDMA increased the mechanical strength of a hydrogel when compared with HA derivative hydrogels. In HA-MA: HA-SH hydrogels, the 50:50 concentration possessed a storage modulus (G') of 40,000 Pa when testing the oscillation amplitude. In contrast, 50% PEGDMA with water showed a G' of approximately 150,000 Pa. In HA-MA: PEGDMA and HA-SH: PEGDMA hydrogels, the 50:50 concentration produced a G' of approximately 250,000 and 150,000 respectively. The addition of HA appeared to increase the storage modulus of the hydrogels as can be seen with the HA-MA, however, HA-SH was in line with what had been observed in the PEGDMA water hydrogels. The introduction of 10% PEGDMA in the blend samples produced results similar to that observed with the 60% HA-MA 40% HA-SH samples. This shows a slight increase in mechanical strength as the blend contains 50% HA-SH which is known to have a lower storage modulus.

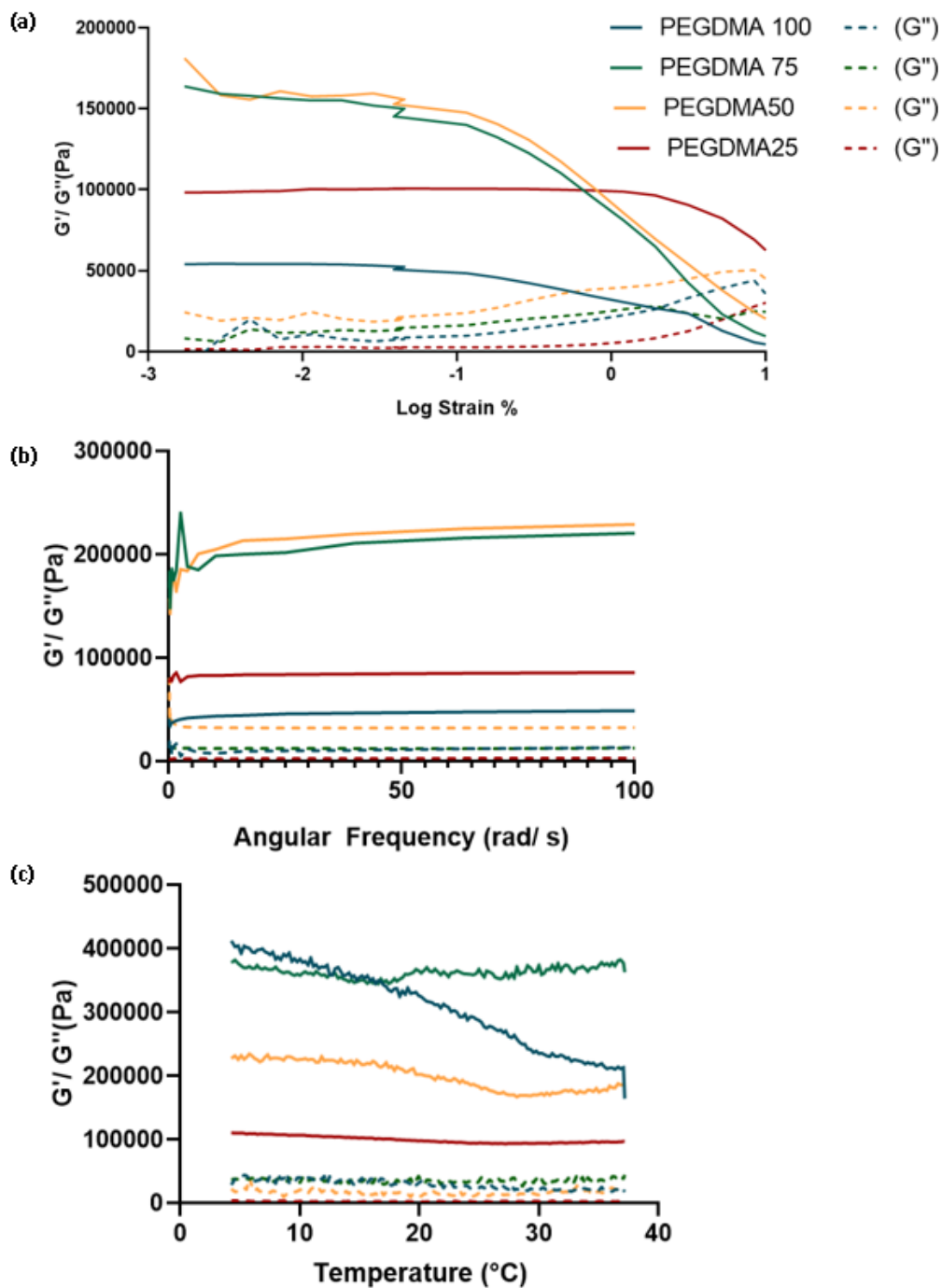


Figure 59. Rheological analysis of PEGDMA in deionised water hydrogels. (a) Amplitude, (b) Frequency and (c) temperature ramp of various concentrations of PEGDMA. Data is the mean \pm SEM of 3 independent experiments (N=3), conducted in triplicate (n=3). Data was analysed using GraphPad Prism V8.01.

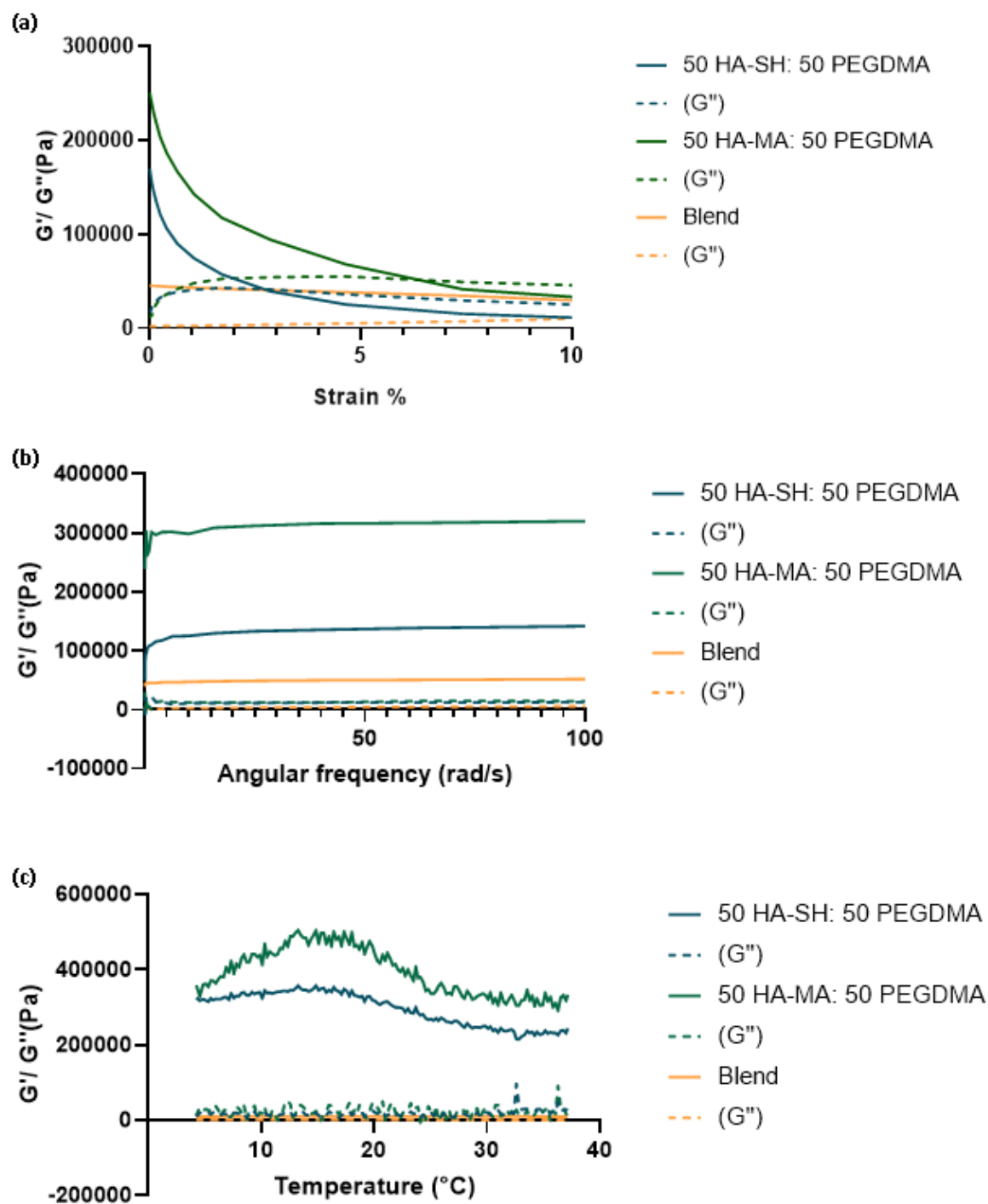


Figure 60. Rheological comparison between 50 HA-SH: PEGDMA, 50 HA-MA: PEGDMA and hybrid blend hydrogels. (a) Amplitude, (b) Frequency and (c) temperature ramp. Blend refers to the hybrid hydrogel blend formulation of 50% HA-SH: 40% HA-MA: 10% PEGDMA. Data is the mean \pm SEM of 3 independent experiments (N=3), conducted in triplicate (n=3). Data was analysed using GraphPad Prism V8.01.

7.2.4 Swelling Studies

Initially, PEGDMA was tested with various ratios of water in the matrix to determine the swelling capacity of concentrations of PEGDMA ranging from 25 % wv to 100 % wv. As was expected, the Q ratio increased proportionally to decreasing PEGDMA concentration. Similarly, when PEGDDMA was introduced to a HA-SH matrix, the Q ratio decreased proportionally to increasing PEGDMA concentration. This result was repeated for the HA-ME samples with significant differences observed when comparing samples with increasing PEGDMA. The inclusion of PEGDMA into the hybrid hydrogel blend, aided in controlling the swelling of the hydrogel with the hybrid blend performing significantly differently to the 50 % wv HA-SH: HA-MA and 100% HA-MA hydrogels. This result provides greater control over the swelling of the hydrogel which is a critical parameter of any medical device.

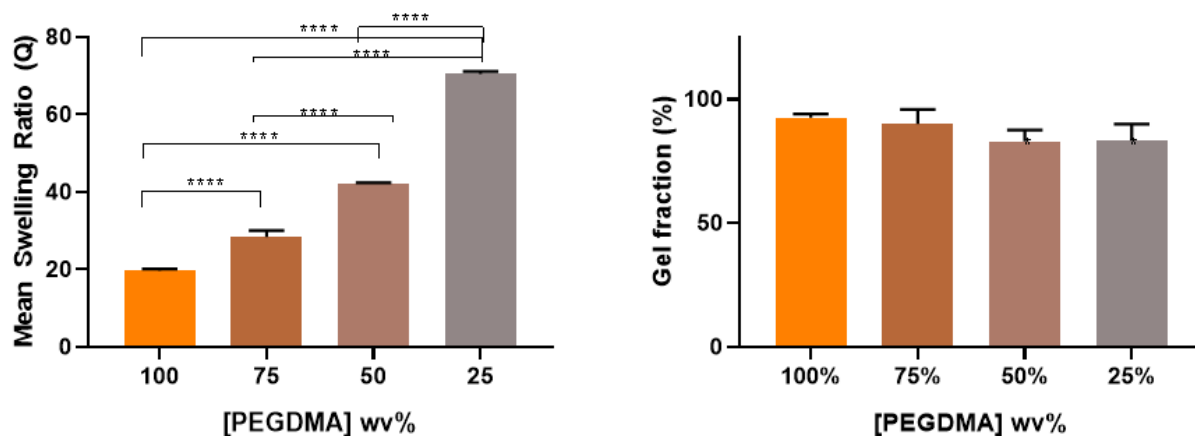


Figure 61. Mean swelling ratio and Gel fraction of PEGDMA in water hydrogel samples. Data is the mean \pm SEM of 3 independent experiments (N=3), performed in triplicate (n=3). **** $P < 0.0001$ when comparing concentrations using one-way ANOVA with Tukey posttests in GraphPad Prism V8.01.

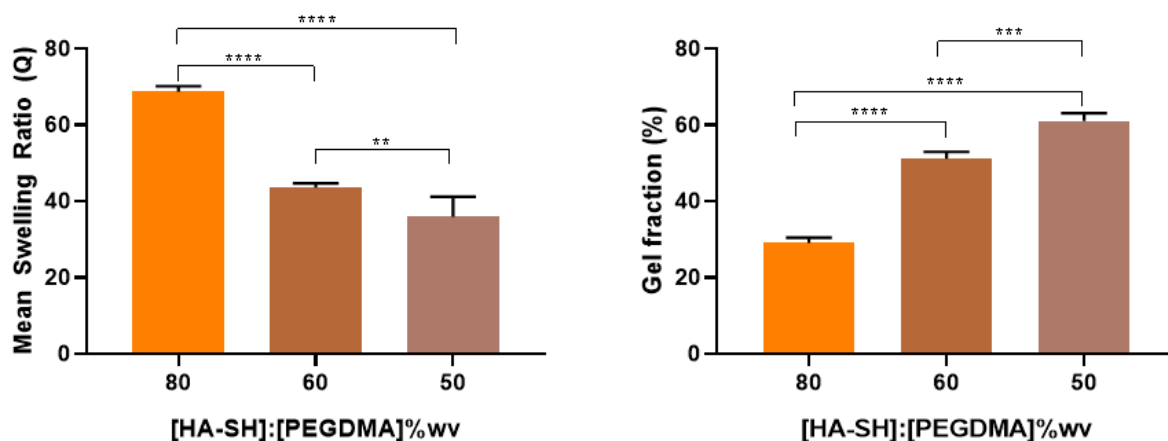


Figure 62. Mean swelling ratio and Gel fraction of HA-SH: PEGDMA hydrogel samples. Data is the mean \pm SEM of 3 independent experiments (N=3), performed in triplicate (n=3). ** $P < 0.01$, *** $P < 0.001$, **** $P < 0.0001$ when comparing concentrations using one-way ANOVA with Tukey posttests in GraphPad Prism V8.01.

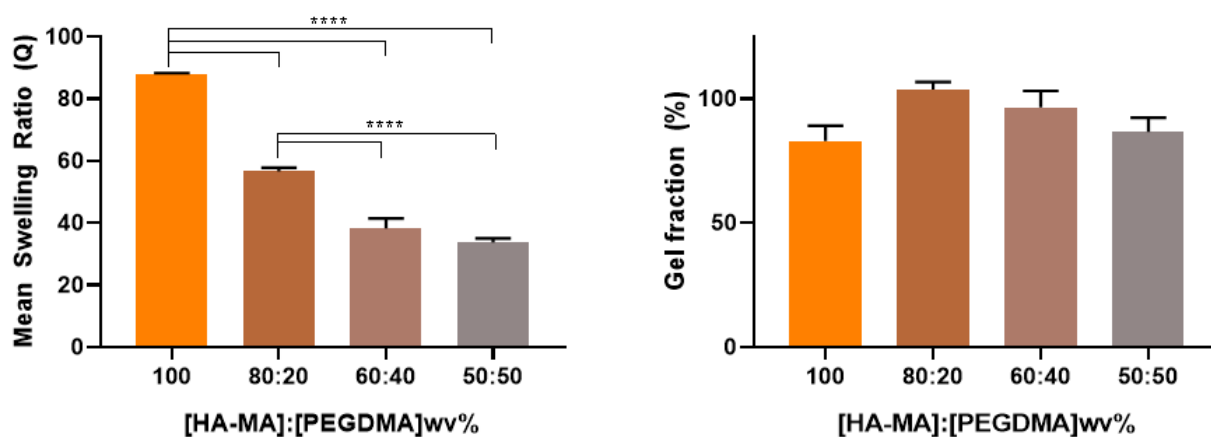


Figure 63. Mean swelling ratio and Gel fraction of HA-MA: PEGDMA hydrogel samples. Data is the mean \pm SEM of 3 independent experiments (N=3), performed in triplicate (n=3). **** $P < 0.0001$ when comparing concentrations using one-way ANOVA with Tukey posttests in GraphPad Prism V8.01.

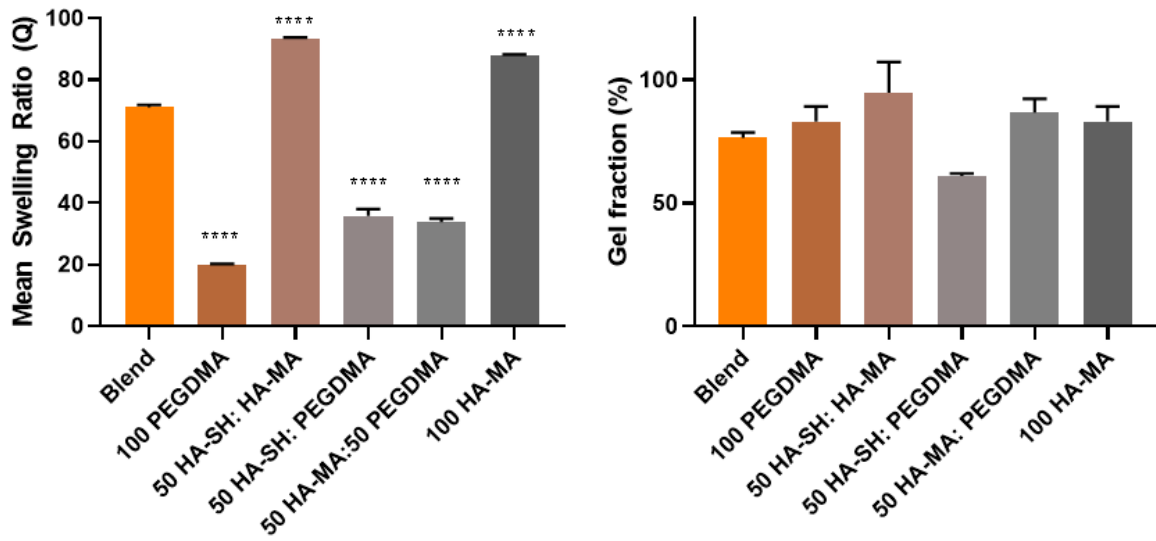


Figure 64. Mean swelling ratio and Gel fraction of the hybrid blend hydrogel sample vs the other hydrogel formulations. Blend refers to the hybrid hydrogel formulation of 50 % HA-SH: 40 % HA-MA: 10 % PEGDMA hydrogel sample. Data is the mean \pm SEM of 3 independent experiments (N=3), performed in triplicate (n=3). **** $P < 0.0001$ when comparing samples vs Blend hydrogel using one-way ANOVA with Tukey posttests in GraphPad Prism V8.01.

7.2.5 Degradation of hybrid hydrogels

The inclusion of thiol into the polymer matrix has been shown throughout this thesis to enhance degradation of the hydrogel. However, this degradation occurs at a rate insufficient to allow for recovery of a nerve. In order to allow for guidance of a regenerating nerve, the NGC would be required to stay in place for approximately 6 weeks (Carvalho, Oliveira and Reis, 2019) to allow for axonal sprouting, migration and myelination. Conversely, PEGDMA has been shown to degrade slowly (Burke *et al.*, 2019), which could potentially cause issues such as scar tissue formation. The purpose of this study was to evaluate the effect of PEGDMA inclusion in the hybrid hydrogel blend with a view to modulating the degradation rate to sustain regeneration of a peripheral nerve.

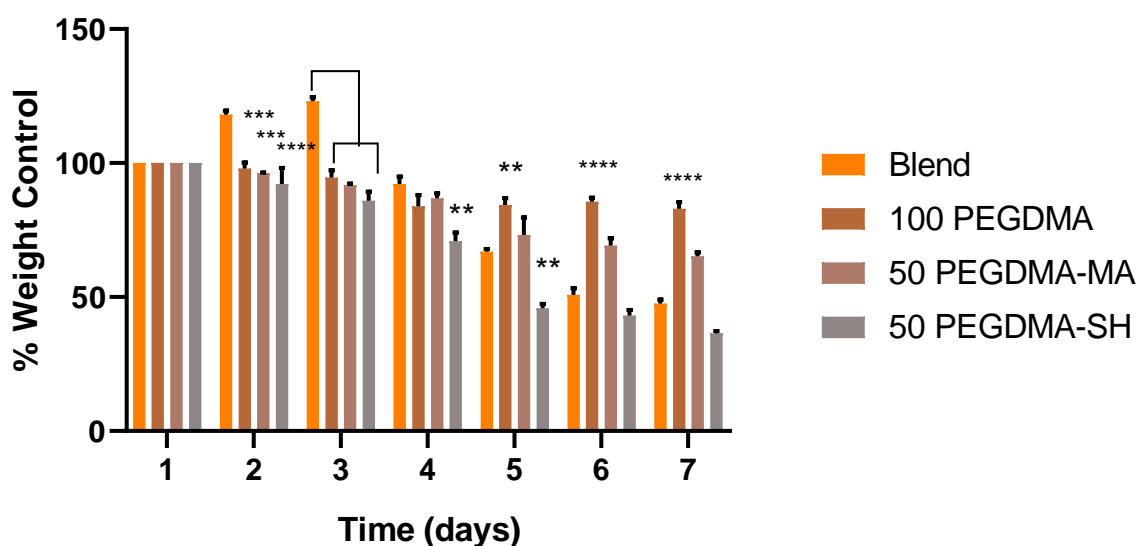


Figure 65. *In vitro* degradation of hybrid blend hydrogels compared with 100 %wv PEGDMA, 50 %wv PEGDMA: HA-MA and 50 %wv PEGDMA: HA-HA-MA: HA-SH. Data is the mean \pm SEM of 3 experiments (N=3), conducted in triplicate (n=3). Blend refers to the hybrid hydrogel blend formulation of 50% HA-SH: 40% HA-MA: 10% PEGDMA. Data is expressed as % weight control of the starting weight of each sample at equilibrium swelling. ** $P < 0.01$, *** $P < 0.001$, **** $P < 0.0001$ vs Blend when compared using two-way ANOVA with Tukey posttests in GraphPad Prism V8.01.

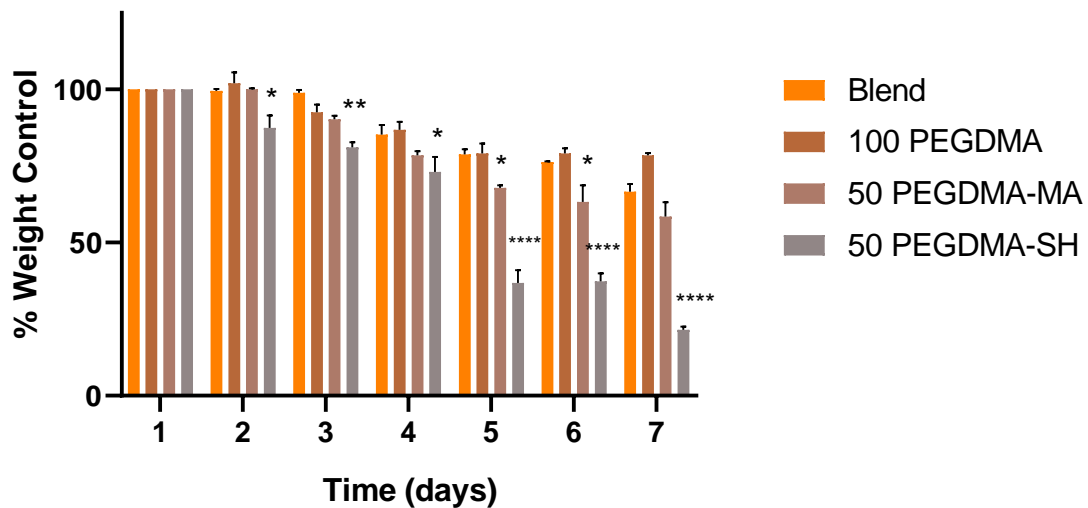


Figure 66. Accelerated (5 mM NaOH) degradation of hybrid blend hydrogels compared with 100 %wv PEGDMA, 50 %wv PEGDMA: HA-MA and 50 %wv PEGDMA: HA-HA-MA: HA-SH. Data is the mean \pm SEM of 3 experiments (N=3), conducted in triplicate (n=3). Data is expressed as % weight control of the starting weight of hydrogel samples at equilibrium swelling. Blend refers to the hybrid hydrogel blend formulation of 50% HA-SH: 40% HA-MA: 10% PEGDMA. * $P < 0.05$, ** $P < 0.01$, *** $P < 0.001$, **** $P < 0.0001$ vs Blend when compared using two-way ANOVA with Tukey posttests in GraphPad Prism V8.01.

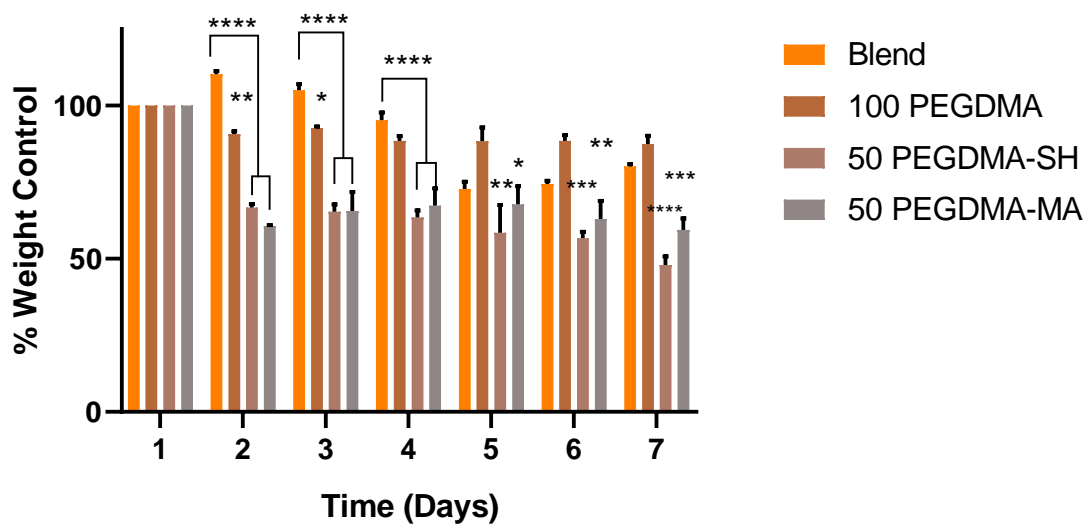


Figure 67. Accelerated (5 M NaOH) degradation of hybrid blend hydrogels compared with 100 %wv PEGDMA, 50 %wv PEGDMA: HA-MA and 50 %wv PEGDMA: HA-HA-MA: HA-SH. Data is the mean \pm SEM of 3 experiments (N=3), conducted in triplicate

(n=3). Data is expressed as % weight control of the starting weight of hydrogel samples at equilibrium swelling. Blend refers to the hybrid hydrogel blend formulation of 50% HA-SH: 40% HA-MA: 10% PEGDMA. * $P < 0.05$, ** $P < 0.01$, *** $P < 0.001$, **** $P < 0.0001$ vs Blend when compared using two-way ANOVA with Tukey posttests in GraphPad Prism V8.01.

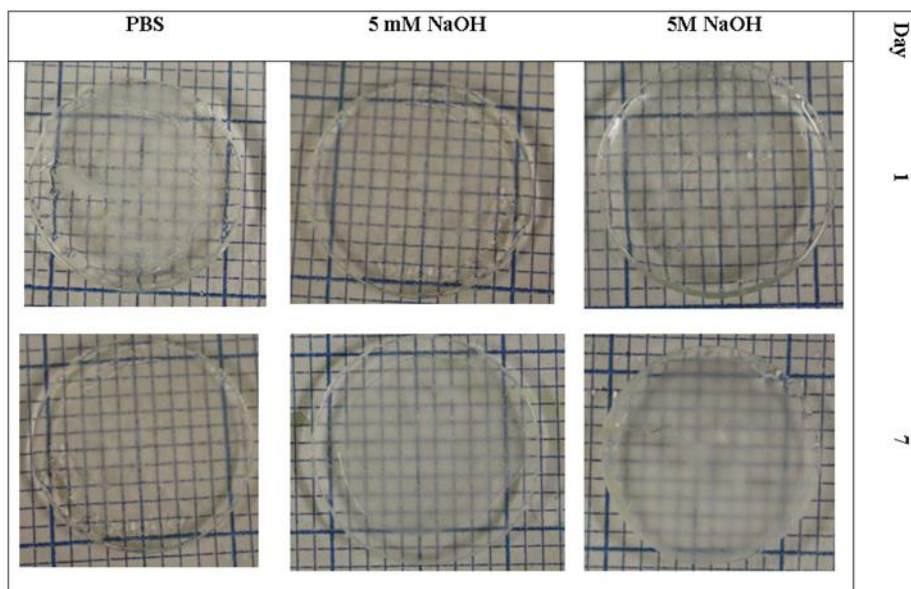


Figure 68. *In vitro* (PBS pH 7.4), 5 mM NaOH and 5 M NaOH degradation samples of 100 %wv PEGDMA on day 1 vs day 7. Images were captured using a canon 450D DSLR camera and used unedited.

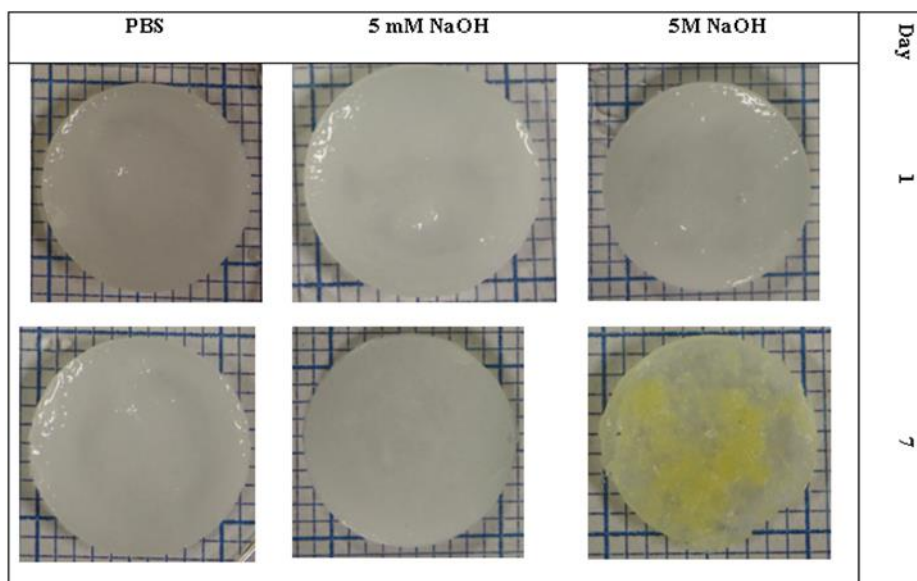


Figure 69. *In vitro* (PBS pH 7.4), 5 mM NaOH and 5 M NaOH degradation samples of 50 %wv PEGDMA: HA-MA on day 1 vs day 7. Images were captured using a canon 450D DSLR camera and used unedited.

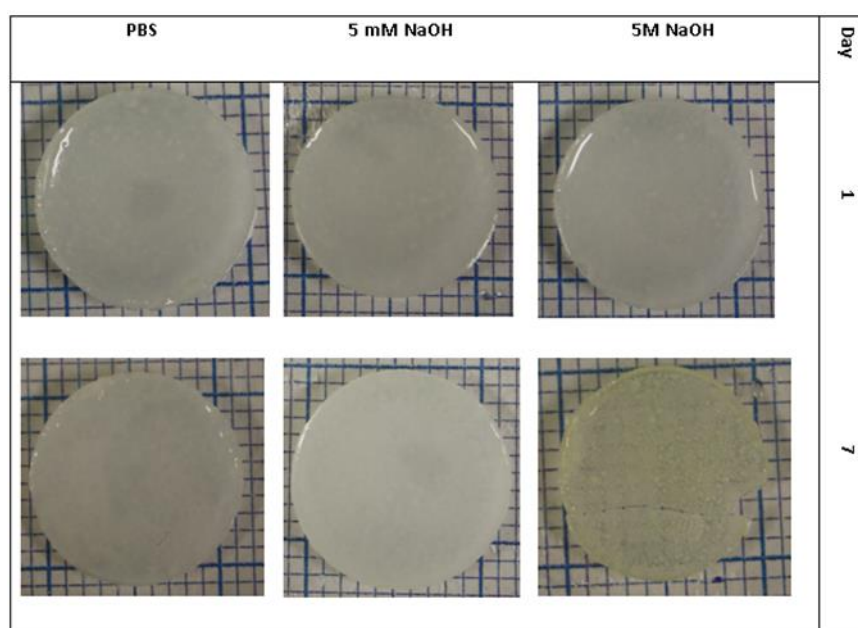


Figure 70. *In vitro* (PBS pH 7.4), 5 mM NaOH and 5 M NaOH degradation samples of 50 %wv PEGDMA: HA-SH on day 1 vs day 7. Images were captured using a canon 450D DSLR camera and used unedited.

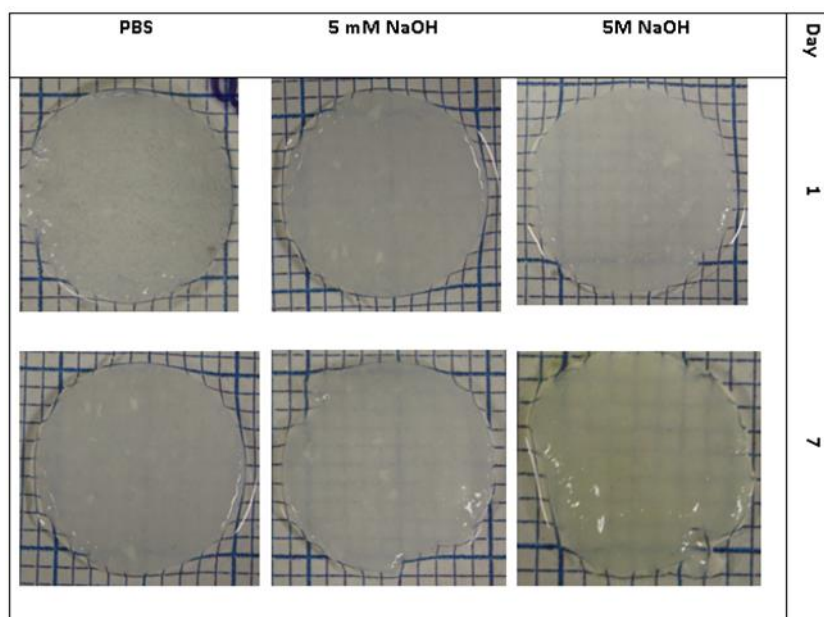


Figure 71. *In vitro* (PBS pH 7.4), 5 mM NaOH and 5 M NaOH degradation samples of hybrid hydrogels on day 1 vs day 7. Images were captured using a canon 450D DSLR camera and used unedited.

In Figure 65, the hybrid blend showed significantly different degradation by weight in *in vitro* (pH 7.4) conditions to the 50 % wv PEGDMA : HA-SH at every time point up until day 6 where there was no longer a significant difference between samples. The blend also showed significantly different results to the PEGDMA only sample in that the weight of the hybrid blend initially increased, a result which has been seen throughout this thesis in thiol containing samples (> 50 % wv). On day 4, the samples were no longer significantly different and after this point, the hybrid hydrogel began to decrease in weight dramatically. This result shows that the development of the hybrid blend modulated the degradation rate in such a way that the degradation rate was faster than that of PEGDMA, but slower than 50 % wv PEGDHA-MA: HA-SH.

The hybrid blend only differed significantly from the 50 % wv PEGDMA: HA-MA hydrogel on days 2 and 3, after which point the difference was no longer significant.

Figure 66 shows a similar conclusion in accelerated degradation (5mM NaOH) in that the 50 % wv PEGDMA: HA-SH sample had the fastest degradation rate. The 100 % wv PEGDMA had the slowest degradation but still degraded substantially more over the 7 day

period than what was observed in *in vitro* (pH 7.4) conditions. The hybrid blend degraded very slowly in 5 mM NaOH and showed no significant difference when compared to the 100 %wv PEGDMA sample.

Similarly, Figure 67 exhibits accelerated degradation (5 M NaOH) and from day 4 onward, the blend showed no significant difference to the PEGDMA sample. 50 %wv PEGDMA: HA-MA and 50 %wv PEGDMA: HA-SH also showed reduced degradation when comparing Figure 67 and 66.

However, when analysing the images taken of hydrogels on day 1 and day 7, it's evident that although degradation may not be evident by weight change, degradation of HA in the samples is very evident in the 5 M NaOH conditions by the presence of substantial yellowing. Cracking and chipping of samples was also evident in accelerated conditions.

7.2.6 Cytocompatibility testing of hybrid hydrogels

The cytocompatibility of hydrogels was evaluated using the direct contact and elution assays as outlined in ISO 10993-5 which details recommendations for the cytotoxicity testing of medical devices as detailed in section 3.8. Figure 72 shows the results obtained via the direct contact assay where hydrogels were formed in tissue culture plates and then sterilised and swollen in cell culture media. Once swollen, cells were seeded on top and allowed to grow for 20 hours before assaying with resazurin. Resazurin provides an ideal assay reagent for the testing of hydrogels as the fluorescent resorufin accumulates extracellularly in the media and therefore, cells do not need to be recovered. This makes it a more robust and reliable method for assaying cell viability on polymeric substrates than the MTT assay. In these assays, a suitable control hydrogel could not be identified, and so, all test conditions were expressed as % of control where the control was a tissue culture well with media and cells but no hydrogel. ISO 10993-5 typically recommends that samples are placed on top of a monolayer of cells, however, in this case it would have inflicted physical trauma to the cells. In this scenario, the ISO standard states that where necessary, cells can be seeded on the surface of the sample. The direct contact assay provides vital insight into how the cells respond to a representative model of conduit materials *in vitro*. As may be seen in Figure 72, significant cytotoxicity was observed in neuronal cells grown on all hydrogels with the exception of 50% HA-MA: HA-SH. In glial cells, cytotoxicity was only observed in samples containing PEGDMA.

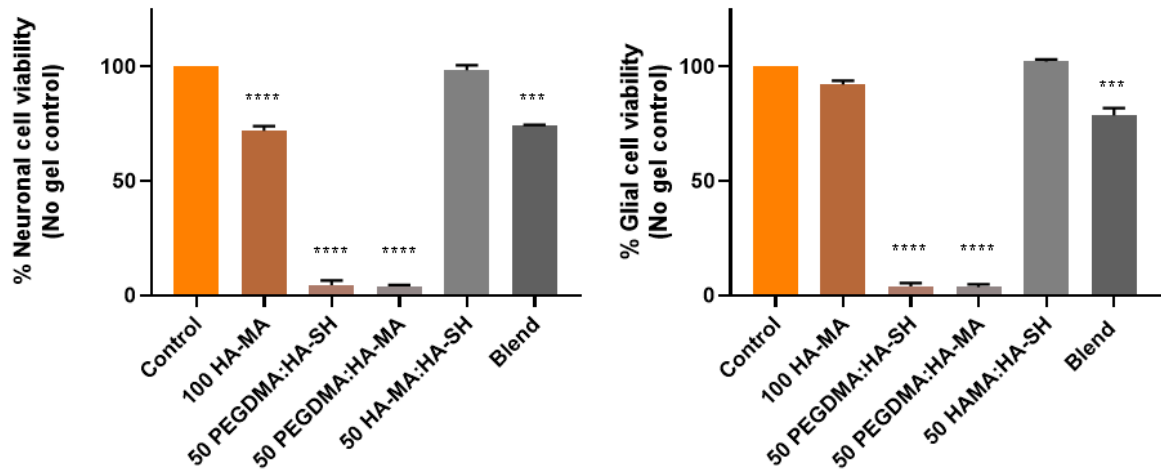


Figure 72. UV cured hydrogels induced significant toxicity in direct contact testing of neuronal and glial cell lines. Direct contact assay for neuronal (left) and glial (right) cells on various hydrogels. Data is expressed as % control where the control contained no hydrogel (cells in media only). Data is the mean \pm SEM of 3 experiments (N=3), conducted in triplicate (n=3). *** $P < 0.001$, **** $P < 0.0001$ vs control when compared using one-way ANOVA with Tukey posttests. Data was analysed using GraphPad Prism V8.01.

To evaluate if this was due to the inability of cells to adhere to the hydrogels, we tested the eluates of the hydrogels on both neuronal and glial cell lines as outlined in ISO 10993-5 (as outlined in section 3.8) which details recommendations for elution testing. Elution testing, as described in section 3.4.8.1, provides a method of testing leachates which can have wider implications in the body for a medical device due to the easier dispersal of compounds. Figure 73, samples (iii)-(vii) induced significant toxicity in neuronal cells, with sample (iii) 50% HA-MA: PEGDMA causing the most severe decrease in cell viability, reducing it to approximately 24%. The glial cells in Figure 73 did not show the same extent of toxicity as the neuronal cells, with only the 50% HA-MA: PEGDMA hydrogel and the 50% HA-SH: 40% HA-MA: 10% PEGDMA hybrid hydrogel showing significant decreases in viability.

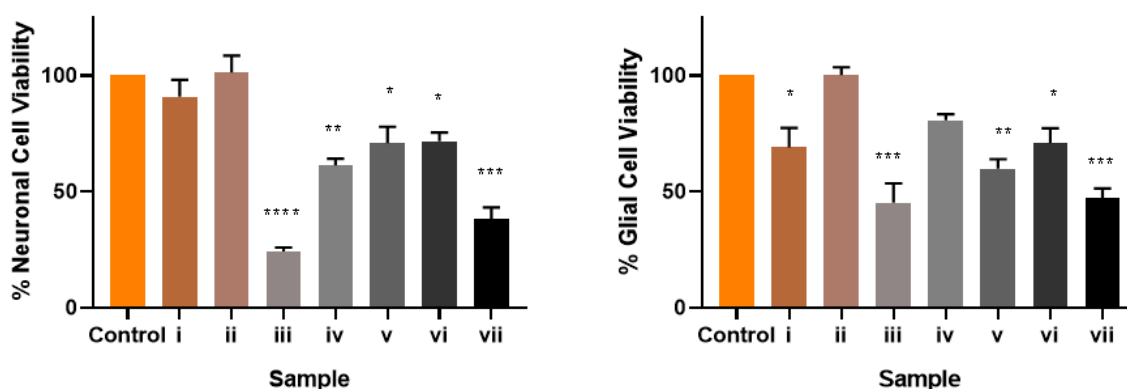


Figure 73. Elution assay of hydrogels in neuronal and glial cell lines. Elution assay for neuronal (left) and glial (right) cells from various hydrogels. (i) 100 % wv PEGDMA, (ii) 50 % PEGDMA-water, (iii) 50 % PEGDMA: HA-MA, (iv) 50% PEGDMA: HA-SH, (v) 100% HA-MA, (vi) 50 % HA-MA:HA-SH, (vii) Hybrid blend hydrogel (50% HA-SH: 40% HA-MA: 10% PEGDMA). Data is expressed as % of no hydrogel eluent (cells in media only). * $P < 0.05$, ** $P < 0.01$, *** $P < 0.001$, **** $P < 0.0001$ vs control when compared using one-way ANOVA with Tukey posttests. Data is the mean \pm SEM of 3 experiments (N=3), conducted in triplicate (n=3). Data was analysed using GraphPad Prism V8.01.

7.3 DISCUSSION

The aim of this chapter was to ameliorate the mechanical properties of HA hydrogels by integrating a synthetic polymer, PEGDMA, which has superior mechanical properties and long residence time *in vivo*, into the polymer matrix. Through a series of ratio testing, an optimal formulation was composed of 50 %wv HA-SH: 40 %wv HA-MA and 10 %wv PEGDMA, (referred to as hybrid blend hereafter). This formulation provided slightly improved mechanical properties, improved degradation profile and also modulated the cytocompatibility of hydrogel. PEGDMA was a necessary addition to counter the poor mechanical properties of HA hydrogels, however, as can be seen in Figure 72, direct contact with 50 %wv PEGDMA gels resulted in significant cytotoxicity in both cell lines. The hybrid hydrogel however, introduced 10 %wv PEGDMA while maintaining cell viability of approximately 60 % in both cell lines, therefore finding a balance between properties. In this manner, it has allowed the introduction of a synthetic polymer which will greatly aid in manufacturing and applicability, without complete compromise of cytocompatibility. When comparing the compressive strength, only the 100 %wv PEGDMA sample possessed a compressive strength suitable for a NGC (> 0.5 MPa), however, the hybrid hydrogel had a compressive strength that was not significantly different from the 50 %wv PEGDMA: HA-SH sample, despite only containing 10 %wv PEGDMA. This shows the impact of the tri-polymer matrix system in improving mechanical properties.

In rheological testing, the hybrid hydrogel blend possessed a lower storage modulus than both 50 %wv PEGDMA: HA samples. However, the hybrid blend sample showed greater stability in storage modulus across increasing strain, whereas the storage modulus of PEGDMA containing samples dramatically decreased when exposed to increasing strain. This is evidence of the capabilities of the hybrid blend to withstand the strains of the peripheral nervous system *in vivo*. All samples were stable across temperatures ranging from 4- 37 °C.

The inclusion of 10 %wv PEGDMA had a significant effect on the Q ratio of samples during swelling studies. When comparing the hybrid blend to 50 %wv HA-MA: HA-SH, a significant difference can be observed with the blend possessing a Q ratio of approximately 70% whereas the 50 %wv HA-MA: HA-SH hydrogel possesses a Q ratio of approximately 95. Therefore, the inclusion of a 10 %wv quantity of PEGDMA induced a reduction of approximately 25 in the Q ratio. Control over swelling rates is a vital parameter of any

medical device as uncontrolled swelling can induce immune responses as well as having a significant impact on drug delivery (Bordbar-Khiabani and Gasik, 2022).

The degradation of PEGDMA is significantly slower than that of HA containing samples which could potentially cause issues for use as a medical device. However, the inclusion of 10 %wv PEGDMA in the hybrid hydrogel provided sufficient resilience to degradation which was significantly better than that of the 50 %wv PEGDMA: HA-SH sample. This effect could be seen in *in vitro physiological conditions* and accelerated degradation conditions (Figure 65-72). By tailoring the ratio of PEGDMA: HA-SH with HA-MA, it could potentially be possible to tailor the degradation profile to the extent of injury and recovery time required.

Cytotoxicity testing of hydrogel samples through direct contact assays revealed significant toxicity in the presence of 50 %wv PEGDMA. This is in contrast to what has been published in literature (Chang, Ching and HA-SHimoto, 2022), although the authors do report a loss of viability of approximately 60 % in the presence of a 60 %wv PEGDMA hydrogel. The molecular weight used in their study was 1000, whereas this project utilised a MW of 600 for cost and ease of manufacturing. Figure 73 reveals less cytotoxicity in the presence of the eluate of 50 %wv PEGDMA sample (iii), although still significantly more cytotoxic than the control of only media and cells. Conversely, the hybrid hydrogel eluate proved to be more cytotoxic, reducing cell viability to below 50 % in both cell lines, while direct contact assay revealed cell viability of approximately 60 %. This would indicate the presence of soluble parts which were causing cytotoxic effects in neuronal and glial cell lines.

This chapter has shown that the mechanical properties of the hydrogels can be improved by the inclusion of synthetic polymers such as PEGDMA, however, their inclusion must be carefully considered due to the cytotoxicity identified in neuronal and glial cell lines. Using a low percentage of synthetic PEGDMA allows for an increase in mechanical properties, without sacrificing biocompatibility. The following chapter will investigate whether the more highly crosslinked network of 3D prints could overcome the cytotoxicity observed in the UV cured hydrogels.

CHAPTER 8. STEREO LITHOGRAPHY 3D PRINTING

8.1 PREFACE

Stereolithography 3D printing has the potential to induce greater mechanical properties due to the tighter interconnected network and greater degree of crosslinking it imparts. In this section, samples of 100 %wv PEGDMA, 50 %wv PEGDMA: HA-MA, 50 %wv PEGDMA: HA-SH and the 50 %wv HA-SH: 40 %wv HA-MA: 10 %wv PEGDMA hybrid blend were 3D printed and compared in terms of their mechanical, physical and biological properties. This was crucial in terms of sample development as the UV cured hybrid blend hydrogel showed approximately 40 % toxicity in the direct contact assay and approximately 60 % toxicity in elution assays. Therefore, it was necessary to determine the effect of modified HA in the representative endpoint design. In almost all cases, properties of 3D printed samples exceeded those of UV photo-cured samples. This section provided proof of concept for the final NGC formulation.

8.2 RESULTS

8.2.1 ATR-FTIR of 3D printed samples

Following 3D printing, samples were placed in a UV chamber for post-curing before rinsing and drying in a vacuum oven to rid the samples of excess water. FTIR analysis of photo-cured samples as shown in Figure 74 revealed a loss of peaks at 1553 and 1236 cm^{-1} (highlighted in Figure 36 above) which arise from the C=C stretching and C-O stretching of methacrylate in PEGDMA and HA-MA. This confirms polymerisation has taken place. Generally, the broad absorption band at 3700-3200 cm^{-1} corresponds to the vibrations from O-H stretching in HA. PEGDMA dominates the spectra in all cases with only the peaks at approximately 3400 cm^{-1} and 1640 cm^{-1} indicating the presence of HA in the polymer matrix.

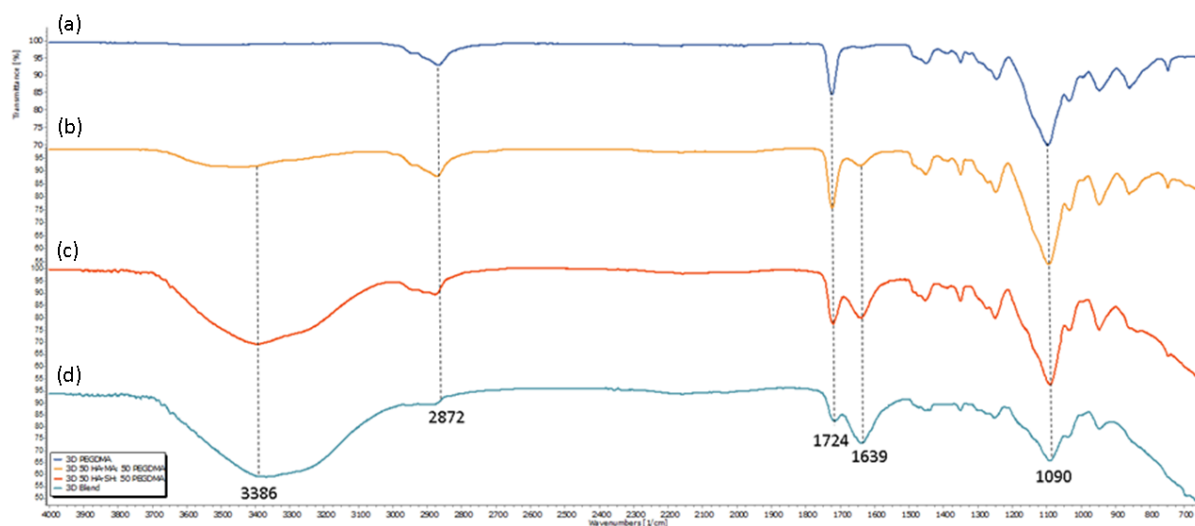


Figure 74. ATR-FTIR of stereolithography 3D printed samples with key peaks highlighted. (a) 100 %wv PEGDMA, (b) 50 %wv PEGDMA: HA-MA, (c) 50 %wv PEGDMA: HA-SH, (d) Hybrid Blend.

8.2.2 Compression testing of 3D printed samples

Compression testing of 3D printed samples did not reveal a significant increase in compressive strength of all samples in comparison with hydrogel gel samples. In the case of the Young's modulus, the 3D printed samples, with the exception of PEGDMA, performed poorer. In particular, the 50 % wv PEGDMA: HA blends performed much poorer than their hydrogel counterparts. These samples when 3D printed were brittle and peeling of layers was evident showing opposing forces within the printed structure, potentially due to the differing viscosities between HA and PEGDMA.

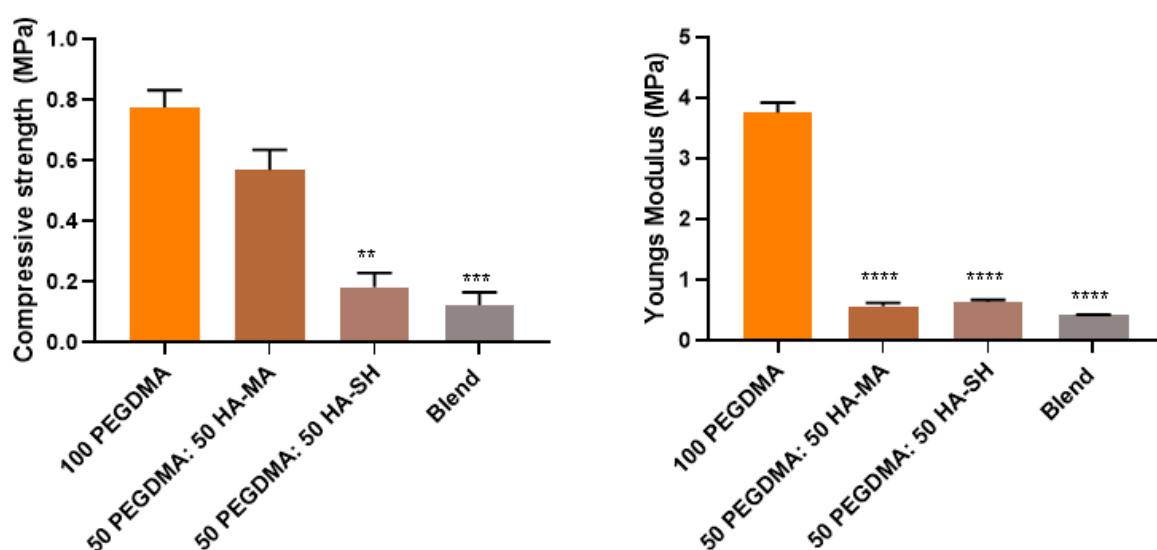


Figure 75. Compressive strength and Young's modulus of 3D printed samples. Data is the mean \pm SEM of 3 independent experiments (N=3), conducted in triplicate (n=3). ** $P < 0.01$, *** $P < 0.001$, **** $P < 0.0001$ vs 100% PEGDMA when compared using two-way ANOVA with Tukey posttests in GraphPad Prism V8.01.

8.2.3 Rheological characterisation of 3D printed samples

Rheological characterisation of samples revealed much greater storage moduli in 3D printed samples when compared to their hydrogel counterparts. This increased energy storage is due to the more highly cross linked matrix within samples. This is a necessary characteristic as the storage modulus indicates the amount of energy a sample can store before deformation which is a critical factor in the design of any medical device formulation. Although the 3D blend shows a lower storage modulus when compared to the 50 %wv PEGDMA samples of approximately one third, it is more stable across a variety of strain (%) and produces one third of the strength with one fifth of the concentration of PEGDMA. This lower concentration counteracts the toxicity and viscosity differential issues observed in samples containing a greater percentage of PEGDMA.

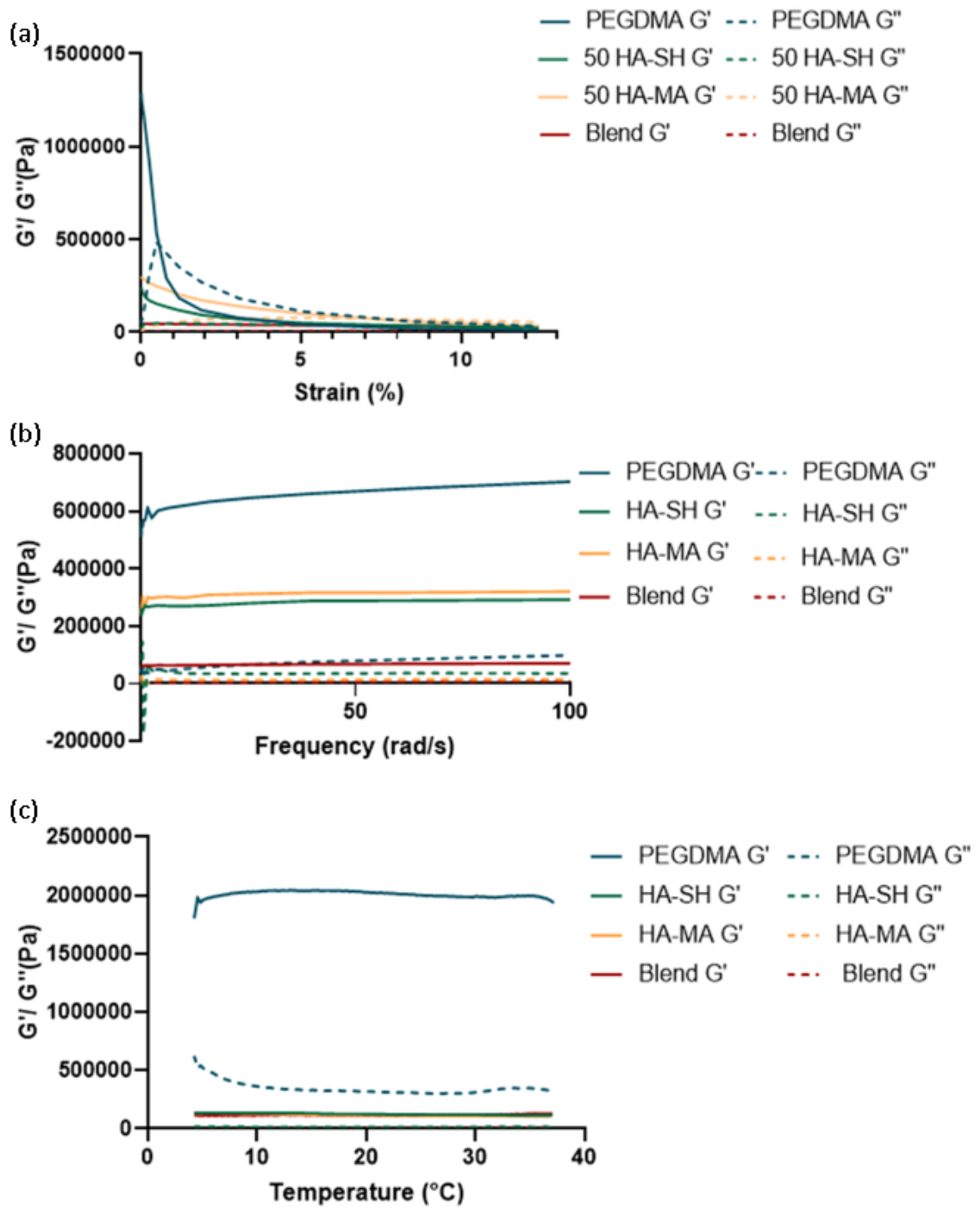


Figure 76. Rheological characterisation of 3D printed samples. (a) Amplitude, (b) Frequency and (c) temperature ramp. Data is the mean \pm SEM of 3 independent experiments (N=3), conducted in triplicate (n=3). Data was analysed using GraphPad Prism V8.01.

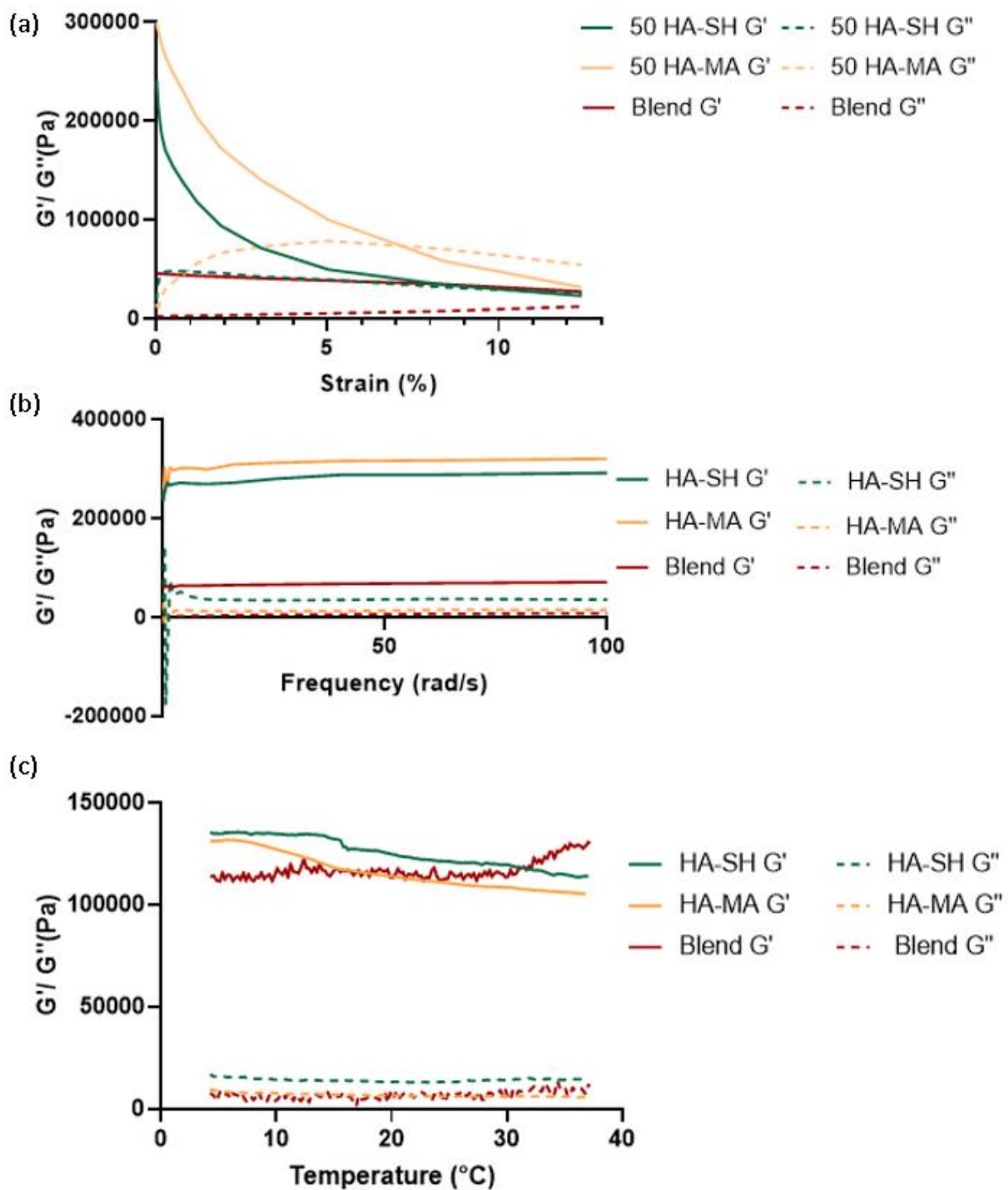


Figure 77. Rheological characterisation of 3D printed samples. Image excludes 100 % wv PEGDMA to allow for proper visualisation, (a) Amplitude, (b) Frequency and (c) temperature ramp. Data is the mean \pm SEM of 3 independent experiments (N=3), conducted in triplicate (n=3). Data was analysed using GraphPad Prism V8.01.

8.2.4 Swelling studies

It was hypothesised that the denser crosslinked network would affect the swelling behaviour of samples. However, this did not prove to be the case for the hybrid blend. 50 %wv PEGDMA: HA-MA and 50 %wv PEGDMA: HA-SH, surprisingly, experienced great increases in the Q ratio after 3D printing. This is believed to be due to the delamination observed in the printed samples, potentially due to the viscosity differences between PEGDMA and HA-MA. Both the hybrid blend and 100 %wv PEGDMA samples were in line with what was observed in the hydrogel samples.

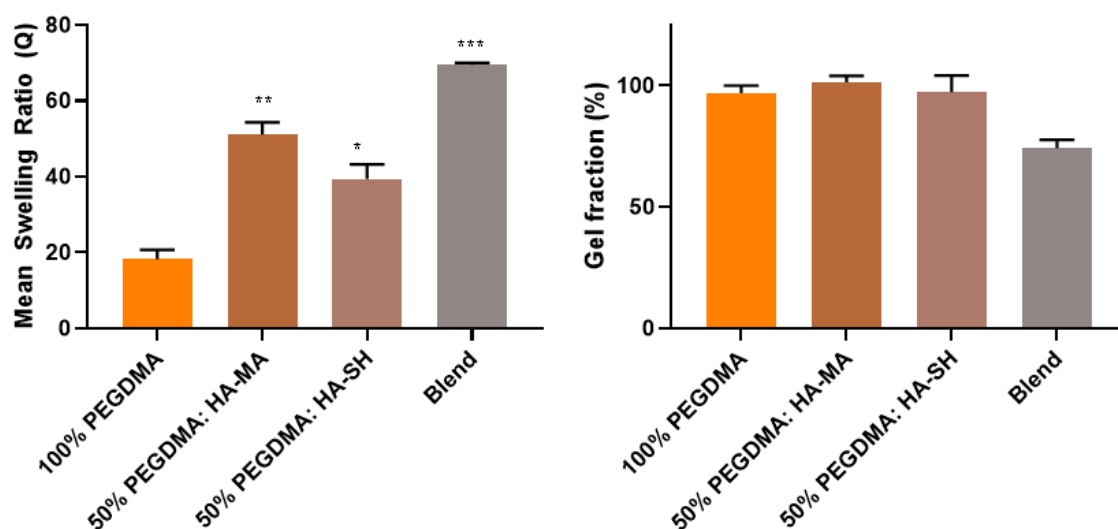


Figure 78. Mean swelling ratio and Gel fraction of 3D printed samples. Data is the mean \pm SEM of 2 independent experiments (N=2), performed in triplicate (n=3). * $P < 0.05$, ** $P < 0.01$, *** $P < 0.001$ vs PEGDMA when compared using one-way ANOVA with Tukey posttests in GraphPad Prism V8.01.

8.2.5 Degradation testing of 3D printed samples

3D printed samples have a more tightly knit architecture due to the higher degree of cross-linking in the polymer matrix and therefore the assumption is made that this tighter network would impart a greater resistance to degradation. However, as can be seen in this trial, the hybrid hydrogel blend degraded at a faster rate than the other samples in the *in vitro* physiological condition (PBS pH 7.4). This is most likely due to the higher concentration of HA in the sample allowing for greater water binding and stretching of polymer chains. This result was not replicated in the accelerated conditions. The accelerated conditions utilised 5 mM and 5M NaOH to accelerate the degradation of the polymer network as outlined in section 3.5.6.2.2. All images were captured using a Canon 450D DSLR camera without flash in order to capture the macroscopic changes in sample structure over the course of a 7 day degradation study. These images appear in Figures 82-85.

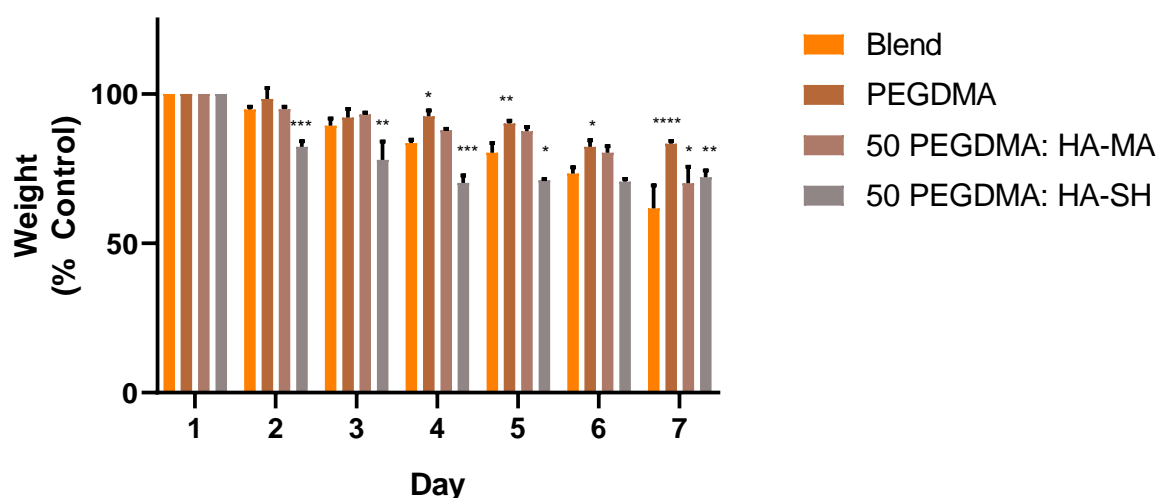


Figure 79. *In vitro* degradation (pH 7.4) of hybrid blend 3D prints compared with 100 %wv PEGDMA, 50 %wv PEGDMA: HA-MA and 50 %wv PEGDMA: HA-SH. Data is the mean \pm SEM of 3 experiments (N=3), conducted in triplicate (n=3). Samples are expressed as % control of the starting weight of 3D prints at equilibrium swelling. * $P < 0.05$, ** $P < 0.01$, *** $P < 0.001$, **** $P < 0.0001$ vs Blend when compared using two-way ANOVA with Tukey posttests in GraphPad Prism V8.01.

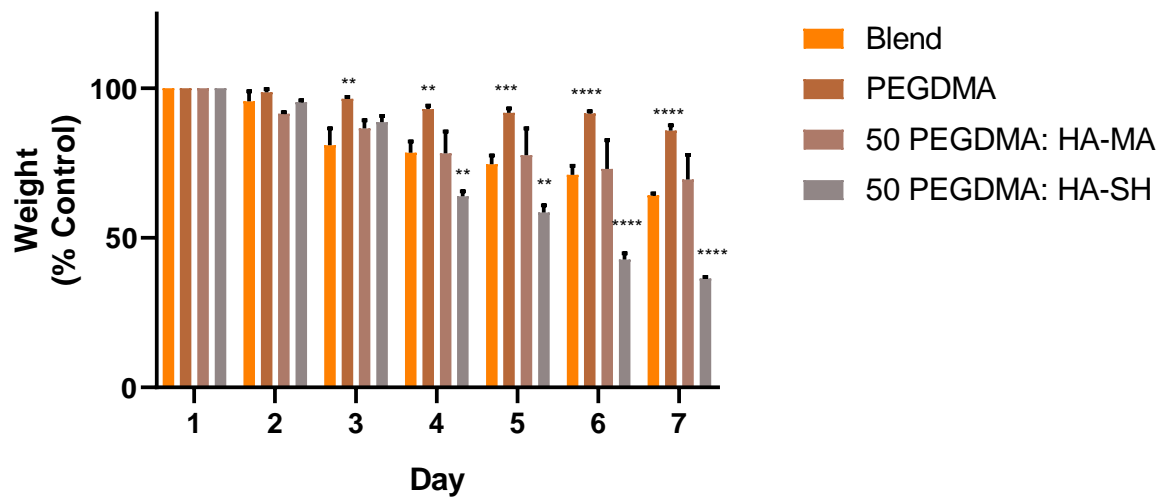


Figure 80. Accelerated (5 mM NaOH) degradation of hybrid blend 3D prints compared with 100 %wv PEGDMA, 50 %wv PEGDMA: HA-MA and 50 %wv PEGDMA: HA-SH. Data is the mean \pm SEM of 3 experiments (N=3), conducted in triplicate (n=3). Samples are expressed as % control of the starting weight of 3D prints at equilibrium swelling. $**P < 0.01$, $***P < 0.001$, $****P < 0.0001$ vs Blend when compared using two-way ANOVA with Tukey posttests in GraphPad Prism V8.01.

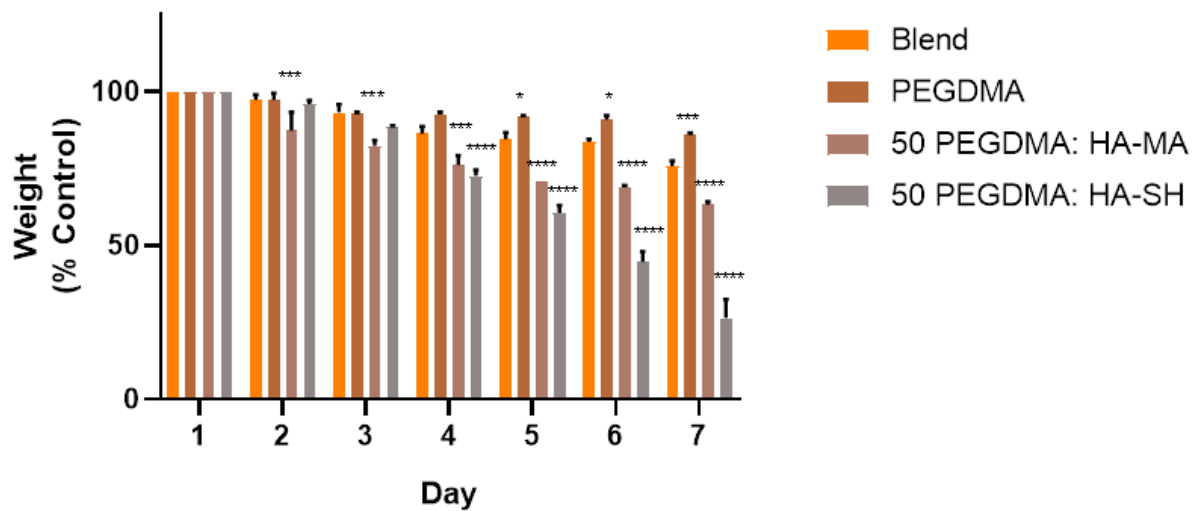


Figure 81. Accelerated (5 M NaOH) degradation of hybrid blend 3D prints compared with 100 %wv PEGDMA, 50 %wv PEGDMA: HA-MA and 50 %wv PEGDMA: HA-SH. Data is the mean \pm SEM of 3 experiments (N=3), conducted in triplicate (n=3). Samples are expressed as % control of the starting weight of 3D prints at equilibrium swelling. * $P < 0.05$, ** $P < 0.01$, *** $P < 0.001$, **** $P < 0.0001$ vs Blend when compared using two-way ANOVA with Tukey posttests in GraphPad Prism V8.01.

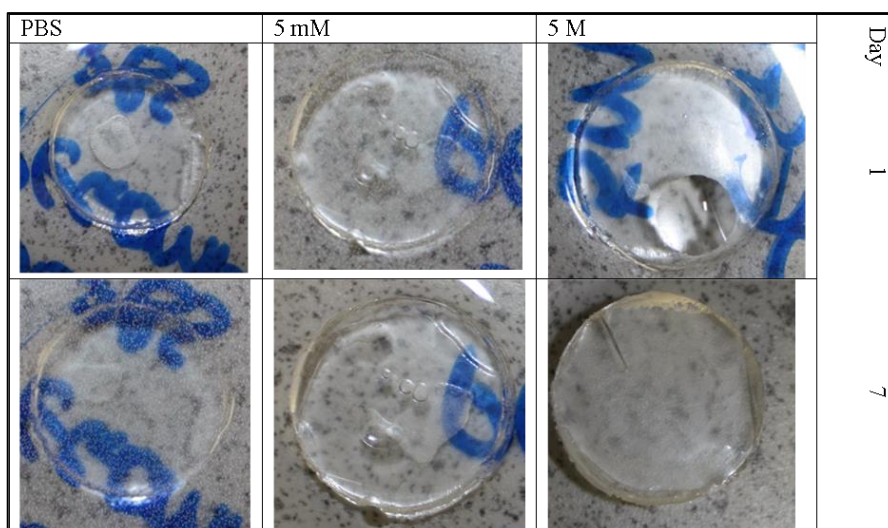


Figure 82. 100 %wv PEGDMA samples on day 1 and day 7 of the degradation study. PEGDMA 3D printed samples showed great resilience to degradation. A small hairline fracture appeared on the outer surface of the print exposed to 5 M NaOH on day 7 but colour and regularity appeared consistent.

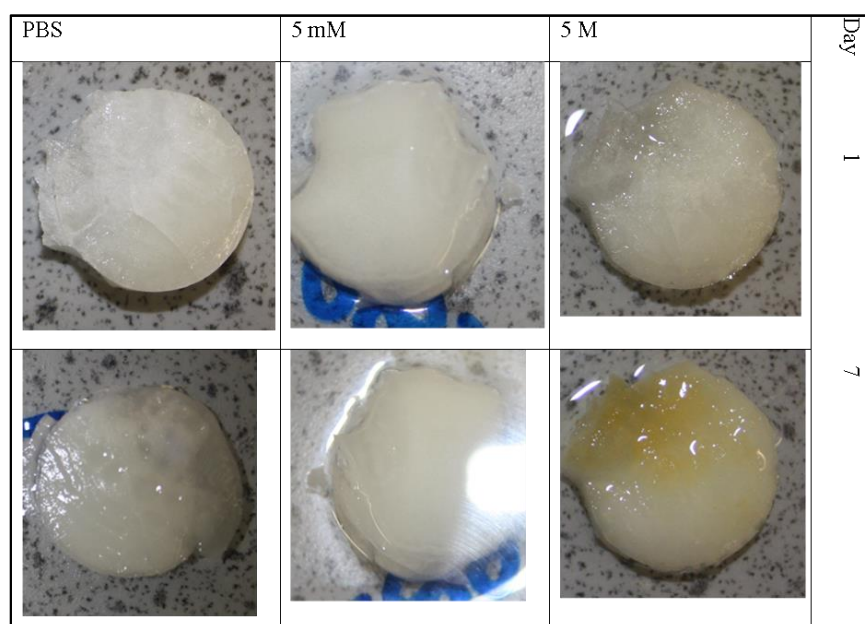


Figure 83. 50 %wv PEGDMA: HA-MA samples on day 1 and day 7 of the degradation study. 50 %wv PEGDMA: HA-MA samples appeared cracked and delaminated immediately after 3D printing which introduced weak points. The samples began to break up over the course of 7 days and also showed discolouration on day 7 of 5 M NaOH exposure.

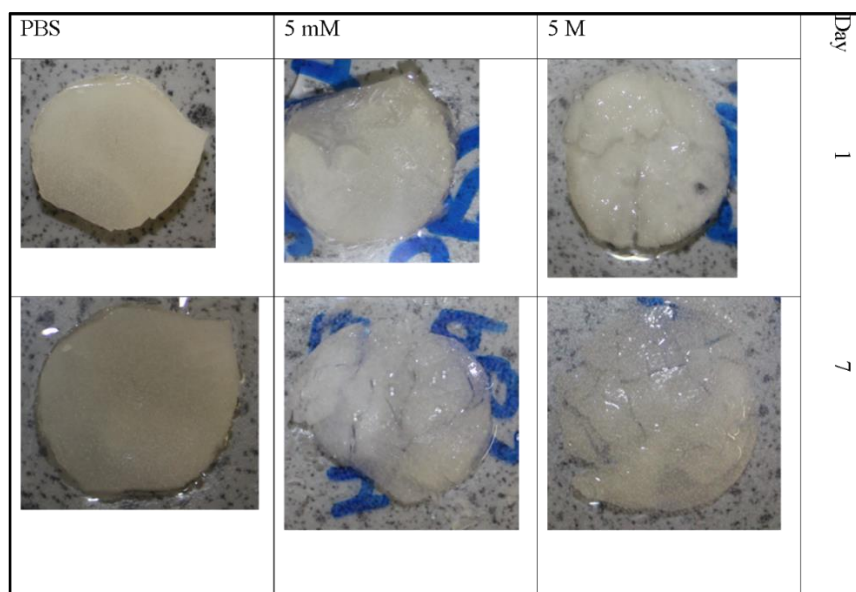


Figure 84. 50 %wv PEGDMA: HA-SH samples on day 1 and day 7 of the degradation study. 50 %wv PEGDMA: HA-SH exhibited similar cracking and delamination to that observed in Figure 83. In the presence of 5 mM and 5M NaOH, the samples disintegrated by day 7.

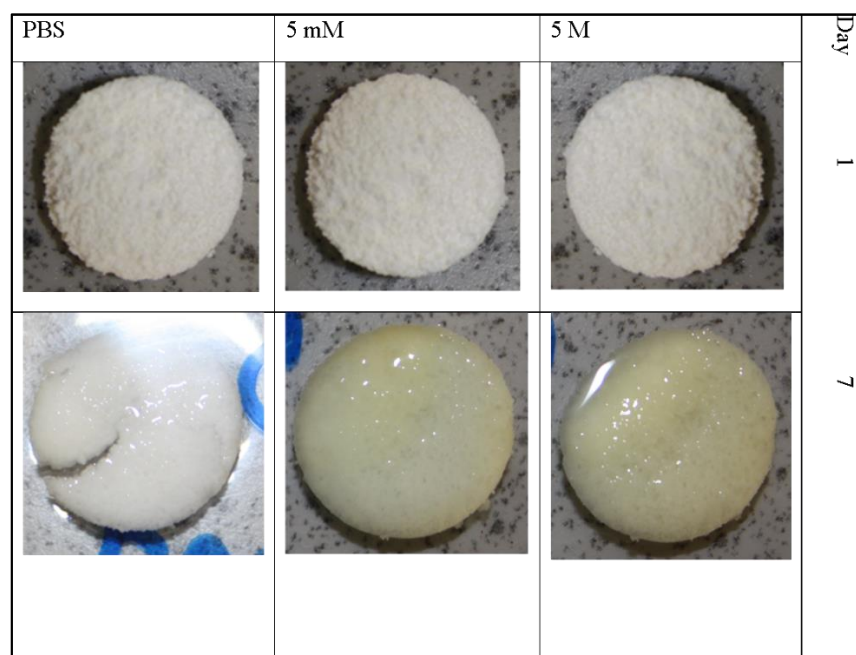


Figure 85. Hybrid blend 3D printed samples on day 1 and day 7 of the degradation study. The hybrid 3D print showed decent resilience to degradation. In the presence of PBS, the sample showed splitting due to the swelling behaviour of the material. In the presence of 5 mM and 5 M NaOH, samples exhibited consistent regularity but both samples appeared yellowed.

8.2.6 Cytotoxicity testing of 3D printed samples

Initial cytotoxicity testing of 3D printed sample leachates revealed almost 100 % toxicity in neuronal and glial cell lines exposed to leachates of the 3D printed blend, as per Figure 86 and 87, which was very concerning. Further investigation revealed that this may have been due to retention of unreacted photo-initiator (TPO) which has been shown to be cytotoxic in a dose dependent manner (Popal *et al.*, 2018). Due to the more porous nature of the hybrid blend sample (Figure 85), it can be assumed that this retention of TPO was the cause of the observed toxicity levels. To confirm this, fresh samples were prepared and washed x3 in methanol before drying to solubilise and leach out the unreacted water insoluble photo-initiator in the polymer matrix. On repeating the elution assays with these revised samples as outlined in section 3.5.6.1, no toxicity was observed (Figures 88 and 89) which confirmed the hypothesis that the 3D printed sample is biocompatible in contrast to the hydrogels of the same polymer mixtures examined in chapter 7, however, efforts must be taken to remove any unreacted TPO.

3D prints were prepared as outlined in section 3.5.3 and prepared as detailed above. After methanol washing, the samples were dried and UV sterilised. The samples were then placed in complete culture medium in 6 well plates and incubated overnight. After 24 h incubation, the leachate medium was extracted from the 6 well plate and used as treatment media for neuronal and glial cells which had been seeded in 24 well plates, 24 h previously. The cells were incubated for a further 20 h in the presence of the treatment media before assaying using the resazurin reduction assay by adding resazurin directly to the medium to a final concentration of 0.02 % wv.

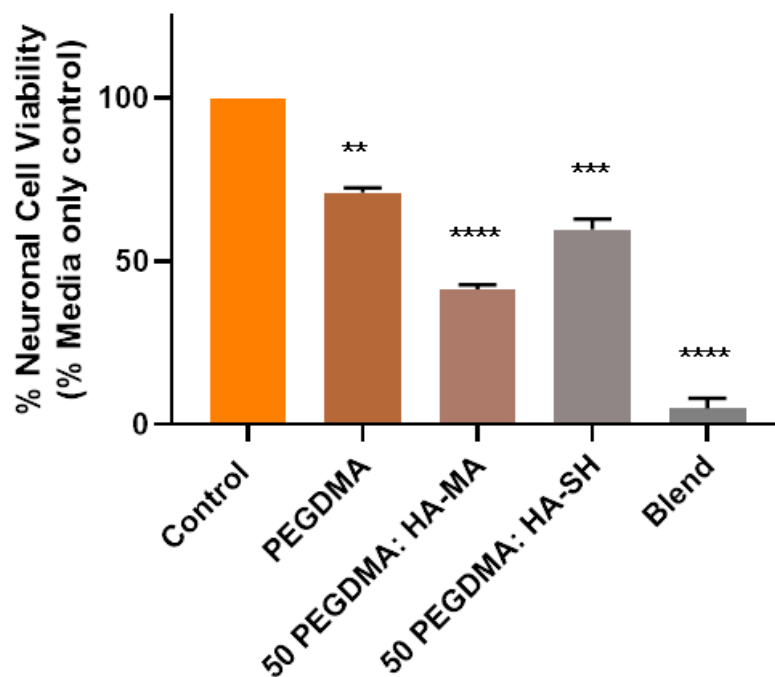


Figure 86. Resazurin reduction assay of 3D print leachates in neuronal cells without residual TPO removal. Data is presented as % control of cells in complete culture medium. Data is the mean \pm SEM of 2 experiments (N=2), conducted in triplicate (n=3). ** $P < 0.01$, *** $P < 0.001$, **** $P < 0.0001$ vs Control when compared using two-way ANOVA with Tukey posttests in GraphPad Prism V8.01.

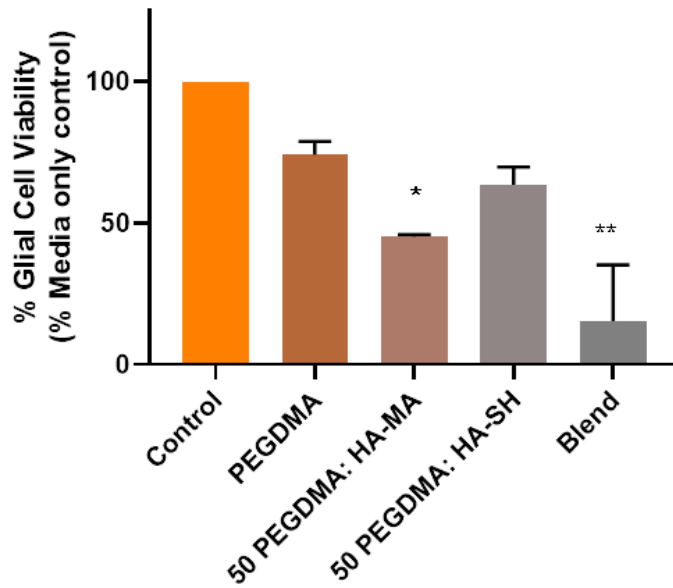


Figure 87. Resazurin reduction assay of 3D print leachates in neuronal cells without residual TPO removal. Data is presented as % control of cells in complete culture medium. Data is the mean \pm SEM of 2 experiments (N=2), conducted in triplicate (n=3). ** $P < 0.01$, *** $P < 0.001$, **** $P < 0.0001$ vs Control when compared using two-way ANOVA with Tukey posttests in GraphPad Prism V8.01.

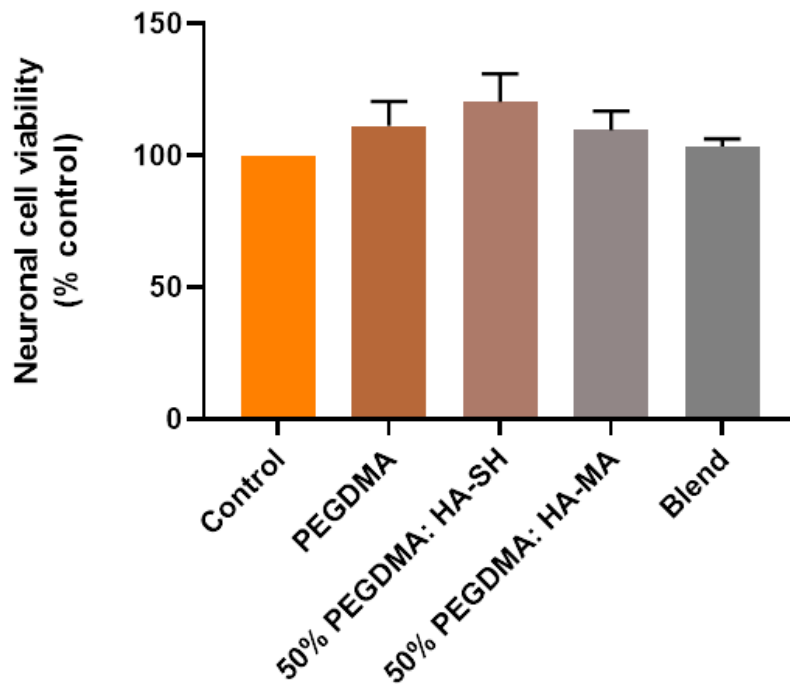


Figure 88. Resazurin reduction assay of 3D print leachates in neuronal cells with residual TPO removal. Data is presented as % control of cells in complete culture medium. Data is the mean \pm SEM of 3 experiments (N=3), conducted in triplicate (n=3). $P > 0.05$ vs Control when compared using two-way ANOVA with Tukey posttests in GraphPad Prism V8.01.

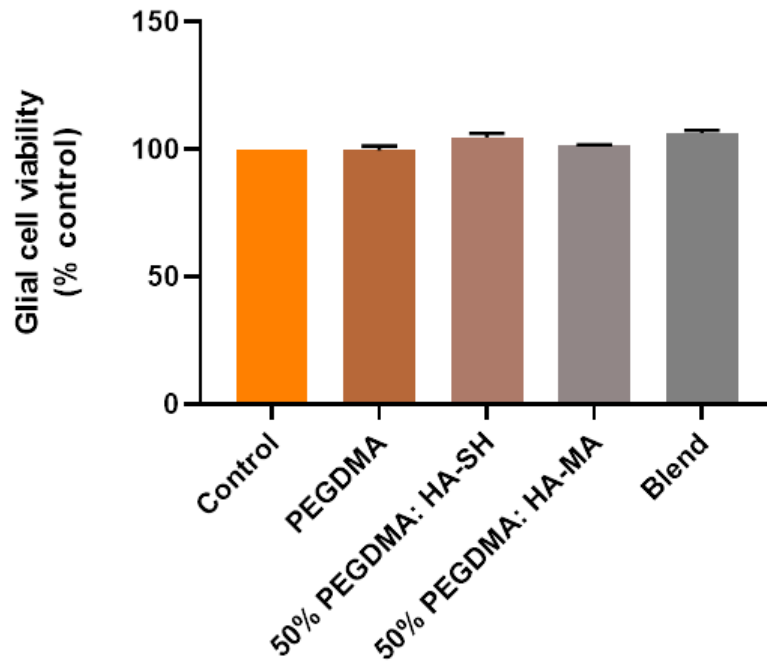


Figure 89. Resazurin reduction assay of 3D print leachates in glial cells with residual TPO removal. Data is presented as % control of cells in complete culture medium. Data is the mean \pm SEM of 3 experiments (N=3), conducted in triplicate (n=3). $P > 0.05$ vs Control when compared using two-way ANOVA with Tukey posttests in GraphPad Prism V8.01.

8.3 DISCUSSION

The aim of this chapter was to utilise the optimised formulation from chapter 7 in SLA 3D printing to compare and contrast the physicochemical and biological properties of hydrogel vs 3D printed samples. In the hydrogel samples demonstrated in chapter 7, the elution assay displayed enhanced toxicity over the direct contact assay. While completing these experiments, it was thought that this toxicity was due to soluble parts eluting out of the samples. However, after further experimentation involving the 3D prints, it is now believed that this increased toxicity could be due to unreacted photo-initiator which, in the case of the UV cured hydrogels, was Irgacure 2959. This photo-initiator was chosen due to its reported low toxicity (Ghazali *et al.*, 2023) at concentrations below and including 0.1 %wv, however, it is possible that prolonged exposure to unreacted photo-initiator may increase neuronal and glial cell lines susceptibility to other compounds such as PEGDMA (Oral and Basal, 2022). This was determined due to similar results exhibited by 3D printed samples which were later determined to be due to the presence of the unreacted photo-initiator TPO. Once this unreacted compound had been leached out of samples using methanol, no toxicity was observed in the presence of the 3D printed samples.

It was hypothesized that 3D printing would increase the mechanical strength of samples due to the tighter network created by the layer by layer deposition of polymer and laser excitation (Ayrilmis *et al.*, 2019). 3D printed samples were prepared by first preparing a 5 %wv solution of modified HA and stirring overnight to ensure complete dissolution. TPO was chosen as the photo-initiator as it possessed the appropriate excitation and emission wavelengths to be compatible with the Form 2 3D printer. However, TPO is insoluble in aqueous solution, such as the HA solution, and therefore it was dissolved in the minimum amount of methanol to ensure adequate dispersion. This methanolic stock of TPO was then added to PEGDMA such that the final concentration of TPO was 1 %wv. To this, the HA solution was added dropwise while stirring until the desired concentration in each sample was reached. Of the 3D prints produced, PEGDMA had the best transparency (Figure 82), and the hybrid blend of 50 HA-SH, 40 HA-MA, 10 PEGDMA %wv was completely opaque (Figure 85). The hybrid blend had evident pores and a spongy like texture whereas the PEGDMA print appeared glass-like. The 50 %wv PEGDMA blends had issues with delamination, and peeling layers could be observed. This is most likely due to opposing viscosities between HA and PEGDMA (Bao, Paunović and Leroux, 2022). Samples were chemically analysed using FTIR which confirmed the presence of HA in all samples by the

peak at approximately 1640 cm^{-1} . Compression testing of samples revealed a slight increase in compressive strength of PEGDMA samples by approximately 0.1 MPa when compared to UV photo-polymerised hydrogels. Interestingly, the 50 %wv PEGDMA blends exhibited a marked increase in compressive strength, particularly the 50 %wv PEGDMA: HA-MA blend which increased in compressive strength by approximately 0.4 MPa. The 50 %wv PEGDMA: HA-SH blend experienced an increase in compressive strength of 0.1 MPa as shown by Figure 75. This increase was also observed when analysing the rheological behaviour of 3D printed samples, where the 3D printed samples exhibited significantly greater storage moduli in comparison to their hydrogel counterparts. Although the hybrid blend contained only 20 % of the PEGDMA that the 50 %wv PEGDMA blends possessed, they displayed 33.34 % of the storage modulus of the 50 %wv PEGDMA blends. This means that some of the mechanical properties can be obtained from PEGDMA in lower concentrations, whilst modulating the cytocompatibility and viscosity differential issues observed.

Swelling studies, shown in Figure 78, revealed an increase in swelling ratio in the 50 %wv PEGDMA blends when compared to the hydrogel samples but this is thought to be due to the delamination discussed earlier and as demonstrated by Takahashi et al., (2021). Both the PEGDMA and the hybrid blend sample performed similarly to the UV photo-polymerised hydrogel samples, showing that 3D printing had no significant effect on the predictability of swelling behaviour.

Degradation of 3D printed samples provided an interesting insight into HA degradation, as the hybrid sample showed greater resilience to accelerated (5M) degradation than the 50 %wv PEGDMA blends, but significantly greater degradation in *in vitro* physiological (pH 7.4) conditions. This indicates that the degradation of the hybrid blend is dependent on the water binding ability and solubility of HA, which is far greater at pH 7.4 than in pH 2.2 (5 M). The samples shown in Figures 82- 85 depict the hydrogels under all degradation conditions. Across the board, PEGDMA proved the most resilient to degradation. The addition of HA to the matrix increased the rate of degradation in PEGDMA samples, which was in agreement with the results observed in hydrogel samples (Section 7.2.5). Furthermore, the introduction of thiol significantly increased the rate of degradation of PEGDMA samples. The 50 %wv PEGDMA blend samples both experienced peeling, cracking and disintegration under all conditions, whereas the 100 %wv PEGDMA sample only experienced cracking after 7 day incubation in 5M NaOH. The hybrid 3D printed

sample experienced cracking after 7 days in pH 7.4, whereas in accelerated conditions no splitting could be observed. Exposure to NaOH did cause yellowing in some samples due to degradation.

Initial cytotoxicity testing, as shown in Figures 86 and 87, revealed significant toxicity in all samples. However, after removal of TPO from the 3D printed matrix, this toxicity was completely negated (Figures 88 and 89). TPO has been found to be cytotoxic as discussed earlier, and therefore, removal of unreacted TPO from the 3D printed product is an important consideration before commercialisation is possible. This could mean that an alternative to TPO needs to be sought or that TPO could be removed through post-processing.

**CHAPTER 9. NEUROTROPHIC COMPOUNDS FOR
PERIPHERAL NERVE REPAIR**

9.1 PREFACE

The use of polymeric materials alone in a nerve conduit design may not be sufficient to encourage axonal outgrowth and migration. However, the use of nerve growth factors is very costly and difficult to scale up and standardise for industry (Stewart *et al.*, 2020). For this reason, alternative materials with potentially neurotrophic effects were investigated for inclusion. The primary candidates were N-acetyl cysteine, melatonin and tyrosol. N-acetyl cysteine (NAC) was initially selected as a modifying agent for HA as it would serve the purpose of introducing a thiol, while also having potential neurotrophic benefits. However, the degree of modification obtained when utilising NAC was less than ideal (< 10%) and when dissolved in tissue culture media, it drastically dropped the pH, leading to a hostile environment for cells in culture. For these reasons, it was quickly excluded from screening. Melatonin and tyrosol were the resultant lead candidates (more information on these can be found in section 2.6) and were subjected to a battery of tests as outlined in section 3.6.1 to evaluate the extent of proliferative effects, if any, these drugs would impart on neuronal, SH-SY5Y, and glial, RT4 D6P2T, cell lines.

9.2 RESULTS

9.2.1 Initial efficacy screening of potential neurotrophic compounds

An initial literature review revealed two leading drug candidates which were potent antioxidants and had potential for neurotrophic activity (Section 2.6). Melatonin had been previously shown to promote peripheral nerve repair through Parkin-mediated mitophagy (Li *et al.*, 2022) and also have an anti-inflammatory effect on SH-SY5Y cells which had been treated with methamphetamine (Wongprayoon and Govitrapong, 2015). Tyrosol, on the other hand, has not been utilised in this way. However, salidroside, which is a glucoside of tyrosol, has been shown to promote peripheral nerve regeneration following crush injury to the sciatic nerve in rats (Sheng *et al.*, 2013). In the body, biosynthesis pathways convert tyrosol to salidroside (Liu *et al.*, 2022). For this reason, both compounds were screened in neuronal and glial cell lines as outlined in section 3.6.2.

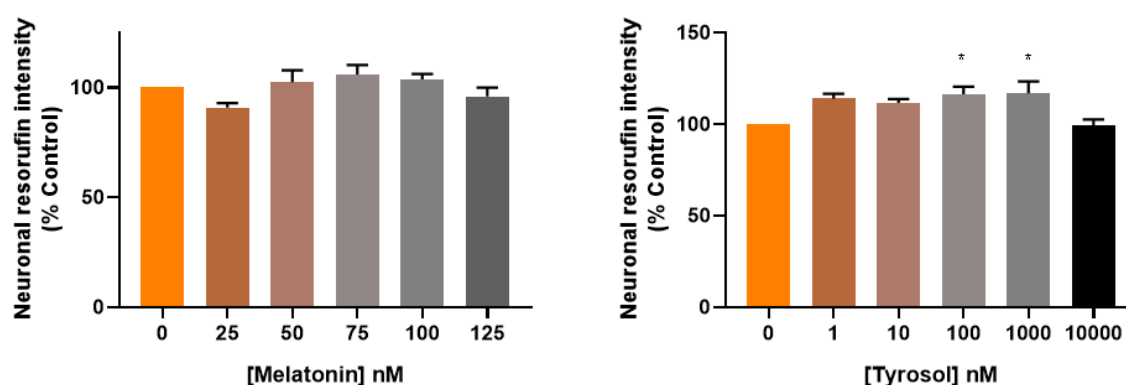


Figure 90. Tyrosol increased the resorufin intensity observed for neuronal cells. Data is presented as % of control (media + cells, no drug), assayed with the resazurin reduction assay. Data is the mean \pm SEM of 6 independent experiments (N=6), performed in triplicate (n=3). * $P < 0.05$ vs control when compared using one-way ANOVA with Tukey posttests in GraphPad Prism V8.01.

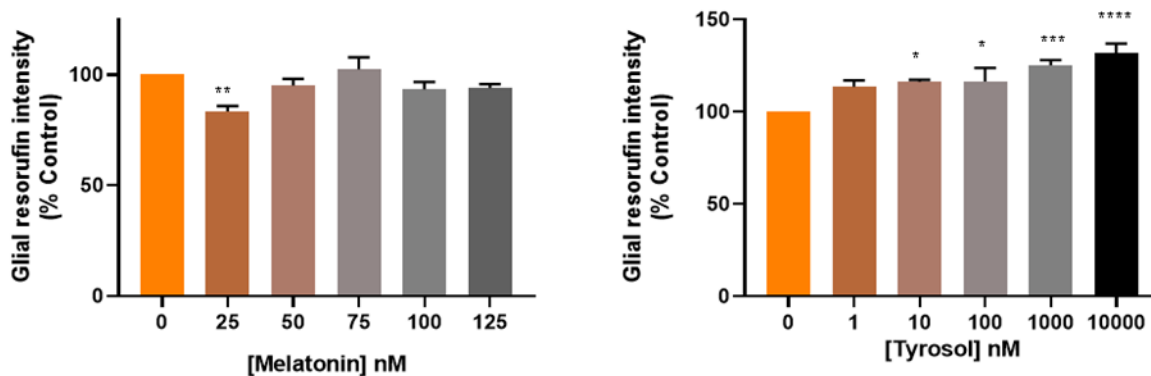


Figure 91. Tyrosol increased the resorufin intensity observed in glial cells in a dose dependent manner. Data is presented as % of control (media + cells, no drug), assayed with the resazurin reduction assay. Data is the mean \pm SEM of 6 independent experiments (N=6), performed in triplicate (n=3). * $P < 0.05$ vs control when compared using one-way ANOVA with Tukey posttests.in GraphPad Prism V8.01.

In neuronal cells, no significant effect was observed in the presence of melatonin when assayed with resazurin. However, in the presence of tyrosol, a significant increase in resorufin intensity was observed at concentrations of 100 nM and 1000 nM. The resorufin intensity of glial cells decreased significantly in the presence of 25 mM Melatonin but then recovered over the rest of the concentration range when assayed with resazurin. Resorufin intensity significantly increased in direct proportionality to tyrosol concentration from 10 nM to 10000 nM in glial cells. Due to the significant increase in the resorufin intensity observed in cells treated with tyrosol, it was vital to further investigate this to see if it was a true increase in cell proliferation or just an increase in metabolic activity as a result of the antioxidant potential of tyrosol.

9.2.2 Proliferative effect of Tyrosol in neuronal and glial cell lines

As resazurin assays showed such promising results for tyrosol in both neuronal and glial cell lines, it was decided to use the BrdU assay to confirm if this was a true increase in proliferation or not. Resazurin relies upon cell metabolism to convert the resazurin dye to resorufin which can then be detected fluorescently. However, BrdU is incorporated into the cell DNA during proliferation as it is a thymidine analogue and provides a reliable and robust method to quantify cell proliferation, independent of metabolism or the effect of mitochondria. The BrdU assay was performed as outlined in section 3.6.2.2 using relevant concentrations of tyrosol- 1000 nM and 10000 nM to investigate cell proliferation. Data was expressed as % control where the control refers to cells without drug treatment, which have been exposed to each step of the BrdU assay. Also included in the assay were negative controls of blanks with and without BrdU reagent.

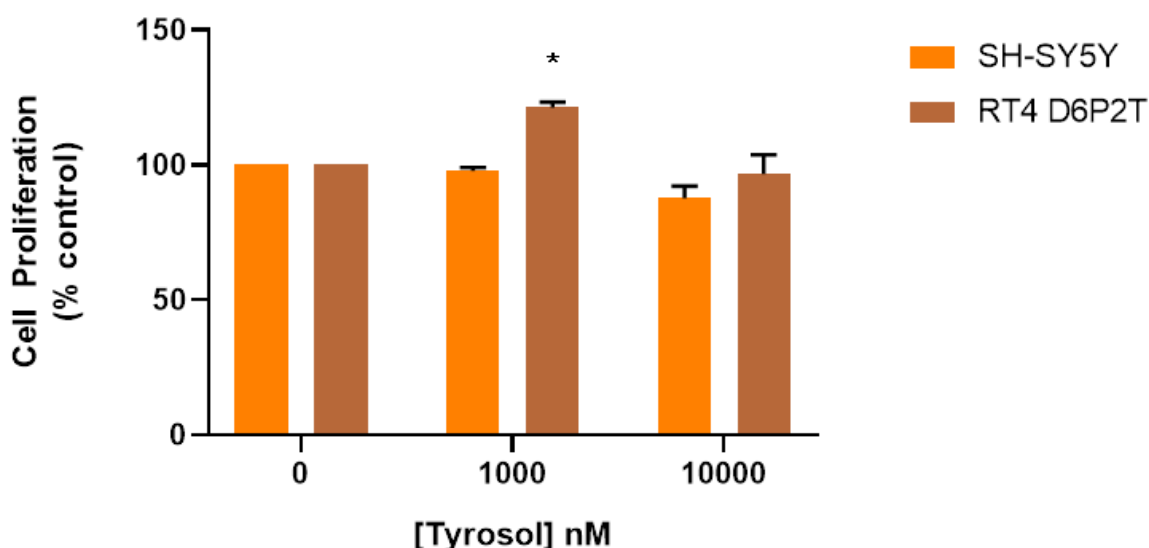


Figure 92. 1000 nm Tyrosol increases glial cell proliferation. Data is presented as % control of the no drug treatment control. * $P < 0.05$ vs control (0 nM Tyrosol) when compared using one-way ANOVA with Tukey posttests. Data is the mean \pm SEM of 3 independent experiments (N=3), performed in triplicate (n=3). Data was analysed using GraphPad Prism V8.01.

No significant effect on proliferation was observed in neuronal cells exposed to tyrosol. A significant increase in cell number was detected in glial cells treated with 1000 nM, but not

10000 nM tyrosol. Although no significance was detected in the neuronal cell line with the BrdU assay, this does not invalidate the earlier result observed with resazurin. The reliance of resazurin on mitochondrial enzymatic activity means that resazurin is more likely to detect subtle changes in cellular respiration and metabolism such as those that occur during mitosis. Therefore, resazurin may detect changes in proliferation more sensitively. Additionally, the BrdU assay involves a number of wash steps during which cells could be lost which can alter the reliability of the assay and shadow subtle increases in cell viability.

9.2.3 Tyrosol drug dissolution: UV Spectroscopy

As tyrosol had shown pro-proliferative results in glial cell lines, hydrogels and 3D prints were produced of PEGDMA, 50 %wv PEGDMA: HA-MA, 50 %wv PEGDMA: HA-SH and the hybrid blend to evaluate two questions: 1. The effect of tyrosol in conjunction with the polymer constructs and 2. If material choice would impact the dissolution or efficacy of the drugs. Tyrosol standards were prepared from an initial stock concentration of 1 mM in PBS and diluted until they fit within the linear range (approximately 0- 1.2A) when reading samples at 280 nm. An absorbance of 280 nm was used for tyrosol due to the phenolic nature of this compound. These samples were then read and recorded on a UV spectrophotometer in photometric mode as shown in Figure 93. The equation of the line was $Y= 303.6x +0.01459$ and an R^2 value of 0.9977 was obtained. This standard curve was then used to determine the concentration of drug detected at each sampling interval.

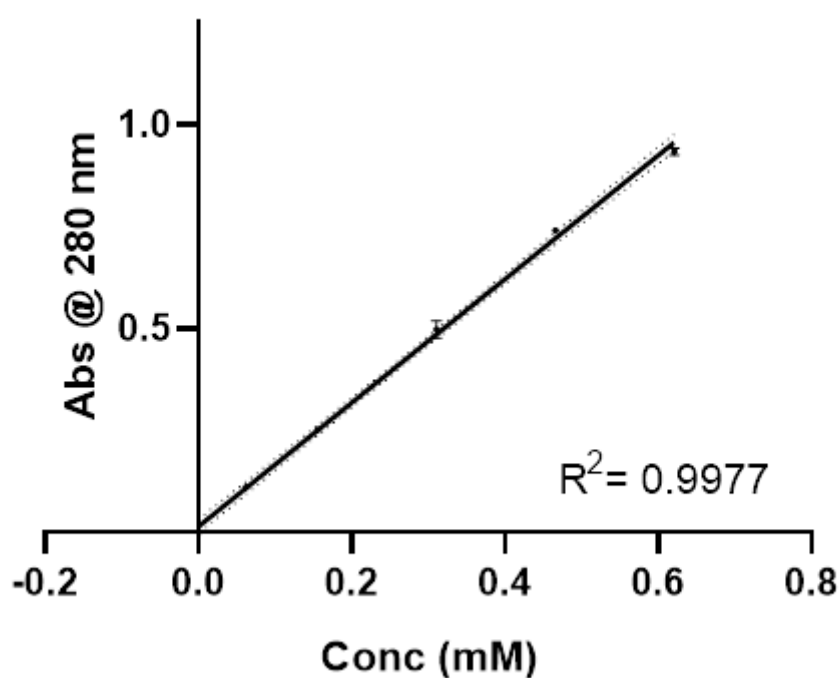


Figure 93. Standard curve of tyrosol standards in PBS. Standard curve of Tyrosol Abs @ 280 nm vs Tyrosol conc (mM). Data is the mean \pm SEM of 2 independent experiments (N=2), conducted in triplicate (n=3). Data was analysed using GraphPad Prism V8.01.

9.2.3.1 Tyrosol drug loaded samples

Tyrosol loaded hydrogels were prepared as outlined in section 3.7.1 and tyrosol loaded prints were prepared as outlined in section 3.7.2. The drug loaded samples were then placed in PBS and samples were taken at regular intervals with complete solution changes at each interval. Cumulative drug release over 24 hours was then plotted and compared across samples to determine their release profile.

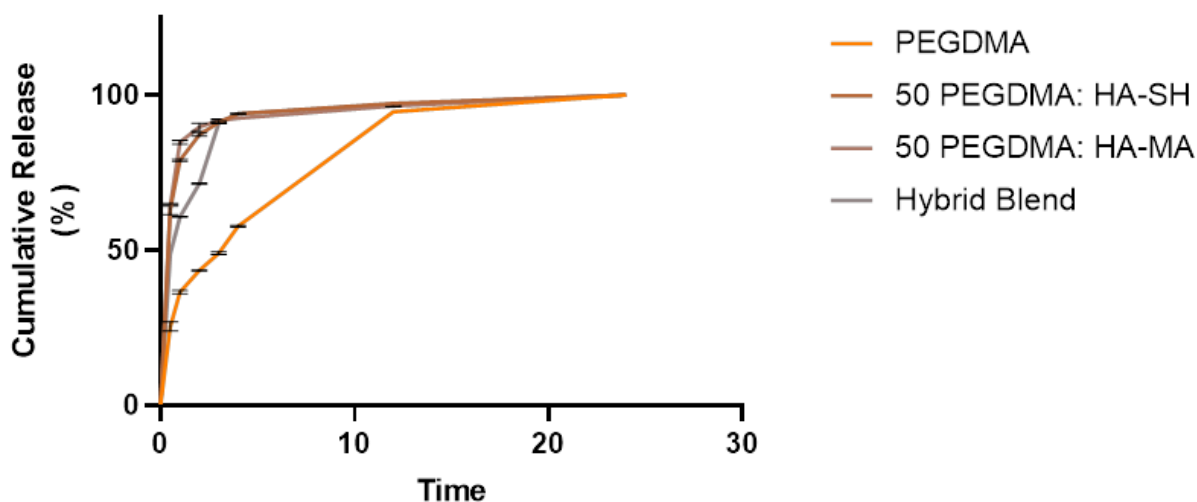


Figure 94. Cumulative tyrosol drug release from hydrogel samples. Graph illustrating drug release from hydrogels of PEGDMA, 50 PEGDMA: HA-SH, 50 PEGDMA: HA-MA and the hybrid blend. $P > 0.05$, no significance, vs control (Control of 0 h time-point of each condition) when compared using one-way ANOVA with Tukey posttests. Data is the mean \pm SEM of 2 independent experiments (N=2), performed in triplicate (n=3). Data was analysed in GraphPad Prism V8.01.

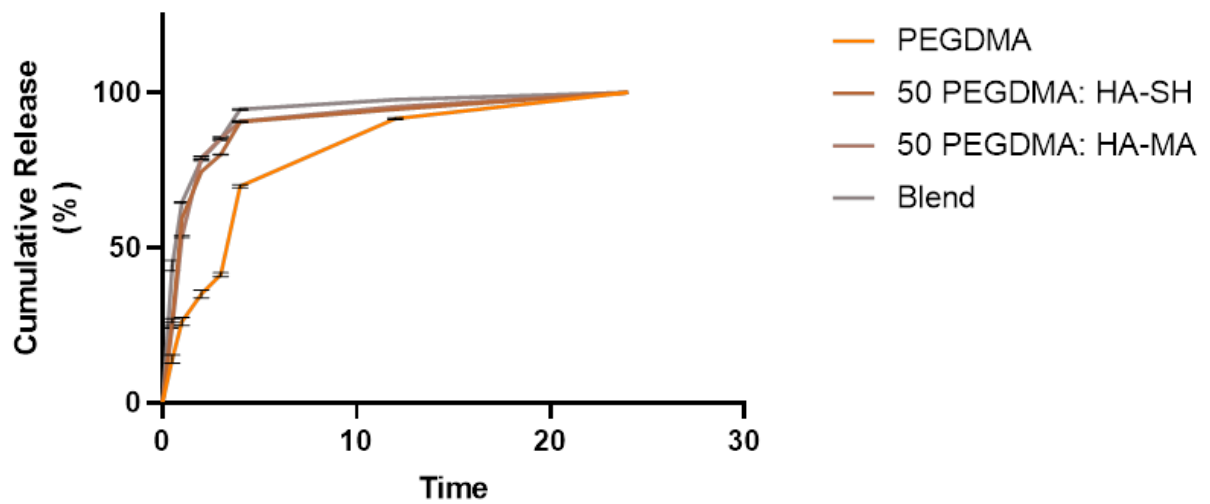


Figure 95. Cumulative tyrosol drug release from 3D printed samples. Graph illustrating drug release from 3D prints of PEGDMA, 50 PEGDMA: HA-SH, 50 PEGDMA: HA-MA and the hybrid blend. $P > 0.05$, no significance, vs control (Control of 0 h time-point of each condition) when compared using one-way ANOVA with Tukey posttests. Data is the mean \pm SEM of 2 independent experiments (N=2), performed in triplicate (n=3). Data was analysed in GraphPad Prism V8.01.

9.2.4 Tyrosol Drug Dissolution: RP-HPLC

In order to support the results obtained from UV spectroscopy, reverse-phase HPLC was utilised. In this approach, a concentration that was 100x greater than previously used, 100 mM, was loaded into samples in an attempt to evaluate the maximum drug loading capacity of these systems. As tyrosol is a potent anti-oxidant, it was important to evaluate whether loading higher dosages would affect the ability to form the interconnected polymer matrix. The initial concentration found to be effective in glial cells was 1000 nM or 1 μ M. Therefore, a standard curve was prepared from 0 to 100 mM as shown in Figure 96 and values were interpolated from this. The R^2 value obtained after fitting the best fit line was 0.9999 and the equation of the line was $Y = 86816x + 20048$. The interpolated values were then plot as shown in Figure 97.

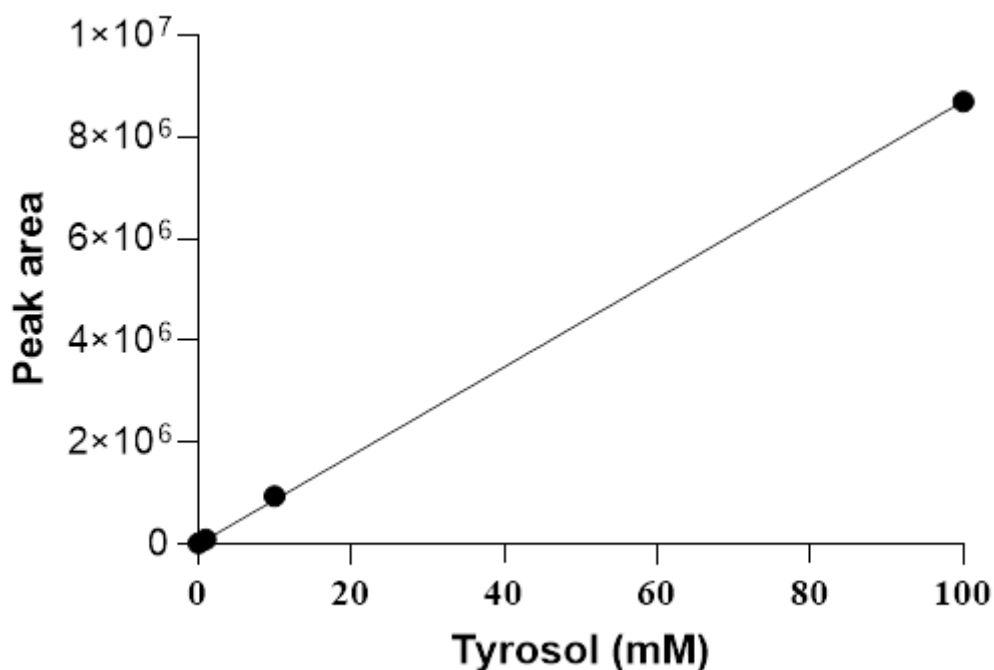


Figure 96. Standard curve of tyrosol standards for RP-HPLC. Data is the mean \pm SD of 1 experiment (N=1), conducted in triplicate (n=3). Data was analysed using GraphPad Prism V8.01.

9.2.4.1 Detection of tyrosol from 3D prints and hydrogels: RP-HPLC

Tyrosol loaded hydrogels and 3D prints were prepared as outlined in section 3.7.1 and 3.7.2. These samples were placed in PBS and aliquots were retrieved at specific time points over a 24 h period. The concentration of tyrosol was determined via RP-HPLC and the tyrosol standard curve shown in Figure 96.

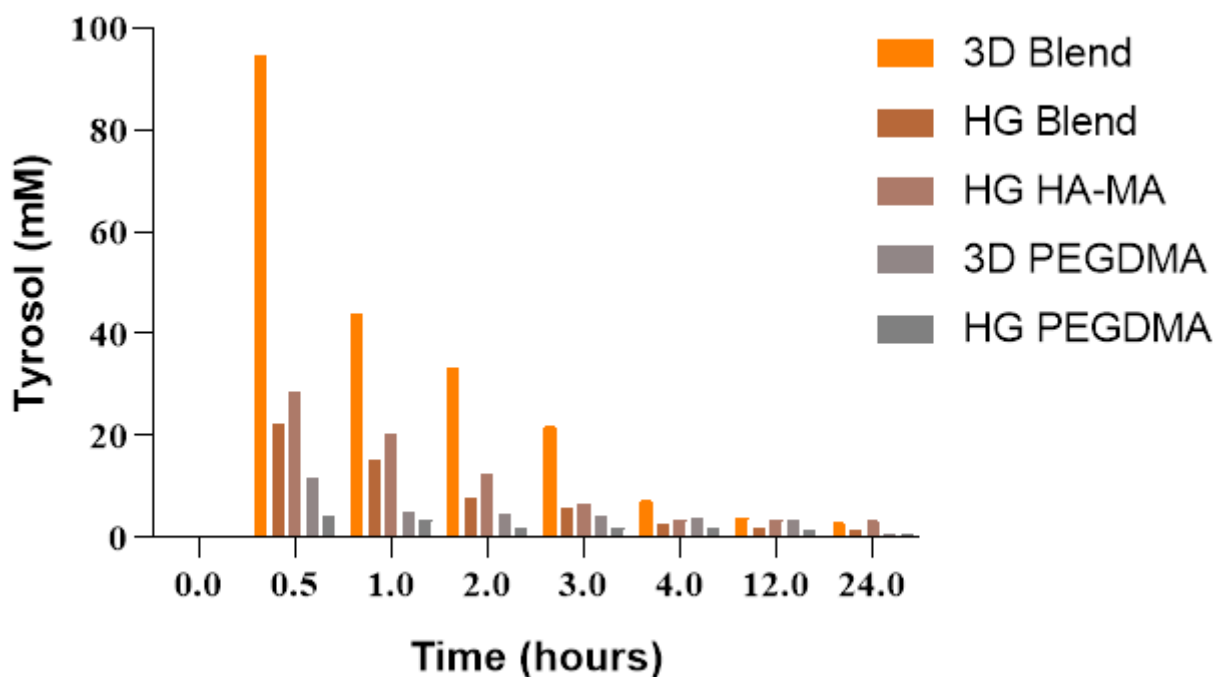


Figure 97. Interpolated values for the concentration of tyrosol in hydrogel (HG) and 3D printed (3D) samples. Data is the mean \pm SD of 1 experiment (N=1), conducted in triplicate (n=3). Data was analysed using GraphPad Prism V8.01.

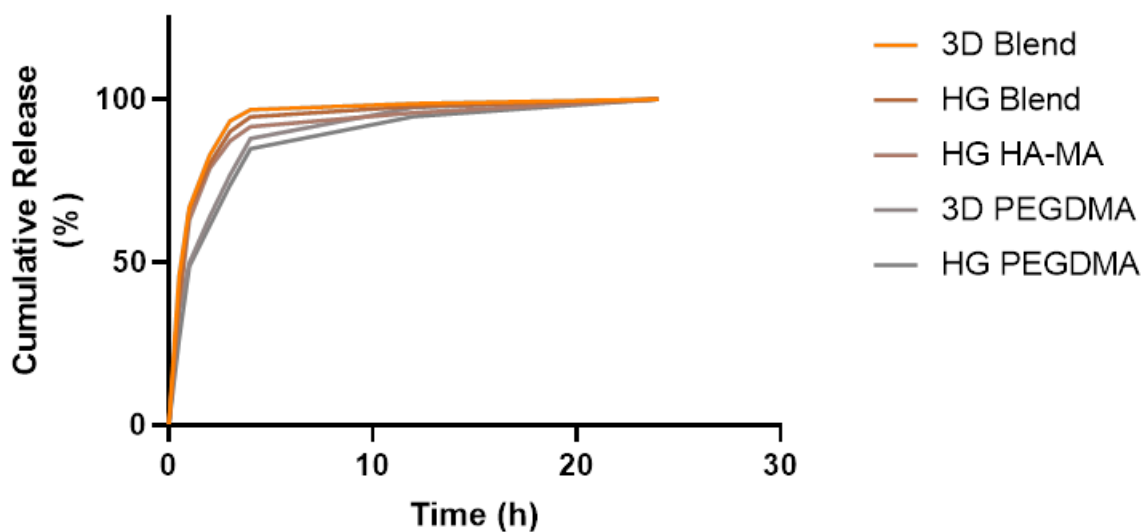


Figure 98. Cumulative release profile for tyrosol from different polymer constructs as determined by RP-HPLC. Cumulative release expressed as % of total tyrosol released. $P > 0.05$, no significance, when comparing different release profiles using two-way ANOVA with Tukey posttests. Data is the mean \pm SD of 1 experiment, conducted in triplicate. Data was analysed using GraphPad Prism V8.01.

9.2.5 Tyrosol elution from 3D printed formulations

Since it was successfully shown through UV spectroscopy and RP-HPLC that tyrosol is released from the polymer formulations in both hydrogel and 3D printed form, it was vital to see the combined effect of 3D printed formulation with tyrosol in the presence of neuronal and glial cells to determine if eluted tyrosol would show the same efficacy seen previously in section 9.2.2 where tyrosol showed a proliferative effect on glial cell lines through the BrdU assay. A tyrosol loading of 1000 times per 3D print was utilised, as any effective drug delivery device should be capable of delivering a drug quantity significantly in excess of the clinically relevant concentration. An initial loading of concentration of 1 mM was utilised for 3D printed samples. 3D prints were placed in sterile 6 well plates with complete cell culture media for 24h at 37 °C and 5% CO₂, the media was then removed from each well and used as treatment media for the cells. Results were presented vs control in order to identify if any significant increases or decreases in resorufin intensity were observed.

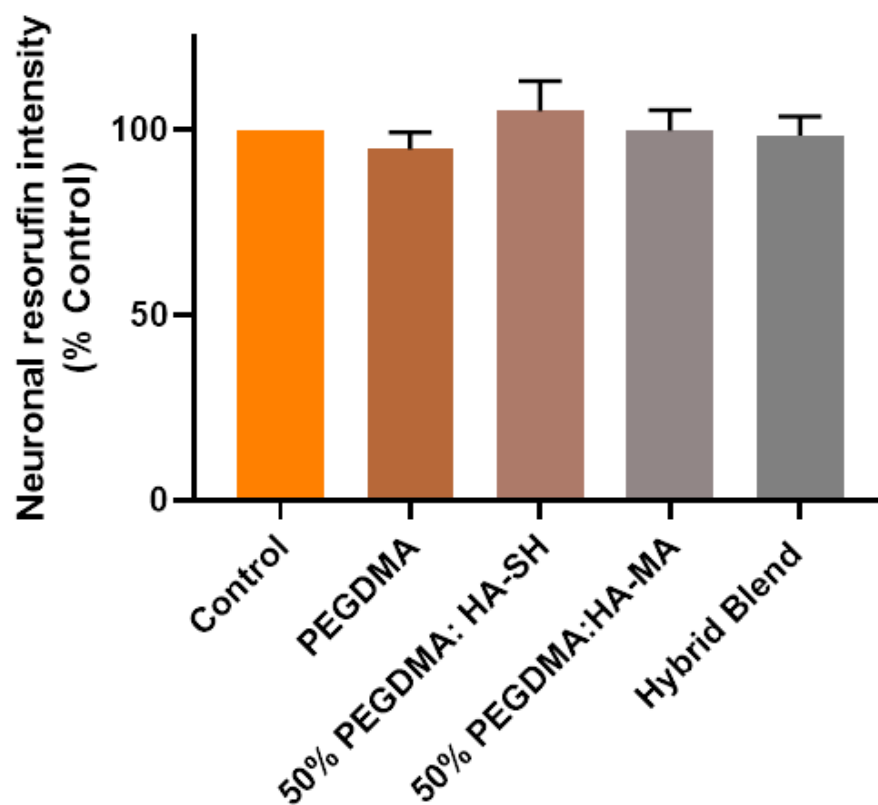


Figure 99. Elution assay of tyrosol loaded (1 mM) 3D prints in neuronal cells. Data is the mean \pm SEM of 3 independent experiments (N=3), conducted in triplicate (n=3). Data is expressed as % of cell only control (no 3D printed sample). $P > 0.05$, no significance, when analysed using one-way ANOVA with Tukey posttests. Data was analysed using GraphPad Prism V8.01.

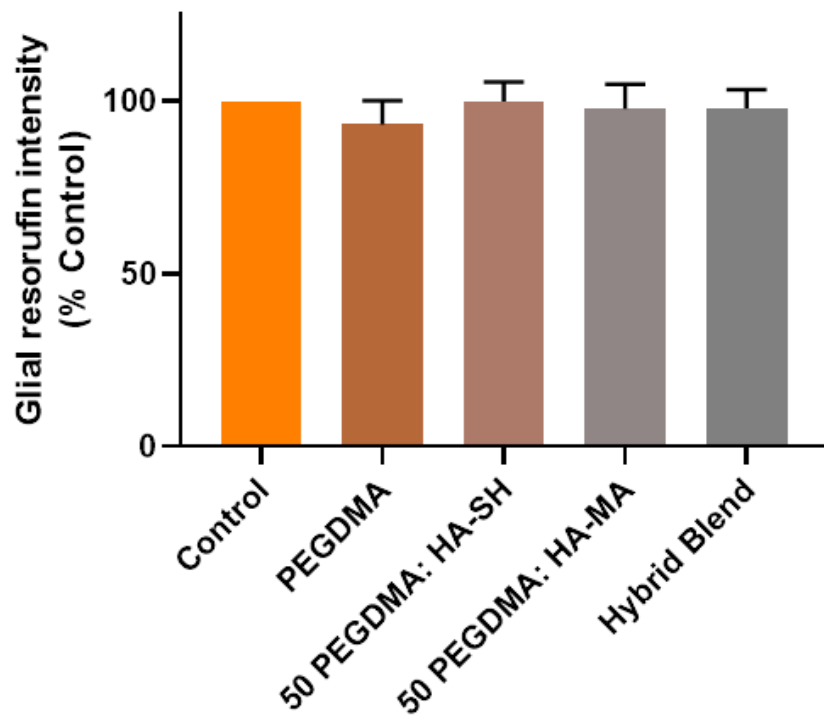


Figure 100. Elution assay of tyrosol loaded (1 mM) 3D prints in glial cells. Data is the mean \pm SEM of 3 independent experiments (N=3), conducted in triplicate (n=3). Data is expressed as % of cell only control (no 3D printed sample). $P > 0.05$, no significance, when analysed using one-way ANOVA with Tukey posttests. Data was analysed using GraphPad Prism V8.01.

9.3 DISCUSSION

Resazurin had revealed increased resorufin intensity results in both cell lines as shown in Figures 90 and 91, which were indicative of pro-proliferative effects. However, as tyrosol has been shown to be a potent antioxidant (Casadey *et al.*, 2021), it was important to confirm whether this result was due to a true increase in cell proliferation and not due to increased metabolism or mitochondrial activity. This is due to the resazurin assay relying upon mitochondrial enzymatic activity to convert the non-fluorescent resazurin to the fluorescent resorufin. Therefore, the brdU assay was chosen due to its selectivity and robustness in detecting proliferation. During cell proliferation, the thymidine analogue brdU gets incorporated into cell DNA where it can then be detected by an antibody probe which can bind to the labelled DNA after denaturation. The amount of brdU detected is directly proportional to the number of proliferating cells (Gratzner, 1982).

Utilising this assay, 1000 nM tyrosol was found to increase proliferative in glial cells. No significant effect was observed in neuronal cells, despite the fact that tyrosol also increased resorufin intensity in neuronal cells in the resazurin assay. This lack of significance does not negate this result however, as there is justification to believe that resazurin would be more sensitive in detecting subtle changes in the proliferation of cells (Bose, Rajeshkumar and Jatin, 2022).

Following this result, it was decided to trial UV photo-polymerisation of tyrosol containing hydrogels. As photo-polymerisation relies upon the generation of free radicals, there was concern that the inclusion of an antioxidant such as Tyrosol would inhibit gelation. A 1000X concentration (1 mM tyrosol) was included into the hydrogel formulation to evaluate the effect of tyrosol on gelation and to assess the drug dissolution from the hydrogels. UV-vis spectroscopy was used for this purpose initially where it was revealed that approximately 90% of the drug was released within the first 12 hours of dissolution in pH 7.4. The hybrid blend showed the fastest release profile, having released approximately 97 % of the drug within 12 hours from both hydrogel and 3D printed formulation, however, this was not significant when compared to the other formulations. 100 % wv PEGDMA in both hydrogel and 3D print format appeared to provide a more sustained release of tyrosol, however, this too was insignificant.

In order to confirm the results of the UV-vis spectrophotometer, RP-HPLC was selected as it has greater sensitivity and selectivity than UV-Vis spectroscopy. HPLC confirmed the

results observed in UV-Vis spectroscopy, revealing that approximately 97 % of the drug was released within the first 12 hours from the hybrid blend, and approximately 94 % and 95 % of tyrosol released in the first 12 hours from PEGDMA and HA-MA respectively. The total drug released from the samples exceeded the concentration initially loaded into each sample (100 mM), however this is expected as samples were not washed between collections, with only solutions being changed between time points. Therefore, residual tyrosol would be present at each time point. Despite this, this method still proved to be a robust and reliable method for comparison between conditions and it highlighted the enhanced drug retention of the 3D blend vs the hydrogel blend and all other samples.

Despite the pro-proliferative results observed in Figure 86, this result could not be replicated when exposing cells to 3D print eluted tyrosol. These prints were printed with a 1 mM concentration of tyrosol, however, the final concentration of tyrosol in the media was not quantified so the actual concentration the cells were exposed to is unknown. From the release profiles obtained via UV-Vis spectroscopy and HPLC, it would be fair to assume that within 24 hours, 100% release should have occurred but these results are not directly indicative of the final NGC within the body. Cell culture media, although a great medium for the culturing and growth of cells, is not directly comparable to *in vivo* conditions and the exact constituents and concentration of those constituents is not known. Therefore, the release of drug from the polymer samples into the media may not be the most reliable representation of the conduit and drug delivery via the conduit.

However, these results have effectively shown that the final formulation could be used to deliver tyrosol through the NGC formulation with complete release occurring within 24 hours. As initial results showed the proliferative potential of tyrosol, future work should involve the quantification of tyrosol eluted in cell culture media, optimisation of concentration to ensure the effective concentration is eluted within the given timeframe, and finally *in vivo* testing of the final NGC formula with tyrosol to evaluate tissue response to the NGC and tyrosol elution.

**CHAPTER 10. CONCLUSIONS AND FUTURE
CONSIDERATIONS**

Patient outcomes should be at the centre of focus for clinicians when devising a treatment strategy, however, in the majority of cases the best treatment may not be the most readily available treatment. Additionally, in the case of PNI, the injury has usually occurred sometime before treatment is sought. In cases where treatment is immediately sought, autografts have been found to have decent clinical outcomes (Matejčík, 2002), despite ongoing issues with immunosuppression and chronic pain in times of less immediate care. A better and more personalised treatment option is required to improve patient outcomes and attempt to restore full functionality of the affected body part.

Interest in HA has boomed over the last decade with uses in cosmetics, supplements and numerous bioengineering applications. Most of this interest stems from the unique ability of HA to bind 1000 times its weight in water (Tian *et al.*, 2021), which imparts great healing abilities from keeping a hydrated lattice structure around wounds. This, in addition to the anti-adhesive nature of HA, has been shown to prevent the occurrence of glial scarring and neuroma formation in peripheral nerve regeneration (Agenor *et al.*, 2017).

In this study, low to moderate MW (30-50 kDa HA) was characterised in two cell lines, a neuronal cell line, SH-SY5Y and a glial cell line, RT4 D6P2T. Due to the unique nature of HA, traditional assays required modification to ensure that they were robust and reliable enough to cater for a viscous polymer. For instance, it was determined that a synergistic toxic effect was occurring between MTT and HA, particularly in SH-SY5Y, and therefore the assay was adapted to include cell counts at each wash step of the normal assay procedure. This result was then validated through the use of the trypan blue assay and the modified resazurin assay which was modified to include the same mechanical forces as an MTT assay.

Additionally, a coating procedure was utilised to ensure equal direct contact of the cells with the HA substrate. This procedure was validated using Alcian Blue, a stain typically used for the staining of mucosa. Once baseline cell responses had been determined for HA of different MW, it was decided to proceed with 30-50 kDa HA as this gave distinct advantages such its workability in manufacturing and lack of decreased resorufin intensity responses. This response is collaborated in research by Kim *et al.*, 2018, who stated better cell adhesion was observed by inclusion of low MW HA when compared to high MW HA. Although cell adhesion to the conduit would not be a vital factor in clinical settings, it was necessary to ensure contact of the cells with the HA coating to facilitate the testing of the entire system, HA and drug, in isolation and synergy.

30-50 kDa HA was modified using gentle procedures with thiol and methacrylate. In both cases, modification was calculated to be approximately $20 \pm 9\%$. The modification procedure for thiolation of HA was developed based on the work by Jin *et al.*, 2018, who modified HA with N-acetyl cysteine for the delivery of the cancer drug, Paclitaxel. However, when this method was repeated, a low degree of modification was obtained. Therefore, an optimised methodology utilising cysteamine was introduced which proved to be more effective for this project. The modified HA was characterised extensively using methods such as FTIR, NMR, HPLC, and colorimetric assays such as the Ellmans assay. The effect of modification on the cytocompatibility of HA was then evaluated in both cell lines using resazurin and neutral red. It was vital to use two different assays to ensure robustness as resazurin relies upon the metabolic activity of cells, whereas neutral red relies upon uptake and membrane integrity of cells. In the case of glial cells, HA-SH was found to increase both resorufin intensity and neutral red uptake at a concentration of 0.01 %wv HA-SH. Conversely, HA-MA was found to decrease resorufin intensity and neutral red uptake at concentrations greater than 0.5 %wv in neuronal cells, and at 1 %wv in glial cells. Following cytocompatibility testing, the effect of modification on hyaluronidase degradation was evaluated. As Figure 47 shows, thiolation of HA increases the rate of degradation by hyaluronidase, whereas methacrylation significantly increased the resistance of HA to hyaluronidase degradation. This result indicates that it is possible to tailor degradation *in vivo* through alteration of modification degree and monomer ratio. This finding is in agreement with Tsanaktsidou, Kammona and Kiparissides, (2019), who found that increasing the degree of modification of methacrylate, increased the resistance to degradation of HA. In a wider context, by altering the rate of degradation factors such as drug release, residence time and applicability can all be expanded.

Hydrogels were developed using various formulations of modified HA. These samples were then extensively characterised to find a polymer profile suitable for 3D printing. Once leading formulations were selected, UV photo-polymerised samples of this reduced sample range were produced and characterised to establish their chemical, mechanical and biological characters. These HA hydrogels were found to have especially poor mechanical properties in terms of compressive strength, and therefore it was decided to introduce a synthetic polymer with improved mechanical performance, PEGDMA. However, as can be seen in Figures 72 and 73, cells grown directly on 50 %wv PEGDMA blend samples exhibited significant toxicity. There is conflicting evidence in the literature for PEGDMA

cytotoxicity with some authors reporting PEGDMA as non-cytotoxic (Chang, Ching and Hashimoto, 2022), whereas others discuss the leaching of cytotoxic components from PEGDMA constructs (Johannsmeier *et al.*, 2020). Largely, the evidence would indicate that the effect of PEGDMA on cytocompatibility is dependent on cell type and sample preparation. Therefore, the formulation needed to be optimised prior to 3D printing to modulate this toxicity.

An optimised formula was selected for 3D printing which consisted of 10% PEGDMA, 40 % HA-MA and 50 % HA-SH. This blend was selected as it was postulated to be sufficient to increase the mechanical strength of the samples, control the degradation of the potential NGC formulation *in vivo* while also modulating the toxicity observed in the presence of PEGDMA and HA-MA samples. In order to test this theory, 3D printed samples were prepared of 100 % PEGDMA, 50 % PEGDMA: HA-MA, 50 % PEGDMA: HA-SH and the hybrid blend. All samples were characterised both physicochemically and biologically and their responses were compared.

The 50 %wv PEGDMA blend samples were found to crack and delaminate, potentially due to opposing forces within the sample arising from differing viscosities. This caused an unusual increase in swelling behaviour and accelerated degradation in all conditions. Although the blend had significantly lower rheological properties than 100 %wv PEGDMA, the inclusion of 10 %wv PEGDMA to the polymer matrix resulted in a significant increase in storage modulus. In terms of degradation, in most cases the hybrid blend outperformed the 50 % wv PEGDMA blends due to the delamination issues they were experiencing as discussed earlier. This enhanced performance is likely due to the greater level of cross-linking within the hybrid sample due to reduced steric hindrance.

The hybrid blend formulation was selected as the matrix for drug delivery and three drug candidates were screened for inclusion- NAC, melatonin and tyrosol. NAC was quickly disregarded due to the effect on pH at even low concentrations. Tyrosol was found to significantly increase resorufin intensity in both cell lines when assayed using resazurin. BrdU was employed to confirm this result and the increase in proliferation observed in glial cells was reliably confirmed when exposed to 1000 nM tyrosol. Tyrosol drug loadings of 1000X the effective concentration were tested in both hydrogel and 3D printed format using UV spectroscopy. In all cases, approximately 97% of the drug was released within the first 12 hours of dissolution in pH 7.4. This shows that all formulations release tyrosol effectively,

however this would most likely need to be modulated or the dose optimised as typically, day 2 of peripheral nerve regeneration in the body would require the highest dose of neurotrophic compounds to accelerate axonal sprouting (Bareyre *et al.*, 2011). When cells were exposed to eluted tyrosol from both hydrogels and 3D prints, no significant increases or decreases in cell viability were observed. However, the concentration of tyrosol eluted into the cell culture media was not quantified, and therefore it is possible that the effective concentration of 1000 nM was not what was used as a treatment for the neuronal and glial cell line. Despite this result, there are still benefits to the inclusion of tyrosol in the HA NGC due to its powerful free radical scavenging ability. Figures 86 and 87 show the cytotoxicity exhibited by residual unreacted TPO, which highlights the necessity of a free radical scavenger when utilising photoinitiators for medical devices.

The initial aim of this project was to investigate the utility of low MW HA for peripheral nerve regeneration. The reason for this was because much of the research has focused on high MW HA for its anti-inflammatory potential. However, recent research has shown that low MW molecules increase cell motility (Abatangelo *et al.*, 2020) and even improve regeneration in bone when compared to high MW HA (Kuo *et al.*, 2021). This aim has been achieved through the completion of multiple objectives such as investigating the effect of low MW HA in neuronal and glial cell lines, and examining the impact of modification on HA. Following initial characterisation, HA was UV photo-crosslinked and later, 3D printed in various formulations. Once a lead formulation was selected, neurotrophic compounds were investigated for inclusion. Tyrosol was selected as it increased glial cell proliferation which is vital factor in peripheral nerve regeneration as Schwann cells have been found to promote peripheral nerve regeneration from axonal sprouting to guidance of the migrating axon (Min, Parkinson and Dun, 2021). Ultimately, this research has provided proof of concept for a 3D printed conduit which could be developed based on patient need, providing a personalised therapeutic approach. However, further work would be required before clinical application could take place.

Throughout this project, the focus has been on producing a formulation which could eventually be optimised into a NGC for nerve repair. This was done by ensuring robust and reproducible methods were developed and optimised for the benchtop testing of materials in isolation and synergistically for physical and biological responses. However, there were some caveats to how this research was conducted. Ideally, primary cells such as dorsal root ganglion (DRG) would have been used to provide a more true response to the materials and

drugs tested. In using immortalised secondary cell lines from different species, it can be difficult to translate the responses to those from human primary nerve cells. Additionally, due to time and resource constraints, the polymer formulations were only tested in cylindrical disk format to provide comparable testing formats between hydrogels and 3D prints. The final blend formulation from this thesis would not have had the mechanical strength to withstand printing of a tube structure for a NGC, however with further formula optimisation the mechanical properties could have been further improved to facilitate this.

There is a huge body of research which has been produced in the last 5 years regarding new NGC technologies for peripheral nerve repair, however, many have failed to realise their clinical potential. The primary reason for this is that many of these NGCs are developed in academic research laboratories, using elaborate technologies which are difficult to scale up and translate to an industrial setting.

With regard to scale up, if a new technology requires significant investment in equipment and training, it is less likely to be successful. Additionally, there are significant challenges with regard to throughput, quality control, purification, product delivery and stability. The process described in this thesis involves low MW HA which can be mass produced via recombinant bacterial culture and can be modified in mild conditions, utilising water as a solvent. The primary advantage of this, is that it does not require any specialised equipment, facilities or skillset. Purification via dialysis and lyophilisation are processes commonly used in industrial settings and have the potential for automation which is a vital criterion in the current climate (Schuett *et al.*, 2020). Additionally, there are numerous 3D printed medical devices already in production such as SLA printed dental and orthopaedic implants. SLA allows for high resolution and fine details which make it optimal for these applications (Mamo, Adamiak and Kunwar, 2023).

Another key consideration in taking this technology to clinic would be end product sterilisation prior to packaging. Typically, ethylene oxide or gamma radiation are used for this purpose, however, these methods can have negative effects on a range of materials such as property modification which would be costly to rectify later. Therefore, the effect of terminal sterilisation techniques on the final conduit would need to be fully investigated to ensure no deleterious effects arise as a result of sterilisation (Pohan *et al.*, 2020). Long term storage is another key concern which would be addressed by storage of the NGC in the

lyophilised state for stability. The conduit would likely then need to be pre-swollen in plasma prior to implantation.

Perhaps most significantly, is the regulatory framework which surrounds implantable devices. In the US, past NGCs have been approved based on two main pathways: the 510(k) process which allows for approval of devices which very closely resemble and build on pre-existing devices, or the de-novo pathway which is sought via pre-market approval (Pohan *et al.*, 2020). A major benefit of the technology developed in this project, is its growth factor free nature. This project has proven the efficacy of the compound tyrosol to enhance glial cell proliferation in RT4 D6P2T cells. Although not a direct replacement for growth factors such as BDNF, the neurotrophic effects exhibited by tyrosol could enhance regeneration of peripheral nerves *in vivo* whilst also ensuring a low cost process, and a simpler regulatory application process.

Future directions for this research include further optimising the mechanical properties of the formulation to achieve a recommended compressive strength of approximately 0.8 MPa, and to facilitate the 3D printing of the NGC tube structure. This could be done through further optimisation of formulation or by utilising engineering techniques such as over-moulding. Drug delivery and cell responses to the NGC could then be tested both *in vitro* and *in vivo* through collaboration. Sustained drug release could be increased through the utilisation of micelle or microsphere technology within the hydrogel, so these will all be investigated. Finally, terminal sterilisation methods will be investigated to ensure clinical readiness of this technology such that regulatory approval could be sought to proceed with clinical trials. Additionally, other applications for the HA formulation will be investigated such as expanding foams which would maximise on the swelling potential of HA.

CHAPTER 11. REFERENCES

1. Abatangelo, G. *et al.* (2020) ‘Hyaluronic Acid: Redefining Its Role’, *Cells*, 9(7), p. 1743. Available at: <https://doi.org/10.3390/cells9071743>.
2. Abrahão, N.M. *et al.* (2021) ‘Bilateral facial paralysis secondary to temporal bone trauma: A case report and literature review’, *Clinical Case Reports*, 9(6), p. e04272. Available at: <https://doi.org/10.1002/ccr3.4272>.
3. Abrego, C.J.G. *et al.* (2022) ‘Multiscale Characterization of the Mechanical Properties of Fibrin and Polyethylene Glycol (PEG) Hydrogels for Tissue Engineering Applications’, *Macromolecular Chemistry and Physics*, 223(1), p. 2100366. Available at: <https://doi.org/10.1002/macp.202100366>.
4. Abu-Niaaj, L.F., Harris, G. and Pixley, S. (2020) ‘The Role of Magnesium Biodegradable Material in Peripheral Nerve Repair’, *The FASEB Journal*, 34(S1), pp. 1–1. Available at: <https://doi.org/10.1096/fasebj.2020.34.s1.06824>.
5. Agenor, A. *et al.* (2017) ‘Hyaluronic acid/carboxymethyl cellulose directly applied to transected nerve decreases axonal outgrowth’, *Journal of Biomedical Materials Research. Part B, Applied Biomaterials*, 105(3), pp. 568–574. Available at: <https://doi.org/10.1002/jbm.b.33576>.
6. Althagafi, A. and Nadi, M. (2023) ‘Acute Nerve Injury’, in *StatPearls*. Treasure Island (FL): StatPearls Publishing. Available at: <http://www.ncbi.nlm.nih.gov/books/NBK549848/> (Accessed: 23 May 2023).
7. Amar, S.K., Donohue, K.B. and Gust, K.A. (2023) ‘Cellular and molecular responses to ethyl-parathion in undifferentiated SH-SY5Y cells provide neurotoxicity pathway indicators for organophosphorus impacts’, *Toxicological Sciences*, 191(2), pp. 285–295. Available at: <https://doi.org/10.1093/toxsci/kfac125>.
8. Andrade del Olmo, J. *et al.* (2021) ‘Biocompatible hyaluronic acid-divinyl sulfone injectable hydrogels for sustained drug release with enhanced antibacterial properties against *Staphylococcus aureus*’, *Materials Science and Engineering: C*, 125, p. 112102. Available at: <https://doi.org/10.1016/j.msec.2021.112102>.
9. Andrade del Olmo, J. *et al.* (2022) ‘Self-healing, antibacterial and anti-inflammatory chitosan-PEG hydrogels for ulcerated skin wound healing and drug delivery’, *Biomaterials Advances*, 139, p. 212992. Available at: <https://doi.org/10.1016/j.bioadv.2022.212992>.
10. Arslantunali, D. *et al.* (2014) ‘Peripheral nerve conduits: technology update’, *Medical Devices: Evidence and Research*, 7, pp. 405–424. Available at: <https://doi.org/10.2147/MDER.S59124>.

11. Asuzu, P.C. *et al.* (2022) 'Cell Culture-Based Assessment of Toxicity and Therapeutics of Phytochemical Antioxidants', *Molecules*, 27(3), p. 1087. Available at: <https://doi.org/10.3390/molecules27031087>.
12. Ates, G. *et al.* (2017) 'Assaying Cellular Viability Using the Neutral Red Uptake Assay', *Methods in Molecular Biology (Clifton, N.J.)*, 1601, pp. 19–26. Available at: https://doi.org/10.1007/978-1-4939-6960-9_2.
13. Ayırmis, N. *et al.* (2019) 'Effect of printing layer thickness on water absorption and mechanical properties of 3D-printed wood/PLA composite materials', *The International Journal of Advanced Manufacturing Technology*, 102(5), pp. 2195–2200. Available at: <https://doi.org/10.1007/s00170-019-03299-9>.
14. Baazaoui, N. and Iqbal, K. (2022) 'Alzheimer's Disease: Challenges and a Therapeutic Opportunity to Treat It with a Neurotrophic Compound', *Biomolecules*, 12(10), p. 1409. Available at: <https://doi.org/10.3390/biom12101409>.
15. Balazs, E.A. *et al.* (1967) 'Hyaluronic acid in synovial fluid. I. Molecular parameters of hyaluronic acid in normal and arthritic human fluids', *Arthritis & Rheumatism*, 10(4), pp. 357–376. Available at: <https://doi.org/10.1002/art.1780100407>.
16. Balazs, E.A., Laurent, T.C. and Jeanloz, R.W. (1986) 'Nomenclature of hyaluronic acid', *Biochemical Journal*, 235(3), p. 903. Available at: <https://doi.org/10.1042/bj2350903>.
17. Bao, Y., Paunović, N. and Leroux, J.-C. (2022) 'Challenges and Opportunities in 3D Printing of Biodegradable Medical Devices by Emerging Photopolymerization Techniques', *Advanced Functional Materials*, 32(15), p. 2109864. Available at: <https://doi.org/10.1002/adfm.202109864>.
18. Bareyre, F.M. *et al.* (2011) 'In vivo imaging reveals a phase-specific role of STAT3 during central and peripheral nervous system axon regeneration', *Proceedings of the National Academy of Sciences*, 108(15), pp. 6282–6287. Available at: <https://doi.org/10.1073/pnas.1015239108>.
19. Bayır, U.Ö. *et al.* (2022) 'The effect of pulsed radiofrequency application on nerve healing after sciatic nerve anastomosis in rats', *Ultrastructural Pathology*, 46(4), pp. 313–322. Available at: <https://doi.org/10.1080/01913123.2022.2066237>.
20. Bhandari, P.S. (2019) 'Management of peripheral nerve injury', *Journal of Clinical Orthopaedics and Trauma*, 10(5), pp. 862–866. Available at: <https://doi.org/10.1016/j.jcot.2019.08.003>.

21. Bharadwaz, A., Dhar, S. and Jayasuriya, A.C. (2023) 'Full factorial design of experiment-based and response surface methodology approach for evaluating variation in uniaxial compressive mechanical properties, and biocompatibility of photocurable PEGDMA-based scaffolds', *Biomedical Materials*, 18(2), p. 025019. Available at: <https://doi.org/10.1088/1748-605X/acb7bd>.
22. Bjelle, A., Andersson, T. and Granath, K. (1983) 'Molecular Weight Distribution of Hyaluronic Acid of Human Synovial Fluid in Rheumatic Diseases', *Scandinavian Journal of Rheumatology*, 12(2), pp. 133–138. Available at: <https://doi.org/10.3109/03009748309102899>.
23. Blom, C.L., Mårtensson, L.B. and Dahlin, L.B. (2014) 'Nerve injury-induced c-Jun activation in Schwann cells is JNK independent', *BioMed Research International*, 2014, p. 392971. Available at: <https://doi.org/10.1155/2014/392971>.
24. Bordbar-Khiabani, A. and Gasik, M. (2022) 'Smart Hydrogels for Advanced Drug Delivery Systems', *International Journal of Molecular Sciences*, 23(7), p. 3665. Available at: <https://doi.org/10.3390/ijms23073665>.
25. Bosch-Queralt, M., Fledrich, R. and Stassart, R.M. (2023) 'Schwann cell functions in peripheral nerve development and repair', *Neurobiology of Disease*, 176, p. 105952. Available at: <https://doi.org/10.1016/j.nbd.2022.105952>.
26. Bose, A., Rajeshkumar, R. and Jatin, M. (2022) 'Benzophenone And Pyrazine Derivatives Differential Effects On Ovarian Cancer (SK-OV-3) Cell Line', *NeuroQuantology*, 20(17), pp. 1473–1478. Available at: <https://doi.org/10.48047/NQ.2022.20.17.NQ880182>.
27. Brull, R. *et al.* (2015) 'Pathophysiology and Etiology of Nerve Injury Following Peripheral Nerve Blockade', *Regional Anesthesia & Pain Medicine*, 40(5), pp. 479–490. Available at: <https://doi.org/10.1097/AAP.0000000000000125>.
28. Buckley, C. *et al.* (2022) 'Hyaluronic Acid: A Review of the Drug Delivery Capabilities of This Naturally Occurring Polysaccharide', *Polymers*, 14(17), p. 3442. Available at: <https://doi.org/10.3390/polym14173442>.
29. Burke, G. *et al.* (2019) 'Evaluation of the materials properties, stability and cell response of a range of PEGDMA hydrogels for tissue engineering applications', *Journal of the Mechanical Behavior of Biomedical Materials*, 99, pp. 1–10. Available at: <https://doi.org/10.1016/j.jmbbm.2019.07.003>.

30. Burke, G. *et al.* (2019) 'Preparation of Biodegradable Polyethylene Glycol Dimethacrylate Hydrogels via Thiol-ene Chemistry', *Polymers*, 11(8), p. 1339. Available at: <https://doi.org/10.3390/polym11081339>.
31. Campoccia, D. *et al.* (1996) 'Quantitative assessment of the tissue response to films of hyaluronan derivatives', *Biomaterials*, 17(10), pp. 963–975. Available at: [https://doi.org/10.1016/0142-9612\(96\)84670-9](https://doi.org/10.1016/0142-9612(96)84670-9).
32. Carreño, E.A. *et al.* (2021) 'Considerations and Technical Pitfalls in the Employment of the MTT Assay to Evaluate Photosensitizers for Photodynamic Therapy', *Applied Sciences*, 11(6), p. 2603. Available at: <https://doi.org/10.3390/app11062603>.
33. Carvalho, C.R., Oliveira, J.M. and Reis, R.L. (2019) 'Modern Trends for Peripheral Nerve Repair and Regeneration: Beyond the Hollow Nerve Guidance Conduit', *Frontiers in Bioengineering and Biotechnology*, 7. Available at: <https://www.frontiersin.org/articles/10.3389/fbioe.2019.00337> (Accessed: 25 April 2023).
34. Casadey, R. *et al.* (2021) 'Antioxidant and antimicrobial properties of tyrosol and derivative-compounds in the presence of vitamin B2. Assays of synergistic antioxidant effect with commercial food additives', *Food Chemistry*, 335, p. 127576. Available at: <https://doi.org/10.1016/j.foodchem.2020.127576>.
35. Chaala, M. *et al.* (2023) 'Accelerated Simple Preparation of Curcumin-Loaded Silk Fibroin/Hyaluronic Acid Hydrogels for Biomedical Applications', *Polymers*, 15(3), p. 504. Available at: <https://doi.org/10.3390/polym15030504>.
36. Chang, S.-Y., Ching, T. and HA-SHimoto, M. (2022) 'Bioprinting using PEGDMA-based hydrogel on DLP printer', *Materials Today: Proceedings*, 70, pp. 179–183. Available at: <https://doi.org/10.1016/j.matpr.2022.09.017>.
37. Chelyshev, Y.A., Kabdesh, I.M. and Mukhamedshina, Y.O. (2022) 'Extracellular Matrix in Neural Plasticity and Regeneration', *Cellular and Molecular Neurobiology*, 42(3), pp. 647–664. Available at: <https://doi.org/10.1007/s10571-020-00986-0>.
38. Chen, L. and Hu, G. (2020) 'Mediating Knowledge through Expressing Surprises: A Frame-based Analysis of Surprise Markers in Research Articles across Disciplines and Research Paradigms', *Discourse Processes*, 57(8), pp. 659–681. Available at: <https://doi.org/10.1080/0163853X.2020.1737348>.

39. Chen, L. and Hu, G. (2020) 'Surprise markers in applied linguistics research articles: A diachronic perspective', *Lingua*, 248, p. 102992. Available at: <https://doi.org/10.1016/j.lingua.2020.102992>.
40. Chen, Y.-S. *et al.* (2023) 'Additive manufacturing of Schwann cell-laden collagen/alginate nerve guidance conduits by freeform reversible embedding regulate neurogenesis via exosomes secretion towards peripheral nerve regeneration', *Biomaterials Advances*, 146, p. 213276. Available at: <https://doi.org/10.1016/j.bioadv.2022.213276>.
41. Cho, J. *et al.* (2020) 'Comparing Absorbable and Nonabsorbable Suture Materials for Repair of Achilles Tendon Rupture: A Magnetic Resonance Imaging-Based Study', *Diagnostics*, 10(12), p. 1085. Available at: <https://doi.org/10.3390/diagnostics10121085>.
42. Cohen, B.H. *et al.* (2016) 'Multifocal Neuropathy: Expanding the Scope of Double Crush Syndrome', *The Journal of Hand Surgery*, 41(12), pp. 1171–1175. Available at: <https://doi.org/10.1016/j.jhssa.2016.09.009>.
43. Coleman, M.P. and Höke, A. (2020) 'Programmed axon degeneration: from mouse to mechanism to medicine', *Nature Reviews Neuroscience*, 21(4), pp. 183–196. Available at: <https://doi.org/10.1038/s41583-020-0269-3>.
44. Contreras, E. *et al.* (2023) 'Repair of Long Peripheral Nerve Defects in Sheep: A Translational Model for Nerve Regeneration', *International Journal of Molecular Sciences*, 24(2), p. 1333. Available at: <https://doi.org/10.3390/ijms24021333>.
45. Crotty, M. (1998) *The Foundations of Social Research: Meaning and Perspective in the Research Process*. SAGE.
46. D'Eon, M.F. (2020) 'Being a post-positivist is exhausting: The daunting commitment to an uncertain truth', *Canadian Medical Education Journal*, 11(5), pp. e1–e4. Available at: <https://doi.org/10.36834/cmej.71151>.
47. D'Este, M., Eglin, D. and Alini, M. (2014) 'A systematic analysis of DMTMM vs EDC/NHS for ligation of amines to Hyaluronan in water', *Carbohydrate Polymers*, 108, pp. 239–246. Available at: <https://doi.org/10.1016/j.carbpol.2014.02.070>.
48. Dai, H. and Li, S. (2015) 'Optimized design of regeneration material for the treatment of peripheral nerve injury', *undefined* [Preprint]. Available at: <https://www.semanticscholar.org/paper/Optimized-design-of-regeneration-material-for-the-Dai-Li/e4124f4be63cf3dbc4ab5a3d897ee019c545463e> (Accessed: 27 April 2022).

49. Daminato, E., Bianchini, G. and Causin, V. (2022) 'New Directions in Aesthetic Medicine: A Novel and Hybrid Filler Based on Hyaluronic Acid and Lactose Modified Chitosan', *Gels*, 8(5), p. 326. Available at: <https://doi.org/10.3390/gels8050326>.
50. Delfi, M. *et al.* (2021) 'Self-assembled peptide and protein nanostructures for anti-cancer therapy: Targeted delivery, stimuli-responsive devices and immunotherapy', *Nano Today*, 38, p. 101119. Available at: <https://doi.org/10.1016/j.nantod.2021.101119>.
51. Ding, Y.-W. *et al.* (2022) 'Advances in modified hyaluronic acid-based hydrogels for skin wound healing', *Biomaterials Science*, 10(13), pp. 3393–3409. Available at: <https://doi.org/10.1039/D2BM00397J>.
52. Dravid, A. *et al.* (2021) 'Optimised techniques for high-throughput screening of differentiated SH-SY5Y cells and application for neurite outgrowth assays', *Scientific Reports*, 11(1), p. 23935. Available at: <https://doi.org/10.1038/s41598-021-03442-1>.
53. Dubový, P. (2011) 'Wallerian degeneration and peripheral nerve conditions for both axonal regeneration and neuropathic pain induction', *Annals of Anatomy - Anatomischer Anzeiger*, 193(4), pp. 267–275. Available at: <https://doi.org/10.1016/j.aanat.2011.02.011>.
54. Ducic, I., Safa, B. and DeVinney, E. (2017) 'Refinements of nerve repair with connector-assisted coaptation', *Microsurgery*, 37(3), pp. 256–263. Available at: <https://doi.org/10.1002/micr.30151>.
55. Edizer, D.T. *et al.* (2019) 'Effects of Melatonin and Dexamethasone on Facial Nerve Neuroorrhaphy', *The Journal of International Advanced Otolaryngology*, 15(1), pp. 43–50. Available at: <https://doi.org/10.5152/iao.2018.3273>.
56. Eleftheriadou, D. *et al.* (2020) 'A combined experimental and computational framework to evaluate the behavior of therapeutic cells for peripheral nerve regeneration', *Biotechnology and Bioengineering*, n/a(n/a). Available at: <https://doi.org/10.1002/bit.28105>.
57. Elsayed, A.-S.E. *et al.* (2019) 'Pathological evaluation of dorsal root ganglia and spinal cord and sciatic nerve following a chronic constriction injury of the sciatic nerve in rats', *Kafrelsheikh Veterinary Medical Journal*, 17(1), pp. 63–77. Available at: <https://doi.org/10.21608/kvmj.2019.110202>.

58. Entekhabi, E. *et al.* (2021) 'Fabrication and in vitro evaluation of 3D composite scaffold based on collagen/hyaluronic acid sponge and electrospun polycaprolactone nanofibers for peripheral nerve regeneration', *Journal of Biomedical Materials Research Part A*, 109(3), pp. 300–312. Available at: <https://doi.org/10.1002/jbm.a.37023>.
59. Espíndola, M.R. *et al.* (2022) 'In vitro assessment for cytotoxicity screening of new antimalarial candidates', *Brazilian Journal of Pharmaceutical Sciences*, 58, p. e18308. Available at: <https://doi.org/10.1590/s2175-97902022e18308>.
60. Eyler, R.W., Klug, E.D. and Diephuis, Floyd. (1947) 'Determination of Degree of Substitution of Sodium Carboxymethylcellulose', *Analytical Chemistry*, 19(1), pp. 24–27. Available at: <https://doi.org/10.1021/ac60001a007>.
61. Fader, K.A. *et al.* (2022) 'Circulating neurofilament light chain as a promising biomarker of AAV-induced dorsal root ganglia toxicity in nonclinical toxicology species', *Molecular Therapy - Methods & Clinical Development*, 25, pp. 264–277. Available at: <https://doi.org/10.1016/j.omtm.2022.03.017>.
62. Fadia, N.B. *et al.* (2020) 'Long-gap peripheral nerve repair through sustained release of a neurotrophic factor in nonhuman primates', *Science Translational Medicine*, 12(527), p. eaav7753. Available at: <https://doi.org/10.1126/scitranslmed.aav7753>.
63. Fedotcheva, N. and Beloborodova, N. (2022) 'Influence of Microbial Metabolites and Itaconic Acid Involved in Bacterial Inflammation on the Activity of Mitochondrial Enzymes and the Protective Role of Alkalization', *International Journal of Molecular Sciences*, 23(16), p. 9069. Available at: <https://doi.org/10.3390/ijms23169069>.
64. Galano, A. *et al.* (2012) 'A Quantum Chemical Study on the Free Radical Scavenging Activity of Tyrosol and Hydroxytyrosol', *Theoretical Chemistry Accounts*, 131, p. 1173. Available at: <https://doi.org/10.1007/s00214-012-1173-3>.
65. Gao, S. *et al.* (2023) 'Recent advances on nerve guide conduits based on textile methods', *Smart Materials in Medicine*, 4, pp. 368–383. Available at: <https://doi.org/10.1016/j.smaim.2022.12.001>.
66. Garg, H.G. and Hales, C.A. (2004) *Chemistry and Biology of Hyaluronan*. 1st ed. Elsevier. Available at: <http://gen.lib.rus.ec/book/index.php?md5=f3fdc80834f8d3a057180095f4b5e6b5> (Accessed: 15 March 2023).

67. Gaudin, R. *et al.* (2016) 'Approaches to Peripheral Nerve Repair: Generations of Biomaterial Conduits Yielding to Replacing Autologous Nerve Grafts in Craniomaxillofacial Surgery', *BioMed Research International*, 2016, p. e3856262. Available at: <https://doi.org/10.1155/2016/3856262>.
68. Ghazali, H.S. *et al.* (2023) 'A high-absorbance water-soluble photoinitiator nanoparticle for hydrogel 3D printing: synthesis, characterization and in vitro cytotoxicity study', *Scientific Reports*, 13(1), p. 8577. Available at: <https://doi.org/10.1038/s41598-023-35865-3>.
69. Giusti, G. *et al.* (2014) 'The influence of nerve conduits diameter in motor nerve recovery after segmental nerve repair', *Microsurgery*, 34(8), pp. 646–652. Available at: <https://doi.org/10.1002/micr.22312>.
70. Gonzalez, R.J. and Tarloff, J.B. (2001) 'Evaluation of hepatic subcellular fractions for Alamar blue and MTT reductase activity', *Toxicology in Vitro*, 15(3), pp. 257–259. Available at: [https://doi.org/10.1016/S0887-2333\(01\)00014-5](https://doi.org/10.1016/S0887-2333(01)00014-5).
71. Gratzner, H.G. (1982) 'Monoclonal Antibody to 5-Bromo- and 5-Iododeoxyuridine: A New Reagent for Detection of DNA Replication', *Science*, 218(4571), pp. 474–475. Available at: <https://doi.org/10.1126/science.7123245>.
72. Guionneau, N. von *et al.* (2020) 'Mechanisms and outcomes of the supercharged end-to-side nerve transfer: a review of preclinical and clinical studies', *Journal of Neurosurgery*, 134(5), pp. 1590–1598. Available at: <https://doi.org/10.3171/2020.3.JNS191429>.
73. Habib, H. (2021) 'Positivism and Post-positivistic Approaches to Research', p. 1000.
74. Hai, M. *et al.* (2002) 'Comparative analysis of Schwann cell lines as model systems for myelin gene transcription studies', *Journal of Neuroscience Research*, 69(4), pp. 497–508. Available at: <https://doi.org/10.1002/jnr.10327>.
75. Hanoux, V. *et al.* (2018) 'Increase in hyaluronic acid degradation decreases the expression of estrogen receptor alpha in MCF7 breast cancer cell line', *Molecular and Cellular Endocrinology*, 476, pp. 185–197. Available at: <https://doi.org/10.1016/j.mce.2018.05.008>.
76. Hao, Y. *et al.* (2014) 'Visible light cured thiol-vinyl hydrogels with tunable degradation for 3D cell culture', *Acta Biomaterialia*, 10(1), pp. 104–114. Available at: <https://doi.org/10.1016/j.actbio.2013.08.044>.

77. Harrer, D. *et al.* (2021) 'Is hyaluronic acid the perfect excipient for the pharmaceutical need?', *International Journal of Pharmaceutics*, 601, p. 120589. Available at: <https://doi.org/10.1016/j.ijpharm.2021.120589>.
78. Hasiba-Pappas, S. *et al.* (2023) 'Does Electrical Stimulation through Nerve Conduits Improve Peripheral Nerve Regeneration?—A Systematic Review', *Journal of Personalized Medicine*, 13(3), p. 414. Available at: <https://doi.org/10.3390/jpm13030414>.
79. Hassan, H.S. *et al.* (2022) 'Assessment of antimicrobial, cytotoxicity, and antiviral impact of a green zinc oxide/activated carbon nanocomposite', *Scientific Reports*, 12(1), p. 8774. Available at: <https://doi.org/10.1038/s41598-022-12648-w>.
80. Hewson, D.W., Bedforth, N.M. and Hardman, J.G. (2018) 'Peripheral nerve injury arising in anaesthesia practice', *Anaesthesia*, 73(S1), pp. 51–60. Available at: <https://doi.org/10.1111/anae.14140>.
81. Hoda, S.A. (2019) 'Underwood's Pathology: A Clinical Approach', *American Journal of Clinical Pathology*, 151(1), p. 127. Available at: <https://doi.org/10.1093/ajcp/aqy140>.
82. Hogan, Q.H. (2008) 'Pathophysiology of Peripheral Nerve Injury During Regional Anesthesia', *Regional Anesthesia and Pain Medicine*, 33(5), pp. 435–441. Available at: <https://doi.org/10.1016/j.rapm.2008.03.002>.
83. Hones, K.M. *et al.* (2023) 'Outcomes following use of VersaWrap nerve protector in treatment of patients with recurrent compressive neuropathies', *Frontiers in Surgery*, 10. Available at: <https://www.frontiersin.org/articles/10.3389/fsurg.2023.1123375> (Accessed: 28 May 2023).
84. Hossain Rakin, R. *et al.* (2021) 'Tunable metacrylated hyaluronic acid-based hybrid bioinks for stereolithography 3D bioprinting', *Biofabrication*, 13(4), p. 044109. Available at: <https://doi.org/10.1088/1758-5090/ac25cb>.
85. Houshyar, S., Bhattacharyya, A. and Shanks, R. (2019) 'Peripheral Nerve Conduit: Materials and Structures', *ACS Chemical Neuroscience*, 10(8), pp. 3349–3365. Available at: <https://doi.org/10.1021/acscchemneuro.9b00203>.
86. Hsu, S., Chang, W.-C. and Yen, C.-T. (2017) 'Novel flexible nerve conduits made of water-based biodegradable polyurethane for peripheral nerve regeneration', *Journal of Biomedical Materials Research Part A*, 105(5), pp. 1383–1392. Available at: <https://doi.org/10.1002/jbm.a.36022>.

87. Huang, G. and Huang, H. (2018) 'Application of hyaluronic acid as carriers in drug delivery', *Drug Delivery*, 25(1), pp. 766–772. Available at: <https://doi.org/10.1080/10717544.2018.1450910>.
88. Hussain, G. *et al.* (2020) 'Current Status of Therapeutic Approaches against Peripheral Nerve Injuries: A Detailed Story from Injury to Recovery', *International journal of biological sciences*, 16, pp. 116–134. Available at: <https://doi.org/10.7150/ijbs.35653>.
89. International Organisation for Standardisation (ISO) (2002) *ISO-10993-17-2002.pdf*. Available at: <https://cdn.standards.iteh.ai/samples/23955/753ca68e498441aa87ba2e96a8cbec4e/ISO-10993-17-2002.pdf> (Accessed: 28 May 2023).
90. International Organisation for Standardisation (ISO) (2009) *ISO-10993-5-2009.pdf*. Available at: <https://nhiso.com/wp-content/uploads/2018/05/ISO-10993-5-2009.pdf> (Accessed: 28 May 2023).
91. Ioncioaia, B. (2023) 'A New Model for Basic Microsurgical Nerve Repair Simulation: Making the Most Out of Less', *Archives of Plastic Surgery*, pp. 220–221. Available at: <https://doi.org/10.1055/s-0042-1758544>.
92. Ito, T. *et al.* (2004) 'Hyaluronan regulates transforming growth factor-beta1 receptor compartmentalization', *The Journal of Biological Chemistry*, 279(24), pp. 25326–25332. Available at: <https://doi.org/10.1074/jbc.M403135200>.
93. Jabbari, F., Babaeipour, V. and Saharkhiz, S. (2023) 'Comprehensive review on biosynthesis of hyaluronic acid with different molecular weights and its biomedical applications', *International Journal of Biological Macromolecules*, 240, p. 124484. Available at: <https://doi.org/10.1016/j.ijbiomac.2023.124484>.
94. Jellish, W.S. and Oftadeh, M. (2018) 'Peripheral Nerve Injury in Cardiac Surgery', *Journal of Cardiothoracic and Vascular Anesthesia*, 32(1), pp. 495–511. Available at: <https://doi.org/10.1053/j.jvca.2017.08.030>.
95. Jiang, H. *et al.* (2019) 'Proteomic Study of a Parkinson's Disease Model of Undifferentiated SH-SY5Y Cells Induced by a Proteasome Inhibitor', *International Journal of Medical Sciences*, 16(1), pp. 84–92. Available at: <https://doi.org/10.7150/ijms.28595>.
96. Jiang, Z. *et al.* (2019) 'Rat sciatic nerve regeneration across a 10-mm defect bridged by a chitin/CM-chitosan artificial nerve graft', *International Journal of*

- Biological Macromolecules*, 129, pp. 997–1005. Available at:
<https://doi.org/10.1016/j.ijbiomac.2019.02.080>.
97. Jin, X. *et al.* (2018) ‘N-acetylcysteine modified hyaluronic acid-paclitaxel conjugate for efficient oral chemotherapy through mucosal bioadhesion ability’, *Colloids and Surfaces B: Biointerfaces*, 172, pp. 655–664. Available at:
<https://doi.org/10.1016/j.colsurfb.2018.09.025>.
98. Johannsmeier, S. *et al.* (2019) ‘Hydrogels for light delivery in in vivo optogenetic applications’, in *Clinical and Preclinical Optical Diagnostics II (2019)*, paper 11075_16. *European Conference on Biomedical Optics*, Optica Publishing Group, p. 11075_16. Available at: <https://doi.org/10.1117/12.2525324>.
99. Johannsmeier, S. *et al.* (2020) ‘PEGDMA Hydrogels for Cell Adhesion and Optical Waveguiding’, *ACS Applied Bio Materials*, 3(10), pp. 7011–7020. Available at:
<https://doi.org/10.1021/acsabm.0c00885>.
100. Kamil, K. *et al.* (2020) ‘Hydroxytyrosol Promotes Proliferation of Human Schwann Cells: An In Vitro Study’, *International Journal of Environmental Research and Public Health*, 17(12), p. 4404. Available at:
<https://doi.org/10.3390/ijerph17124404>.
101. Kang, N.-U., Lee, S.-J. and Gwak, S.-J. (2022) ‘Fabrication Techniques of Nerve Guidance Conduits for Nerve Regeneration’, *Yonsei Medical Journal*, 63(2), pp. 114–123. Available at: <https://doi.org/10.3349/ymj.2022.63.2.114>.
102. Kaplan, S. (2011) ‘Effects of Melatonin on Peripheral Nerve Regeneration’, *Recent patents on endocrine, metabolic & immune drug discovery*, 5, pp. 100–8. Available at: <https://doi.org/10.2174/187221411799015336>.
103. Katiyar, K.S. *et al.* (2020) ‘Tissue Engineered Axon Tracts Serve as Living Scaffolds to Accelerate Axonal Regeneration and Functional Recovery Following Peripheral Nerve Injury in Rats’, *Frontiers in Bioengineering and Biotechnology*, 8. Available at: <https://doi.org/10.3389/fbioe.2020.00492>.
104. Khan, H. and Perera, N. (2020) ‘Peripheral nerve injury: an update’, *Orthopaedics and Trauma*, 34(3), pp. 168–173. Available at:
<https://doi.org/10.1016/j.mporth.2020.03.011>.
105. Khetan, S. and Corey, O. (2019) ‘Maintenance of stem cell viability and differentiation potential following cryopreservation within 3-dimensional hyaluronic acid hydrogels’, *Cryobiology*, 90, pp. 83–88. Available at:
<https://doi.org/10.1016/j.cryobiol.2019.08.001>.

106. Khunmanee, S., Jeong, Y. and Park, H. (2017) 'Crosslinking method of hyaluronic-based hydrogel for biomedical applications', *Journal of Tissue Engineering*, 8, p. 2041731417726464. Available at: <https://doi.org/10.1177/2041731417726464>.
107. Killion, J. (2013) *Development of novel hydrogel based composites for bone tissue engineering applications*. Thesis. Available at: <https://research.thea.ie/handle/20.500.12065/2632> (Accessed: 3 May 2023).
108. Killion, J. *et al.* (2011) 'Mechanical properties and thermal behaviour of PEGDMA hydrogels for potential bone regeneration application', *Journal of the mechanical behavior of biomedical materials*, 4, pp. 1219–27. Available at: <https://doi.org/10.1016/j.jmbbm.2011.04.004>.
109. Kim, S. *et al.* (2018) 'Versatile biomimetic conductive polypyrrole films doped with hyaluronic acid of different molecular weights', *Acta Biomaterialia*, 80, pp. 258–268. Available at: <https://doi.org/10.1016/j.actbio.2018.09.035>.
110. Konofaos, P., Bassilios Habre, S. and Wallace, R.D. (2018) 'End-to-Side Nerve Repair: Current Concepts and Future Perspectives', *Annals of Plastic Surgery*, 81(6), pp. 736–740. Available at: <https://doi.org/10.1097/SAP.0000000000001663>.
111. Kothari, C.R. (2004) *Research Methodology: Methods and Techniques*. New Age International.
112. Kouyoumdjian, J.A. (2006) 'Peripheral nerve injuries: A retrospective survey of 456 cases', *Muscle & Nerve*, 34(6), pp. 785–788. Available at: <https://doi.org/10.1002/mus.20624>.
113. Kovalevich, J. and Langford, D. (2013) 'Considerations for the use of SH-SY5Y neuroblastoma cells in neurobiology', *Methods in Molecular Biology (Clifton, N.J.)*, 1078, pp. 9–21. Available at: https://doi.org/10.1007/978-1-62703-640-5_2.
114. Kovalevich, J., Santerre, M. and Langford, D. (2021) 'Considerations for the Use of SH-SY5YSH-SY5Y NeuroblastomaNeuroblastoma Cells in Neurobiology', in S. Amini and M.K. White (eds) *Neuronal Cell Culture: Methods and Protocols*. New York, NY: Springer US (Methods in Molecular Biology), pp. 9–23. Available at: https://doi.org/10.1007/978-1-0716-1437-2_2.
115. Köwitsch, A., Zhou, G. and Groth, T. (2018) 'Medical application of glycosaminoglycans: a review: Medical Application of Glycosaminoglycans', *Journal of Tissue Engineering and Regenerative Medicine*, 12(1), pp. e23–e41. Available at: <https://doi.org/10.1002/term.2398>.

116. Krauss, E.M., Weber, R.V. and Mackinnon, S.E. (2022) '52 - Nerve Injury, Repair, and Reconstruction', in R.D. Farhadieh et al. (eds) *Plastic Surgery - Principles and Practice*. Elsevier, pp. 803–825. Available at: <https://doi.org/10.1016/B978-0-323-65381-7.00052-6>.
117. Kumar, R. *et al.* (2022) 'Biomimetic Nanocomposites for Biomedical Applications', in *Biorenewable Nanocomposite Materials, Vol. 1: Electrocatalysts and Energy Storage*. American Chemical Society (ACS Symposium Series, 1410), pp. 163–196. Available at: <https://doi.org/10.1021/bk-2022-1410.ch007>.
118. Kuo, P.-J. *et al.* (2021) 'Estimation of the Effect of Accelerating New Bone Formation of High and Low Molecular Weight Hyaluronic Acid Hybrid: An Animal Study', *Polymers*, 13(11), p. 1708. Available at: <https://doi.org/10.3390/polym13111708>.
119. Kwan, M.K. *et al.* (1992) 'Strain, stress and stretch of peripheral nerve Rabbit experiments in vitro and in vivo', *Acta Orthopaedica Scandinavica*, 63(3), pp. 267–272. Available at: <https://doi.org/10.3109/17453679209154780>.
120. Kwon, M.Y. *et al.* (2019) 'Influence of hyaluronic acid modification on CD44 binding towards the design of hydrogel biomaterials', *Biomaterials*, 222, p. 119451. Available at: <https://doi.org/10.1016/j.biomaterials.2019.119451>.
121. Lai, J.-Y. (2012) 'Solvent Composition is Critical for Carbodiimide Cross-Linking of Hyaluronic Acid as an Ophthalmic Biomaterial', *Materials*, 5(10), pp. 1986–2002. Available at: <https://doi.org/10.3390/ma5101986>.
122. Lakkala, P. *et al.* (2023) 'Additive manufacturing technologies with emphasis on stereolithography 3D printing in pharmaceutical and medical applications: A review', *International Journal of Pharmaceutics: X*, 5, p. 100159. Available at: <https://doi.org/10.1016/j.ijpx.2023.100159>.
123. Larramendy, M. and Soloneski, S. (2018) *Genotoxicity: A Predictable Risk to Our Actual World*. BoD – Books on Demand.
124. Laurent, T.C. *et al.* (1987) 'Urinary excretion of hyaluronan in man', *Scandinavian Journal of Clinical and Laboratory Investigation*, 47(8), pp. 793–799. Available at: <https://doi.org/10.3109/00365518709168948>.
125. Lavogina, D. *et al.* (2022) 'Revisiting the Resazurin-Based Sensing of Cellular Viability: Widening the Application Horizon', *Biosensors*, 12(4), p. 196. Available at: <https://doi.org/10.3390/bios12040196>.

126. Leckenby, J.I. *et al.* (2020) ‘A Retrospective Case Series Reporting the Outcomes of Avance Nerve Allografts in the Treatment of Peripheral Nerve Injuries’, *Plastic and Reconstructive Surgery*, 145(2), pp. 368e–381e. Available at: <https://doi.org/10.1097/PRS.0000000000006485>.
127. Lee, H. *et al.* (2022) ‘Injectable Self-Crosslinkable Thiolated Hyaluronic Acid for Stem Cell Therapy of Atopic Dermatitis’, *ACS Biomaterials Science & Engineering*, 8(4), pp. 1613–1622. Available at: <https://doi.org/10.1021/acsbiomaterials.1c01374>.
128. Li, B. *et al.* (2022) ‘Melatonin promotes peripheral nerve repair through Parkin-mediated mitophagy’, *Free Radical Biology & Medicine*, 185, pp. 52–66. Available at: <https://doi.org/10.1016/j.freeradbiomed.2022.04.016>.
129. Li, J. *et al.* (2023) ‘Development and systematic characterization of GelMA/alginate/PEGDMA/xanthan gum hydrogel bioink system for extrusion bioprinting’, *Biomaterials*, 293, p. 121969. Available at: <https://doi.org/10.1016/j.biomaterials.2022.121969>.
130. Li, Jiqing *et al.* (2019) ‘The Role of Hyaluronidase for the Skin Necrosis Caused by Hyaluronic Acid Injection-Induced Embolism: A Rabbit Auricular Model Study’, *Aesthetic Plastic Surgery*, 43(5), pp. 1362–1370. Available at: <https://doi.org/10.1007/s00266-019-01398-2>.
131. Li, R. (no date) ‘A Novel Thiolated Hyaluronic acid Hydrogel for Spinal Cord Injury Repair’, p. 80.
132. Li, S. *et al.* (2020) ‘Self-healing hyaluronic acid hydrogels based on dynamic Schiff base linkages as biomaterials’, *Carbohydrate Polymers*, 250, p. 116922. Available at: <https://doi.org/10.1016/j.carbpol.2020.116922>.
133. Li, Xiangling *et al.* (2023) ‘Electrical stimulation accelerates Wallerian degeneration and promotes nerve regeneration after sciatic nerve injury’, *Glia*, 71(3), pp. 758–774. Available at: <https://doi.org/10.1002/glia.24309>.
134. Li, Y. *et al.* (2022) ‘Hyaluronic acid-methacrylic anhydride/polyhexamethylene biguanide hybrid hydrogel with antibacterial and proangiogenic functions for diabetic wound repair’, *Chinese Chemical Letters*, 33(12), pp. 5030–5034. Available at: <https://doi.org/10.1016/j.ccllet.2022.03.116>.
135. Li, Z. *et al.* (2014) ‘Multilayer coextrusion of rheologically modified main chain liquid crystalline polymers and resulting orientational order’, *Polymer*, 55(19), pp. 4966–4975. Available at: <https://doi.org/10.1016/j.polymer.2014.08.009>.

136. Liu, H. *et al.* (2017) ‘Salidroside promotes peripheral nerve regeneration based on tissue engineering strategy using Schwann cells and PLGA: in vitro and in vivo’, *Scientific Reports*, 7(1), p. 39869. Available at: <https://doi.org/10.1038/srep39869>.
137. Liu, Y. *et al.* (2022) ‘Biosynthesis and biotechnological production of salidroside from *Rhodiola* genus plants’, *Phytochemistry Reviews*, 21(5), pp. 1605–1626. Available at: <https://doi.org/10.1007/s11101-021-09800-1>.
138. Liu, Z. *et al.* (2022) ‘Low-Stiffness Hydrogels Promote Peripheral Nerve Regeneration Through the Rapid Release of Exosomes’, *Frontiers in Bioengineering and Biotechnology*, 10, p. 922570. Available at: <https://doi.org/10.3389/fbioe.2022.922570>.
139. Lizarraga-Valderrama, L.R. *et al.* (2021) ‘Preclinical study of peripheral nerve regeneration using nerve guidance conduits based on polyhydroxyalkanoates’, *Bioengineering & Translational Medicine*, 6(3), p. e10223. Available at: <https://doi.org/10.1002/btm2.10223>.
140. Lü, L. *et al.* (2012) ‘Exocytosis of MTT formazan could exacerbate cell injury’, *Toxicology in Vitro*, 26(4), pp. 636–644. Available at: <https://doi.org/10.1016/j.tiv.2012.02.006>.
141. Luo, Z., Dai, Y. and Gao, H. (2019) ‘Development and application of hyaluronic acid in tumor targeting drug delivery’, *Acta Pharmaceutica Sinica B*, 9(6), pp. 1099–1112. Available at: <https://doi.org/10.1016/j.apsb.2019.06.004>.
142. Ma, H. *et al.* (2022) ‘Effects and Progress of Photo-Crosslinking Hydrogels in Wound Healing Improvement’, *Gels*, 8(10), p. 609. Available at: <https://doi.org/10.3390/gels8100609>.
143. Macedo, G.E. *et al.* (2022) ‘Effect of fungal indoor air pollutant 1-octen-3-ol on levels of reactive oxygen species and nitric oxide as well as dehydrogenases activities in *Drosophila melanogaster* males’, *Journal of Toxicology and Environmental Health, Part A*, 85(14), pp. 573–585. Available at: <https://doi.org/10.1080/15287394.2022.2054887>.
144. Mahar, M. and Cavalli, V. (2018) ‘Intrinsic mechanisms of neuronal axon regeneration’, *Nature Reviews Neuroscience*, 19(6), pp. 323–337. Available at: <https://doi.org/10.1038/s41583-018-0001-8>.
145. Mai, J.K. and Paxinos, G. (2011) *The Human Nervous System*. Academic Press.
146. Mamo, H.B., Adamiak, M. and Kunwar, A. (2023) ‘3D printed biomedical devices and their applications: A review on state-of-the-art technologies, existing

- challenges, and future perspectives’, *Journal of the Mechanical Behavior of Biomedical Materials*, 143, p. 105930. Available at: <https://doi.org/10.1016/j.jmbbm.2023.105930>.
147. Masgutov, R. *et al.* (2019) ‘Adipose-Derived Mesenchymal Stem Cells Applied in Fibrin Glue Stimulate Peripheral Nerve Regeneration’, *Frontiers in Medicine*, 6. Available at: <https://doi.org/10.3389/fmed.2019.00068>.
 148. Masri, B.A. *et al.* (2020) ‘Tourniquet-induced nerve compression injuries are caused by high pressure levels and gradients – a review of the evidence to guide safe surgical, pre-hospital and blood flow restriction usage’, *BMC Biomedical Engineering*, 2(1), p. 7. Available at: <https://doi.org/10.1186/s42490-020-00041-5>.
 149. Matejčík, V. (2002) ‘Peripheral nerve reconstruction by autograft’, *Injury*, 33(7), pp. 627–631. Available at: [https://doi.org/10.1016/S0020-1383\(02\)00073-6](https://doi.org/10.1016/S0020-1383(02)00073-6).
 150. Mathot, F. *et al.* (2020) ‘Introducing human adipose-derived mesenchymal stem cells to Avance® nerve grafts and NeuraGen® nerve guides’, *Journal of Plastic, Reconstructive & Aesthetic Surgery*, 73(8), pp. 1473–1481. Available at: <https://doi.org/10.1016/j.bjps.2020.03.012>.
 151. Matos Cruz, A.J. and De Jesus, O. (2023) ‘Neurotmesis’, in *StatPearls*. Treasure Island (FL): StatPearls Publishing. Available at: <http://www.ncbi.nlm.nih.gov/books/NBK559108/> (Accessed: 23 May 2023).
 152. Mauch, J.T. *et al.* (2019) ‘A Systematic Review of Sensory Outcomes of Digital Nerve Gap Reconstruction With Autograft, Allograft, and Conduit’, *Annals of Plastic Surgery*, 82(4S), p. S247. Available at: <https://doi.org/10.1097/SAP.0000000000001851>.
 153. McMurtry, A. (2020) ‘Relief for the exhausted post-positivist: New epistemological choices transcend positivism, relativism, and even post-positivism’, *Canadian Medical Education Journal*, 11(6), pp. e197–e198. Available at: <https://doi.org/10.36834/cmej.71217>.
 154. Meek, M.F. and Coert, J.H. (2008) ‘US Food and Drug Administration/Conformit Europe-Approved Absorbable Nerve Conduits for Clinical Repair of Peripheral and Cranial Nerves’, *Annals of Plastic Surgery*, 60(1), p. 110. Available at: <https://doi.org/10.1097/SAP.0b013e31804d441c>.
 155. Menorca, R.M.G., Fussell, T.S. and Elfar, J.C. (2013a) ‘Peripheral Nerve Trauma: Mechanisms of Injury and Recovery’, *Hand clinics*, 29(3), pp. 317–330. Available at: <https://doi.org/10.1016/j.hcl.2013.04.002>.

156. Min, Q., Parkinson, D.B. and Dun, X.-P. (2021) 'Migrating Schwann cells direct axon regeneration within the peripheral nerve bridge', *Glia*, 69(2), pp. 235–254. Available at: <https://doi.org/10.1002/glia.23892>.
157. Morin, J.-édéric, Olsson, C. and Atikcan, E.Ö. (2021) *Research Methods in the Social Sciences: an A-Z of Key Concepts*. Oxford University Press.
158. Mosmann, T. (1983) 'Rapid colorimetric assay for cellular growth and survival: Application to proliferation and cytotoxicity assays', *Journal of Immunological Methods*, 65(1), pp. 55–63. Available at: [https://doi.org/10.1016/0022-1759\(83\)90303-4](https://doi.org/10.1016/0022-1759(83)90303-4).
159. Murphy, E.J. *et al.* (2023) 'Polysaccharides—Naturally Occurring Immune Modulators', *Polymers*, 15(10), p. 2373. Available at: <https://doi.org/10.3390/polym15102373>.
160. Nakamura, Y. *et al.* (2020) 'Repair of temporal branch of the facial nerve with novel polyglycolic acid-collagen tube: a case report of two cases', *Nagoya Journal of Medical Science*, 82(1), pp. 123–128. Available at: <https://doi.org/10.18999/nagjms.82.1.123>.
161. Narayan, S.K., Arumugam, M. and Chittoria, R. (2019) 'Outcome of human peripheral nerve repair interventions using conduits: a systematic review', *Journal of the Neurological Sciences*, 396, pp. 18–24. Available at: <https://doi.org/10.1016/j.jns.2018.10.012>.
162. Nassimizadeh, M., Nassimizadeh, A.K. and Power, D. (2019) 'Managing the nerve gap: New tools in the peripheral nerve repair toolbox', *Journal of Musculoskeletal Surgery and Research*, 3, p. 4. Available at: https://doi.org/10.4103/jmsr.jmsr_98_18.
163. Oral, N. and Basal, G. (2022) 'The effects of crosslinker ratio and photoinitiator type on the properties of pnipam hydrogel', *Journal of Polymer Research*, 30(1), p. 34. Available at: <https://doi.org/10.1007/s10965-022-03419-2>.
164. Oudshoorn, M.H.M. *et al.* (2007) 'Synthesis of methacrylated hyaluronic acid with tailored degree of substitution', *Polymer*, 48(7), pp. 1915–1920. Available at: <https://doi.org/10.1016/j.polymer.2007.01.068>.
165. Pandey, S. and Mudgal, J. (2022) 'A Review on the Role of Endogenous Neurotrophins and Schwann Cells in Axonal Regeneration', *Journal of Neuroimmune Pharmacology*, 17(3), pp. 398–408. Available at: <https://doi.org/10.1007/s11481-021-10034-3>.

166. Panzer, K.V. *et al.* (2020) ‘Tissue Engineered Bands of Büngner for Accelerated Motor and Sensory Axonal Outgrowth’, *Frontiers in Bioengineering and Biotechnology*, 8. Available at: <https://doi.org/10.3389/fbioe.2020.580654>.
167. Papakonstantinou, E., Roth, M. and Karakiulakis, G. (2012) ‘Hyaluronic acid: A key molecule in skin aging’, *Dermato-Endocrinology*, 4(3), pp. 253–258. Available at: <https://doi.org/10.4161/derm.21923>.
168. Parker, B.J. *et al.* (2021) ‘Nerve guidance conduit development for primary treatment of peripheral nerve transection injuries: A commercial perspective’, *Acta Biomaterialia*, 135, pp. 64–86. Available at: <https://doi.org/10.1016/j.actbio.2021.08.052>.
169. Pohan, G. *et al.* (2020) ‘Effect of Ethylene Oxide Sterilization on Polyvinyl Alcohol Hydrogel Compared with Gamma Radiation’, *Tissue Engineering Part A*, 26(19–20), pp. 1077–1090. Available at: <https://doi.org/10.1089/ten.tea.2020.0002>.
170. Popal, M. *et al.* (2018) ‘Cytotoxic and genotoxic potential of the type I photoinitiators BAPO and TPO on human oral keratinocytes and V79 fibroblasts’, *Dental Materials*, 34(12), pp. 1783–1796. Available at: <https://doi.org/10.1016/j.dental.2018.09.015>.
171. Qie, X. *et al.* (2021) ‘Interaction between β -lactoglobulin and chlorogenic acid and its effect on antioxidant activity and thermal stability’, *Food Hydrocolloids*, 121, p. 107059. Available at: <https://doi.org/10.1016/j.foodhyd.2021.107059>.
172. Rahman, I., Kode, A. and Biswas, S.K. (2006) ‘Assay for quantitative determination of glutathione and glutathione disulfide levels using enzymatic recycling method’, *Nature Protocols*, 1(6), pp. 3159–3165. Available at: <https://doi.org/10.1038/nprot.2006.378>.
173. Rakin, R.H. *et al.* (2021) ‘Tunable metacrylated hyaluronic acid-based hybrid bioinks for stereolithography 3D bioprinting’, *Biofabrication*, 13(4), p. 044109. Available at: <https://doi.org/10.1088/1758-5090/ac25cb>.
174. Rangasami, V.K. *et al.* (2021) ‘Harnessing hyaluronic acid-based nanoparticles for combination therapy: A novel approach for suppressing systemic inflammation and to promote antitumor macrophage polarization’, *Carbohydrate Polymers*, 254, p. 117291. Available at: <https://doi.org/10.1016/j.carbpol.2020.117291>.
175. Raut, S. and Johnson, R. (2023) ‘Acute nerve injuries in the hand: common patterns and treatment strategies’, *Orthopaedics and Trauma*, 37(2), pp. 111–117. Available at: <https://doi.org/10.1016/j.mporth.2023.01.004>.

176. Repellin, M. *et al.* (2023) ‘Alcian Blue Staining to Visualize Intracellular Hyaluronic Acid-Based Nanoparticles’, in C. Pellicciari, M. Biggiogera, and M. Malatesta (eds) *Histochemistry of Single Molecules: Methods and Protocols*. New York, NY: Springer US (Methods in Molecular Biology), pp. 313–320. Available at: https://doi.org/10.1007/978-1-0716-2675-7_25.
177. Repetto, G., del Peso, A. and Zurita, J.L. (2008a) ‘Neutral red uptake assay for the estimation of cell viability/cytotoxicity’, *Nature Protocols*, 3(7), pp. 1125–1131. Available at: <https://doi.org/10.1038/nprot.2008.75>.
178. Ristagno, G. *et al.* (2012) ‘Hydroxytyrosol Attenuates Peripheral Neuropathy in Streptozotocin-Induced Diabetes in Rats’, *Journal of Agricultural and Food Chemistry*, 60(23), pp. 5859–5865. Available at: <https://doi.org/10.1021/jf2049323>.
179. Rodriguez-Collazo, E. and Laube Ward, K. (2021) ‘Conduit-assisted Allograft Neurorrhaphy for the Treatment of Intractable Lower Extremity Pain Due to Neuromas-in-continuity’, *Plastic and Reconstructive Surgery Global Open*, 9(11), p. e3867. Available at: <https://doi.org/10.1097/GOX.0000000000003867>.
180. Salma-Ancane, K. *et al.* (2022) ‘Effect of crosslinking strategy on the biological, antibacterial and physicochemical performance of hyaluronic acid and ϵ -polylysine based hydrogels’, *International Journal of Biological Macromolecules*, 208, pp. 995–1008. Available at: <https://doi.org/10.1016/j.ijbiomac.2022.03.207>.
181. Sarnat, H.B. (2023) ‘Axonal pathfinding during the development of the nervous system’, *Annals of the Child Neurology Society*, 1(1), pp. 13–23. Available at: <https://doi.org/10.1002/cns3.2>.
182. Schuett, T. *et al.* (2020) ‘Automated Polymer Purification Using Dialysis’, *Polymers*, 12(9), p. 2095. Available at: <https://doi.org/10.3390/polym12092095>.
183. Schumann, J. *et al.* (2015) ‘Differences in CD44 Surface Expression Levels and Function Discriminates IL-17 and IFN- γ Producing Helper T Cells’, *PLOS ONE*, 10(7), p. e0132479. Available at: <https://doi.org/10.1371/journal.pone.0132479>.
184. Sciabica, S. *et al.* (2023) ‘A Safe-by-Design Approach for the Synthesis of a Novel Cross-Linked Hyaluronic Acid with Improved Biological and Physical Properties’, *Pharmaceuticals*, 16(3), p. 431. Available at: <https://doi.org/10.3390/ph16030431>.
185. Selyanin, M.A. *et al.* (2015) ‘The history of hyaluronic acid discovery, foundational research and initial use’, *Hyaluronic Acid: Preparation, Properties, Application in Biology and Medicine*, pp. 1–8.

186. Serafin, A., Culebras, M. and Collins, M.N. (2023) ‘Synthesis and evaluation of alginate, gelatin, and hyaluronic acid hybrid hydrogels for tissue engineering applications’, *International Journal of Biological Macromolecules*, 233, p. 123438. Available at: <https://doi.org/10.1016/j.ijbiomac.2023.123438>.
187. Sheng, J., Ling, P. and Wang, F. (2015) ‘Constructing a recombinant hyaluronic acid biosynthesis operon and producing food-grade hyaluronic acid in *Lactococcus lactis*’, *Journal of Industrial Microbiology and Biotechnology*, 42(2), pp. 197–206. Available at: <https://doi.org/10.1007/s10295-014-1555-8>.
188. Sheng, Q.-S. *et al.* (2013) ‘Salidroside promotes peripheral nerve regeneration following crush injury to the sciatic nerve in rats’, *Neuroreport*, 24(5), pp. 217–223. Available at: <https://doi.org/10.1097/WNR.0b013e32835eb867>.
189. Shih, M. (2012) ‘In vitro assessment of cytotoxicity, genotoxicity, and bioavailability of copper in HepG2 cells’.
190. Siengalewicz, P., Mulzer, J. and Rinner, U. (2014) ‘Synthesis of Esters and Lactones’, in *Heteroatom Manipulation*. Elsevier Ltd, pp. 355–410. Available at: <https://doi.org/10.1016/B978-0-08-097742-3.00612-1>.
191. Singh, S., Rai, A.K. and Prakash Tewari, R. (2023) ‘Recent advancement in hyaluronic acid-based hydrogel for biomedical engineering application: A mini-review’, *Materials Today: Proceedings*, 78, pp. 138–144. Available at: <https://doi.org/10.1016/j.matpr.2022.12.208>.
192. Sneiders, D. *et al.* (2019) ‘Outcomes of Single versus Double Fascicular Nerve Transfers for Restoration of Elbow Flexion in Patients with Brachial Plexus Injuries: A Systematic Review and Meta-Analysis’, *Plastic and Reconstructive Surgery*, 144(1), p. 155. Available at: <https://doi.org/10.1097/PRS.0000000000005720>.
193. Snetkov, P. *et al.* (2020) ‘Hyaluronic Acid: The Influence of Molecular Weight on Structural, Physical, Physico-Chemical, and Degradable Properties of Biopolymer’, *Polymers*, 12(8), p. 1800. Available at: <https://doi.org/10.3390/polym12081800>.
194. Snider, W.D. *et al.* (2002) ‘Signaling the Pathway to Regeneration’, *Neuron*, 35(1), pp. 13–16. Available at: [https://doi.org/10.1016/S0896-6273\(02\)00762-6](https://doi.org/10.1016/S0896-6273(02)00762-6).
195. Som, P.M., Miles, B. and Bakst, R. (2019) ‘Perineural Invasion and Its Interrelationship with Neural Repair: A Review’, *Neurographics*, 9(5), pp. 308–319. Available at: <https://doi.org/10.3174/ng.1800066>.

196. Stazi, M. *et al.* (2021) ‘Melatonin promotes regeneration of injured motor axons via MT1 receptors’, *Journal of Pineal Research*, 70(1), p. e12695. Available at: <https://doi.org/10.1111/jpi.12695>.
197. Steenhuis, H.-J. and Bruijn, E. (2006) ‘Empirical research in OM: three paradigms [004-0203]’, in.
198. Stewart, C.E. *et al.* (2020) ‘Machine intelligence for nerve conduit design and production’, *Journal of Biological Engineering*, 14(1), p. 25. Available at: <https://doi.org/10.1186/s13036-020-00245-2>.
199. Stocco, E. *et al.* (2021) ‘Bioactivated Oxidized Polyvinyl Alcohol towards Next-Generation Nerve Conduits Development’, *Polymers*, 13(19), p. 3372. Available at: <https://doi.org/10.3390/polym13193372>.
200. Sulek, J. *et al.* (2022) ‘Cytotoxicity of Methacrylate Dental Resins to Human Gingival Fibroblasts’, *Journal of Functional Biomaterials*, 13(2), p. 56. Available at: <https://doi.org/10.3390/jfb13020056>.
201. Sumarwoto, T.-, Poetera, C.Y. and Abimanyu, D. (2021) ‘Peripheral nerve injury and its regeneration processes: a biomolecular point of view’, *Bali Medical Journal*, 10(2), pp. 927–934. Available at: <https://doi.org/10.15562/bmj.v10i2.2343>.
202. Takahashi, R. *et al.* (2021) ‘Tough, permeable and biocompatible microfluidic devices formed through the buckling delamination of soft hydrogel films’, *Lab on a Chip*, 21(7), pp. 1307–1317. Available at: <https://doi.org/10.1039/D0LC01275K>.
203. Talaei, A. *et al.* (2023) ‘Optimizing the composition of gelatin methacryloyl and hyaluronic acid methacryloyl hydrogels to maximize mechanical and transport properties using response surface methodology’, *Journal of Biomedical Materials Research Part B: Applied Biomaterials*, 111(3), pp. 526–537. Available at: <https://doi.org/10.1002/jbm.b.35169>.
204. Tammi, R. *et al.* (1994) ‘Hyaluronan Metabolism in Skin’, *Progress in Histochemistry and Cytochemistry*, 29(2), p. III–77. Available at: [https://doi.org/10.1016/S0079-6336\(11\)80023-9](https://doi.org/10.1016/S0079-6336(11)80023-9).
205. Tengblad, A. *et al.* (1986) ‘Concentration and relative molecular mass of hyaluronate in lymph and blood’, *Biochemical Journal*, 236(2), pp. 521–525. Available at: <https://doi.org/10.1042/bj2360521>.
206. Thirumalaisamy, R. *et al.* (2021) ‘Molecular insights of hyaluronic acid-hydroxychloroquine conjugate as a promising drug in targeting SARS-CoV-2 viral

- proteins’, *Journal of Molecular Structure*, 1238, p. 130457. Available at: <https://doi.org/10.1016/j.molstruc.2021.130457>.
207. Tian, W. *et al.* (2021) ‘Reveal the Relationship Between Hyaluronic Acid and Water Using Aquaphotomics’, *Asian Journal of Complementary and Alternative Medicine*, 9. Available at: <https://doi.org/10.53043/2347-3894.acam90006>.
208. Tian, X. *et al.* (2022) ‘A rethinking of collagen as tough biomaterials in meat packaging: assembly from native to synthetic’, *Critical Reviews in Food Science and Nutrition*, 0(0), pp. 1–21. Available at: <https://doi.org/10.1080/10408398.2022.2111401>.
209. Tiwari, S. and Bahadur, P. (2019) ‘Modified hyaluronic acid based materials for biomedical applications’, *International Journal of Biological Macromolecules*, 121, pp. 556–571. Available at: <https://doi.org/10.1016/j.ijbiomac.2018.10.049>.
210. Tsanaktsidou, E., Kammona, O. and Kiparissides, C. (2019) ‘On the synthesis and characterization of biofunctional hyaluronic acid based injectable hydrogels for the repair of cartilage lesions’, *European Polymer Journal*, 114, pp. 47–56. Available at: <https://doi.org/10.1016/j.eurpolymj.2019.02.024>.
211. Turathum, B., Gao, E.-M. and Chian, R.-C. (2021) ‘The Function of Cumulus Cells in Oocyte Growth and Maturation and in Subsequent Ovulation and Fertilization’, *Cells*, 10(9), p. 2292. Available at: <https://doi.org/10.3390/cells10092292>.
212. Turgut, M. and Kaplan, S. (2011) ‘Effects of Melatonin on Peripheral Nerve Regeneration’, *Recent Patents on Endocrine, Metabolic & Immune Drug Discovery*, 5(2), pp. 100–108. Available at: <https://doi.org/10.2174/187221411799015336>.
213. Turner, N.J. *et al.* (2004) ‘A novel hyaluronan-based biomaterial (Hyaff-11®) as a scaffold for endothelial cells in tissue engineered vascular grafts’, *Biomaterials*, 25(28), pp. 5955–5964. Available at: <https://doi.org/10.1016/j.biomaterials.2004.02.002>.
214. Tzagiollari, A. *et al.* (2022) ‘Biodegradable and Biocompatible Adhesives for the Effective Stabilisation, Repair and Regeneration of Bone’, *Bioengineering*, 9(6), p. 250. Available at: <https://doi.org/10.3390/bioengineering9060250>.
215. Varier, P. *et al.* (2022) ‘A Brief Review of In Vitro Models for Injury and Regeneration in the Peripheral Nervous System’, *International Journal of Molecular Sciences*, 23(2), p. 816. Available at: <https://doi.org/10.3390/ijms23020816>.
216. Vasvani, S., Kulkarni, P. and Rawtani, D. (2020) ‘Hyaluronic acid: A review on its biology, aspects of drug delivery, route of administrations and a special emphasis on

- its approved marketed products and recent clinical studies’, *International Journal of Biological Macromolecules*, 151, pp. 1012–1029. Available at: <https://doi.org/10.1016/j.ijbiomac.2019.11.066>.
217. Venkata Krishna, D. and Ravi Sankar, M. (2023) ‘Engineered approach coupled with machine learning in biofabrication of patient-specific nerve guide conduits - Review’, *Bioprinting*, 30, p. e00264. Available at: <https://doi.org/10.1016/j.bprint.2023.e00264>.
218. Ventura-Hunter, C. *et al.* (2022) ‘Glycerol methacrylate-based copolymers: Reactivity ratios, physicochemical characterization and cytotoxicity’, *European Polymer Journal*, 178, p. 111478. Available at: <https://doi.org/10.1016/j.eurpolymj.2022.111478>.
219. Vigetti, D. *et al.* (2014) ‘Hyaluronan: Biosynthesis and signaling’, *Biochimica et Biophysica Acta (BBA) - General Subjects*, 1840(8), pp. 2452–2459. Available at: <https://doi.org/10.1016/j.bbagen.2014.02.001>.
220. Vijayavenkataraman, S. (2020) ‘Nerve guide conduits for peripheral nerve injury repair: A review on design, materials and fabrication methods’, *Acta Biomaterialia*, 106, pp. 54–69. Available at: <https://doi.org/10.1016/j.actbio.2020.02.003>.
221. Wang, G. and Yang, L. (2019) ‘Development History, Progress and Future Prospects of Biomechanics and Biorheology in Chongqing University: For Specially Celebrating the Centennial of Professor Yuan-Cheng Fung’, *Molecular & Cellular Biomechanics*, 16(S2), pp. 10–10. Available at: <https://doi.org/10.32604/mcb.2019.08410>.
222. Wang, K. *et al.* (2020) ‘Using cross-linked hyaluronic acid gel to prevent postoperative lumbar epidural space adhesion: in vitro and in vivo studies’, *European Spine Journal*, 29(1), pp. 129–140. Available at: <https://doi.org/10.1007/s00586-019-06193-w>.
223. Wang, K.-K. *et al.* (1998) ‘Hyaluronic acid enhances peripheral nerve regeneration in vivo’, *Microsurgery*, 18(4), pp. 270–275. Available at: [https://doi.org/10.1002/\(SICI\)1098-2752\(1998\)18:4<270::AID-MICR11>3.0.CO;2-V](https://doi.org/10.1002/(SICI)1098-2752(1998)18:4<270::AID-MICR11>3.0.CO;2-V).
224. Wareham, L.K., Risner, M.L. and Calkins, D.J. (2020) ‘Protect, Repair, and Regenerate: Towards Restoring Vision in Glaucoma’, *Current Ophthalmology Reports*, 8(4), pp. 301–310. Available at: <https://doi.org/10.1007/s40135-020-00259-5>.

225. Weigel, P.H. and DeAngelis, P.L. (2007) ‘Hyaluronan Synthases: A Decade-plus of Novel Glycosyltransferases *’, *Journal of Biological Chemistry*, 282(51), pp. 36777–36781. Available at: <https://doi.org/10.1074/jbc.R700036200>.
226. Weigel, P.H., Hascall, V.C. and Tammi, M. (1997) ‘Hyaluronan Synthases *’, *Journal of Biological Chemistry*, 272(22), pp. 13997–14000. Available at: <https://doi.org/10.1074/jbc.272.22.13997>.
227. Wongprayoon, P. and Govitrapong, P. (2015) ‘Melatonin attenuates methamphetamine-induced neuroinflammation through the melatonin receptor in the SH-SY5Y cell line’, *Neurotoxicology*, 50, pp. 122–130. Available at: <https://doi.org/10.1016/j.neuro.2015.08.008>.
228. Xia, L. *et al.* (2023) ‘LncRNA HAGLR promotes the proliferation, migration, and neurotrophic factor production of Schwann cells via miR-204/CDK5R1 after sciatic nerve injury’, *Journal of Neuropathology & Experimental Neurology*, 82(4), pp. 324–332. Available at: <https://doi.org/10.1093/jnen/nlad010>.
229. Yang, C.-Y. *et al.* (2021) ‘Neural tissue engineering: the influence of scaffold surface topography and extracellular matrix microenvironment’, *Journal of Materials Chemistry B*, 9(3), pp. 567–584. Available at: <https://doi.org/10.1039/D0TB01605E>.
230. Yang, X. *et al.* (2022) ‘Multifunctional chitin-based hollow nerve conduit for peripheral nerve regeneration and neuroma inhibition’, *Carbohydrate Polymers*, 289, p. 119443. Available at: <https://doi.org/10.1016/j.carbpol.2022.119443>.
231. Yang, Y. *et al.* (2023) ‘A multi-responsive targeting drug delivery system for combination photothermal/chemotherapy of tumor’, *Journal of Biomaterials Science, Polymer Edition*, 34(2), pp. 166–183. Available at: <https://doi.org/10.1080/09205063.2022.2112310>.
232. Yao, Z. *et al.* (2022) ‘Magnesium-Encapsulated Injectable Hydrogel and 3D-Engineered Polycaprolactone Conduit Facilitate Peripheral Nerve Regeneration’, *Advanced Science*, 9(21), p. 2202102. Available at: <https://doi.org/10.1002/advs.202202102>.
233. Yao, Z.-Y. *et al.* (2021) ‘Versatile strategies for bioproduction of hyaluronic acid driven by synthetic biology’, *Carbohydrate Polymers*, 264, p. 118015. Available at: <https://doi.org/10.1016/j.carbpol.2021.118015>.

234. Zhang, Y. and Xing, X. (2018) ‘Classifications of Soft-Tissue Injuries’, in Y. Zhang (ed.) *Clinical Classification in Orthopaedics Trauma*. Singapore: Springer, pp. 635–638. Available at: https://doi.org/10.1007/978-981-10-6044-1_13.
235. Zhao, C. *et al.* (2006) ‘Surface Treatment of Flexor Tendon Autografts with Carbodiimide-Derivatized Hyaluronic Acid: An in Vivo Canine Model’, *JBJS*, 88(10), p. 2181. Available at: <https://doi.org/10.2106/JBJS.E.00871>.
236. Zheng, B. and Tuszynski, M.H. (2023) ‘Regulation of axonal regeneration after mammalian spinal cord injury’, *Nature Reviews Molecular Cell Biology*, pp. 1–18. Available at: <https://doi.org/10.1038/s41580-022-00562-y>.
237. Zheng, T. *et al.* (2022) ‘YR/DFO@DCNT functionalized anisotropic micro/nano composite topography scaffolds for accelerating long-distance peripheral nerve regeneration’, *Composites Part B: Engineering*, 246, p. 110242. Available at: <https://doi.org/10.1016/j.compositesb.2022.110242>.
238. Zuchero, J.B. (2014) ‘Purification and Culture of Dorsal Root Ganglion Neurons’, *Cold Spring Harbor protocols*, 2014(8), pp. 813–814. Available at: <https://doi.org/10.1101/pdb.top073965>.

APPENDICES

APPENDIX 1. JOURNAL PUBLICATIONS



Review

Hyaluronic Acid: A Review of the Drug Delivery Capabilities of This Naturally Occurring Polysaccharide

Clara Buckley ^{1,2}, Emma J. Murphy ^{1,3}, Therese R. Montgomery ⁴ and Ian Major ^{1,*}

¹ PRISM Research Institute, Technological University of the Shannon, N87 HD68 Athlone, Ireland

² Biosciences Research Institute, Technological University of the Shannon, V94 ECST Limerick, Ireland

³ LIFE Research Institute, Technological University of the Shannon, V94 ECST Limerick, Ireland

⁴ School of Science and Computing, Atlantic Technological University, H91 T8NW Galway, Ireland

* Correspondence: ian.major@tus.ie

Abstract: The inclusion of physiologically active molecules into a naturally occurring polymer matrix can improve the degradation, absorption, and release profile of the drug, thus boosting the therapeutic impact and potentially even reducing the frequency of administration. The human body produces significant amounts of polysaccharide hyaluronic acid, which boasts exceptional biocompatibility, biodegradability, and one-of-a-kind physicochemical features. In this review, we will examine the clinical trials currently utilizing hyaluronic acid and address the bright future of this versatile polymer, as well as summarize the numerous applications of hyaluronic acid in drug delivery and immunomodulation.

Keywords: naturally-occurring polymers; polysaccharide; immunotherapies; bioactives; heteropolysaccharides; drug-delivery



Citation: Buckley, C.; Murphy, E.J.; Montgomery, T.R.; Major, I.

Hyaluronic Acid: A Review of the Drug Delivery Capabilities of This Naturally Occurring Polysaccharide. *Polymer* 2022, 14, 3442. <https://doi.org/10.3390/polymer14173442>

Academic Editor: Sergio Costari

Received: 2 August 2022

Accepted: 19 August 2022

Published: 23 August 2022

Publisher's Note: MDPI stays neutral with regard to jurisdictional claims in published maps and institutional affiliations.



Copyright: © 2022 by the authors. Licensee MDPI, Basel, Switzerland. This article is an open access article distributed under the terms and conditions of the Creative Commons Attribution (CC BY) license (<https://creativecommons.org/licenses/by/4.0/>).

1. Introduction

Hyaluronic acid (HA) is a naturally occurring mucopolysaccharide that belongs to a group of heteropolysaccharides referred to as glycosaminoglycans (GAGs) [1–3]. Mucopolysaccharides are long chain sugar molecules commonly found in mucus or joint fluid in the body. Endogenous HA is found throughout the human body in the vitreous humour, joints, umbilical cord, connective tissue, and skin. Naturally, occurring HA is commonly isolated from sources such as rooster comb for industrial applications requiring an animal source. However, it can also be synthesized using biotechnological processes and recombinant DNA technologies in bacterial expression systems such as *Lactococcus*. A species of bacteria that can naturally produce HA and therefore HA can be isolated from, is *Streptococcus*. However, *Streptococcus* is a pathogen that produces several endotoxins, rendering end-stage product isolation difficult. As a result, other approaches such as cell-free HA synthesis or genetic engineering of microorganisms that do not create endotoxins have been developed [4]. This freely accessible natural polysaccharide has a wide range of applications due to its unique physicochemical and bioactive properties, which will be explored in depth throughout this review. Furthermore, HA is biocompatible and biodegradable, making it a safe biomaterial for biomedical applications such as biomedical engineering, as well as finding applications in the cosmetics industry, wound healing, and drug delivery [5–7]. Through this review, we will first discuss the discovery of HA, followed by an in-depth analysis of its physicochemical and bioactive properties, as well as its synthesis and degradation, functionalization, and applications in drug delivery, wound healing, and cancer therapeutics. In conclusion, we will review the potentially bright future of HA, with a particular emphasis on ongoing as well as forthcoming clinical trials.



Contents lists available at ScienceDirect

International Journal of Biological Macromolecules

journal homepage: www.elsevier.com/locate/ijbiomac

Modification of hyaluronic acid to enable click chemistry photo-crosslinking of hydrogels with tailorable degradation profiles

Giara Buckley^a, Therese R. Montgomery^b, Tomasz Szank^c, Brian A. Murray^d, Cormac Quigley^b, Ian Major^{a,*}

^a *NSRF Research Institute, Technological University of the Shannon, Athlone NS7 ND68, Ireland*

^b *School of Science and Computing, Atlantic Technological University, Galway NS1 1BNW, Ireland*

^c *Simonsium Research Institute, Technological University of the Shannon, Athlone NS7 ND68, Ireland*

^d *Department of Science, Technological University Dublin - Tallaght Campus, Dublin D24 EK7D, Ireland*

ARTICLE INFO

Keywords:
Hyaluronic acid
Photopolymerisation
Click-chemistry

ABSTRACT

Hyaluronic acid (HA) is a naturally occurring mucopolysaccharide that, due to its inherent bioactivity and extracellular matrix-like structure, has the potential to be utilised extensively in tissue engineering. However, this glycosaminoglycan lacks the properties required for cellular adhesion and photo-crosslinking by UV light, which significantly hinders this polymer's applicability. This research presents a method for modifying hyaluronic acid via thiolation and methacrylation to generate a novel photo-crosslinkable polymer with improved physicochemical properties, biocompatibility and the potential to customize biodegradability according to the ratio of monomers used. A decrease in stiffness proportional to increasing thiol concentration was observed when testing the compressive strength of hydrogels. Conversely, it was noted that the storage moduli of hydrogels increased proportionally to thiol concentration indicating a greater degree of cross-linking with the addition of thiol. The addition of thiol to HA increased the biocompatibility of the material in both neuronal and glial cell lines and improved the degradability of methacrylated HA. Due to the enhanced physicochemical properties and biocompatibility imparted by the introduction of thiolated HA, this novel hydrogel system could have numerous bioengineering applications.

1. Introduction

Hyaluronic acid (HA) is a naturally occurring mucopolysaccharide that belongs to the glycosaminoglycan (GAGs) family of heteropolysaccharides. GAGs have multiple functions in the human body, including roles in cell development and proliferation [1] and wound healing [2]. Due to their essential roles in the extracellular matrix, many GAGs, such as heparin sulfate and HA, are of great interest as biomaterials. Interestingly, HA is the only GAG that lacks sulfation and, as a result, cannot bind to a core protein to create a proteoglycan [3]. HA is created endogenously in the human body and is present in all bodily fluids, from synovial fluid to urine [4]. It is this endogenous character that makes it of particular interest over polymers with similar properties such as chitosan or pectin. Certain bacterial species, such as *Streptococcus*, have evolved the ability to synthesise HA; nevertheless, the presence of endotoxins renders them an undesirable and laborious source of HA for industrial purposes. Biotechnological production of HA

primarily utilises genetically modified strains of *Lactobacillus*, which, unlike *Streptococcus*, do not create endotoxins and are generally regarded as safe (GRAS) [5].

Due to its unique viscoelastic properties, HA has been at the forefront of biomaterials for many years [6]. These properties enable the use of HA in a variety of forms, from microgels [7], nanogels [8], and cryogels [9] to nanoparticle conjugates [10]. In addition, HA has an exceptional ability to bind water, which permits a variety of applications ranging from topical to injectable hydrogels [11]. Native HA is easily degraded by endogenous enzymes known as hyaluronidases, which is a significant limitation [12]. These enzymes cleave the glycosidic bond, degrading the HA polysaccharide from a high-molecular-weight (HMW) chain to low-molecular-weight (LMW) oligos (10 kilodaltons (kDa)) that have very different effects on the body. Numerous investigations have demonstrated that HMW HA (>1000 kDa) has anti-immunogenic and anti-angiogenic effects, whereas LMW HA is immune-stimulatory and pro-angiogenic [13,14]. Due to the viscosity exhibited even at low concentrations, HMW HA can be difficult to work with depending on the

* Corresponding author.
E-mail address: ian.major@tusa.ie (I. Major).

<https://doi.org/10.1016/j.ijbiomac.2023.124459>

Received 22 December 2022; Received in revised form 16 March 2023; Accepted 11 April 2023

Available online 16 April 2023

0141-8130/© 2023 The Author(s). Published by Elsevier B.V. This is an open access article under the CC BY license (<http://creativecommons.org/licenses/by/4.0/>).



An assessment of the transparency of contemporary technology education research employing interview-based methodologies

Jeffrey Buckley^{1,2} · Latif Adams³ · Ifeoluwapo Aribilola¹ · Iram Arshad¹ · Muhammad Azeem¹ · Lauryn Bracken³ · Colette Breheny¹ · Ciara Buckley¹ · Ismael Chimello⁴ · Alison Fagan³ · Daniel P. Fitzpatrick³ · Diana Garza Herrera¹ · Guilherme Daniel Gomes¹ · Shaun Grassick³ · Elaine Halligan¹ · Amit Hirway¹ · Tomás Hyland¹ · Muhammad Babar Imtiaz¹ · Muhammad Bilal Khan¹ · Eduardo Lanzagorta Garcia¹ · Paul Lennon^{1,5} · Eyman Manaf¹ · Jing Meng⁴ · Mohd Sufino Zuhaily Mohd Sufian^{4,6} · Adrielle Moraes¹ · Katja Magdalena Osterwald³ · Anastasia Platonava⁴ · Clodagh Reid¹ · Michèle Renard³ · Laura G. Rodriguez-Barroso¹ · Bianca Simonassi-Paiva³ · Maulshree Singh¹ · Tomasz Szank³ · Mehwish Tahir¹ · Sowmya Vijayakumar¹ · Cormac Ward³ · Xinyu Yan^{1,7} · Ismin Zainol¹ · Lin Zhang¹

Accepted: 10 August 2021

© The Author(s), under exclusive licence to Springer Nature B.V. 2021

Abstract

A high level of transparency in reported research is critical for several reasons, such as ensuring an acceptable level of trustworthiness and enabling replication. Transparency in qualitative research permits the identification of specific circumstances which are associated with findings and observations. Thus, transparency is important for the repeatability of original studies and for explorations of the transferability of original findings. There has been no investigation into levels of transparency in reported technology education research to date. With a position that increasing transparency would be beneficial, this article presents an analysis of levels of transparency in contemporary technology education research studies which employed interviews within their methodologies, and which were published within the *International Journal of Technology and Design Education* and *Design and Technology Education: An International Journal* ($n=38$). The results indicate room for improvement, especially in terms of documenting researcher positionality, determinations of data saturation, and how power imbalances were managed. A discussion is presented on why it is important to improve levels of transparency in reported studies, and a guide on areas to make transparent is presented for qualitative and quantitative research.

Keywords Replicability · Transparency · Trustworthiness · Repeatability · Reporting practices · Qualitative research · Technology education research

✉ Jeffrey Buckley
jbuckley@kth.se

Extended author information available on the last page of the article

Published online: 20 August 2021

Springer



How transparent are quantitative studies in contemporary technology education research? Instrument development and analysis

Jeffrey Buckley^{1,2} · Jeovan A. Araujo¹ · Ifeoluwapo Aribilola¹ · Iram Arshad¹ · Muhammad Azeem¹ · Ciara Buckley¹ · Alison Fagan¹ · Daniel P. Fitzpatrick¹ · Diana A. Garza Herrera¹ · Tomás Hyland¹ · Muhammad Babar Imtiaz¹ · Muhammad Bilal Khan¹ · Eduardo Lanzagorta Garcia¹ · Bhagyabati Moharana¹ · Mohd Sufino Zuhaily Mohd Sufian^{1,3} · Katja Magdalena Osterwald¹ · Joseph Phelan¹ · Anastasia Platonava¹ · Clodagh Reid¹ · Michèle Renard¹ · Laura G. Rodriguez Barroso¹ · Jeremiah Scully¹ · Gilberto Silva Nunes Bezerra¹ · Tomasz Szank¹ · Mehwish Tahir¹ · Mairéad Teehan¹ · Sowmya Vijayakumar¹ · Ismin Zainol¹

Accepted: 18 April 2023

© The Author(s), under exclusive licence to Springer Nature B.V. 2023

Abstract

Transparency in the reporting of empirical studies is foundational to a credible knowledge base. Higher levels of transparency, in addition to clarity in writing, also make research more accessible to a diverse readership. Previous research reviewed how transparently reported qualitative, interview-based, studies were in contemporary technology education research (Buckley et al. in *Int J Technol Des Educ*, 2021a. <https://doi.org/10.1007/s10798-021-09695-1>). The results illustrated that no article was fully transparent and that authors tended to be less transparent in some areas, such as the management of power imbalances and a saturation point, than in others, such as the methodology adopted and research setting. This article presents a similar study, however the focus of the investigation was on contemporary quantitative technology education research. An analysis of 46 articles revealed again that no article was fully transparent and that authors tended to be more transparent in some areas than others. Interestingly, the areas where authors of quantitative research tended to be more or less transparent were similar to the areas in which authors of qualitative research tended to be more or less transparent. These results have use in supporting researchers in the clear and transparent reporting of the empirical work and could be useful in the development of guides or support material for academic writing.

Keywords Transparency · Credibility · Technology education research · Quantitative research

✉ Jeffrey Buckley
jeffrey.buckley@tus.ie

Extended author information available on the last page of the article

Published online: 03 May 2023 Springer
Content courtesy of Springer Nature, terms of use apply. Rights reserved.

Review

Polysaccharides—Naturally Occurring Immune Modulators

Emma J. Murphy ^{1,2,3,*}, Gustavo Waltzer Fehrenbach ^{3,4}, Ismin Zainol Abidin ^{3,4}, Ciara Buckley ^{3,4},
Therese Montgomery ⁵, Robert Pogue ⁶, Patrick Murray ^{1,2}, Ian Major ^{3,4} and Emanuele Rezoagli ^{7,8,*}

¹ Shannon Applied Biotechnology Centre, Midwest Campus, Technological University of the Shannon, V94B2S7 Limerick, Ireland; emma.murphy@tusa.ie (E.J.M.); patrick.murray@tusa.ie (P.M.)

² LIFE Health and Biosciences Research Institute, Midwest Campus, Technological University of the Shannon, V94B2S7 Limerick, Ireland

³ PERA, Research Institute, Midlands Campus, Technological University of the Shannon, N07 1D60 Athlone, Ireland; g.fehrenbach@research.tusa.ie (G.W.F.); izabidin@research.tusa.ie (I.Z.A.); c.buckley@research.tusa.ie (C.B.); imajor@tusa.ie (I.M.)

⁴ Applied Polymer Technologies, Midlands Campus, Technological University of the Shannon, N07 1D60 Athlone, Ireland

⁵ School of Science and Computing, Atlantic Technological University, H91 10N9 Galway, Ireland; therese.montgomery@atu.ie

⁶ Universidade Católica de Brasília, CG 7 LOTE 1-Taguatinga, Brasília 71600-010, DF, Brazil; rpogue@ucb.br

⁷ Department of Emergency and Intensive Care, Fondazione IRCCS San Gerardo da Tortona, 20060 Monza, Italy

⁸ School of Medicine and Surgery, University of Milan-Bicocca, 20150 Monza, Italy

* Correspondence: emurphy@tusa.ie (E.J.M.); erezoagli@unimib.it (E.R.)

Abstract: The prevention of disease and infection requires immune systems that operate effectively. This is accomplished by the elimination of infectious and abnormal cells. Innate or biological therapy treats disease by either stimulating or inhibiting the immune system, dependent upon the circumstances. In plants, animals, and microbes, polysaccharides are abundant biomacromolecules. Due to the intricacy of their structure, polysaccharides may interact with and impact the immune response; hence, they play a crucial role in the treatment of several human illnesses. There is an urgent need for the identification of natural biomolecules that may prevent infection and treat chronic disease. This article addresses some of the naturally occurring polysaccharides of known therapeutic potential that have already been identified. This article also discusses extraction methods and immunological modulatory capabilities.

Keywords: polysaccharides; immune modulation; inflammation; naturally occurring polymers



Citation: Murphy, E.J.; Fehrenbach, G.W.; Abidin, I.Z.; Buckley, C.; Montgomery, T.; Pogue, R.; Murray, P.; Major, I.; Rezoagli, E.

Polysaccharides—Naturally Occurring Immune Modulators. *Polymers* **2023**, *15*, 2373. <https://doi.org/10.3390/polym15102373>

Academic Editor: Umiliana Fedrli

Received: 4 March 2023

Revised: 4 May 2023

Accepted: 7 May 2023

Published: 19 May 2023



Copyright: © 2023 by the authors. Licensee MDPI, Basel, Switzerland. This article is an open access article distributed under the terms and conditions of the Creative Commons Attribution (CC BY) license (<https://creativecommons.org/licenses/by/4.0/>).

1. Introduction

Biomaterials have substantially disparate functions and structural properties. They have played a critical role in a wide range of healthcare challenges, fostering significant advancements in several biomedical sectors, such as tissue engineering, medical implants, drug delivery, and immunotherapies [1–3]. Numerous healthcare products use biopolymers either as functional excipients or as active ingredients [4].

Polymers are a large group of natural or synthetic compounds that are comprised of macromolecules. These macromolecules in turn are composed of smaller monomers. Biopolymers are natural polymers that exist in nature, and include proteins, polysaccharides, cellulose, natural rubber, silk, and wool. Polymers can also be biobased, manufactured artificially from natural sources [5]. Synthetic polymers include nylon, polyethylene, polyester, Teflon, and epoxy. Polymeric biomolecules are typically classed based on their monomeric unit [6–9].

Natural polymers are often favoured over synthetic ones for many reasons. They are abundant in nature, thus more accessible, and are easier to modify chemically. Additional advantages are that they are renewable, non-toxic, stable, hydrophilic, biocompatible, and

APPENDIX 2. CONFERENCE ABSTRACTS

Poster number: PT146 (PP)

Theme: Novel treatments & translational neuroscience

The modification of hyaluronic acid (HLA) with n-acetylcysteine (NAC) to enable 3D printing of a robust nerve guidance conduit for peripheral nerve repair

Authors: Ms Ciara Buckley^{1,2}, Dr Ian Major², Dr Therese Montgomery¹

¹Bioscience Research Institute (BRI), Athlone Institute of Technology, Ireland, ²Materials Research Institute (MRI), Athlone Institute of Technology, Ireland

SP = Standard poster

PP = Preregistration poster

BNA2019 POSTER ABSTRACTS

SESSION 3

TUESDAY 16th APRIL

Introduction: Significant research is ongoing as scientists attempt to develop alternative strategies to enhance nerve regeneration following damage or disease. Many therapeutic options currently available are highly invasive and use materials commonly rejected by the body. Effective regeneration is not permitted without the use of a guidance conduit to bridge the defect in the event of a large gap in the peripheral nerve. Without a conduit, there is a high risk of fibrous scar tissue formation which inhibits migration of the regenerating axon. Hyaluronic acid (HLA) is a human endogenous polymer which has been shown to enhance nerve regeneration *in vivo* (1). Through the modification of HLA with N-acetylcysteine (NAC), we hope to combine the nerve regenerating potential of HLA with the anti-oxidant and anti-inflammatory effects of NAC (2) and to produce a superior novel nerve guidance conduit.

Methods: HLA will be modified using the well-characterised Steglich esterification reaction to produce HLA-NAC. Once the nature of the product has been confirmed via ATR-FTIR and NMR, HLA-NAC will be photo-polymerised, to produce a biocompatible polymer of sufficient mechanical strength. Any bioactivity and/or cytotoxicity associated with the above materials will be tested in neuronal and glial cell lines. Following successful testing, the material will be 3D printed as a conduit and undergo further testing in 3D neuronal co-cultures.

Approach for statistical analysis: All assay data will be analysed using one-way Anova with an appropriate post-hoc test to establish significant results. Additionally, all imaging will be performed double-blinded to prevent experimental bias.

References

- Wang, K., Nemeth, I., Seckel, B., Chakalis-Haley, D., Swann, D., Kuo, J., ... Cetrulo, C. (1998). Hyaluronic acid enhances peripheral nerve regeneration *in vivo*. *Microsurgery*.
- Bhatti, J., Nascimento, B., Akhtar, U., Rhind, S., Tien, H., Nathens, A., & Teodoro da Luz, L. (2018). Systematic Review of Human and Animal Studies Examining the Efficacy and Safety of N-Acetylcysteine (NAC) and N-Acetylcysteine Amide (NACA) in Traumatic Brain Injury: Impact on Neurofunctional Outcome and Biomarkers of Oxidative Stress and Inflammation. *Frontiers in Neurology*.

Modification of hyaluronic acid for stereolithography 3D printing of hydrogel nerve conduits

Unique Code: TP001300

Authors: Ciara Buckley - Materials Research Institute Athlone Institute of Technology, Dr. Ian Major - Materials Research Institute Athlone Institute of Technology, Dr. Therese R. Montgomery - Bioscience Research Institute Athlone Institute of Technology,

Topic: Disorders, treatments and translational neuroscience

Introduction:

Peripheral nerve injuries (PNIs) arise from trauma or illness and can result in functional loss in that part of the body. Such injuries are reported in 15-40% of all trauma cases¹.

Despite our extensive knowledge of the pathophysiology and regenerative mechanisms of PNIs, a therapeutic intervention capable of full functional recovery has yet to be developed.

Theoretically, nerve guidance conduits (NGC) can act as a bridge between two injured nerve ends, thus providing structural and trophic support for regenerating axons. Several of these conduits are under clinical investigation but few have made it to market.

Utilising a novel blend of biopolymers, polyethylene glycol dimethacrylate (PEGDMA) and hyaluronic acid (HLA), we hope to identify a suitable biomaterial for the 3D printing of NGC candidates.

Methods:

The effect of low molecular weight (LMW) (30-50kDa) HLA on neuronal (SH-SY5Y) and glial (RT4 D6P2T) cells was investigated using the MTT assay, resazurin reduction (RR) assay and the trypan blue exclusion (TBE) assay. The results were then compared with HLA of increasing MW in order to select the optimal MW which allowed for neuronal and glial cell proliferation and attachment.

Statistical approach:

Statistical analysis was conducted using one-way and two-way ANOVA in Graphpad Prism with Tukey and Sidak's post-hoc tests respectively.

Results and conclusions:

LMW HLA did not induce cytotoxicity with the RR and the TBE assay. However, when assayed using MTT, significant toxicity in both cell lines was observed, with the SH-SY5Y appearing more susceptible. It was determined that this overestimation of cytotoxicity was due to enhanced cell detachment during MTT exposure in SH-SY5Y cells and not HLA-induced cell death, thus bringing into question the suitability of the MTT assay for SH-SY5Y experiments. Future experiments will focus on the modification of LMW HLA for incorporation into a NGC with novel biotherapeutics and PEGDMA.

References:

1. Gong H, Fei H, Xu Q, Gou M, Chen HH. 3D-engineered GelMA conduit filled with ECM promotes regeneration of peripheral nerve. *J Biomed Mater Res.* 2020 Mar;108(3):805–13.

P04-48**A cautionary note on the utility of MTT in toxicity screening***C. Buckley^{1,2}, I. Major¹, T.R. Montgomery²¹ Athlone Institute of Technology, Materials Research Institute, Westmeath, Ireland;² Athlone Institute of Technology, Biosciences Research Institute, Westmeath, Ireland

Introduction: The MTT (3-(4, 5-dimethylthiazolyl-2)-2, 5-diphenyltetrazolium bromide) assay has long been considered the gold standard cytotoxicity assay due to its sensitivity (Carreño *et al.*, 2021) and noted reliability of cellular metabolic activity in a variety of adherent cell lines. The activity of MTT is reliant on the reduction of MTT to its insoluble formazan by nicotinamide adenine dinucleotide phosphate (NADPH)-dependent cellular oxidoreductase enzymes (Larramendy and Soloneski, 2018). However, the rate of formation of these crystals is dependent on the metabolic rate and quantity of mitochondria. This study shows that the suitability of MTT must be considered on an individual project by project basis with regard to cell type and potential synergistic drug interactions.

Methods: The effect of low molecular weight (LMW) (30–50kDa) hyaluronic acid (HLA) on neuronal (SH-SY5Y) and glial (RT4 D6P2T) cell lines was investigated using the MTT assay, resazaurin reduction (RR) assay and the trypan blue exclusion (TBE) assay. The results were then compared to elucidate the accuracy of each of the bioassays used.

Statistical approach: Statistical analysis was conducted using one-way analysis of variance for statistical significance between a single factor, with Tukey post-hoc tests. A two-way analysis of variance with Sidak's post-hoc test was used where more than one independent factor existed. $P < 0.05$ was considered to represent a statistically significant difference.

Results and conclusions: LMW HLA was significantly cytotoxic when assayed using the MTT assay in both cell lines. These results could not be replicated using RR, which works on a similar method of action to the MTT, or the live/dead TBE bioassays. Through investigation, it was determined that the apparent overestimation of cytotoxicity by the MTT assay was due to enhanced cellular detachment of live cells due to the MTT reagent itself and not mechanical disruption through assay procedure.

References

- [1] Carreño, E. A. *et al.* (2021) 'Considerations and Technical Pitfalls in the Employment of the MTT Assay to Evaluate Photosensitizers for Photodynamic Therapy', *Applied Sciences*, 11(6), p. 2603. doi: 10.3390/app11062603.
- [2] Larramendy, M. and Soloneski, S. (2018) *Genotoxicity: A Predictable Risk to Our Actual World*. BoD – Books on Demand.

permeabilised cells and the ETC can be identified. Aiming to assess changes in mitochondrial specific these approaches we assessed the MMP/cytotoxicity, the cell assays in HepG2 cells with a specificity and accuracy of 78%, 73% and 41,100 and 73%, respectively. Compounds flagged as positive in MitoROS assays but not in other assays include compounds in permeabilising mechanisms of action, I and IV inhibitors respectively. OCR, RC and ECAR provide mitochondrial toxicity. An alternative to the Glu/Gal assay. The MitoSOX assay although more detailed in dermal toxicants was provided.

P04-50**An *in vitro* Cell Model for Regulation Utilizing hTERT Dermal Melanocytes***N. Perera¹, M. Spencer², L.¹ LGC, Teddington, UK;² ATCC Cell Systems, Gaithersburg, MD, USA

Skin pigmentation is a complex process involving the synthesis, transport, and packaging of melanin into melanosomes, which are then endocytosed by keratinocytes. Melanocytes play roles in controlling skin pigmentation and production. Mutations in melanocyte genes can lead to skin disorders, including hyper- and hypopigmentation. A model for elucidating melanocyte regulation by the surrounding keratinocytes is needed. However, primary melanocyte variability and limited lifespan are major limitations in more robust human cell culture models and agents which can be used to study melanocyte regulation.

In this study, we immortalized primary melanocytes by expressing hTERT in cells that were immortalized primary melanocytes from more than 35 population.

APPENDIX 3. POSTER PRESENTATIONS

THE SUNDAY TIMES
GOOD UNIVERSITY GUIDE
2018
INSTITUTE OF TECHNOLOGY OF THE YEAR

An investigation into the effect of hyaluronic acid (HLA) polymer size on neuronal and glial cell viability and attachment

¹ Claire Buckley, ² Ian Major, ² Therese R. Montgomery
¹ Biosciences Research Institute, Athlone Institute of Technology
² Materials Research Institute, Athlone Institute of Technology

Introduction

Cytotoxicity testing of LMW HLA

HLA is a human endogenous glycosaminoglycan, discovered by Karl Meyer in 1936. In the vitreous humour of bovine eyes and in a low concentration of the avian callus embryo (CE) found in avian cell nuclei in the body. It is normally synthesised by a class of integral membrane proteins called hyaluronan synthase, and degraded by a family of enzymes called hyaluronidases.

Since HLA was first demonstrated to enhance peripheral nerve repair (PFR) *in vivo* over 21 years ago, there has been an increasing focus on the use of HLA in the development of nerve conduits for PFR (4). Despite the diverse range of polymer lengths reported in the literature, ranging from 100-2000kDa to human amniotic fluid 6000-7000kDa (5), the majority of studies to date have utilised high molecular weight (HMW) HLA, such as that incorporated into a biphasic nerve guidance conduit (hGQ) recently developed by Snijders, A. et al (6), regardless of the high production costs incurred during commercial production.

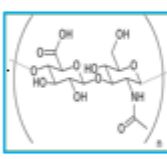


Figure 2.1 Structure of HLA

LMW HLA (8-50kDa and 30-50kDa) reduces the proliferation of SH-SY5Y cells

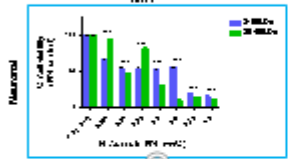


Figure 3.1 Proliferation of SH-SY5Y cells in the presence and absence of HLA. SH-SY5Y cell proliferation was measured using MTT. ***p < 0.001. Error bars represent standard deviation. n = 3.

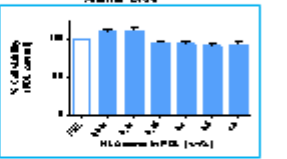


Figure 3.2 Proliferation of SH-SY5Y cells in the presence and absence of HLA. SH-SY5Y cell proliferation was measured using Alamar Blue. ***p < 0.001. Error bars represent standard deviation. n = 3.

LMW HLA significantly reduced SH-SY5Y cell viability and attachment when assayed using MTT (Figure 3.1/3.2) but not when assayed with Alamar blue.

30-50kDa HLA had a significantly greater effect than 8-50kDa on cell viability and attachment in RT4-D6P2T cells (Figure 3.3)

Aims & Objectives

SH-SY5Y cell attachment assay

The aim of this study was to evaluate if low molecular weight (LMW) HLA could reversibly affect neuronal and glial cell viability and attachment, with a view to the future design of a low cost, reversible nerve conduit for nerve repair.

LMW HLA (30-50 kDa) reduces SH-SY5Y cellular attachment but not cell viability



Figure 4.1 Attachment of SH-SY5Y cells to 30-50kDa HLA. SH-SY5Y cell attachment was measured using MTT. ***p < 0.001. Error bars represent standard deviation. n = 3.



Figure 4.2 Attachment of SH-SY5Y cells to 30-50kDa HLA. SH-SY5Y cell attachment was measured using Alamar Blue. ***p < 0.001. Error bars represent standard deviation. n = 3.

Data show the reversible nature of the independent attachment, conducted in triplicate. The cell loss observed in Figure 4.2 combined with the reversible counting shown in Figure 4.1. LMW HLA significantly reduces cellular attachment in SH-SY5Y cells in a dose-dependent manner.

Methods

Discussion

1. Cell models

Two continuous cell lines were used in this study, glial cell line to represent the Schwann cells found in the PNS and human neuronal cell line.

Glial cell line:
The RT4-D6P2T cell line is an immortalised Schwann cell line derived from an adult rat sciatic nerve (RV) induced for peripheral neuropathy (4).

Neuronal cell line: SH-SY5Y is an immortalised human neuroblastoma cell line routinely employed as neuronal model in *in vitro* and *in vivo* used in this study (5,6).

2. Cytotoxicity testing of LMW HLA

- Cell proliferation in the presence and absence of HLA were detected via spectrophotometry, using the viability assay MTT and Alamar Blue. 24-well plates were coated in HLA (8-50kDa and 30-50kDa) overnight followed by 24-hour drug elution. Seeding cells at a density of 0.5-10⁵ cells/well.



Figure 2.1 Flow diagram of cytotoxicity methodology

3. SH-SY5Y cell attachment assay

- The ability of the cells to attach to the 30-50kDa HLA was measured via the viability of detached cells following 24-hour HLA exposure.
- SH-SY5Y cells were counted in 96-well plates throughout various wash steps of the procedure.
- Remaining cells remaining from 30-50kDa were assayed via the MTT assay.
- All statistical analysis was performed using one-way ANOVA in GraphPad Prism version 5.02.



Figure 2.2 Flow diagram of SH-SY5Y cell attachment assay methodology

Due to the reversible nature associated with the reversible and reversible nature of LMW HLA, only for animal studies, the reversible nature of the effect of LMW HLA on neuronal and glial cell lines as an alternative solution for the following reasons:

- Reversible nature of LMW HLA can be easily washed from neuronal surfaces due to its smaller size.
- LMW HLA exhibits less toxicity than HMW allowing easier cell culture based assays.
- LMW HLA exhibits significantly less reduction in attachment (7).

Although no cytotoxicity was observed in the glial cells, LMW HLA had a significant effect on the cell attachment measured in SH-SY5Y cells. This effect was more pronounced when using the 30-50kDa HLA vs. 8-50kDa HLA, higher concentrations only.

Conclusions and Future Work

References

This study has highlighted a reversible and reversible effect of LMW HLA on neuronal cell attachment, although a reversible nature has indicated the effectiveness of LMW HLA as both an animal cell model (8). However, more work will be required to determine the suitability of repeating doses of LMW-HMW HLA (100kDa up to 1M Da) for nerve repair as well as a nerve guidance conduit design for a neural nerve repair. This work was funded by AIT President's Seed Fund 2018.

1. Wang, C. et al. (2017) Cell adhesion and cell-cell communication in the nervous system. *Neuroscience*, 350, 1-15.
 2. Gammie, P. et al. (2017) Cell adhesion and cell-cell communication in the nervous system. *Neuroscience*, 350, 1-15.
 3. Wang, C. et al. (2017) Cell adhesion and cell-cell communication in the nervous system. *Neuroscience*, 350, 1-15.
 4. Wang, C. et al. (2017) Cell adhesion and cell-cell communication in the nervous system. *Neuroscience*, 350, 1-15.
 5. Wang, C. et al. (2017) Cell adhesion and cell-cell communication in the nervous system. *Neuroscience*, 350, 1-15.
 6. Wang, C. et al. (2017) Cell adhesion and cell-cell communication in the nervous system. *Neuroscience*, 350, 1-15.
 7. Wang, C. et al. (2017) Cell adhesion and cell-cell communication in the nervous system. *Neuroscience*, 350, 1-15.
 8. Wang, C. et al. (2017) Cell adhesion and cell-cell communication in the nervous system. *Neuroscience*, 350, 1-15.

THE SUNDAY TIMES
GOOD UNIVERSITY GUIDE
2018
INSTITUTE OF TECHNOLOGY OF THE YEAR



Modification of hyaluronic acid for stereolithography 3D printing of hydrogel nerve conduits

ORCID
IRISH RESEARCH COUNCIL
An Chomhairle um Thaighde in Eirinn

^{1,2}Clara Buckley, ²Ian Major, ¹Therese R. Montgomery
¹Biosciences Research Institute, Athlone Institute of Technology
²Materials Research Institute, Athlone Institute of Technology

Introduction

The peripheral nervous system transmits signals from the brain to the limbs and organs of the body. Peripheral nerve injuries (PNI) resulting from trauma, illness or cancer affect approximately 1 million people in Europe and the US per annum. Such injuries may result in gaps/erosion of the nerve which limits or ceases function in that part of the body and are reported in 15-40% of all trauma cases worldwide (1). Of those who undergo surgery, only 25% regain full function (2). Current therapeutic options such as autografts and allografts involve transplanting a donor nerve to the injured site. However, despite autografts being considered the gold standard for peripheral nerve repair (PNR), the chance of full functional recovery remains low. Since HLA was first demonstrated to enhance PNR *in vivo* over 21 years ago, there has been an increasing focus on the use of HLA in the development of nerve conduits for PNR.

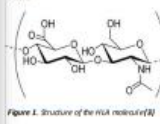


Figure 1. Structure of the HLA repeating unit (3)

Much of this research has focused on *in vivo* studies due, in part, to the unique rheological properties of HLA posing an issue for *in vitro* analysis. The objective of this first initial phase was to undertake an *in vitro* biological screen which would identify the optimal molecular weight of HLA to subject to further testing and to establish the cytotoxicity of HLA.

Given the physicochemical properties of HLA it was not possible to examine its cytotoxicity or neuro-proliferative/differentiation effects using standard *in vitro* assay approaches. Therefore, it was necessary to design and optimise a novel *in vitro* experimental approach which would allow us to assess the suitability of HLA in the presence and absence of various novel biological agents for nerve conduit design.

Aim

To produce a hydrogel nerve conduit which is inherently bioactive

Objectives

- Advanced cell culture and bioassays to determine the optimal molecular weight of hyaluronic acid and the toxicity of hyaluronic acid in neuronal and glial cell lines.
- The modification of hyaluronic acid and subsequent cross-linking to PEGDMA, to achieve a degree of substitution which will not affect cell interactions.
- Stereolithography 3D printing of a multilayer hydrogel conduit which will encourage and support regenerating neurons.

Methods

1. Cell lines

Two continuous cell lines were used in this study, a glial cell line to represent the Schwann cells found in the PNS and a human neuronal cell line. For ease of viewing, only the neuronal data is presented in this poster.

Glial cell line:

The RT4-DG92T cell line is an immortalized Schwann cell line derived from an N-ethyl-N-nitrosourea (ENU) induced rat peripheral neurotumor (4). This cell line was shown to be most similar to a myelinating Schwann cell based on the comparatively high expression of P0 and P0 mRNA (5).

Neuronal cell line:

SH-SY5Y are an immortalized human catecholaminergic cell line routinely employed as a neuronal model *in vitro* and were used undifferentiated for this study (6).

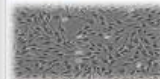


Figure 2. RT4-DG92T (glial) cell line (5)



Figure 3. SH-SY5Y (neuronal) cell line (7)

2. Identification of optimal molecular weight of HLA

HLA of molecular weights ranging from 30-50 kDa to 2200 kDa were screened in neuronal and glial cells using the resazurin and trypan blue exclusion (TBE) assays.

3. Cytotoxicity of HLA

Once the optimal molecular weight of HLA was established, this was subjected to further screening with MTT, resazurin and TBE assays. These assays were modified and validated.



Figure 4. Method flow chart for modified MTT and resazurin assays

Results

2. Identification of the optimal molecular weight of HLA

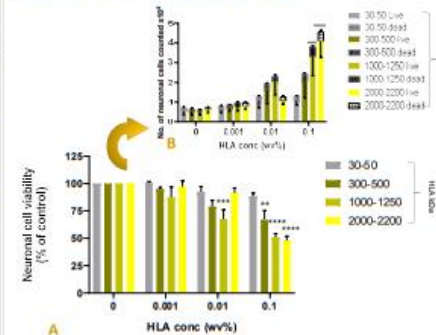


Figure 5. A. Low Molecular weight (LMW) 30-50 kDa HLA does not induce cytotoxicity in neuronal cell lines when assayed with resazurin and trypan blue. B. The effect of HLA on cellular attachment and viability was assessed using the TBE assay.

3. Cytotoxicity of 30-50 kDa HLA in neuronal cell lines

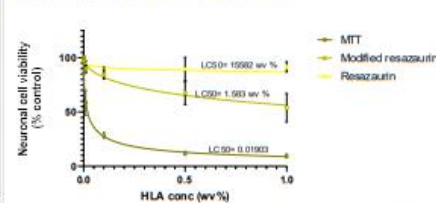


Figure 6. Enhanced MTT toxicity is not related to mechanical disruption of cells. SH-SY5Y cells were grown on 30-50 kDa HLA as before for 30 h before assaying with resazurin.

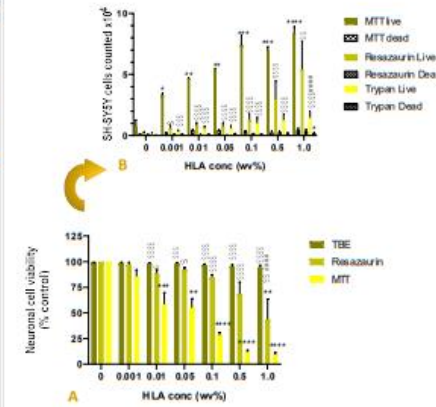


Figure 7. A. MTT enhances HLA toxicity in SH-SY5Y cells. SH-SY5Y cells were grown on 30-50 kDa HLA for 20 h before entering the MTT/resazurin/TBE protocol outlined in Fig. 4 (Count 3).

Discussion

This poster represents the completion of Phase 1. Development. The purpose of this phase was to elucidate the optimal molecular weight of HLA to subject to further testing and to determine the cytotoxicity of HLA. The results presented here have shown that:

- 30-50 kDa hyaluronic acid was the optimal molecular weight for cell attachment as shown in Fig 5
- MTT revealed toxicity of 30-50 kDa in both cell lines but SH-SY5Y cells appeared more susceptible
- These results could not be replicated with the resazurin assay despite MTT and resazurin working on a similar method of action, or the TBE bioassay
- It was determined that the overestimation of cytotoxicity was actually due to enhanced cell detachment during an MTT assay, and not cell death (Fig. 7 B)
- This result was independent of differences in the basic assay methods.

Conclusion

In conclusion, it was determined that there was a potential synergistic relationship occurring between MTT and HLA which resulted in enhanced cytotoxicity in neuronal cell lines.

Future work

The research shown here is the subject of a manuscript currently in preparation and due for submission to 'Toxicology *In Vitro*' in July 2021.

Phase 2: Formulation and testing is currently underway.

- HLA and PEGDMA are being isolated and screened in neuronal and glial cell lines.
- Material properties will be evaluated.

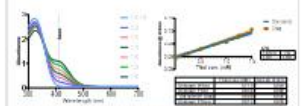


Figure 8. Quantification of thiolation via Ellman's assay. HLA modification was confirmed by the colorimetric quantification of thiols via Ellman's assay @ 412 nm.

Phase 3: Production

- Prototypes will be 3D printed using the modified polymers.
- Potential regeneration enhancing compounds will be screened for inclusion.
- Extensive preclinical testing will be performed.

Acknowledgements

This work was funded by AIT President's Doctoral Scholarship 2018 and the Irish Research Council Government of Ireland Postgraduate Scholarship, 2020.

References

- Gong, H., Fei, H., Xu, Q., Guo, M. and Chen, H., 2019. 3D-engineered GelMA conduit filled with ECM promotes regeneration of peripheral nerve. *Journal of Biomedical Materials Research Part A*, 108(3), pp. 875-883.
- Shapiro, R., 2020. *UK Research And Innovation*. [online]. Available at: <https://gtr.ukri.org/projects?ref=EP/R0104463/2/1> [Accessed 12 Mar 2021].
- Pubchem.ncbi.nlm.nih.gov. 2020. Hyaluronic Acid. [online]. Available at: <https://pubchem.ncbi.nlm.nih.gov/compound/Hyaluronic-Acid> [Accessed 18 March 2021].
- igostandards-wtc.org. 2020. RT4-DG92T ATCC® CRL-2768™ Ratios Nervous Peripheral Ner. [online]. Available at: https://www.igostandards-atc.org/products/ATCR-2768.aspx?geo_country=ie [Accessed 18 March 2021].
- Hu, M., Maja, N., O'Neill, G., Quares, R., Patel, P. Comparative analysis of Schwann cell lines as model systems for myelin gene transcription studies. *J Neurosci Res.* 2002 Aug; 65(9):487-508.
- Jiang, H., Yu, Y., Liu, S., Zhu, M., Dong, X., Wu, J., Zhang, Z., Zhang, M. and Zhang, Y., 2019. Proteomic Study of a Parkinson's Disease Model of Undifferentiated SH-SY5Y Cells Induced by a Proteasome Inhibitor. *International Journal of Medical Sciences*, 16(3), pp.84-92.
- Rowlewich, J. and Langford, O., 2013. Considerations for the Use of SH-SY5Y Neuroblastoma Cells in Neurobiology. *Neural Cell Culture*, pp.9-21.



Introduction

MTT (3-(4,5-dimethylthiazol-2-yl)-2,5-diphenyltetrazolium bromide) is a water soluble tetrazolium salt commonly used in toxicity screening (1). The tetrazolium salt is converted to insoluble purple formazan via tetrazolium ring cleavage by succinate dehydrogenase within mitochondria (2). The MTT assay was used for the cytotoxicity testing of low molecular weight (LMW) hyaluronic acid (HLA) in a neuronal (SH-SY5Y) and glial (RT4 DGP2T) cell line and the results were then compared against two further viability tests; the trypan blue exclusion (TBE) assay and the resazurin reduction (RR) assay. The results of this testing highlighted the requirement for a battery approach in the cytotoxicity testing of drug compounds.

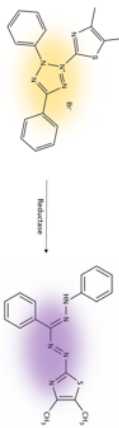
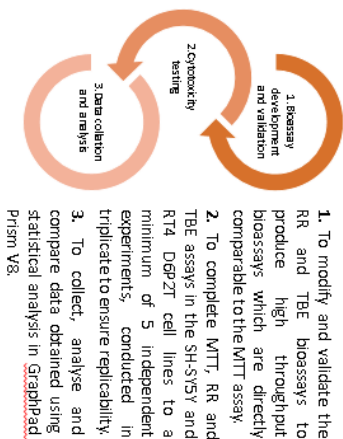


Figure 1. Conversion of MTT to formazan product via the action of MTT reductases

Aims and Objectives

To determine the robustness of the MTT assay in the cytotoxicity testing of LMW HLA, a number of objectives were completed.



Methods

1. Cell lines

Two continuous cell lines were used in this study; a glial cell line, RT4 DGP2T, to represent the Schwann cells found in the peripheral nervous system and a human neuronal cell line, SH-SY5Y, used undifferentiated. For ease of viewing, only the neuronal data is presented in this poster.

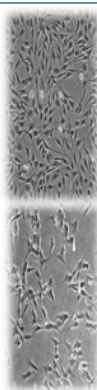


Figure 2. RT4 DGP2T (glial) (Figure 3. SH-SY5Y (neuronal) cell line (4)

2. Cytotoxicity testing

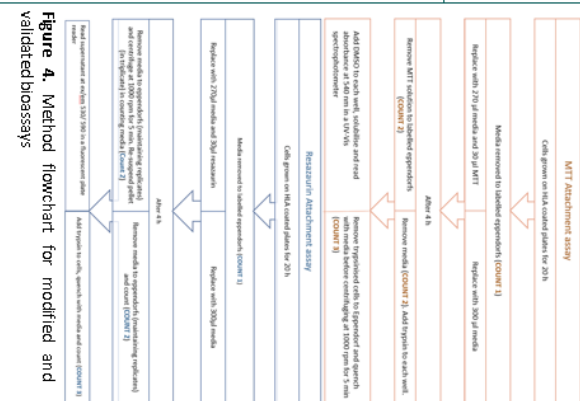


Figure 4. Method flowchart for modified and validated bioassays

Results

1. Enhanced MTT toxicity in neuronal cells

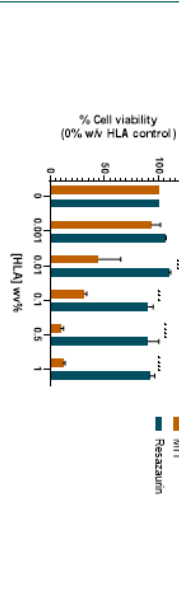


Figure 5. Enhanced cytotoxicity of LMW HLA in neuronal cells by MTT. ****p* < 0.001, *****p* < 0.0001 vs control (0 w/v% HLA).

2. Enhanced toxicity is independent of mechanical disruption

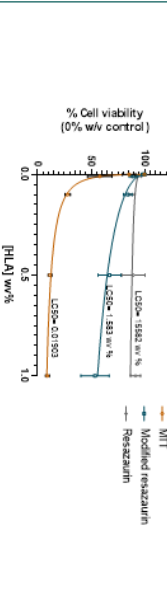


Figure 6. Mechanical cell disruption is not responsible for enhanced MTT toxicity. Data is representative of mean ± SEM of 5 independent experiments, performed in triplicate.

3. MTT enhances HLA toxicity in SH-SY5Y

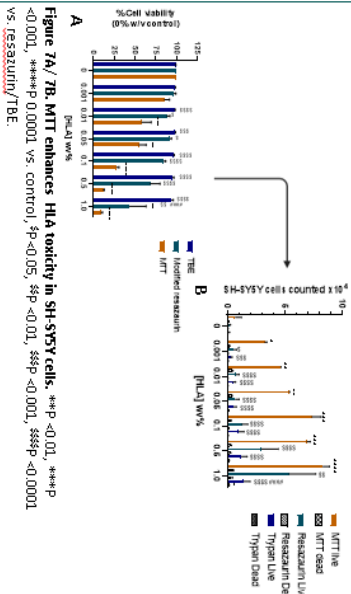


Figure 7a/7b. MTT enhances HLA toxicity in SH-SY5Y cells. ***p* < 0.01, ****p* < 0.001, *****p* < 0.0001 vs. control; †*p* < 0.05, ‡*p* < 0.01, §§*p* < 0.001, §§§*p* < 0.0001 vs. Resazurin/TBE.

Discussion

MTT remains one of the most widely used cytotoxicity assays in research due to how accessible and well characterised it is. However caution should be exercised when utilising MTT. The results presented have shown that:

- MTT revealed toxicity of LMW HLA in both neuronal (SH-SY5Y) and glial (RT4 DGP2T) cell lines, but SH-SY5Y shown here, were more susceptible.
- This enhanced toxicity could not be replicated with the resazurin assay despite the fact that both assays operate via the same mechanism of action.
- The TBE bioassay also failed to replicate the enhanced toxicity observed in the MTT.
- It was determined that the overestimation of cytotoxicity was due to enhanced cell detachment during the MTT assay, and not cell death (Fig. 7b).
- This result was independent of methodological deviations between the three assay protocols.

Conclusion

The MTT assay caused an overestimation of LMW HLA toxicity in neuronal cells. This study has highlighted the need for a battery approach to cytotoxicity testing and careful interpretation of MTT viability results.

Acknowledgements

This work was funded by AIT President's Doctoral Scholarship 2018 and the Irish Research Council Government of Ireland Postgraduate Scholarship 2020

References

1. MTT assay. *Wikipedia*. 2020. URL: https://en.wikipedia.org/wiki/MTT_assay
2. MTT assay. *Wikipedia*. 2020. URL: https://en.wikipedia.org/wiki/MTT_assay
3. MTT assay. *Wikipedia*. 2020. URL: https://en.wikipedia.org/wiki/MTT_assay
4. MTT assay. *Wikipedia*. 2020. URL: https://en.wikipedia.org/wiki/MTT_assay



APPENDIX 4. ADDITIONAL DATA

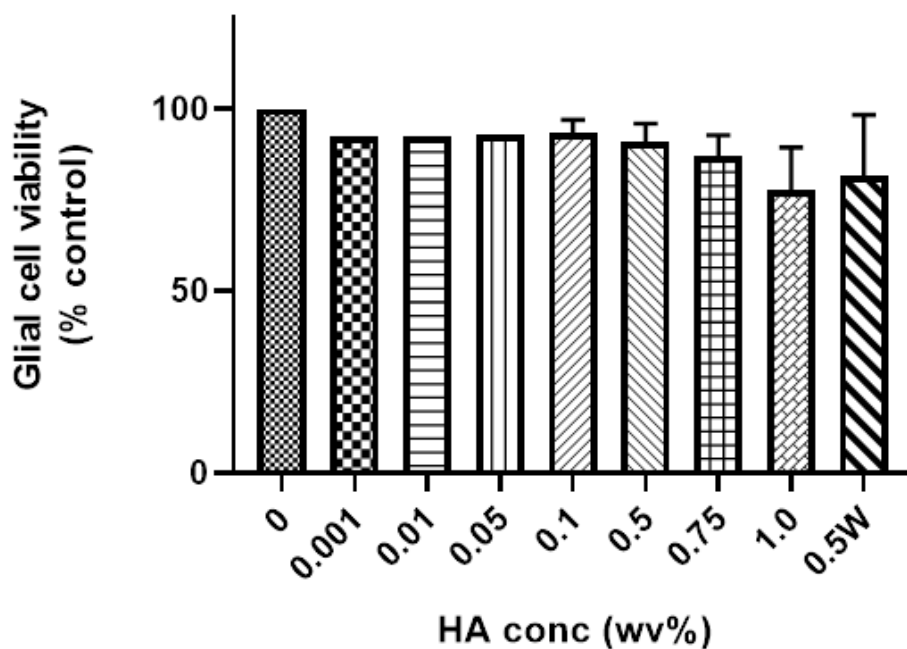


Figure 101. MTT assay of glial cells exposed to 8-50 kDa HA of various concentrations. 0.5W refers to 0.5 %wv HA dissolved in water rather than PDL to provide a comparison. Data is the mean \pm SEM of 5 independent experiments, conducted in triplicate. $P > 0.05$, no significance, when comparing conditions vs control using one-way ANOVA with Tukey posttests.

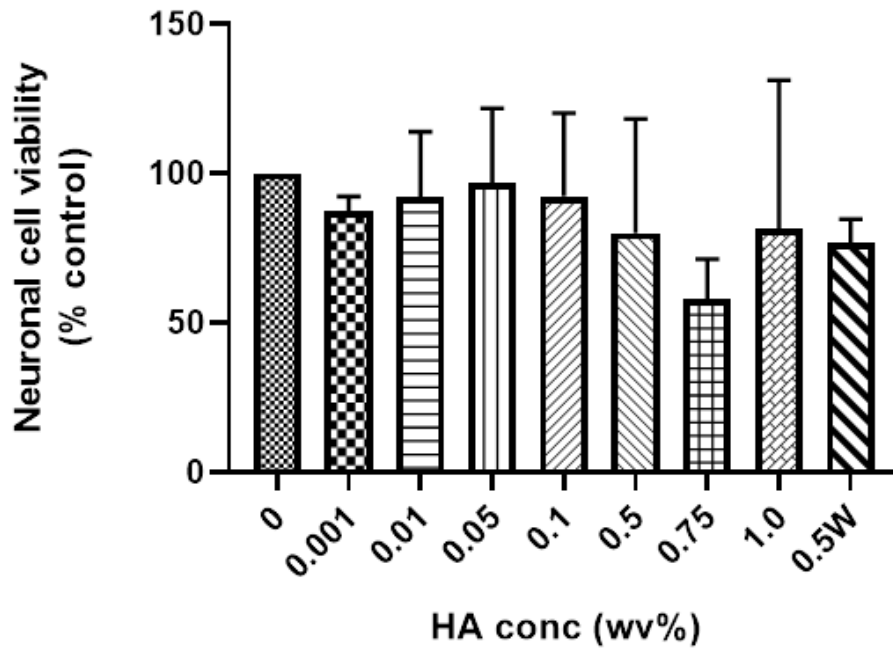


Figure 102. MTT assay of neuronal cells exposed to 8-50 kDa HA of various concentrations. 0.5W refers to 0.5 % wv HA dissolved in water rather than PDL to provide a comparison. Data is the mean \pm SEM of 5 independent experiments, conducted in triplicate. $P > 0.05$, no significance, when comparing conditions vs control using one-way ANOVA with Tukey posttests.

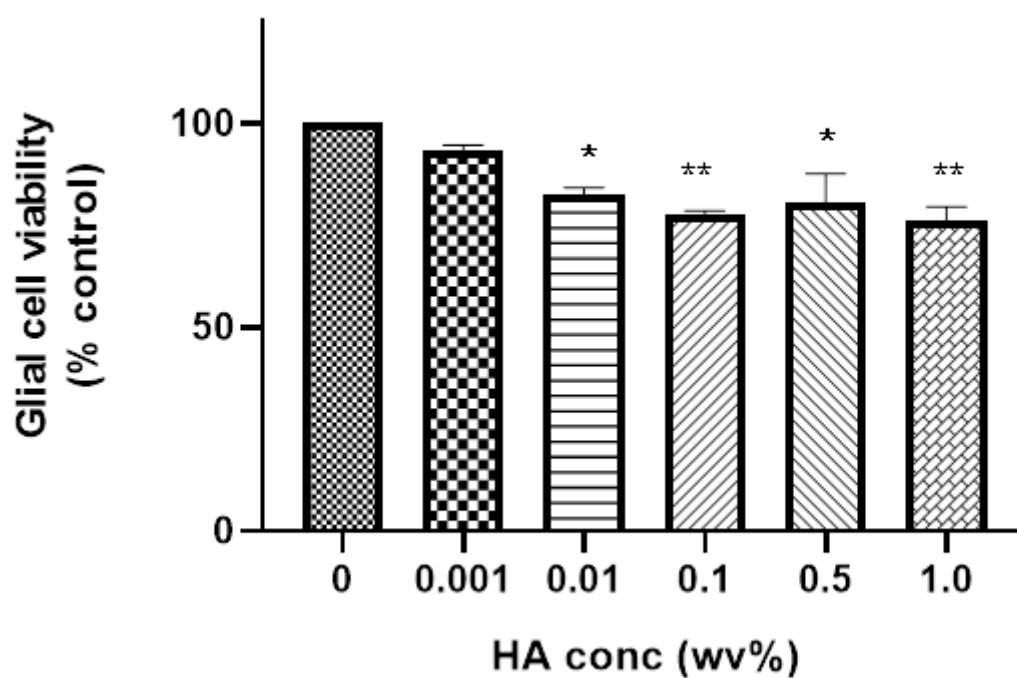


Figure 103. MTT assay of glial cells exposed to 30-50 kDa HA of various concentrations. Data is the mean \pm SEM of 3 independent experiments, conducted in triplicate. * $P < 0.05$, ** $P < 0.01$ vs control when compared using one-way ANOVA with Tukey posttests.

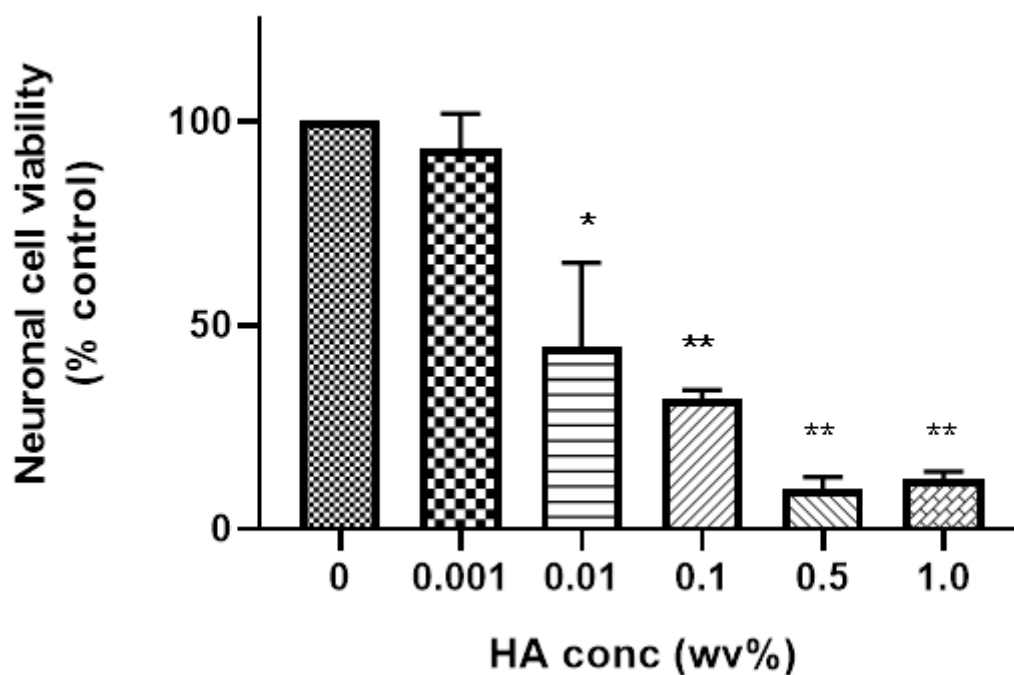


Figure 104. MTT assay of neuronal cells exposed to 30-50 kDa HA of various concentrations. Data is the mean \pm SEM of 3 independent experiments, conducted in triplicate. * $P < 0.05$, ** $P < 0.01$ vs control when compared using one-way ANOVA with Tukey posttests.

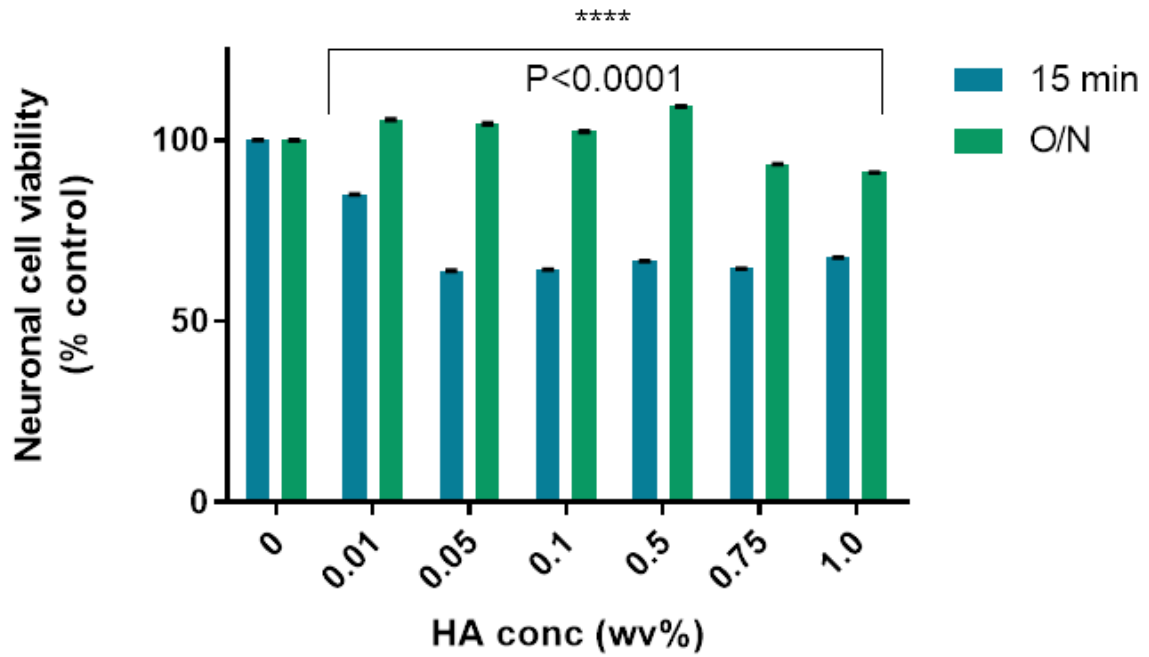


Figure 105. MTT assay of neuronal cells comparing coating times. 15 mins vs O/N referring to a 15 min or overnight incubation of HA in the wells before removal and washing. O/N incubation of HA in the wells resulted in significantly better cell viability. Data is the mean \pm SD of 1 independent experiment, conducted in 6 replicates.

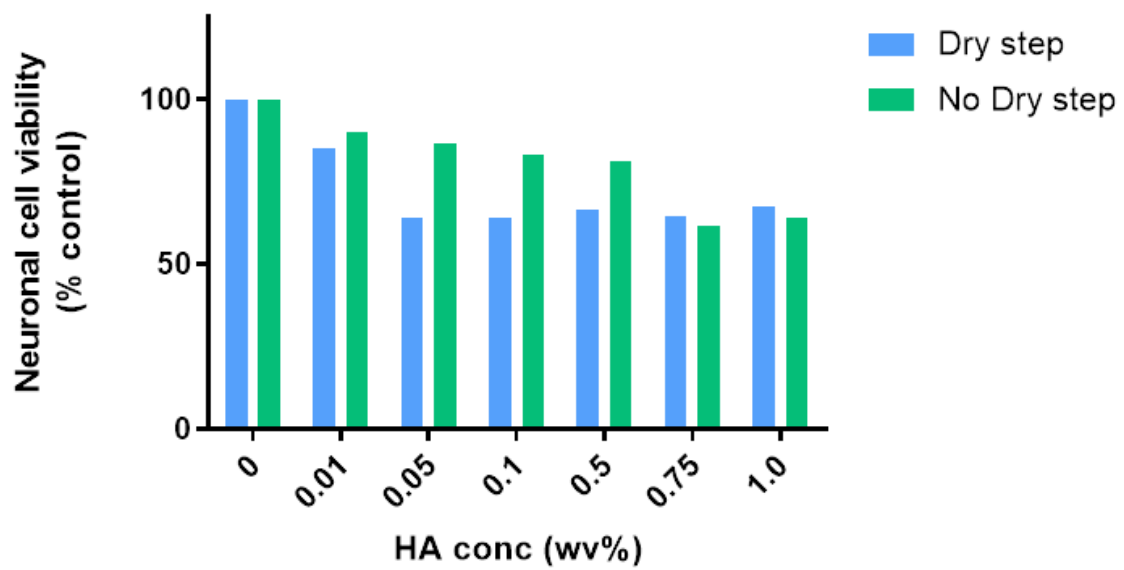


Figure 106. MTT assay of neuronal cells after exposure to HA coating with a dry step vs no dry step. Dry step refers to the period between the removals of HA solution from each well, prior to washing. Data is the mean \pm SD of 1 experiment, performed in 6 replicates.

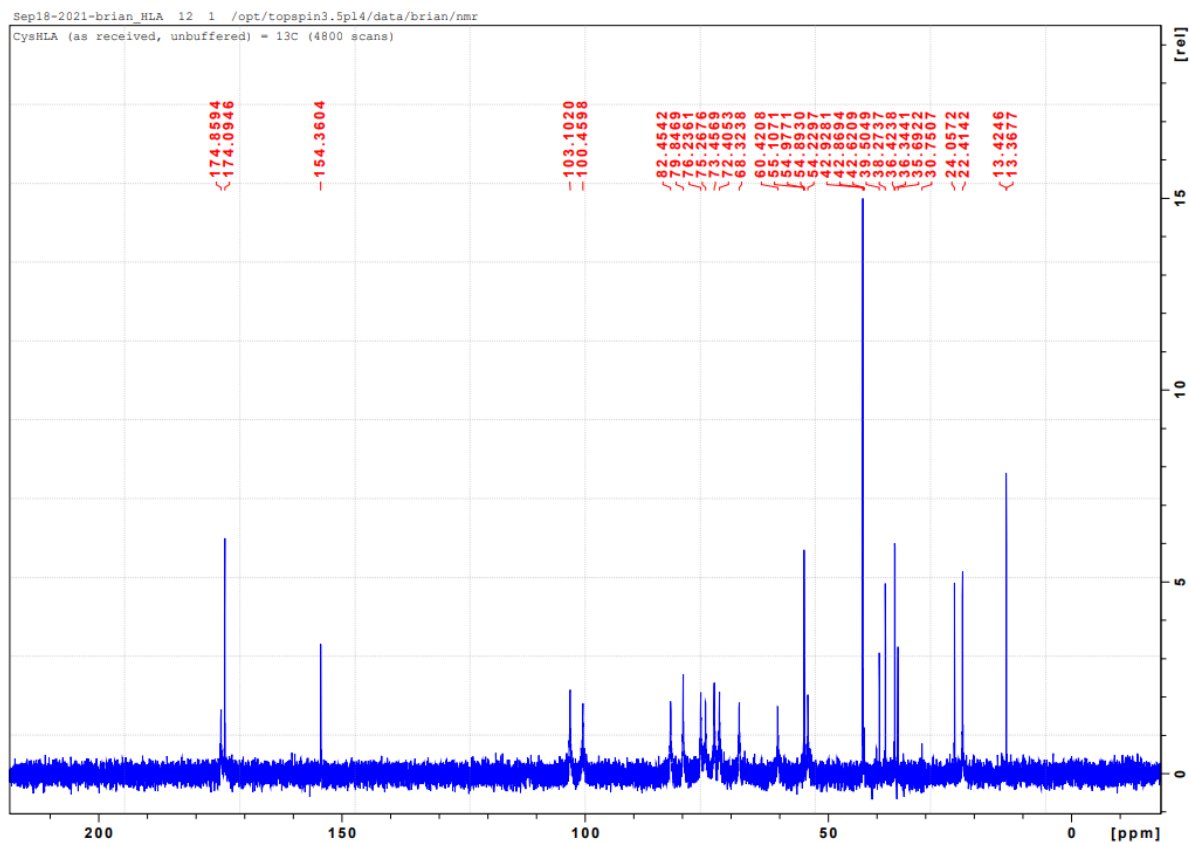


Figure 107. ^{13}C NMR of HA-SH

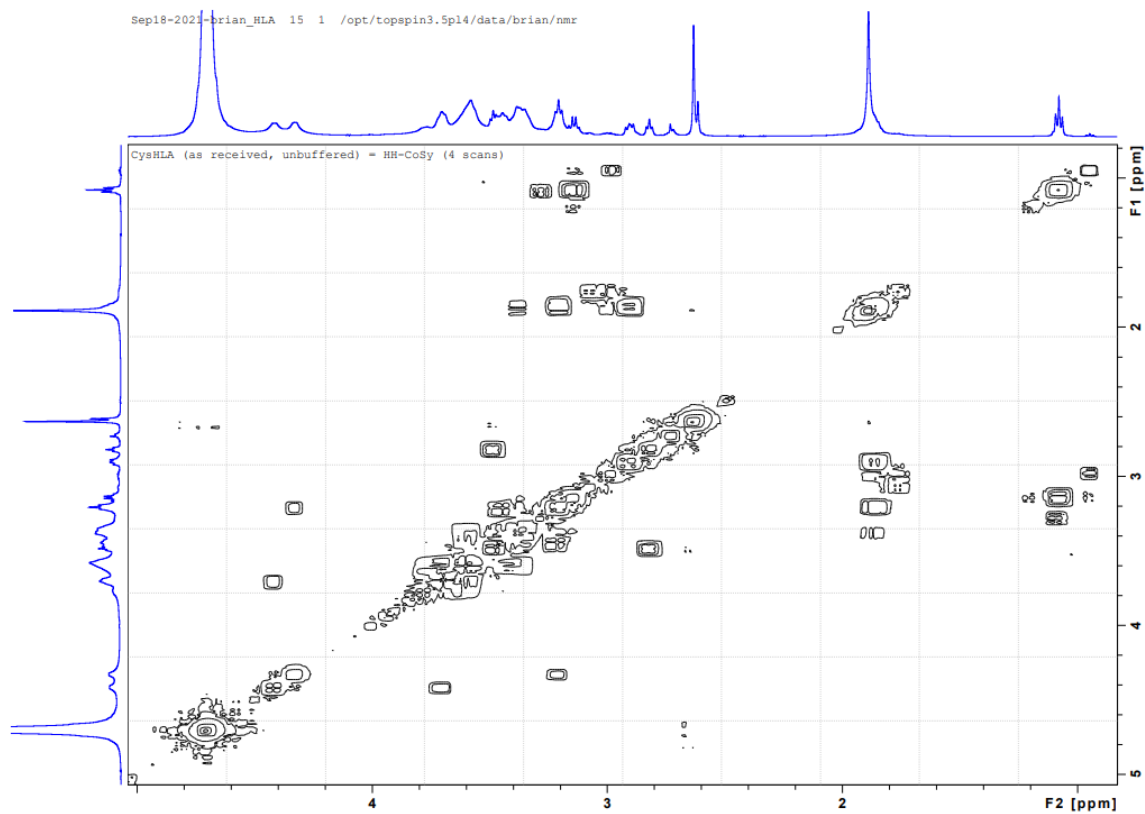


Figure 108. HH-CoSy NMR of HA-SH

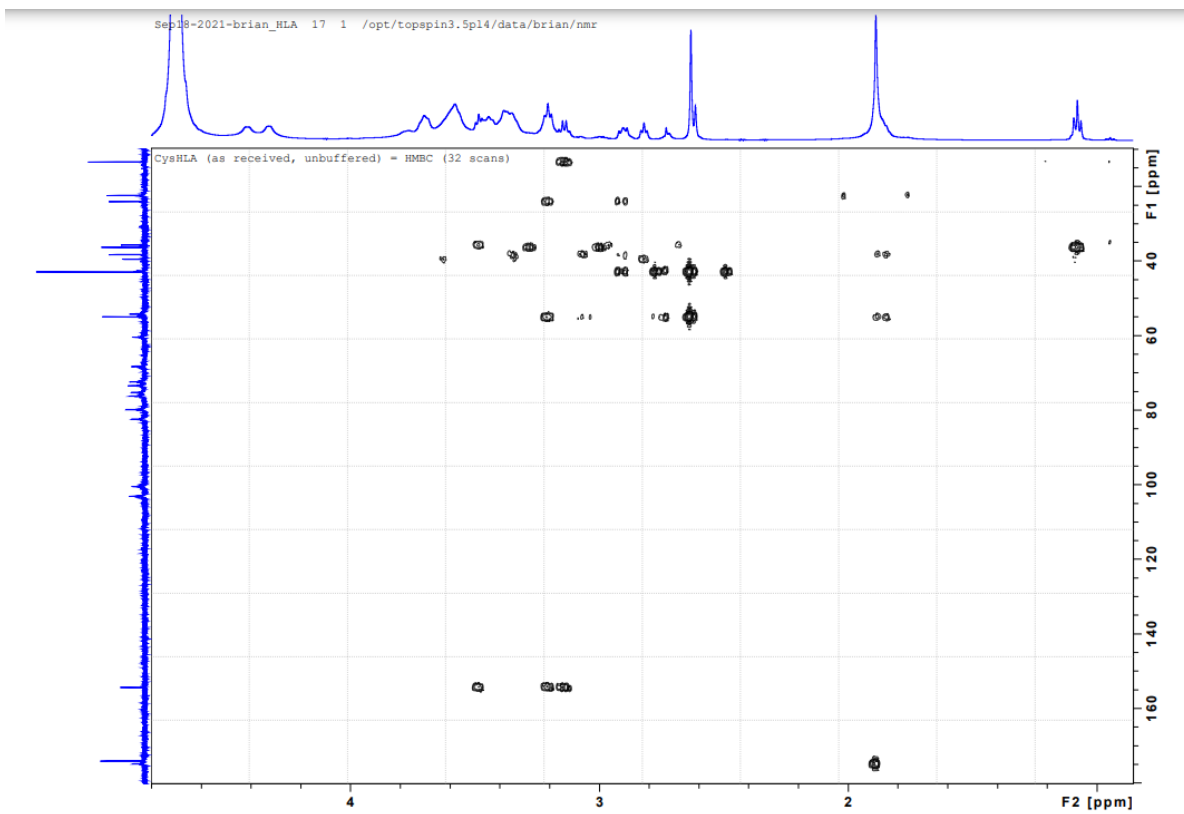


Figure 109. HMBC NMR of HA-SH

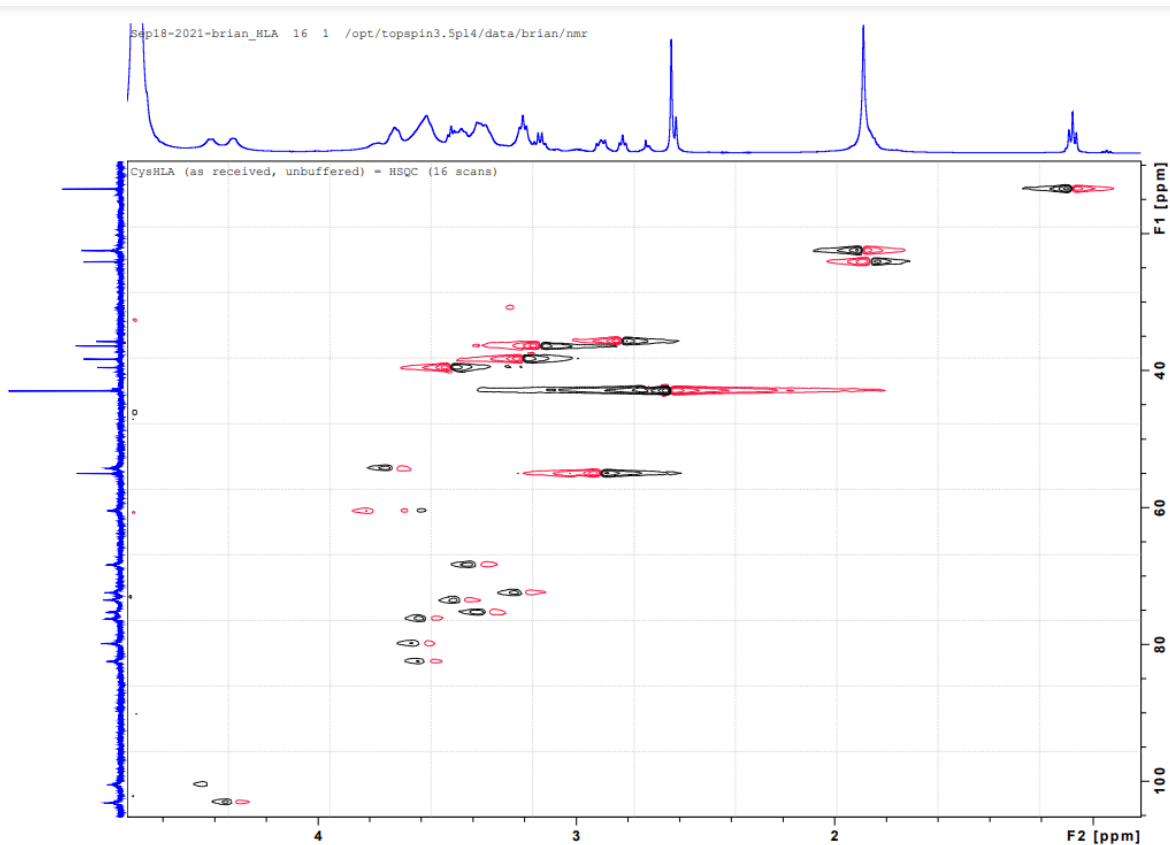


Figure 110. HSQC NMR of HA-SH

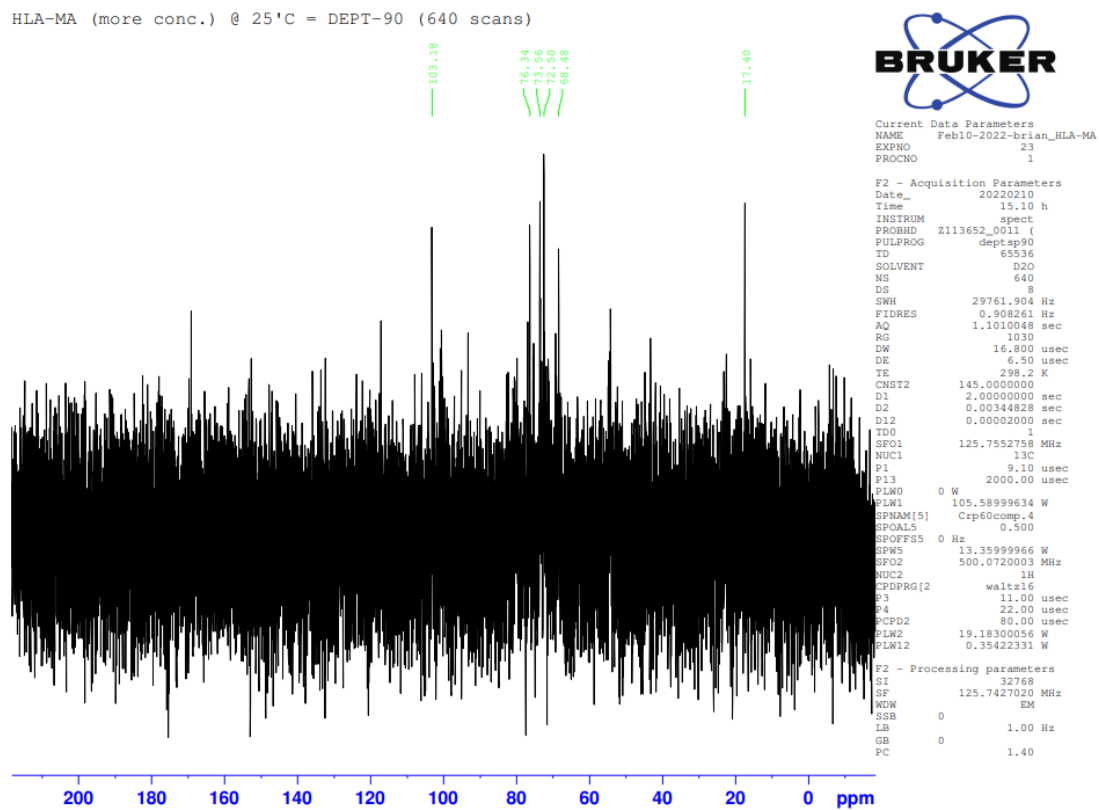


Figure 111. DEPT-90 scan of HA-MA

HLA-MA (more conc.) @ 25°C = HH-CoSy (1 scan)

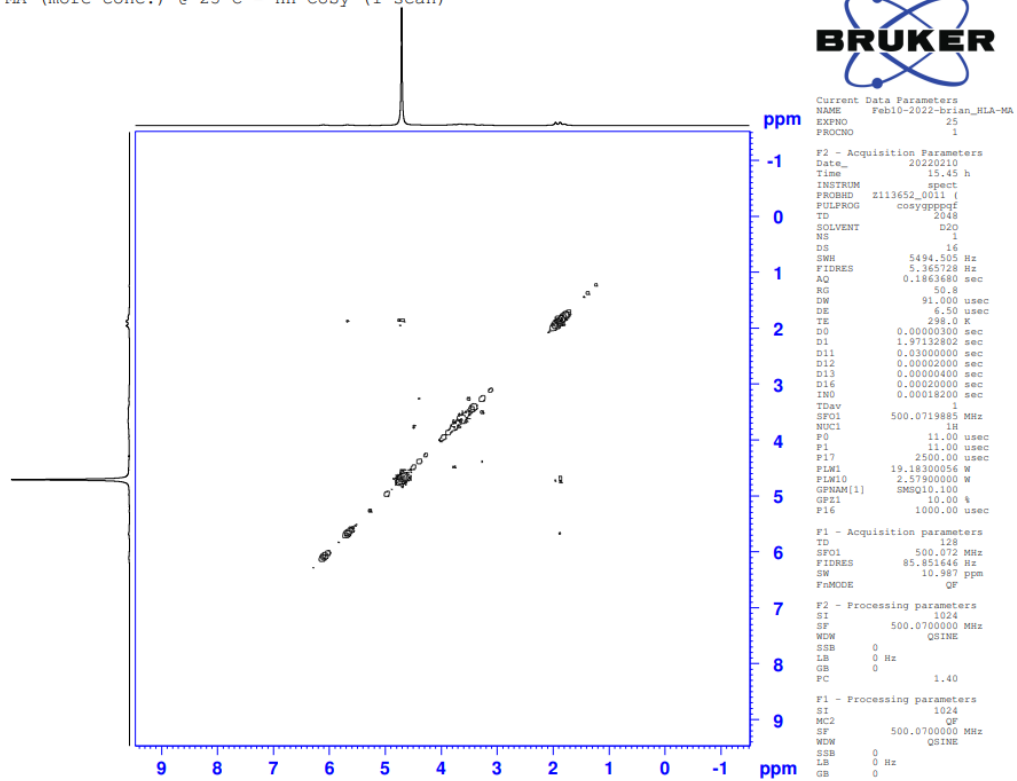


Figure 112. HH-CoSy NMR of HA-MA

HLA-MA (more conc.) @ 25°C = HSQC (2 scans)

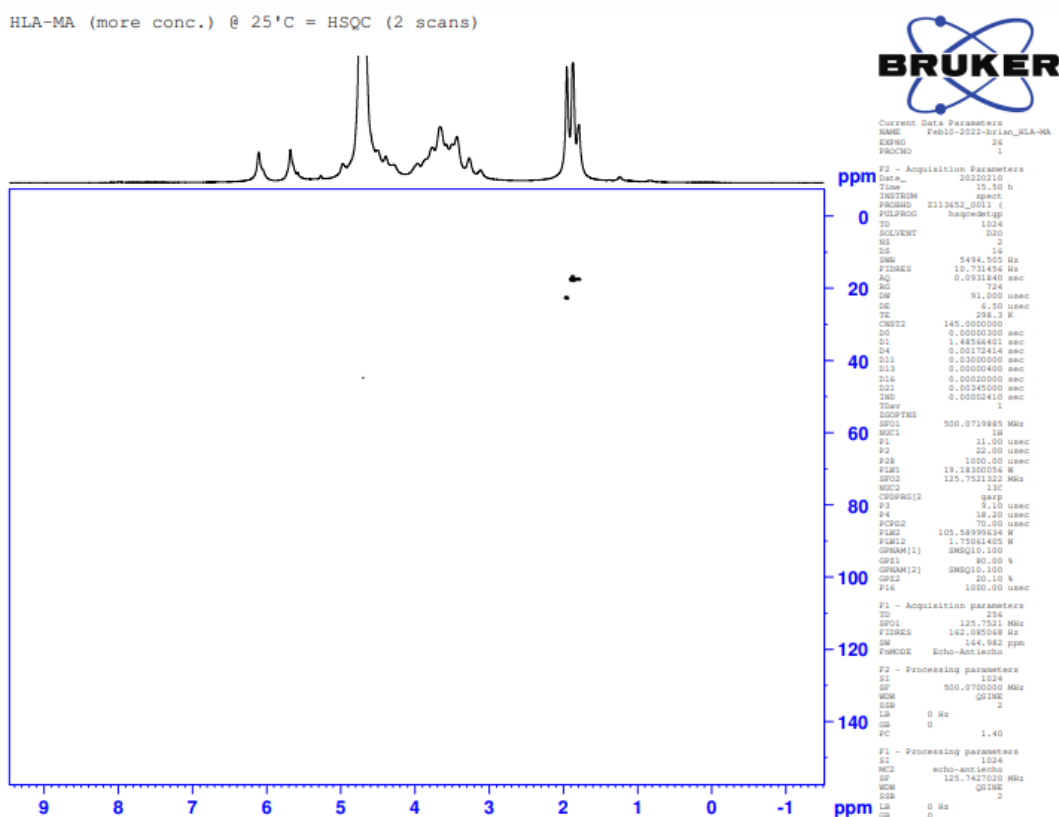


Figure 113. HSQC NMR of HA-MA